U.S.G.S. Award Number: 05HQGR0009

THE LIQUEFACTION SUSCEPTIBILITY, RESISTANCE, AND RESPONSE OF SILTY AND CLAYEY SOILS

Jennifer L. Donahue, Jonathan D. Bray, and Michael F. Riemer

University of California, Berkeley
453 Davis Hall, MC-1710
Berkeley, CA 94720-1710
Tel. (510) 642-9843
Fax. (510) 642-7476
bray@ce.berkeley.edu
URL: http://www.ce.berkeley.edu/~bray/

November 21, 2007

U.S.G.S. Award Number: 05HQGR0009

THE LIQUEFACTION SUSCEPTIBILITY, RESISTANCE, AND RESPONSE OF SILTY AND CLAYEY SOILS

Jennifer L. Donahue, Jonathan D. Bray, and Michael F. Riemer
University of California, Berkeley
453 Davis Hall, MC-1710
Berkeley, CA 94720-1710
Tel. (510) 642-9843
Fax. (510) 642-7476
bray@ce.berkeley.edu
URL: http://www.ce.berkeley.edu/~bray/

ABSTRACT

An experimental research program has been undertaken to assess the cyclic response of soils with significant fines (both plastic and non-plastic). Advanced cyclic testing of low plasticity silty and clayey soils is required to characterize the liquefaction susceptibility of fine-grained soils and to evaluate their liquefaction resistance. Fine-grained soils from Adapazari, Turkey were reconstituted and systemically tested so that the significant characteristics, or combination of characteristics, that primarily control their liquefaction susceptibility and cyclic response could be identified. Replicate testing required development of a modified version of the Slurry Deposition Method and the newly developed In-Place Wet Pluviation Method for specimen preparation.

The reconstituted soils were first subjected to grain size analysis, Atterberg Limits, constant rate of strain consolidation tests, consolidation tests, undrained monotonic triaxial and undrained simple shear tests to develop an understanding and a context for interpreting the cyclic experiments. Using the results of the undrained monotonic triaxial and simple shear tests, the effects on changes to static strength by varying the reconstitution method, effective confining stress, soil index properties, loading rate, and time under confinement were explored. It was found that the reconstitution method and time under confinement were the two most influential variations in testing conditions for monotonic testing.

The cyclic response of the reconstituted fine-grained soils was thoroughly investigated next. The soils were reconstituted by the two aforementioned methods, and the cyclic strength was evaluated by performing 82 tests using the cyclic triaxial and cyclic simple shear devices. This was accomplished by initially testing the reconstituted soil specimens at specified baseline conditions, and then retesting these soils after varying the specimen preparation, time under confinement, void ratio, overconsolidation ratio (OCR), effective confining stress (σ'_m), rate of loading, and initial static shear stress (α). Of the various testing conditions listed above, factors such as specimen preparation, time under confinement, w_c/LL and OCR were found to have the most impact on the soil's cyclic response.

This is part of an ongoing study to develop a database of experimental results upon which to characterize silty soils and to build robust soil constitutive models for advanced dynamic analysis.

ACKNOWLEDGEMENTS

Research supported by the U. S. Geological Survey (U.S.G.S.), Department of Interior, under USGS award number 05HQGR0009. The views and conclusions contained in this document are those of the authors and should not be interpreted as necessarily representing the official policies, either expressed or implied, of the U.S. Government. Additional support was also provided by the National Science Foundation (NSF) under award number CMS-0408760. The financial support of the NSF and USGS is gratefully acknowledged.

Chapter 1 INTRODUCTION

1.1 Research Motivation

The strong shaking produced by the 1999 Kocaeli earthquake (M_w = 7.4) caused widespread damage throughout the northwest region of Turkey. Hundreds of structures in Adapazari were severely damaged as evidenced by building settlement, sliding, and tilting. Many of the affected buildings had sand boils in their vicinity, although often ejecta were not present. The materials underlying the buildings that experienced ground failure were found to be primarily fine-grained soils (Bray et al., 2001a, 2001b). The use of state-of-the-art methods for screening and identification of potentially liquefiable soils (as defined by the consensus paper by Youd et al. 2001) in Adapazari did not commonly identify the problematic soils because of deficiencies in the widely used "Chinese criteria" for fine-grained soils (Bray et al. 2004a). The “Chinese Criteria” is one of the oldest and most commonly accepted liquefaction criteria and will be explained in more detail in Section 1.2.

Recent studies by Bray and Sancio (2006) and Boulanger and Idriss (2006) have developed alternative criteria for identifying soils susceptible to liquefaction. Based primarily on cyclic testing of “undisturbed” specimens of Adapazari silts and clays, Bray and Sancio (2006) found that soils with Plasticity Index (PI) < 12 and water content to liquid limit ratios (w_c/LL) > 0.85 were susceptible to liquefaction, as evidenced by a dramatic loss of strength resulting from increased pore water pressure and reduced effective stress. Liquefaction of fine-grained soils is typically manifested as cyclic mobility with limited flow deformation resulting from a transient loss of shear resistance due to the development of excess pore water pressures. Boulanger and Idriss (2006) use PI < 7 to identify soils exhibiting “sand-like” behavior that are susceptible to liquefaction and PI $\geqq$ 7 to identify soils exhibiting “clay-like” behavior that are judged to not be susceptible to liquefaction. Clay-like soils may soften due to the loss of effective stress resulting from the build-up of positive excess pore pressures, but the term liquefaction is reserved for sand-like soils. Thus, different definitions of liquefaction are, in part, leading to slightly different liquefaction susceptibility criteria. However, both research groups make it clear that fine-grained soils can undergo severe strength loss due to increased pore water pressures that temporarily reduce the effective stress in the soil.

The results of the cyclic testing of non-plastic and plastic silts provide an exceptional opportunity to re-evaluate current liquefaction screening and analysis techniques employed in the U.S. Current guidelines contained in efforts such as the California Hazard Mapping Program are poorly defined regarding the liquefaction of fine-grained soils. The Seismic Hazards Mapping Act, which became operative in the State of California on April 1, 1991, is a model for the nation in identifying and mitigating potential earthquake hazards. The stated purpose of the Act is "to protect public safety from the effects of strong ground shaking, liquefaction, landslides, or other ground failure, and other hazards caused by earthquakes" (in Guidelines for Evaluating and

Mitigating Seismic Hazards in California, Special Publication 117, California Division of Mines and Geology, 1997).

The seismic hazards zone mapping effort and the evaluation/mitigation guidelines for liquefaction-induced ground failure hazards are largely based on the application of the “Chinese Criteria” and "simplified" empirical methods that require re-evaluation and updating as important-case histories emerge. An area of special interest is the liquefaction potential of silty and clayey soils, because the empirical database for liquefaction triggering has only a few data points for soils with fines contents greater than 35%. For instance, only 13 data points for this case are in the Seed et al. (1985) correlation shown in Figure 1.1(i.e. as blackened round circles), which was readopted by the state-of-the-art liquefaction triggering consensus document of Youd et al. (2001).

Tremendous advancements are possible through research of the liquefaction susceptibility and resistance of non-plastic silts and low plasticity clayey silts. Many of the prevalent procedures for evaluating liquefaction are discussed in the document "Recommended Procedures for Implementation of DMG Special Publication 117: Guidelines for Analyzing and Mitigating Liquefaction Hazards in California" edited by Martin and Lew (1999). This important guidance document states, "Clayey soils are those that have a clay content (particle size < 0.005 mm) greater than 15 percent." Moreover, it states, "If clayey soil materials are encountered during site exploration, those materials may be considered non-liquefiable.”

However, research following the 1999 Kocaeli and 1999 Chi-Chi earthquakes has identified a large number of cases where ground failure in silty and clayey soils containing more than 15% clay-size particles caused considerable damage to buildings. For example, Sancio et al. (2002) found that liquefaction in the silts of Adapazari, Turkey was responsible for much of the damage observed in this city. These silty soils typically had clay contents greater than 15%, the results of cyclic triaxial testing of carefully retrieved soil specimens from Adapazari, described in Sancio et al. (2003), show that these soils are actually susceptible to liquefaction, which is contrary to the often relied upon Chinese Criteria.

In this study, a reliable specimen preparation method is required for replicate testing of silty soil specimens of varying characteristics (e.g., different PI, void ratio (e), and overconsolidation ratio (OCR), among other factors). After presenting a modified version of the Slurry Deposition Method and the newly developed In-Place Wet Pluviation Method, preliminary results from a series of cyclic simple shear (CSS) and cyclic triaxial (CTX) tests are presented and discussed.

1.2 Screening and Identification of Liquefiable Fine-Grained Soils

Many of the commonly used procedures for evaluating liquefaction are largely based on field and laboratory testing of clean sands or sands with a limited amount of fines. Wang (1979) was one of the first to establish liquefaction criteria based on the observations from many earthquakes. His criteria stated that soils are susceptible to liquefaction if they meet the following criteria: Percent of particles less than 5 μm < 15% to 20%, and $w_c/LL > 0.9$.

Based on the observations of Wang (1979), Seed and Idriss (1982) developed the "Chinese Criteria" which stated that clayey soils (i.e. points that plot above the A-line on the plasticity chart) can be susceptible to liquefaction only if all three of the following conditions are met: Percent of particles less than 5 μm < 15%, LL < 35, and $w_c/LL > 0.9$.

This criterion became the standard known as the "Chinese Criteria," based on its origin. The "Chinese Criteria" is shown graphically in Figure 1.2. Koester (1992) revised the "Chinese Criteria" and recommended a reduction in the LL conditions due to inconsistencies between the Chinese produced fall cone and western made Casagrande percussion device.

The Youd (1998) paper stated that the "Chinese Criteria" is conservative and proposed the following alternatives for liquefaction criteria. If the material is classified with a "C" in the USCS nomenclature (e.g. CH, CL, SC, and GC), the material can be screened as non-liquefiable. Furthermore, soils may be liquefiable if they meet the following criteria: LL < 35, and Plot below A-line on the Casagrande plasticity chart, or PI < 7

As stated in the previous section, from the "Guidelines for Analyzing and Mitigating Liquefaction Hazards in California," Martin and Lew (1999) state that soils with the following characteristics are not susceptible to liquefaction: Percent of particles less than 5 μm > 15%, This criterion also agrees with the Youd (1998) criteria in that soils that are clayey are not susceptible to liquefaction.

Andrews and Martin (2000) recommend the following liquefaction susceptibility screening criteria to amend the "Chinese Criteria": Percent of particles less than 2 μm < 10%, andLL < 32 In this liquefaction screening criteria, the w_c/LL ratio has been disregarded as a condition for silty soils.

Following the observations and case histories of liquefaction in 1989 Loma Prieta, 1994 Northridge, 1999 Kocaeli, and 1999 Chi-Chi earthquakes, it was found that the liquefaction screening criteria, as stated above, would not have classified many of the soils which exhibited liquefaction as susceptible to liquefaction. Boulanger et al. (1997, 1998), Holzer et al. (1999), and Perlea (2000) all suggest laboratory testing of fine-grained soils for liquefaction potential rather than relying solely upon the use of the "Chinese Criteria."

The liquefaction screening criteria of Polito and Martin (2001) was developed from high quality cyclic triaxial tests on sandy soils with increasing percentages of nonplastic silt fines. They found that with sufficient fines, the sand particles are suspended with the fines, and the liquefaction resistance is controlled by the relative density, D_r. Furthermore, the liquefaction resistance for silts is systematically lower than that for clean sands at a similar D_r. The liquefaction screening criteria state the following conditions: Liquefiable: LL < 25 and PI < 7 Potentially Liquefiable: 25 < LL < 35 and 7 < PI < 10, Susceptible to cyclic mobility: 35 < LL < 50 and 10 < PI < 15. The Polito and Martin (2001) liquefaction screening criteria are given in Figure 1.4.

The liquefaction criteria from Seed et al. (2003) are similar to Polito and Martin (2001) with the following conditions: Liquefiable: LL < 30 and PI < 10, Uncertain: 30 < LL < 40 and 10 < PI < 12 . For those soils that are plotted in the "uncertain" range, laboratory testing of undisturbed samples is recommended. A graphical depiction of the Seed et al. (2003) criteria is given in Figure 1.5.

Thevanayagam (2000) and Thevanayagam and Martin (2002) have developed a different liquefaction screening criteria based on the fines content of the material. This criteria uses three nomenclatures, FC_{th} (Threshold fines content), FC_l (Limiting fines content), and e_f (void ratio of the fines fraction). For each case presented in the papers, the fines content (FC) is compared on a continuum with FC_{th} and FC_l. In a first example, $FC < FC_{th}$, meaning the coarser grains interact and influence response. When there are sufficient fines ($FC > FC_{th}$), two cases are presented where $FC > FC_l$ and $FC < FC_l$. For each case, the coarse particles are essentially "floating" in a matrix of fine silt-size particles. Using these two cases, the papers detail how to find the void ratio of the fine fraction (e_f) which is thought to be the key descriptor of the density, and governs the cyclic response.

Many researchers have broadened this research to specifically investigate the percentage of fines and density of the material in screening for liquefaction susceptibility and resistance. These investigators begin with a clean sand and incrementally increase the amount of fines to assess the liquefaction resistance of the mixtures. Results from Guo and Prakash (1999), Xenaki and Athanasopoulos (2002), and Naeini and Braziar (2003) all suggest that cyclic resistance decreases with an increase in fines until approximately 35-45%. Here the fines will dominate the cyclic response of the soil. After this threshold, the cyclic resistance was found to increase.

Based on the research by Sancio (2003), and Bray and Sancio (2004a, b) it was found that soil deposits may be categorized into three groups: Susceptible to liquefaction or cyclic mobility: $w_c/LL \geq 0.85$ and $PI \leq 12$,Moderately susceptible to liquefaction or cyclic mobility (requires testing): $PI \leq 20$ and $w_c/LL \geq 0.80$, Too clayey to liquefy: $PI > 20$. A graphical representation of the Bray and Sancio (2004a) method is presented in Figure 1.6. Structures founded on these soils, and for that matter, on any soil, may still undergo significant deformations if the cyclic loads approach or exceed the dynamic strength of the soil.

Boulanger and Idriss (2004 and 2006) recommend that soil be categorized into "clay-like" and "sand-like." They also recommend that the first step in evaluating the potential for ground failure in silts and clays during earthquakes is to determine the appropriate framework and engineering procedure for evaluation. They propose that fine-grained soils can confidently be expected to exhibit clay-like behavior if they have $PI \geq 7$, which includes soils in the "transition interval" and all CL soils. If the soil is a CL-ML, the PI criterion may be reduced to $PI \geq 5$. Soils that meet the above criteria are expected to exhibit cyclic softening during earthquake loading. Soils which do not exhibit the above criteria are considered likely to exhibit sand-like behavior (i.e., are liquefiable). These criteria are plotted in Figure 1.7.

The current state-of-the-art and state-of-the-practice for the evaluation of liquefaction triggering is established in the summary reports from the 1996 NCEER and 1998 NCEER/NSF workshops on the evaluation of liquefaction resistance of soils, which were published in the ASCE Journal

of Geotechnical and Geoenvironmental Engineering (Youd et al., 2001). These proceedings recommend the use of the "Chinese Criteria" to confirm the liquefaction susceptibility of silts and clays.

1.3 Scope of Work and Report Organization

The literature reveals arguments both for and against the "Chinese Criteria" for silty sands and silts. This difference of opinion stems from the availability of relevant case histories and interpretation of the cyclic response.

This study is motivated to help improve the understanding of the classification of fine-grained soils (both plastic and non-plastic) by examining aspects of testing from sample preparation, experiment design, and the material response in the context of how they should be characterized for liquefaction potential. The following outlines the major chapters of this dissertation.

Chapter 2 presents the characteristics of the fine-grained soils from Adapazari. The soils were first divided, based on PI, LL, and fines content, into seven batches representative of the fine-grained soils that exhibited liquefaction or cyclic softening in Adapazari during the 1999 Kocaeli earthquake. Atterberg Limits tests, Electron Microscope Analysis, and X-ray Diffraction were all used to characterize the soils.

Chapter 3 discussed the two reconstitution methods developed for testing the fine-grained Adapazari soils. A detailed discussion of specimen preparation using these methods is included for both the cyclic triaxial and cyclic simple shear devices.

Chapter 4 discusses the laboratory testing equipment used to study liquefaction response, with particular emphasis on the benefits and potential problems associated with each device.

Chapter 5 presents the results of the testing series undertaken for both the soil characterization and the static testing on the triaxial and simple shear. For the consolidation and monotonic testing performed within this chapter, varied testing conditions are explored and the resulting effects on static strength are discussed.

Chapter 6 presents the results of the testing series for both the cyclic triaxial and cyclic simple shear. Numerous testing conditions are explored and the resulting increases and decreases in cyclic strength are discussed. Comparisons between test series are examined with emphasis on understanding the generalized liquefaction response for fine-grained soils, and a new criterion for the liquefaction response of fine-grained reconstituted soils based on this testing program is introduced.

Chapter 7 presents the testing series conclusions. The results integrate the static and dynamic tests into a cohesive development of findings. Recommendations for future research are also provided.

All individual test results are available in the Appendices. Appendix A presents the soil characterization laboratory tests such as the constant rate of strain consolidation and consolidation tests for both the triaxial and simple shear devices. Appendix B provides the results for the monotonic tests for the triaxial device with the Slurry Deposition Method and the simple shear device with both the Slurry Deposition Method and In-Place Wet Pluviation Method of specimen reconstitution. Appendix C provides the results of the cyclic tests for the triaxial device with the Slurry Deposition Method and the simple shear device with both the Slurry Deposition Method and In-Place Wet Pluviation Method of specimen reconstitution.

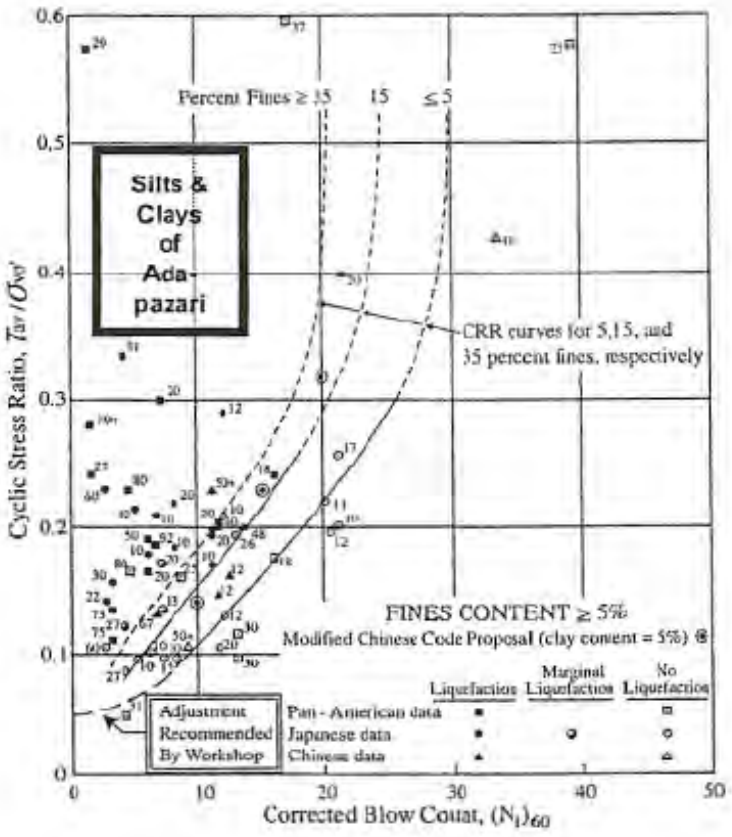

Figure 1.1 Relationship between cyclic stress ratio (CSR) and SPT penetration resistance for sands and silty sands based on field performance data (modified from Youd et al. 2001 after Seed et al. 1985) with range of data for the silts and clays of Adapazari, Turkey shown in the rectangle.

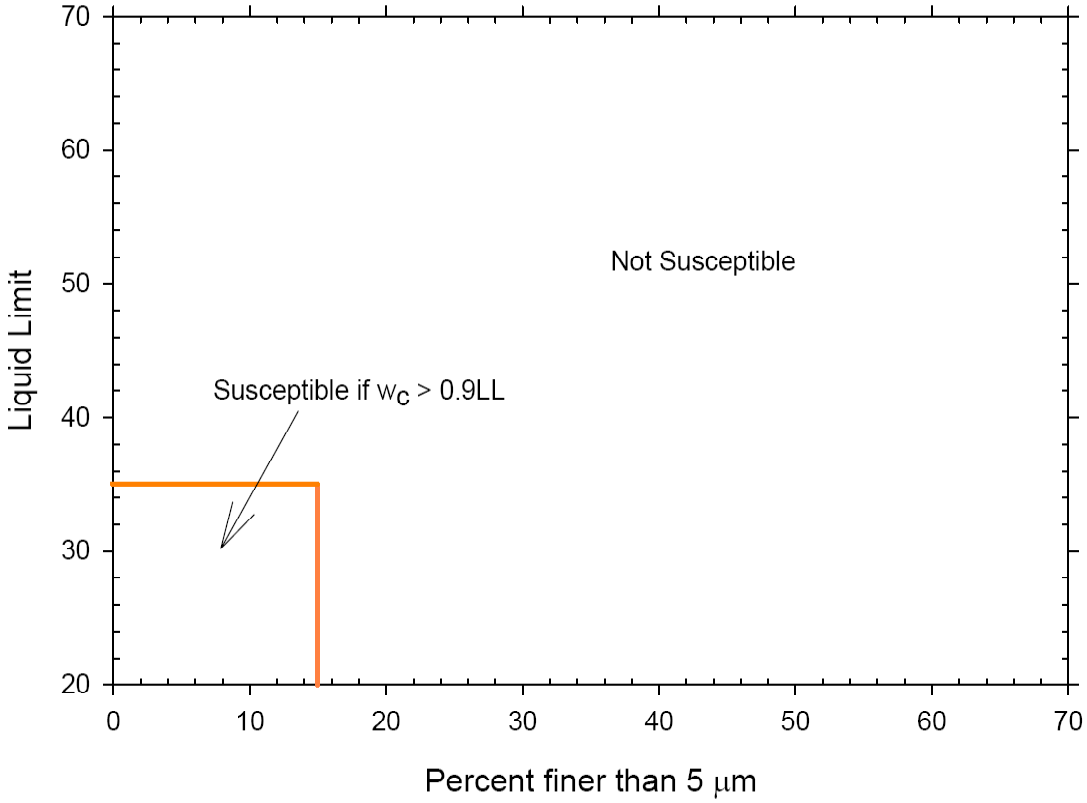

Figure 1.2 "Chinese Criteria" from Seed and Idriss (1982), after Wang (1979) liquefaction screening criteria.

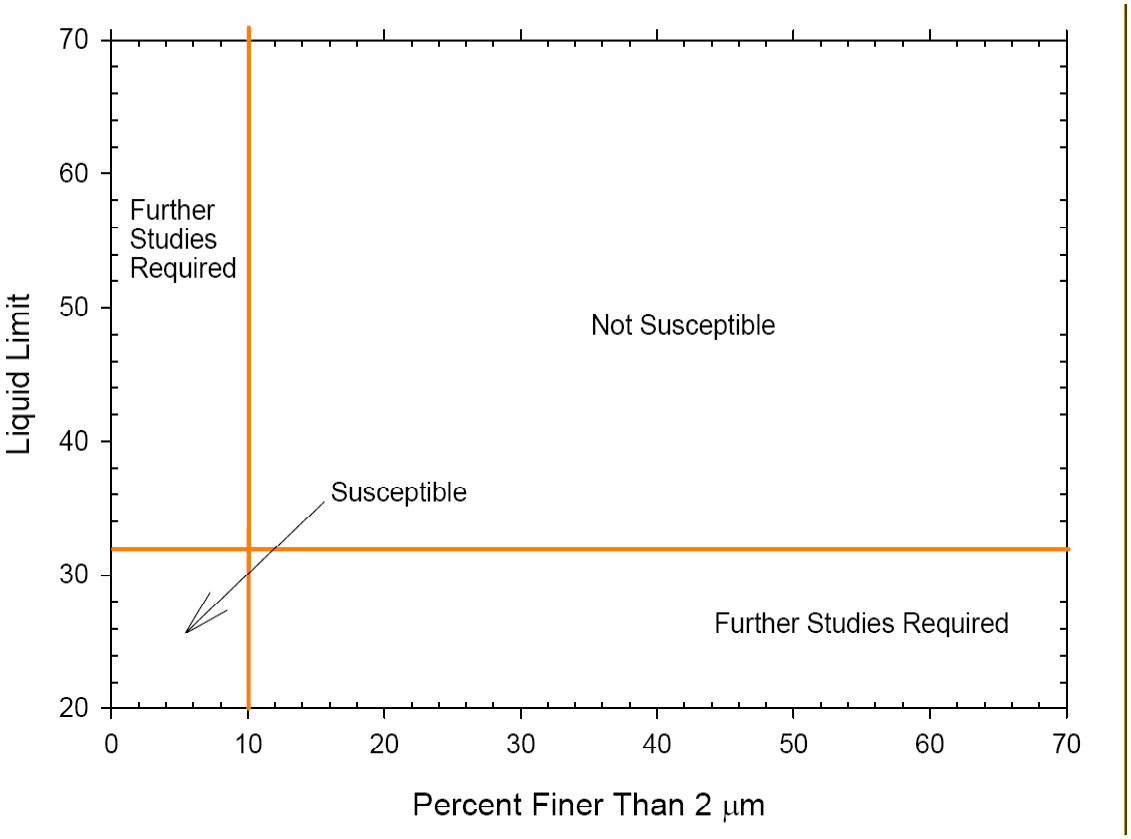

Figure 1.3 Andrews and Martin (2000) liquefaction screening criteria.

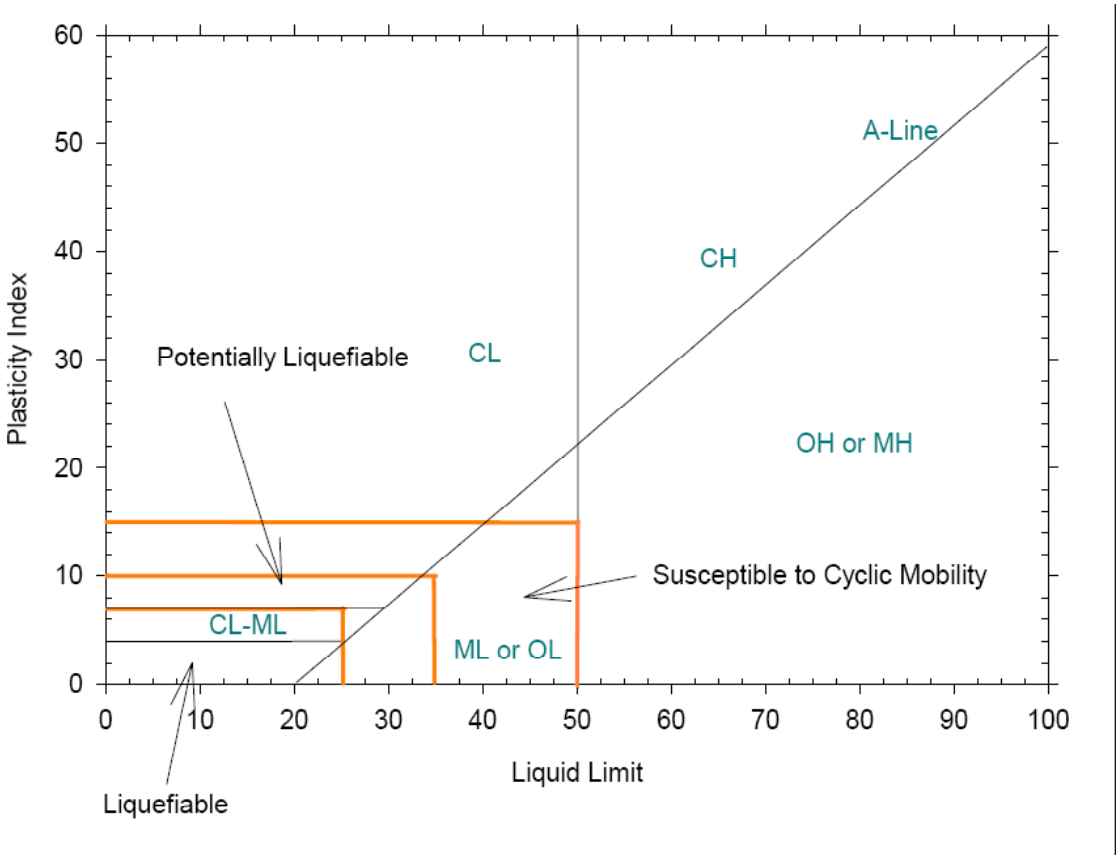

Figure 1.4 Polito and Martin (2001) liquefaction screening criteria.

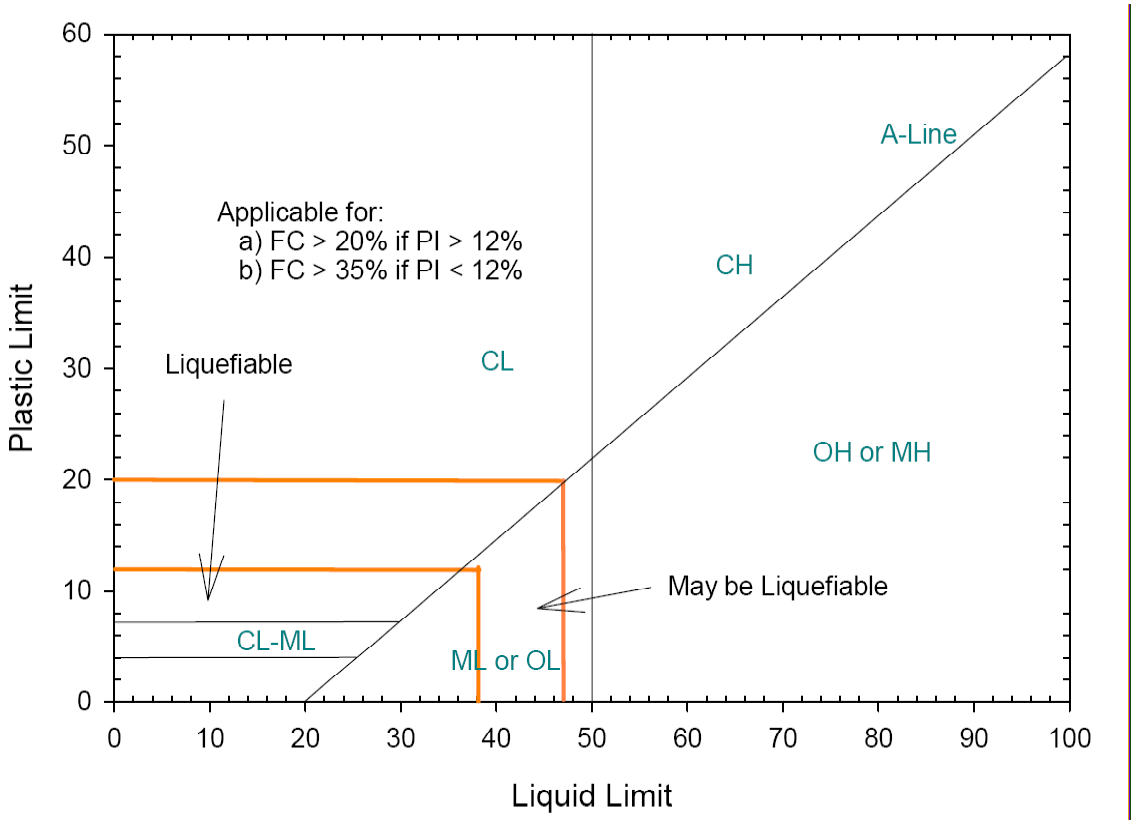

Figure 1.5 Seed et al. (2003) liquefaction screening criteria.

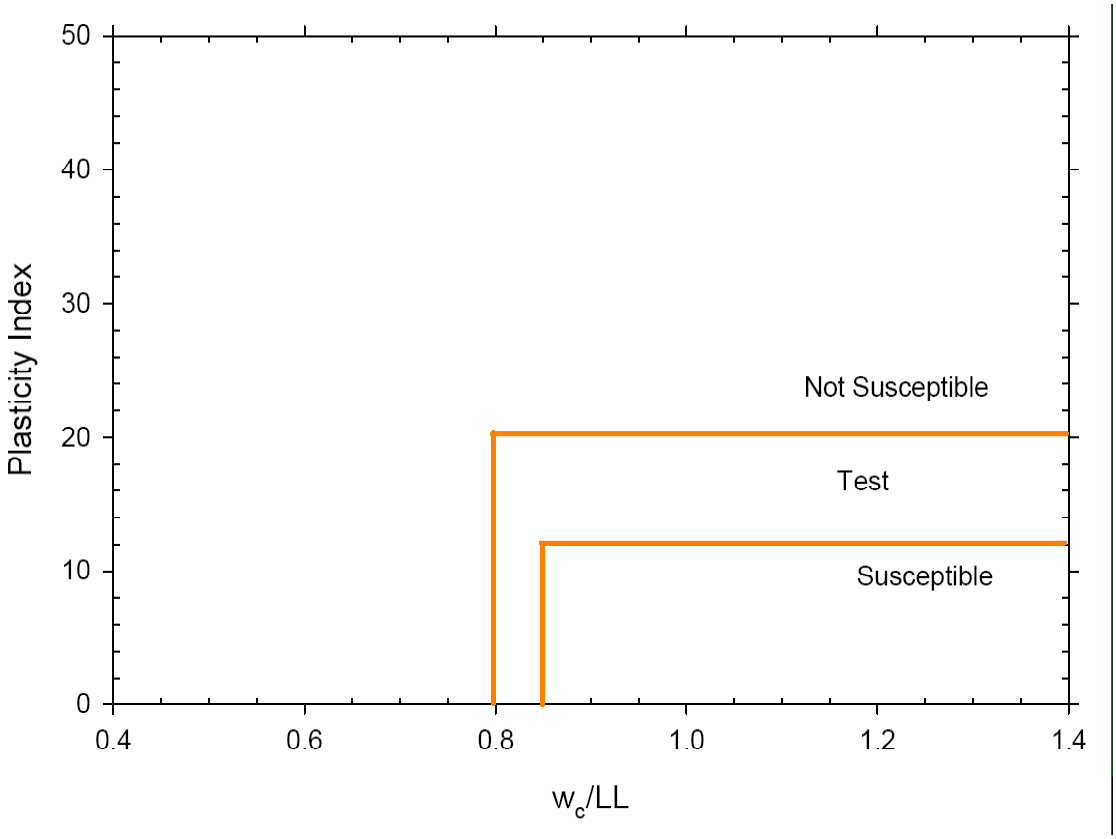

Figure 1.6 Bray and Sancio (2004a) liquefaction screening criteria.

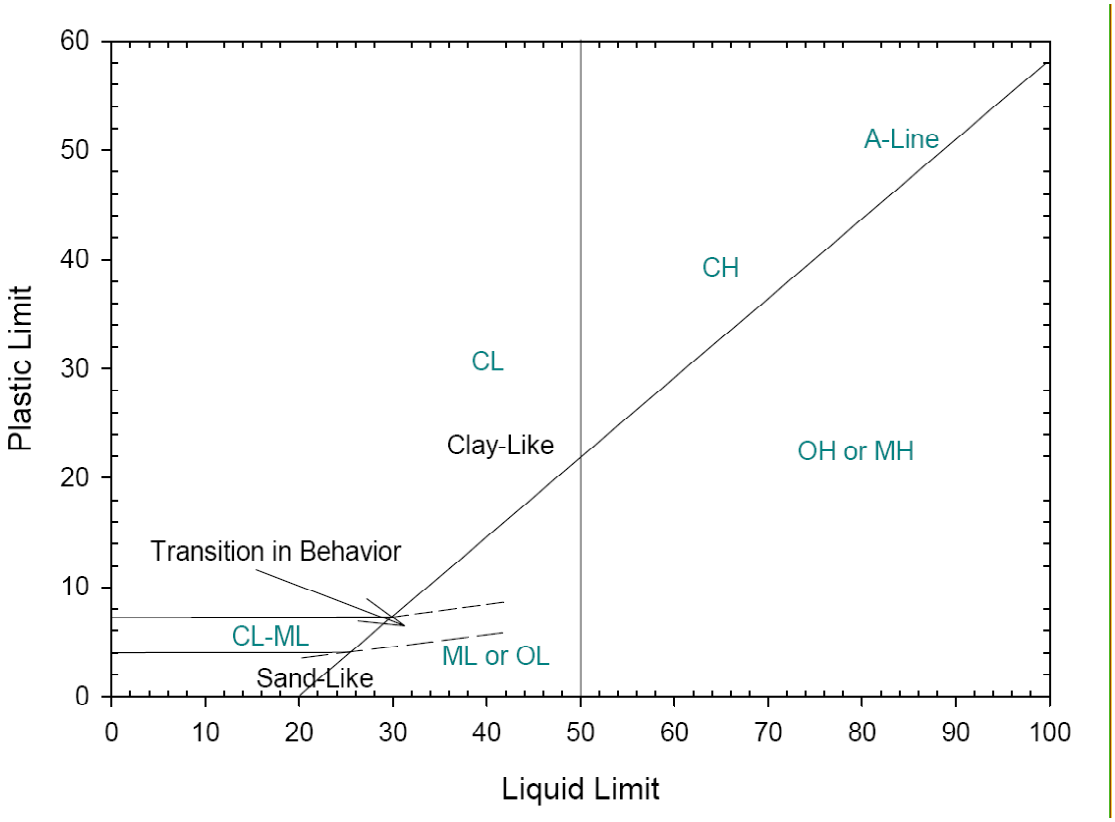

Figure 1.7 Boulanger and Idriss (2004, 2006) liquefaction screening criteria.

Chapter 2 ADAPAZARI FINE-GRAINED SOILS

2.1 General Discussion of Adapazari Soils

Over 402 individual samples were returned from Adapazari, Turkey following an on-site investigation by Sancio (2003). The samples originated from core samples taken from seven sites. Each sample was cataloged according to the following:

- location in Adapazari,
- section of the core,
- depth,
- PI,
- water content,
- liquid limit,
- fines content,
- amount passing 2μm,
- amount passing 5μm, and
- weight.

Using the database of cataloged materials, the samples were divided into seven batches, based on Plasticity Index (PI), Liquid Limit (LL), Fines Content, and particles finer than 5 μm and 2μm. Atterberg Limits tests were performed on each batch and the results are shown in Table 2.1

Table 2.1 Index Properties of Soils A through G

Soil Nomenclature	Plasticity Index	Liquid Limit	Plastic Limit	Unified Soil Classification
A	2	31	29	ML
B	5	32	27	ML
C	5	32	27	ML
D	11	38	27	ML
E	14	39	25	CL
F	7	28	21	CL-ML
G	10	31	21	CL

The samples brought back from Adapazari had been oven dried after testing by Sancio (2003). The batched soils were first put through a grinder with an aperture large enough to not break or crush the sand and silt particles, but small enough to reduce the oven-dried samples to a dry powder. The dry material was then mixed with tap water to bring the water content up to the initial bulking water content, or approximately 12%. This water content is sufficient to hold fines in place and decrease segregation through gravitational processes. The soils remained at this water content in air-proof containers until testing.

2.2 Results of Electron Microscope Analysis

Further analysis was performed by the Scan Electron Microscope at the University of California, Berkeley on the following soil with properties similar to Soil G (Table 2.1).

- Soil Sampled: A6-P5A, Depth: 3.9m, PI: 9, LL: 31, UCSC: CL, Fines Content ~80%

This soil was segregated into five categories: < 1 μm, < 2 μm, < 5 μm, and > 20 μm. This was done by placing a predetermined amount of material in a centrifuge and extracting the materials at precise times.

The photos from the Scan Electron Microscope show the diversity of materials within the silt. Figure 2.1 shows four photographs of particles less than 1 μm. Figure 2.1a and Figure 2.1b show the platy material within this batch. Figure 2.1c and Figure 2.1d show a piece of illite contained within the soil. Figure 2.2 shows a crystalline structure at different scales for material less than 2 μm, and Figure 2.3 shows the same crystalline structure as in Figure 2.2 for particles less than 5 μm. The particles larger than 20 μm demonstrate an even wider array of particle types, shapes, and sizes. Figure 2.4a, for example, shows two interesting objects, a cube near the top left corner and a spherical "brain" shaped particle near the bottom center of the photo. A close-up of the "brain" shaped object in Figure 2.4b reveals a complex crystalline structure. A multi-layered "baklava" shaped platy silt particle is displayed in Figure 1.4c, and two more objects of interest are shown in Figure 1.4d. The first object is the long thin particle, believed to be naturally occurring asbestos. The other object is a perfectly hexagonal particle of unknown origin appearing in the middle of the photograph.

Chapters 3 and 4 explain the difficulties in de-airing the soils. Judging by the photos of the particles in the soil, it is easy to see how air can be trapped within the platy and layered materials.

2.3 Results of X-ray Diffraction

To better understand the mineralogy of the Adapazari soils, three representative soils were sent to Willamette Geological Service in Philomath, OR for X-Ray Diffraction. This service provided the data that formed the basis of the description of soil mineralogy presented below. Each was taken from a unique location and depth. Information about each soil is given below:

- Soil 1: C10-P3A, Depth: 2.3m, PI: 19, LL: 47, UCSC: ML, Fines Content ~100%
- Soil 2: D4-P2B, Depth: 2.0m, PI: 11, LL: 33, UCSC: CL, Fines Content ~ 80%
- Soil 3: F9-P2A, Depth: 1.8m, PI: ~ 0, LL: 29, UCSC: ML, Fines Content ~ 80%

The three soils appear to be genetically related, stemming from similar parent materials. The clay mineral assemblage of the soils includes smectite (or highly expandable randomly interstratified illite/smectite, 80-90% expandable layers), chlorite (intermediate Fe-Mg composition), illite (muscovite in the coarser fractions), and kaolinite (increasing disorder with decreasing particle size). Smectite is the dominant component of the finest clay fraction, but illite is the most abundant clay in the coarser clays.

These soils appear to derive from parent material containing moderately calcic plagioclase, hornblende or amphibole, K-feldspar, quartz, calcite, and a mix of dolomite and ferroan dolomite (possibly as ferroan or as ankerite). Calcite is a major component of the category < 15μm to 2 μm and is present in lesser amounts in the < 2 μm and < 0.5 μm fractions. It is a trace component or absent in the < 0.2 μm clays. The calcite component could be pedogenic, although much of the pedogenic carbonate is very micritic and tends be observed in the finer soil size fractions. The presence of dolomite suggests possible detrital carbonates, although there is the possibility of ankerite in paleosols as a pedogenic phase. In each case, the < 0.2 μm clays are approximately 85% smectite, 10% illite, and 5% other clays (chlorite and kaolinite), with only traces of quartz and calcite.

The mineralogy at 15 to 2 microns, 2 to 0.5 microns, 0.5 to 0.2 microns, and less than 0.2 microns for each of the three soils can be found in Figure 2.5 (Soil 1), Figure 2.6 (Soil 2), and Figure 2.7 (Soil 3). The differences in mineralogy between the three soils is compared for each of the divisions in grain size in Figure 2.8.

2.4 Summary

Of the hundreds of samples brought back from Adapazari, seven representative soil batches were created to use in the exploration of liquefaction resistance and susceptibility. Atterberg Limits tests, Scan Electron Microscope (SEM), and X-ray Diffraction provide a more complete understanding of the composition of the Adapazari soils. From SEM, the diversity and complexity of the soils can be appreciated. The mineralogy of soils taken from different areas within Adapazari suggests that they are genetically related, stemming from similar parent materials. These results provide significant indicators on the micro-scale level that may be used in screening for liquefaction susceptibility.

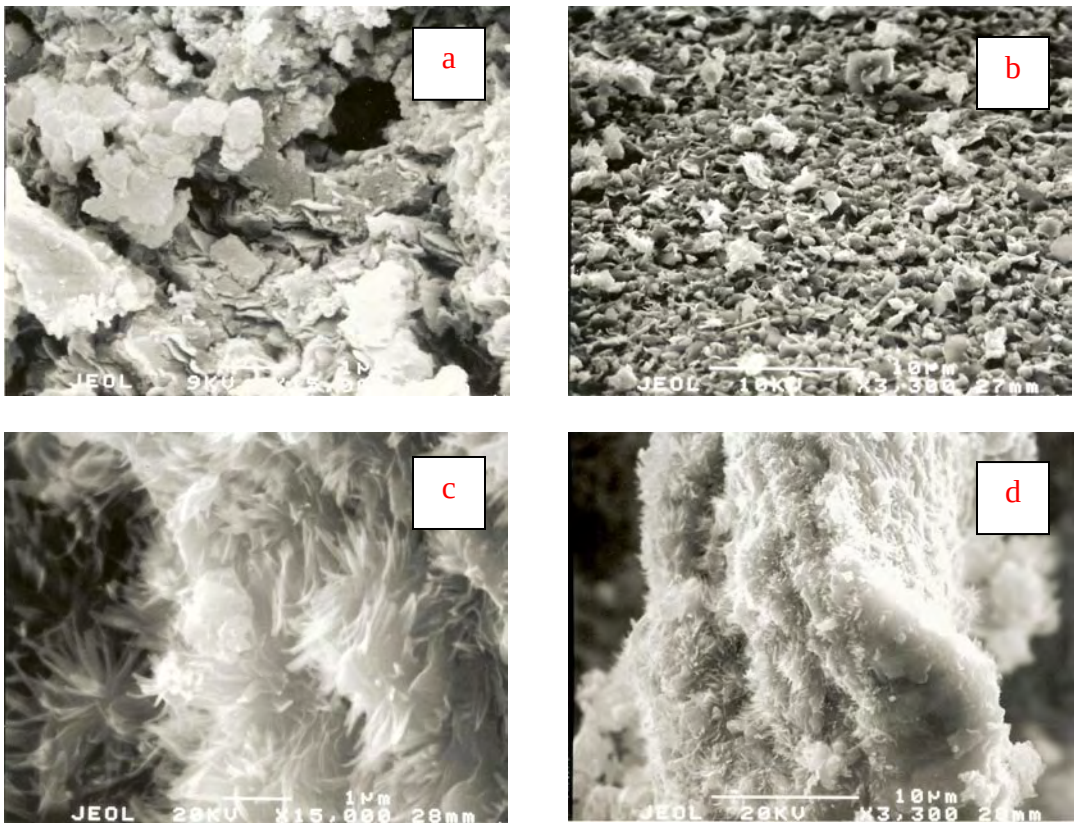

Figure 2.1 Representative photos of particles ≤ 1 micron: a) platy materials at 15,000x zoom, b) material surface at 3,300x zoom, c) illite at 15,000x zoom, and d) illite shown at 3,300x zoom.

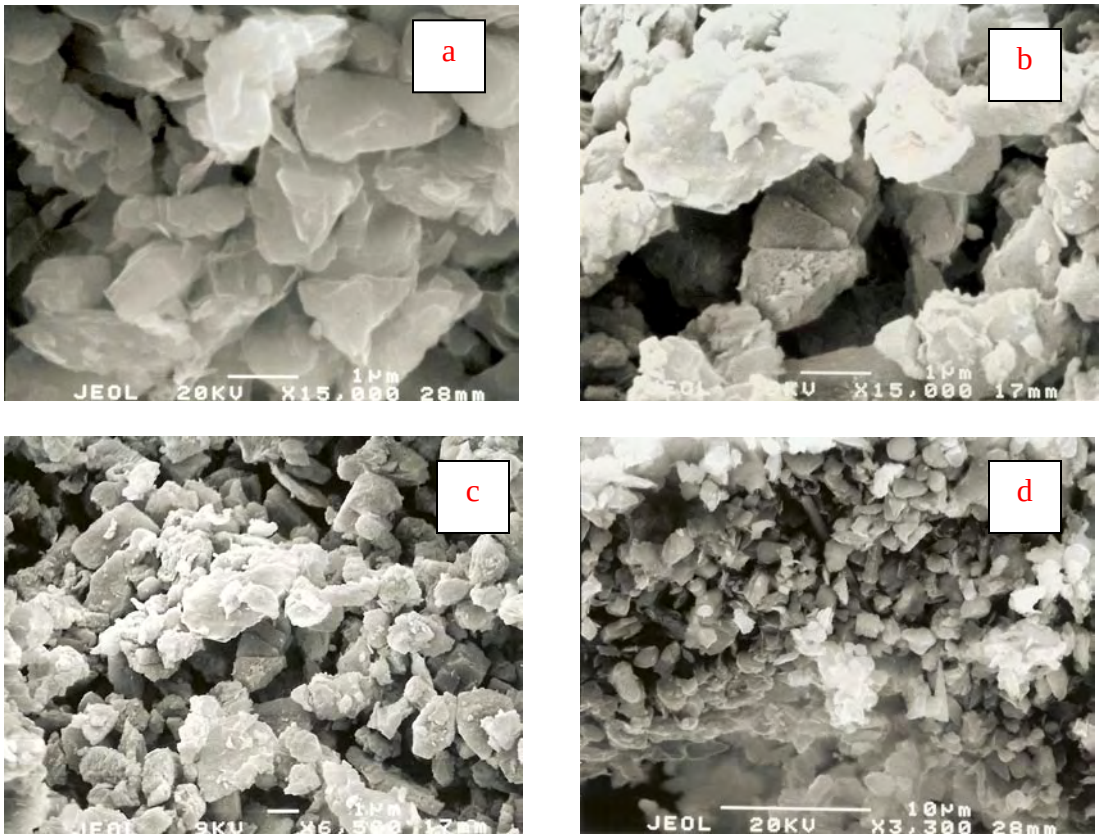

Figure 2.2 Representative photos of particles ≤ 2 microns: a) Crystalline structure at 15,000x zoom b) Similar crystalline structure at 15,000x zoom c) Overview of silt structure at 6,500x zoom, and d) Conglomerate structure at 3,300x zoom.

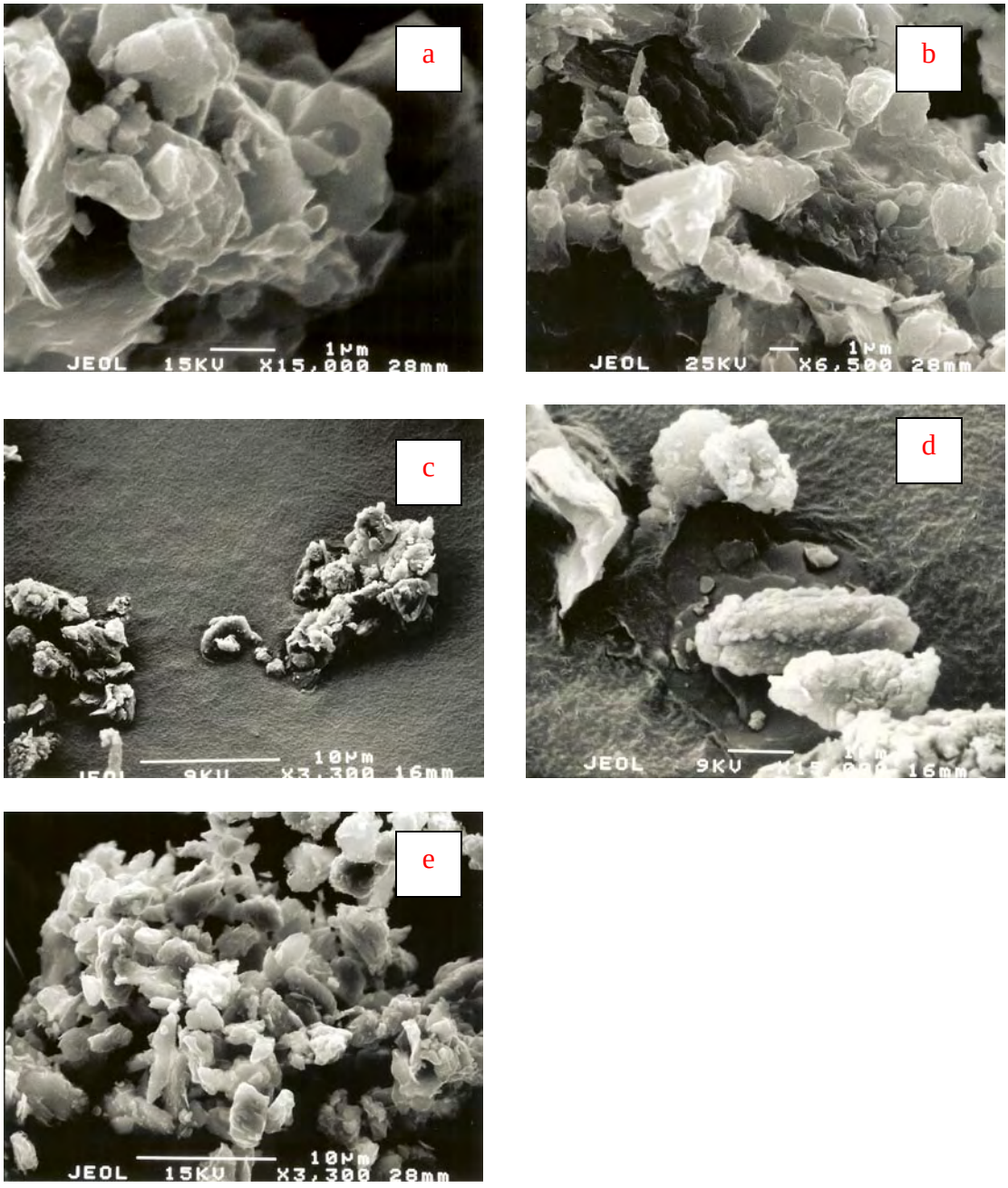

Figure 2.3 Representative photos of particles ≤ 5 microns: a) Texture of silt at 15,000x zoom, b) Flaky texture at 6,500x zoom c) representative pieces of 5- micron at 15,000x zoom, and d) Contrasting representative pieces at 3,300x zoom e) Crystalline structure at 3,300x zoom.

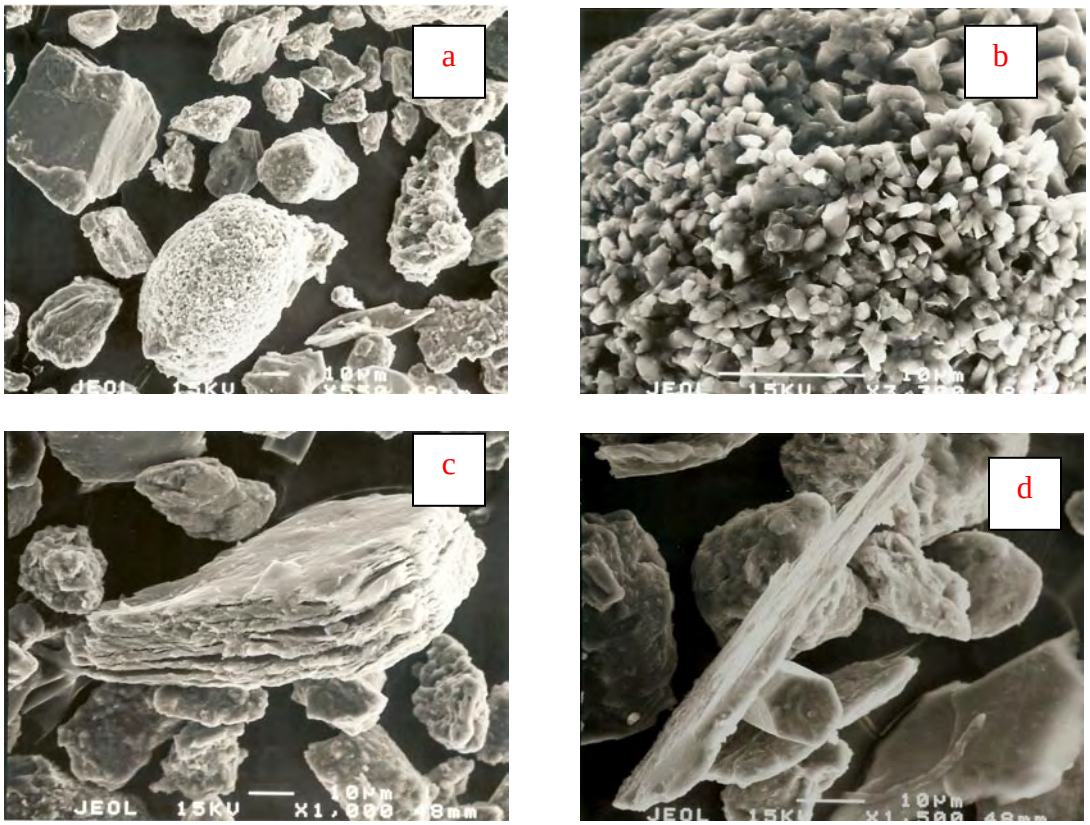

Figure 2.4 Representative photos of particles ≥ 20 microns: a) Two interesting element, one brain-like, the other cubical at 550x zoom, b) close-up of brain-like element at 3,300x zoom, c) platy material at 1,000x zoom, and d) hexagonal element at 1,500x zoom.

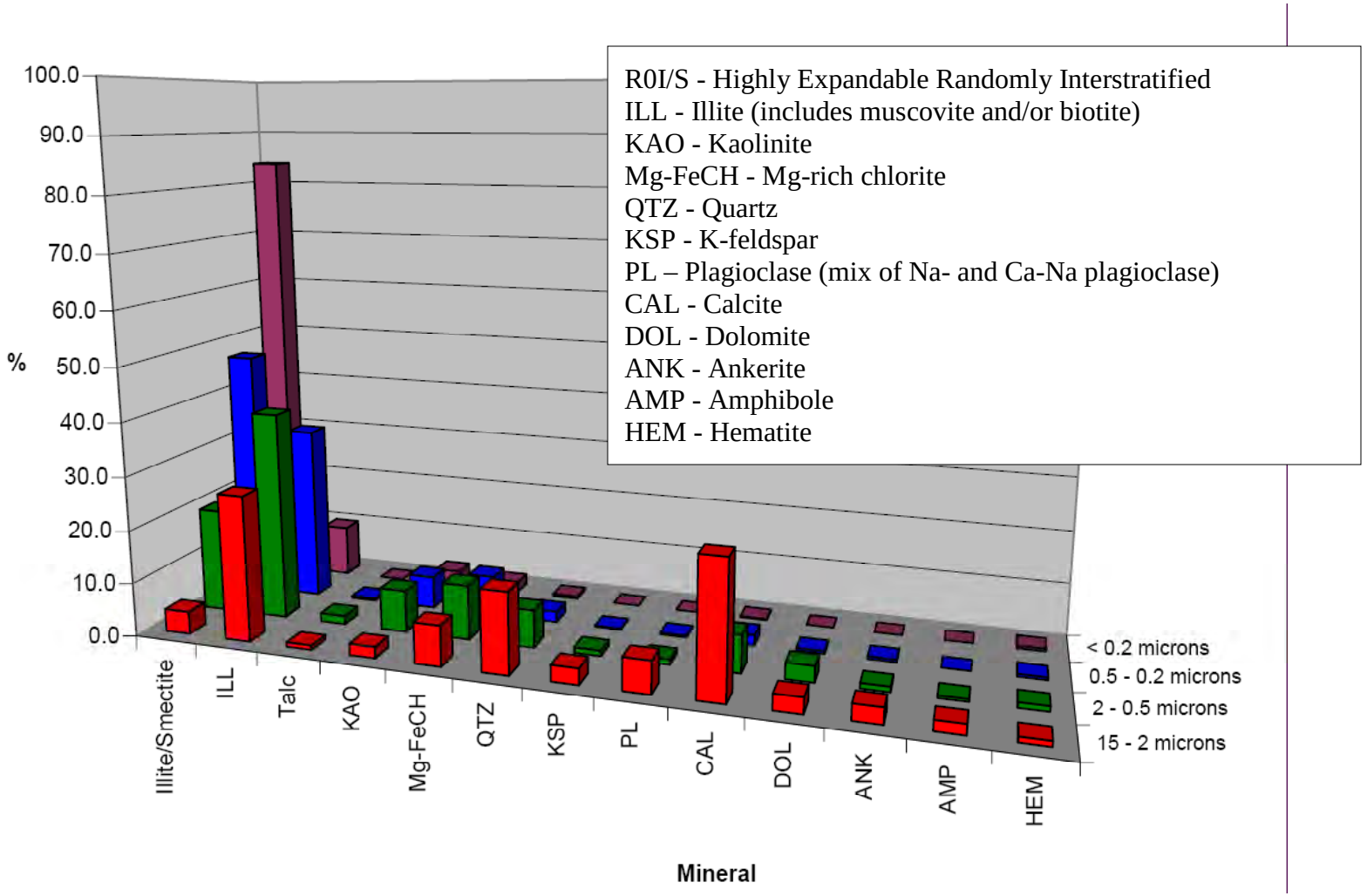

Figure 2.5 Mineral Interpretation for Sample 1 = C10-P3A-M, Depth = 2.3m, PI = 19, LL = 47, USCS = ML, Fines Content ~100% segregated into four sizes (from Willamette Geological Services Report, 2005).

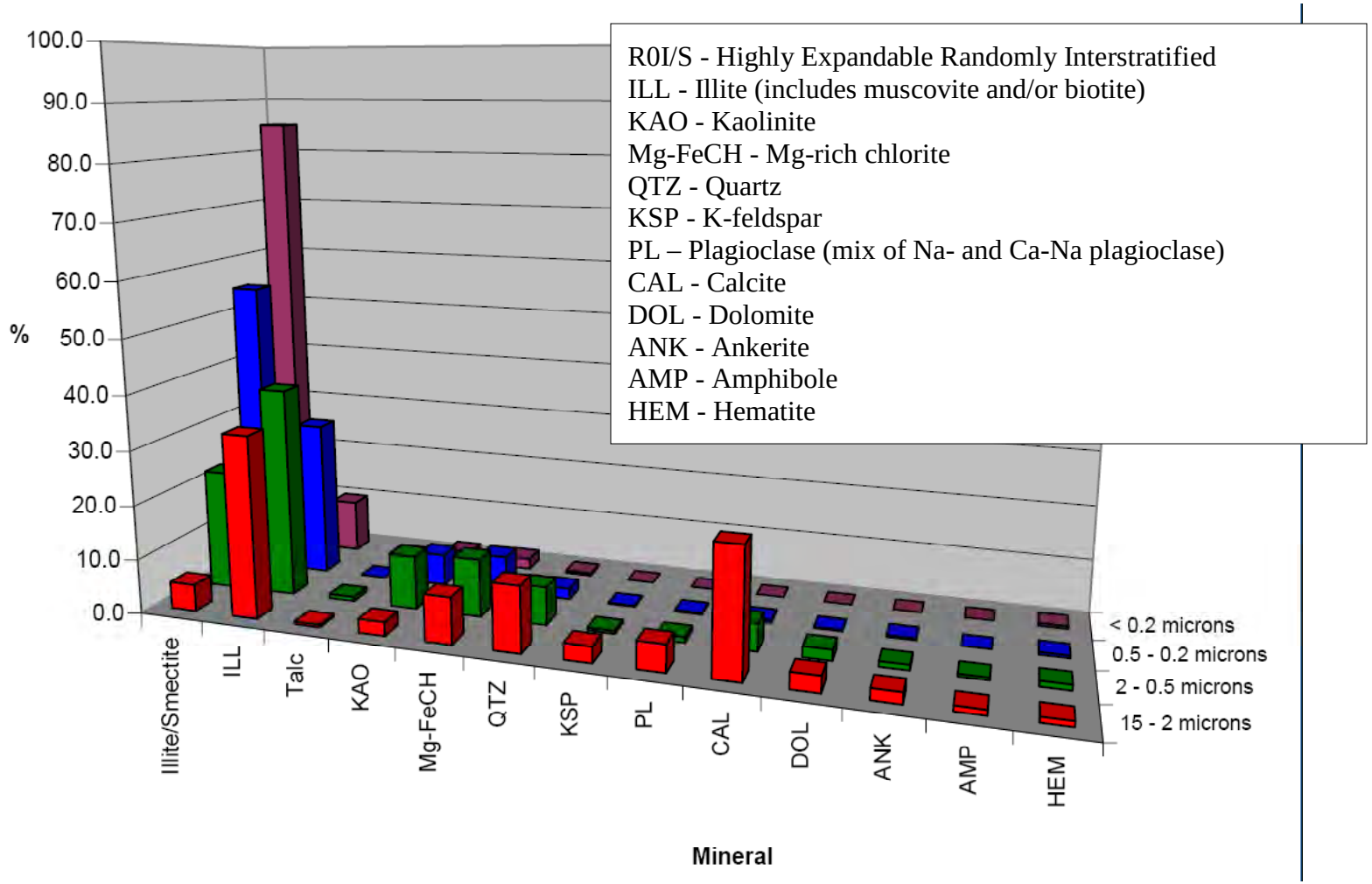

Figure 2.6 Mineral Interpretation for Sample 2 = D4-P2B-B, Depth = 2m, PI = 11, LL = 33, USCS = CL, Fines Content = 84% segregated into four sizes (from Willamette Geological Services Report, 2005).

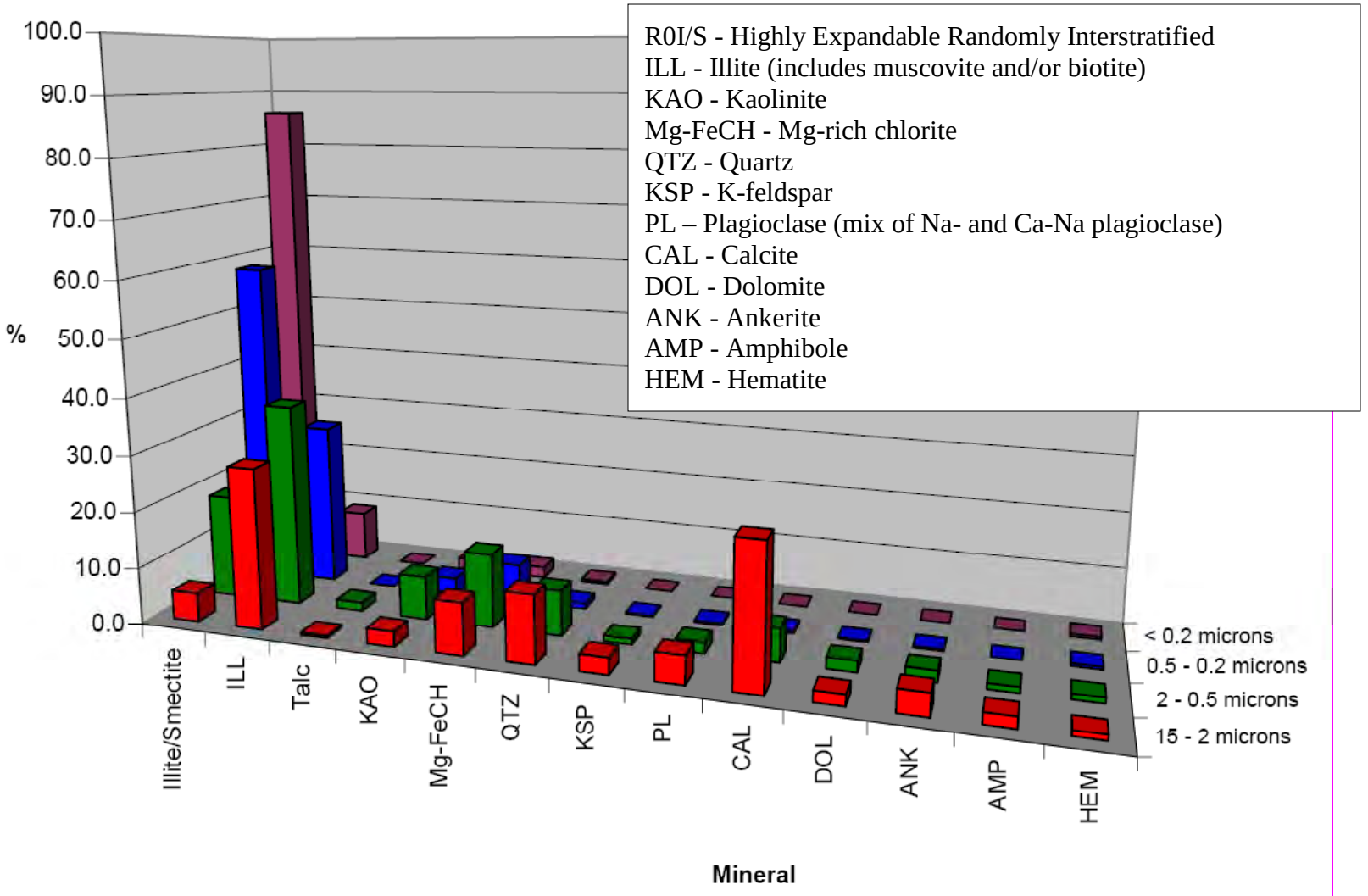

Figure 2.7 Mineral Interpretation for Sample 3 = F9-P2A-T, Depth = 1.8m, PI = ~0, LL = 29, USCS = ML, Fines Content = 81% segregated into four sizes (from Willamette Geological Services Report, 2005).

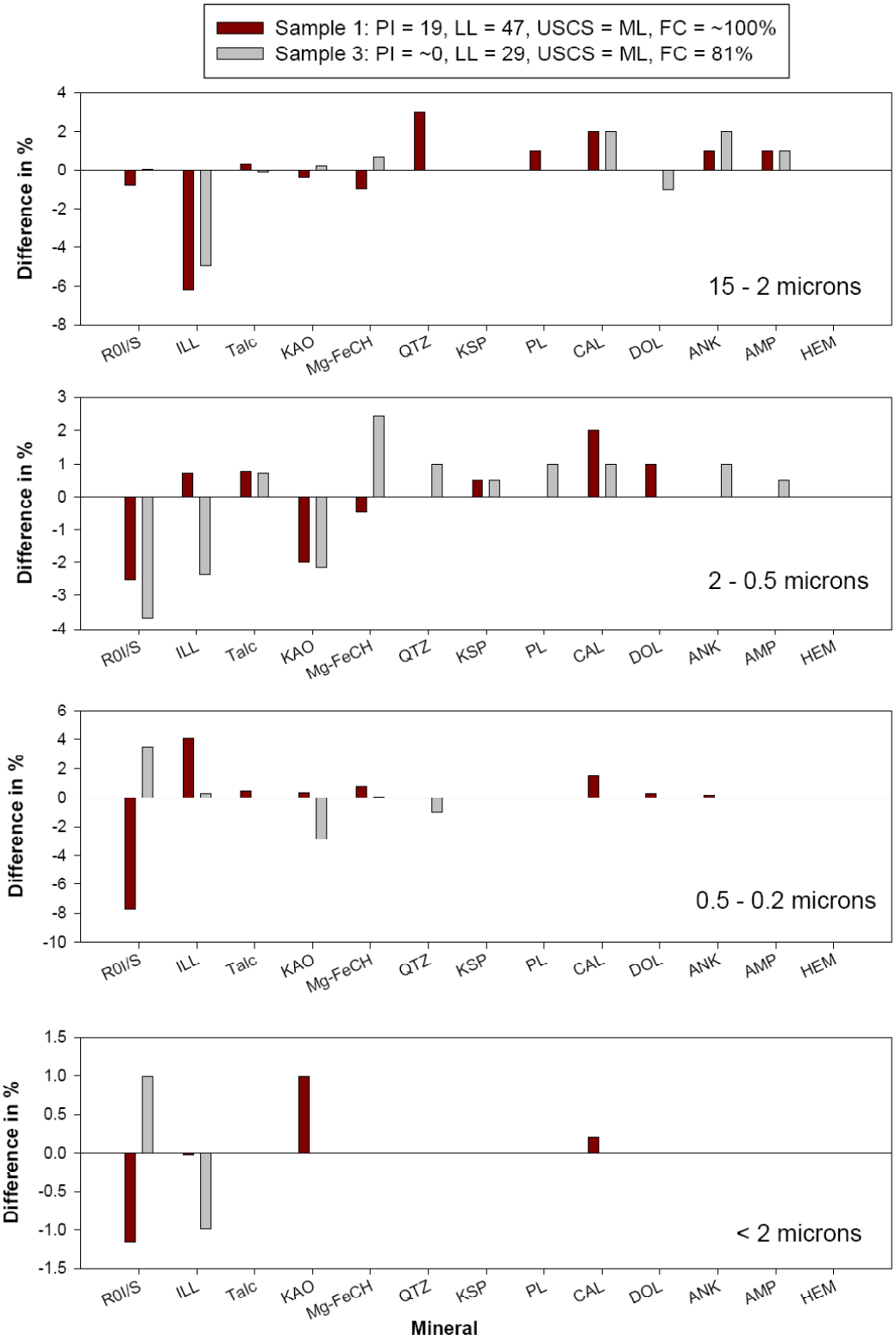

Figure 2.8 Difference charts for mineralogy, percentage of difference in each mineral for Soil 1 and 3 compared to Soil 2: PI = 11, LL = 33, USCS = CL, FC = 84%.

Chapter 3 SPECIMEN PREPARATION METHOD FOR RECONSTITUTED FINE-GRAINED SOIL SPECIMENS

3.1 Introduction

For decades, researchers have relied on reconstituting specimens in order to replicate in situ deposits and develop conclusions on the static and cyclic response of a soil. Field samples, on the other hand, are ideal for gaining information about the likely response of a specific location and soil. The static and cyclic responses of a natural soil are complicated by variability and natural, inherent imperfections. (An example of an imperfection is a sand seam within a mostly clay sample.) While imperfections of real soils are difficult to duplicate, the techniques for reconstituting a natural fabric has made major advancements over the past decade, especially for fine-grained soils. When properly prepared, reconstituted specimens have the advantage of behaving nearly identically. This assures high quality, reliable data for comparing various testing conditions.

Previous research on reconstituted soils has primarily concentrated on sands and clays. Sand specimens are typically easy to construct and can be made to replicate natural soil fabrics (Boulanger, 1990; Kammerer, 2002; and Wu, 2002), although the method of reconstitution can affect the cyclic and static response (Mulilis et al., 1977; Vaid and Sivathayalan, 2000). Reconstitution of fine-grained soils, both plastic and non-plastic, has only recently been investigated because of the complexity of the natural fabric (Zdravkovic, 1996; Wijewickreme and Sanin, 2004).

The fine-grained soils collected in Adapazari, Turkey, as described in Chapter 2, were reconstituted and tested both monotonically and cyclically (Chapter 5 and 6, respectively) to assess the static and cyclic strength. In this chapter, the two methods used to reconstitute these specimens are discussed. A full description of the preparation of the triaxial and the simple shear specimens will be given for each method along with a discussion of the comparisons and contrasts drawn between them.

3.2 Approaches Considered and Selection of Reconstitution

One of the greatest challenges in this program of research was deciding what type of specimen preparation method to use. Several methods of reconstitution were considered:

- Moist Tamping,
- Wet Pluviation,
- Dry Pluviation,
- Slurry Deposition Method, and
- In-Place Wet Pluviation

Moist tamping was discarded because it does not produce specimens that are representative of a natural deposition process. It is also known that specimens prepared in this method can exhibit sharply defined boundaries between layers (Riemer, 1992).

Also discarded was traditional wet pluviation, which consists of pouring a thin slurry of material into a large tub of water and allowing natural sedimentation to occur. The material is then consolidated, cored and tested. This method has the advantage of forming the soil fabric most like that formed in situ by natural fluvial deposition, but it was not suitable to this testing program due to the lack of large quantities of available silt and the long time required to prepare each specimen. Dry pluviation was not utilized because the soils of Adapazari are deposited in a fluvial environment.

Only the Slurry Deposition Method and the In-Place Wet Pluviation Method proved to be useful in this testing program. The Slurry Deposition Method will be explained in detail in Section 3.3 and the In-Place Wet Pluviation Method in Section 3.4.

Inevitably, there are advantages and disadvantages associated with the use of each of the chosen reconstitution methods. Although the Slurry Deposition Method is a viable method that will produce repeatable, uniformly reconstituted specimens designed to isolate specific liquefaction characteristics, it is not representative of a natural deposition process. Conversely, the In-Place Wet Pluviation Method does produce soil fabric that is more representative of a naturally occurring soil, but it is arguable that the inhomogeneities within the specimen may control the response.

The specimen preparation techniques described below were developed after an extensive and exhaustive process of trial and error. The weights and applied pressures produce the optimum conditions for consolidation and consistent void ratios for the soils tested within this program.

3.3 The Slurry Deposition Method for Silty Soils

The primary purpose of the Slurry Deposition Method is to produce uniformly reconstituted specimens that minimize the significant inherent variability found in naturally deposited soils. Such specimens can then be tested in a systematic and controlled manner so that specific liquefaction characteristics can be isolated and evaluated.

To date, most Slurry specimen reconstitution has been performed on sands and silty-sands. The most common technique was developed by Kuerbis and Vaid (1988), and it has been proven to produce uniform, non-segregated samples. The key feature of this method is that soil and de-aired water are combined to form a thick slurry directly within the triaxial mold, and the mold is "vigorously rotated" until the slurry is thoroughly mixed. With a sandy material, this process ensures a homogeneous material.

When applying this method to a silty material, a homogeneous specimen is unattainable. During the mixing phase, the thick slurry of silt does not blend properly because the reduced permeability prohibits movement of the water and fine particles. In order to achieve a homogeneous specimen during the mixing phase, the slurry requires substantially more water.

At this point, the Kuerbis and Vaid (1988) slurry reconstitution method is rendered useless because of the resulting segregation in particle sizes. The particles within the thinner slurry will begin to settle out of suspension due to gravitational processes as soon as the mixing is completed.

Zdravkovic (1996) developed a method of reconstituting silts for use in a cyclic torsional shear device. This method was adopted and modified as described below for the development of specimens for the triaxial and simple shear devices.

3.3.1 Specimen Homogeneity

For this study, it was imperative to prove that the Slurry Deposition Method could be used to create consistent, homogeneous specimens. For this, a triaxial specimen 13 cm in height was prepared, initially consolidated, then subjected to water content and gradation analysis. Water contents from six places within the specimen yielded an average of 28.1% with a standard deviation of 0.11. To perform the gradation testing, the same specimen was divided into 3 parts: top, middle, and bottom, and a control batch of silt still in slurry form was used. These three sections and the control batch were subjected to hydrometer testing and sieve analysis. The results are compared in Figure 3.1. All four gradation lines lie on top of each other. These results strongly suggest that a specimen can be prepared that is homogeneous and that consistency between specimens is possible.

A visual inspection of a simple shear specimen was also performed. The specimen was prepared using the Slurry Deposition Method, oven dried and then cut in half. As seen from Figure 3.2, the specimen does not exhibit segregation or layering.

3.3.2 Specimen Preparation for Triaxial Testing

All triaxial specimens, both monotonic and cyclic, were prepared using the Slurry Deposition Method. The method appears complex with many steps, but is rather simple once understood.

To prepare a Slurry Deposition Method triaxial specimen the following are required:

1. Triaxial Cell,
2. End Caps for Sample:
    a. Bottom end cap with a diameter of 70.9 mm with an embedded bronze porous disk
    b. Top end cap with a diameter of 70.0 mm, and a height of 37.4 mm with an embedded bronze porous disk
3. 2 Porous Stones:
    a. The bottom porous stone should be the same diameter as the bottom end cap
    b. The top porous stone should be slightly smaller in diameter than the inner diameter of the triaxial mold
4. Non-reinforced Membrane,
5. 3 O-rings:
    a. 2 to fit snuggly on bottom and top caps
    b. 1 large enough to fit over triaxial mold
6. Triaxial Mold,
7. Vacuum Container,

8. Non-reinforced membrane cut to half the normal height,
9. Vacuum Chamber,
10. Vacuum Regulator,
11. Loading Rod,
12. Additional End Cap, and
13. Approximately 6 kg Free Weights

Step 1: Mold-Assembly Preparation

To assemble the triaxial cell and mold, first attach the bottom cap to the triaxial cell and place the bottom porous stone on top of the cap. Although the end cap contains a bronze porous disk, the porous stone acts as an additional filter for the fines in the slurry. Place the membrane around the bottom end cap and seal with an O-ring. Finally, place the triaxial mold over the end cap-membrane assembly, ensuring a proper seal with the bottom O-ring. Attach the vacuum lines of the mold to the house vacuum and fold the top of the membrane over the top edge of the mold. Ensure the membrane is stretched taut against the mold to achieve a proper fit and good seal.

Step 2: Soil Preparation

In Chapter 2, the batching of the soil was described and soil batches were brought up to a water content of 12%. This water content is sufficient to hold fines in place while preventing segregation of particles through gravitational processes.

De-aired water is added to approximately 800g (dry weight) of the batched soil to bring the soil up to a water content of approximately 45%. At this water content, the material is a thick slurry with the consistency of pudding, and it is of optimum workability. Transfer the slurry into a vacuum container for additional de-airing. A photograph of the vacuum container used in this study is shown in Figure 3.3. This specially made vacuum container[1] measures 12 inches in height and 4 inches in diameter. The lid seals to the container with a rubber gasket. Apply up to 1 atm (100 kPa) of vacuum to the contents of the container for de-airing purposes. As described above, the soil is initially mixed with de-aired water, but air adheres to the silt during the grinding, batching, and mixing processes, and must be removed.

When the slurry is placed within the container and the vacuum is raised to 1 atm, the slurry violently bubbles as air is pulled from the material. As more air is pulled from the slurry, the rate of bubbling slows. Once the bubbling stops, reduce and remove the vacuum and mix the contents with a long-handled spatula. Mixing is performed to move the slurry material on the bottom of the container closer to the top where it is available to release air. Typically, 5 cycles of vacuuming and stirring are necessary for the triaxial Slurry specimens. By the fifth cycle, relatively no bubbling occurs when the vacuum is applied. This signifies that the material is sufficiently de-aired and ready for the next step.

[1] During the initial testing of the triaxial specimens, even after backpressure saturation, the highest B-value attainable was 0.4 and the cell pressure and backpressure reached the limitations of the triaxial machine. Differential vacuuming was also tried with limited success. The resulting B-values were too low and the specimens could not be tested under saturated conditions. The vacuum container was improvised at this point.

Step 3: Initial Consolidation

With the triaxial mold assembled, transfer the slurry material into the mold, ensuring no air pockets are formed during placement. Set the top porous stone on top of the slurry mixture. Make sure the porous stone can move easily within the mold, then place the top cap on the porous stone. Place the half membrane over the top cap and triaxial mold in order to form a collar. Secure the bottom of the half membrane to the exterior of the mold with a large O-ring. Secure the top of the half membrane to the top cap with the last O-ring. Finally, attach the top drain line of the triaxial cell to the top cap.

The specimen is now ready for initial consolidation. Connect the vacuum regulator to the house vacuum and set to 5 in-Hg (18 kPa). Attach the vacuum chamber to both the regulator and triaxial cell. Slowly open the valves to the specimen, applying 18 kPa to the specimen. If there is a proper seal around the collar, no air bubbles will appear in the vacuum chamber and the collar will adhere to the top cap. Insert the loading rod into the top cap and place the triaxial cell cap over the loading rod. This is done to ensure the top cap remains level during consolidation. Attach the extra top cap to the end of the loading rod. This extra top cap will act as a platform for the free weights. Slowly add up to 6 kg, or 15 kPa, of vertical load. If the vertical load is not added, the internal vacuum will overcome the vacuum supplied by the mold, and the membrane will adhere to the material. This will cause to the specimen to "hourglass," or cause a global decrease in the diameter as the material consolidates. By adding the vertical load, the material will consolidate vertically, and the diameter will remain constant. The low pressure of the vacuum chamber and the vertical load on the specimen can easily be erased during consolidation to the testing effective stress level.

If the top cap and porous stone have been properly seated and the half membrane collar holds a vacuum, the top cap should slowly depress into the mold, dragging the collar down with it. Make sure the O-ring on the top cap is high enough so that it will not inhibit the sliding of the top cap into the mold. The whole assembly is shown in Figure 3.4.

Step 4: Assembly Completion

For the soil tested in this study, the triaxial specimens required consolidation for at least 48 hours; however, 72 hours of consolidation was preferred. After the initial consolidation is complete, remove the weights, extra top cap, loading rod, and triaxial cell cap. Carefully remove the O-ring from the top cap and slide down the drain line. At no time should the drain line be disconnected. Remove the large O-ring from the mold and slide down the drain line. Fold both the collar and membrane over the top cap and ensure there are no wrinkles. Slide the top cap sized O-ring up the drain line to the top cap and over all layers of the collar and membrane. It is essential to have a good seal on the sample. Finally, detach the vacuum lines to the mold and disassemble. It is important to record the change in height of the specimen at each stage of the preparation method.

Using this series of steps, and allowing the specimen to consolidate for three days, yields a specimen that is able to stand erect from what was once a slurry. A photograph of the triaxial specimen prepared by the Slurry Deposition Method is shown in Figure 3.5 and a schematic is presented in Figure 3.6.

The specimen may now be prepared for either monotonic or cyclic testing. Place the triaxial cell chamber over the specimen, reinsert the loading rod, and attach the triaxial cell cap. Fill the chamber with de-aired water in preparation for testing. Testing methods are discussed in Chapter 4.

3.3.3 Specimen Preparation for Simple Shear

The preparation technique for simple shear specimens is less complex than for triaxial specimens. While the triaxial Slurry Deposition Method requires 3 days of preparation to produce a specimen, a simple shear Slurry Deposition Method specimen can be prepared within hours.

To prepare a Slurry Deposition Method simple shear specimen the following are required:

1. End Caps for Sample. Caps have a diameter of 10 cm with built-in porous stones, shown in Figure 3.7,
2. Wire-Reinforced Membrane,
3. 2 Pieces of Filter Paper, 10 cm in diameter,
4. 4 O-rings:
    a. 2 O-rings to fit on bottom and top caps
    b. 2 large, flexible O-rings to fit over simple shear mold
5. Simple Shear Mold,
6. Vacuum Container,
7. Short, non-reinforced membrane. Diameter must be large enough to fit over the simple shear mold,
8. Vacuum Chamber,
9. Vacuum Regulator,
10. 2 Hose Clamps,
11. High Strength Rubber Bands, and
12. 4 kg of Free Weight.

Step 1: Mold-Assembly Preparation

Prior to sample preparation, saturate the top and bottom caps by flowing de-aired water through the porous stones, and check the membrane for leaks or holes. Placed the bottom cap on a level surface and pull the wire-reinforced membrane over the sides of the cap. The bottom edge of the wire reinforcement should be within a few millimeters of the O-ring grove on the cap. Ensure the wire-reinforcement is horizontal and not at an angle. The use of wire-reinforced membranes is further discussed in Section 4.5 of the next chapter.

Place the bottom cap O-ring in the O-ring groove to secure the membrane, and place a piece of filter paper over the embedded porous stone. The filter paper gives an extra layer of protection against the loss of fines. Assemble the mold around the bottom cap and membrane assembly. Fold the top of the membrane over the mold.

Step 2: Soil Preparation

Place 250g (dry weight) of soil directly into the vacuum container and add de-aired water to bring the material up to a water content of approximately 45%. Mix well. Because the mass of

soil for the cyclic simple shear is less than the mass of soil for triaxial test preparation, typically only three cycles of vacuuming and stirring are required. Once the slurry no longer releases air bubbles after a stirring cycle, it is sufficiently de-aired and ready to be transferred. Place the slurry inside the simple shear mold, ensuring no air pockets are formed during placement.

Step 3: Initial Consolidation and Assembly Completion

Place the second piece of filter paper on top of the slurry mixture. Seat the top cap on the filter paper, checking that the entire assembly is level. Place the flexible membrane over the top cap and simple shear mold to create a collar. Use the larger O-rings to seal the collar by placing one over the membrane on the mold and the other on the membrane in the O-ring grove of the top cap. It is useful at this time to place a dial gauge on the top cap. This is done to measure the height of the assembly and determine when primary consolidation is complete. Connect the vacuum regulator to the house vacuum and set it to 4 in-Hg (13 kPa). Attach the vacuum chamber to the regulator and to the top and bottom drain lines of the assembly. Slowly apply 13 kPa of vacuum to the specimen. If there is a proper seal around the collar, no air bubbles will form in the vacuum chamber and the collar will adhere to the top cap.

The top cap will begin to settle into the simple shear mold as the material consolidates. At all times, take care to ensure the top cap remains level. Once primary consolidation ends, remove the collar and two larger O-rings. Unfold the reinforced membrane onto the top cap, and secure it with the top cap O-ring. During this procedure, the top drain line will need to be disconnected to fit the final O-ring in place. Do this as quickly as possible and reattach the top drain line.

In many cases, there is a gap between the wire-reinforced portion of the membrane and the O-rings on the top and bottom caps. A gap of un-reinforced membrane will become a focal point for blistering and the development of holes during testing. The decreased lateral strength of the un-reinforced membrane cannot contain the high excess pore water pressures generated during testing. To remedy this, use high-tension rubber bands to cover any un-reinforced sections of the membrane. A photograph of a specimen with O-rings and rubber bands is shown in Figure 3.8.

Wu (2002), Kammerer (2002) and Anantanavanich (2006) found that in tests with effective overburden stresses greater than or equal to 80 kPa, hose clamps are needed to secure the O-rings in place. This avoids the risk of leakage caused by elevated excess pore water pressures during testing. After placing the rubber bands, attach the hose clamps over the O-rings.

If the O-rings, rubber bands, and hose clamps are properly placed, no air bubbles will form in the vacuum chamber. The simple shear mold can now be removed and the specimen height should be taken.

When the specimen is placed within the simple shear device, as described in Chapter 4, the top platen is bolted onto the top cap. This platen weighs 4 kg. To ensure the proper height for testing, apply 4 kg of free weight to the specimen after the mold has been removed. The 4 kg will cause consolidation and the final height should be taken after the end of primary consolidation. The specimen is now ready to be placed in the simple shear device for monotonic or cyclic testing.

3.4 The In-Place Wet Pluviation Method for Silty Soils

As previously mentioned, traditional wet pluviation is performed in a large tank with large quantities of soil. Because large quantities of the batched soils were not available, an alternative approach was developed in which the soils for each specimen were pluviated directly into the mold. This was accomplished by pouring the silt through a column of water directly into the simple shear mold and allowing it to settle naturally, in a sequence of multiple layers, or lifts. This method is similar to traditional wet pluviation and is intended to produce higher void ratios, lower densities, and a higher water content to liquid limit ratio (w_c/LL), in order to better represent the in situ state of the soils of Adapazari, Turkey. To date, no other researchers have used this method for wet pluviation of fine-grained soils to reconstitute specimens for such testing.

3.4.1 Specimen Layering and Heterogeneity

The main advantage of the In-Place Wet Pluviation Method is that it produces a layered specimen, which is more typical of in situ soils. To demonstrate this, a grain size analysis was performed on the top and bottom sides of layers of an In-Place Wet Pluviation specimen after consolidation to σ'_m = 100 kPa. After isolating the top and bottom portions of the individual layers, the grain size analysis was conducted. More coarse material, by weight, was harvested than the fine material. The results of the grain size analysis for the bottom (coarse) and top (fine) layer portions compared to a thoroughly mixed sample of Soil G are shown in Figure 3.9 and in

Table 3.1.

There is a significant difference between the coarse material curve and fine material curve. The fine material has a much greater fines content (particles finer than 75 μm) and clay content (particle finer than 2 μm) than either the thoroughly mixed or coarse specimens. The thoroughly mixed specimen also has a higher percentage of fines and clay content than the coarse material.

Table 3.1 Grain Size analysis for fine and coarse-grained specimens from Soil G

Specimen	% of Particles < 75 μm	% of Particles < 2 μm	D_{10} (μm)	D_{30} (μm)	D_{60} (μm)	C_u	C_c
Fine Grained Material	93%	36%	-	1.24	8.57	-	-
Thoroughly Mixed Specimen	77%	15%	1.34	12.32	42.58	31.7	2.66
Coarse Grained Material	65%	11%	1.88	25.00	65.00	34.6	5.12

Fine materials do exist within the bottom, coarse-grained sample. One explanation may be that the fine materials were trapped under or within the coarse material during pluviation. As the slurry sedimented, finer particles within the slurry settled with the coarse material. Another explanation is that the specimens do not have discrete layering. These specimens represent

graded bedding commonly formed in nature. Except for the utmost top and bottom of a layer, where the finest and coarsest particles would be found, there should be a gradation, or transition in grain sizes.

An In-Place Wet Pluviation specimen was oven dried and cut in half along the diameter to perform a visual inspection. A photograph of the specimen is given in Figure 3.10. The specimen shows segregation and heterogeneity. The light colored bands are the fine-grained layers and the darker bands are the coarse-grained layers. The top of the specimen shows cracks and fissures resulting from oven drying. These attributes are typical of desiccated clay, and suggest that the top of the specimen is clay-like in nature.

In-Place Wet Pluviation was only used for simple shear specimens because of differences in geometry for the two testing systems. Simple shear specimens have large diameters (10 cm) and are only 2.5 cm tall, compared to triaxial specimens with smaller diameters (7.5 cm) and greater heights (13 cm).

Consider that both a triaxial specimen and simple shear specimen would add the same mass (in this example 83 grams dry weight) for a layer. This means the same volume of slurry would be added to both mold assemblies. Because of the difference in diameters, to retain the same volume, the mold assembly for the triaxial specimen would be twice the height for the simple shear specimen. This makes the assembly unwieldy because of the height and increases the overall time for sedimentation per layer because the soil must sediment through a taller column of water. Additionally, the triaxial specimen will require almost 10 layers to reach the target dry weight of 800 g, compared to 3 layers to reach the target dry weight of 280 g for the simple shear. This increases the overall time for pluviation by a factor of 3. For these reasons, it was determined that only simple shear specimens would be prepared using this method.

3.4.2 Specimen Preparation for Simple Shear

The construction of a simple shear specimen by the In-Place Wet Pluviation Method is similar in many aspects to the Slurry Deposition Method. Unlike the Slurry Deposition specimens, which take approximately 2 hours to construct, In-Place Wet Pluviation specimens require a minimum of 12 days. With the equipment on hand at the UC Berkeley laboratory, up to six specimens can be built at once.

To prepare an In-Place Wet Pluviation simple shear specimen the following materials are required:

1. End Caps for Sample. Caps have the diameter of 10 cm with built-in porous stones, shown in Figure 3.7,
2. Wire-Reinforced Membrane,
3. 2 Pieces of Filter Paper, 10 cm in diameter
4. 4 O-Rings:
    a. 2 to fit on bottom and top caps
    b. 2 large, flexible O-rings to fit over simple shear mold
5. Simple Shear Mold,
6. 2 Hose Clamps,
7. Stainless Steel Collar,

8. Plexiglas Tube,
9. Brass Cap,
10. Vacuum Container,
11. Short, non-reinforced membrane. Membrane should have a diameter large enough to fit over the simple shear mold,
12. Vacuum Chamber,
13. Vacuum Regulator,
14. High Strength Rubber Bands, and
15. 4 kg of Free Weight,

Step 1: Mold-Assembly Preparation

The mold assembly is prepared in the same steps as detailed in the Slurry Deposition Method. Saturate the top and bottom caps by flowing de-aired water through the porous stones, and check the membrane for leaks or holes. Place the bottom cap on a level surface, and pull the wire-reinforced membrane over the sides of the cap, ensuring the reinforcement is also horizontal. Place the bottom cap O-ring in the O-ring groove on the end cap to secure the membrane. Place the filter paper and assemble the mold. Hold the mold in place with a hose clamp, then fold the top membrane down over the mold.

At this point, the In-Place Wet Pluviation Method preparation technique deviates from the Slurry Deposition Method. Place the stainless steel collar over the simple shear mold and membrane. Apply vacuum grease to the stainless steel collar prior to placement, both to ensure the collar will not stick to the membrane and to provide protection against leakage between the collar and membrane. Insert the Plexiglas tube into the stainless steel collar. The Plexiglas tube should also have a layer of vacuum grease around the edge to prevent possible leaks. Seal the bottom cap drain line with a brass cap. Fill the mold assembly with approximately 200 cm^3 of de-aired water, and check the assembly for leaks. A picture of the completed assembly is shown in Figure 3.11.

Step 2: Soil Preparation

Place 83 g (dry weight) of soil directly into the vacuum container and bring the water content up to approximately 200% by adding de-aired water. Mix well. At this water content, the material becomes a thin slurry and the coarse and fines grains separate easily. Because of the high water content, air is more easily released from the soil and typically only two cycles of vacuum and stirring are necessary to produce a de-aired material.

Step 3: Pluviation

To pluviate the material into the mold, a long, thin tube, fitted with a wire mesh at the bottom was utilized. The thin slurry is poured from the vacuum container directly into the mold assembly through the tube. Move the tube around the mold to ensure that material is evenly placed. Make sure to retrieve all fine and coarse particles from the vacuum container.

The sedimentation process for an individual layer should be complete within 72 hours. Figure 3.12 shows four specimens at different stages of the sedimentation process. The specimen No. 1, has rested for 72 hours, and the water column is nearly clear. Specimen, No. 2 has rested for 48 hours, resulting in a somewhat cloudy water column. Specimen, No. 3, has rested 24 hours. If

an object is held behind this water column, it cannot be seen on the other side. Specimen No. 4, has just recently been pluviated.

After 72 hours of settlement time, slowly siphon off the water column, leaving approximately 3 inches of water on top of the sedimented layer. Prepare another 83 g of soils, as described in Step 2, and pluviate as previously described. After an additional 72 hours, siphon the water column a second time, and add the third and final layer. Wait 72 hours for sedimentation and again siphon the water, this time until only ¼ inch of water remains above the top layer.

When all of the layers have been added and allowed to settle, attach the drain line of the bottom cap to a vacuum chamber and apply 7 in-Hg (23 kPa) of vacuum to the specimen to continue drawing down the water. Do not expose the top of the specimen to air. Always leave a thin layer of water to prevent desiccation. At this point, the Plexiglas tube and stainless steel collar can be removed.

The In-Place Wet Pluviated specimens are placed under a vacuum of 23 kPa, not 13 kPa which is used in the construction of all Slurry Deposition Method specimens. When the Slurry specimens were placed under a vacuum of 23 kPa, it was found that this caused the sides of the membrane to cave in. The internal vacuum was too great for the specimen to properly consolidate while maintaining a constant diameter. For this reason, a lower vacuum is required. Conversely, the Pluviated specimens were found to consolidate under the larger vacuum with no decreases in diameter or without the membrane caving in.

Step 4: Initial Consolidation and Assembly Completion

This step is the same as Step 3 for the Simple Shear Slurry Deposition Method and will not be repeated here. The only difference between the two techniques is the In-Place Wet Pluviation specimen is placed under 23 kPa vacuum pressure, as compared to 13 kPa for the Slurry Deposition specimen, as stated in the section above. All other procedures to prepare for testing are the same.

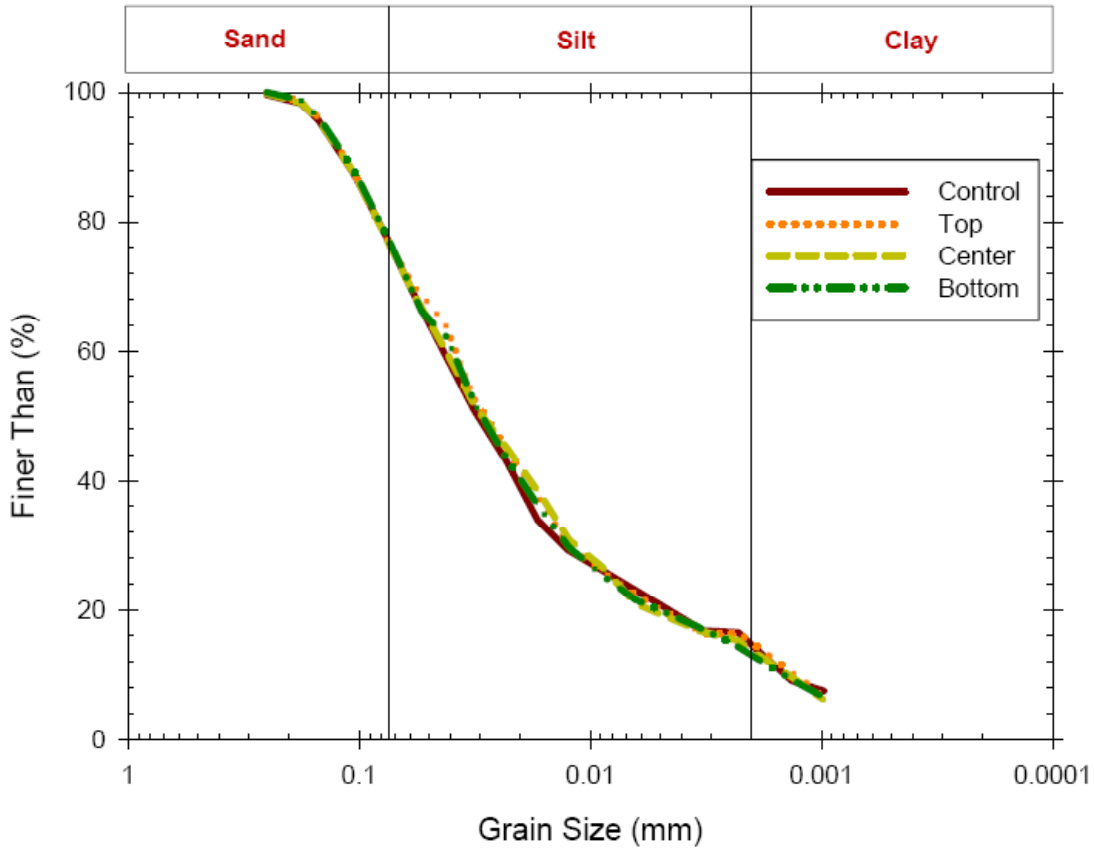

Figure 3.1 Gradation analysis from hydrometer and sieve analysis for Soil "G" prepared using the Slurry Deposition Method.

Figure 3.2 Photograph of simple shear specimen prepared by the Slurry Deposition Method.

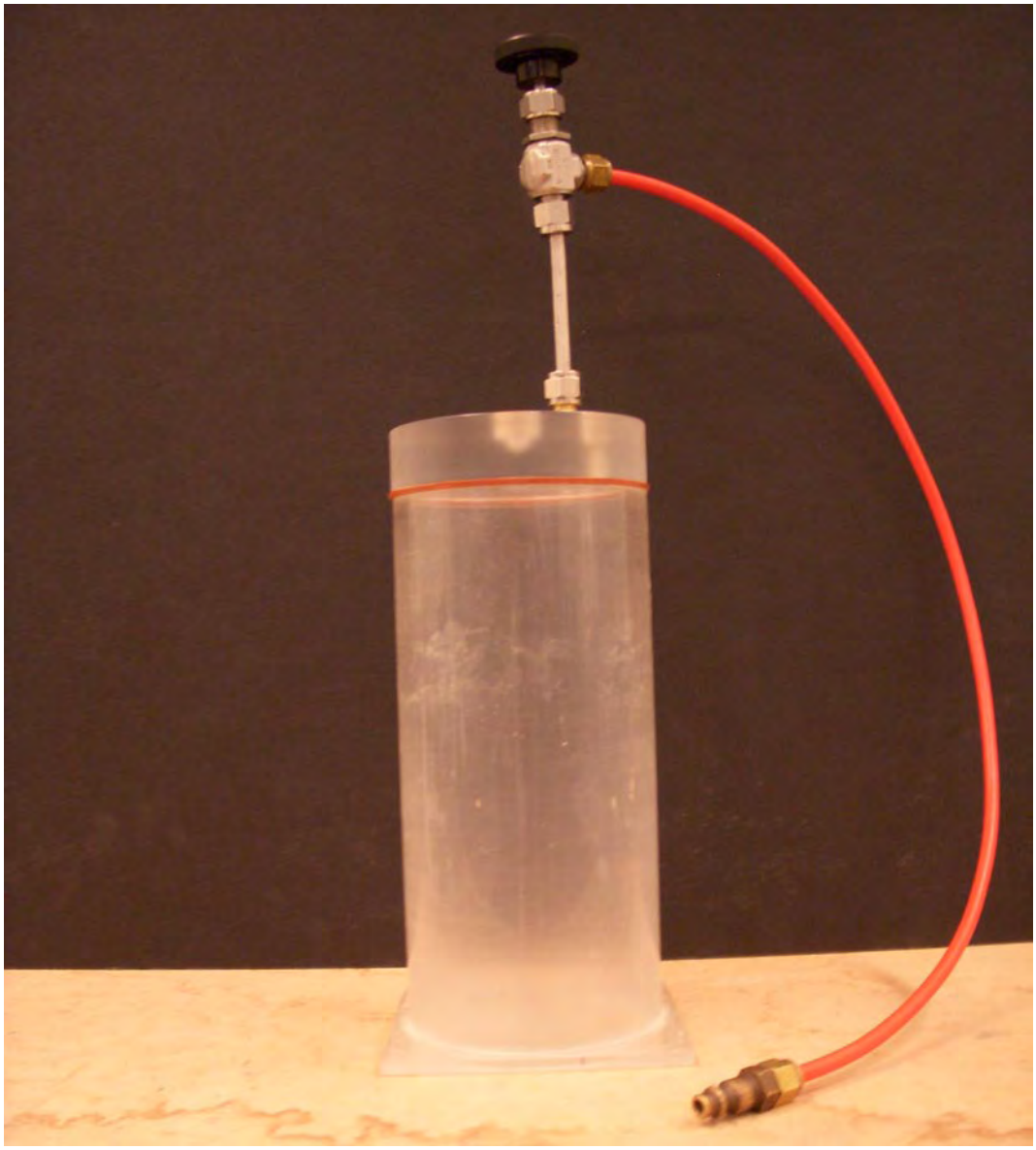

Figure 3.3 Photograph of specially devised vacuum container able to contain a 1 atm vacuum.

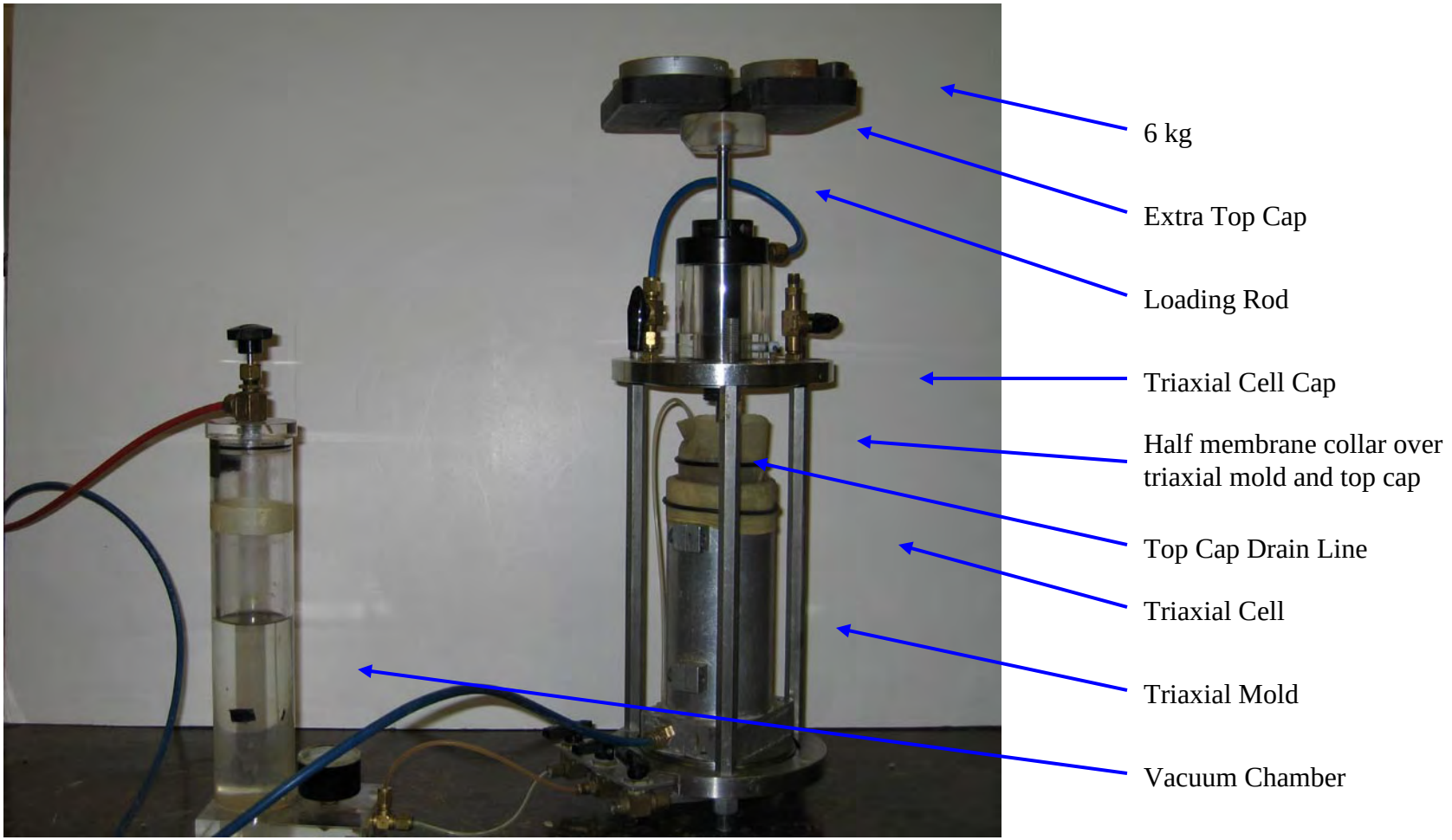

Figure 3.4 Photograph of specimen inside vacuum mold consolidating from a slurry. Specimen is attached to vacuum chamber delivering 5 in-Hg vacuum at top and bottom with a 6 kg load vertically applied.

Figure 3.5 Photograph of specimen once vacuum mold has been removed, while still under confining pressure from vacuum chamber.

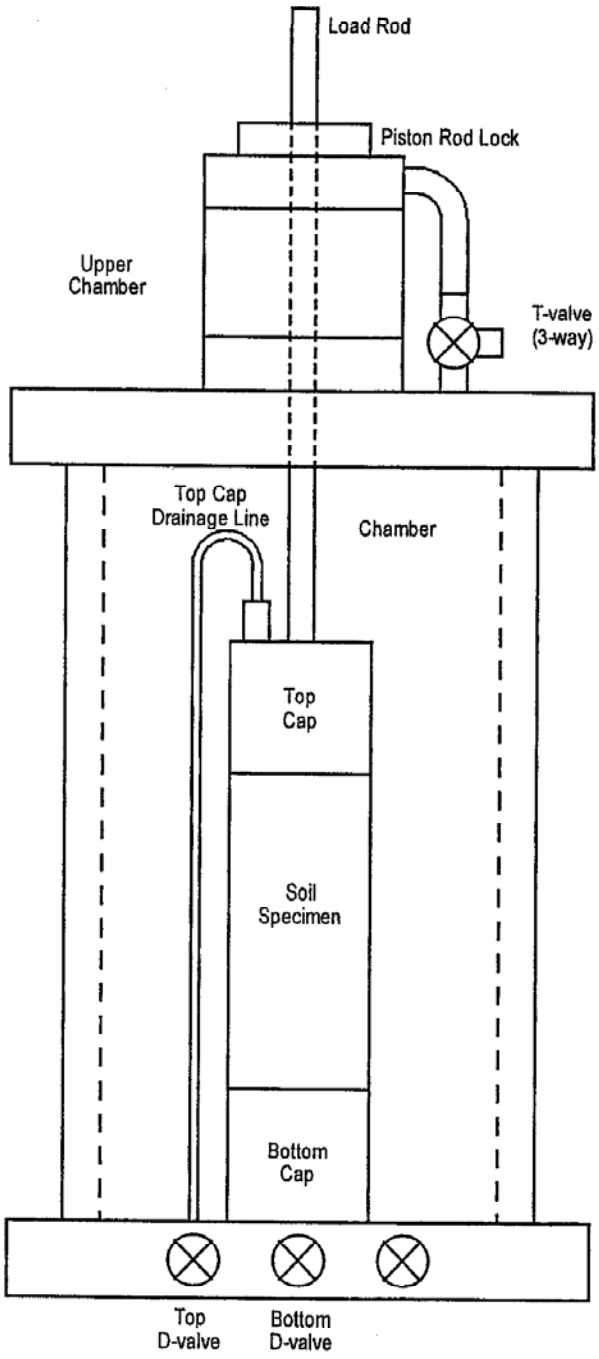

Figure 3.6 Front elevation of the triaxial cell (from Sancio 2003).

Figure 3.7 Photograph of end caps used for simple shear testing. The bluish-gray porous stones are the embedded in the end caps.

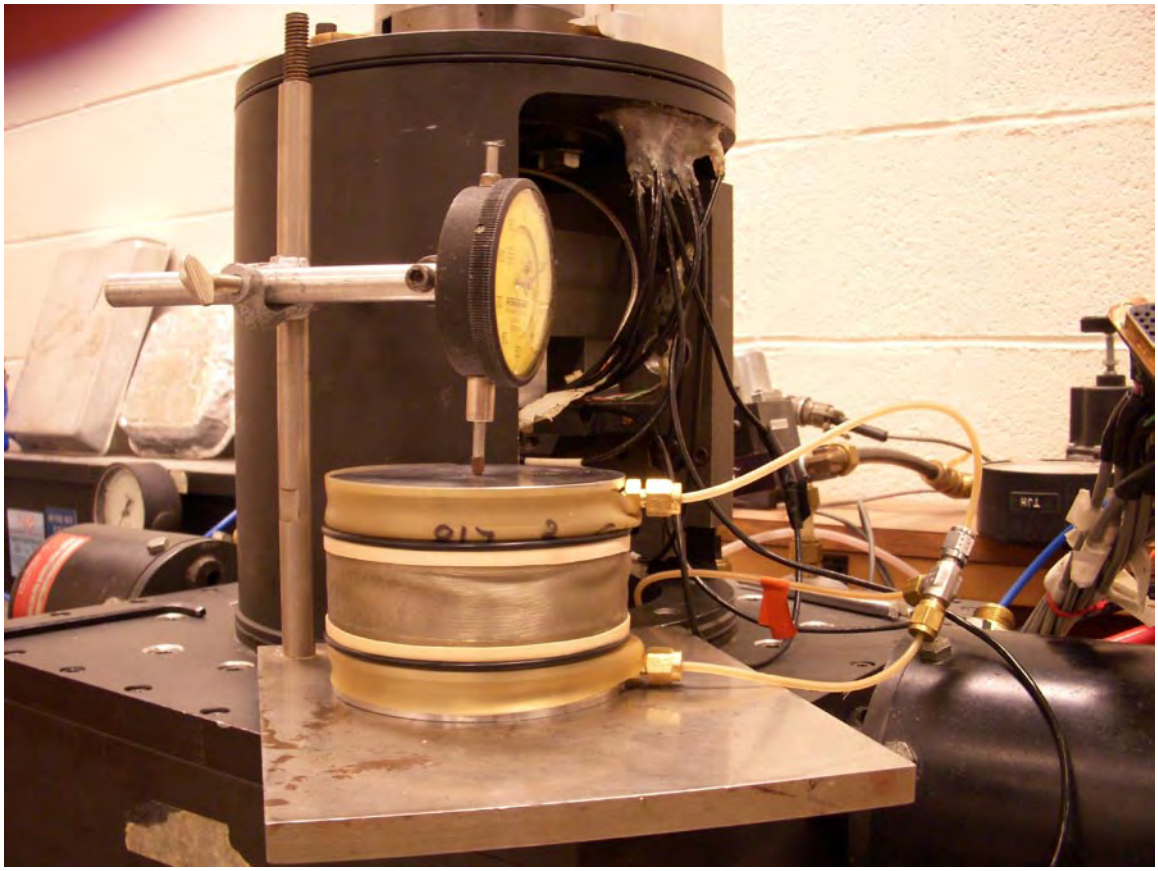

Figure 3.8 Photograph of specimen with O-rings and Rubber bands attached. Drain lines are attached to the top and bottom caps and a dial gauge reads the height of the specimen.

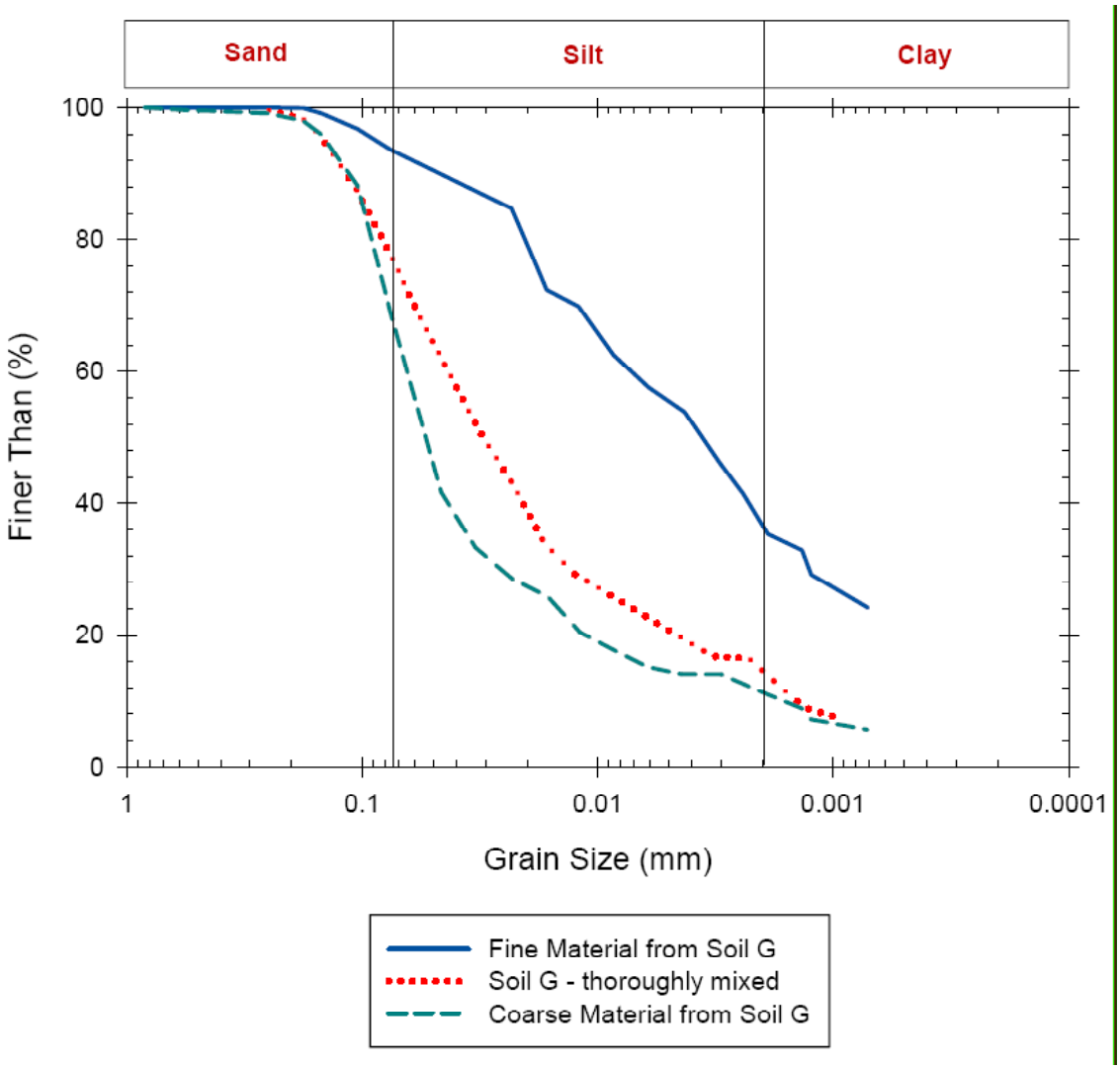

Figure 3.9 Gradation analysis from hydrometer and sieve analysis for Soil "G" prepared using In-Place Wet Pluviation, the fine material is from the top of a layer and the coarse material is from the bottom of a layer. Layers are due to natural segregation during pluviation.

Figure 3.10 Photograph of simple shear specimen prepared by In-Place Wet Pluviation, showing layering within the specimen.

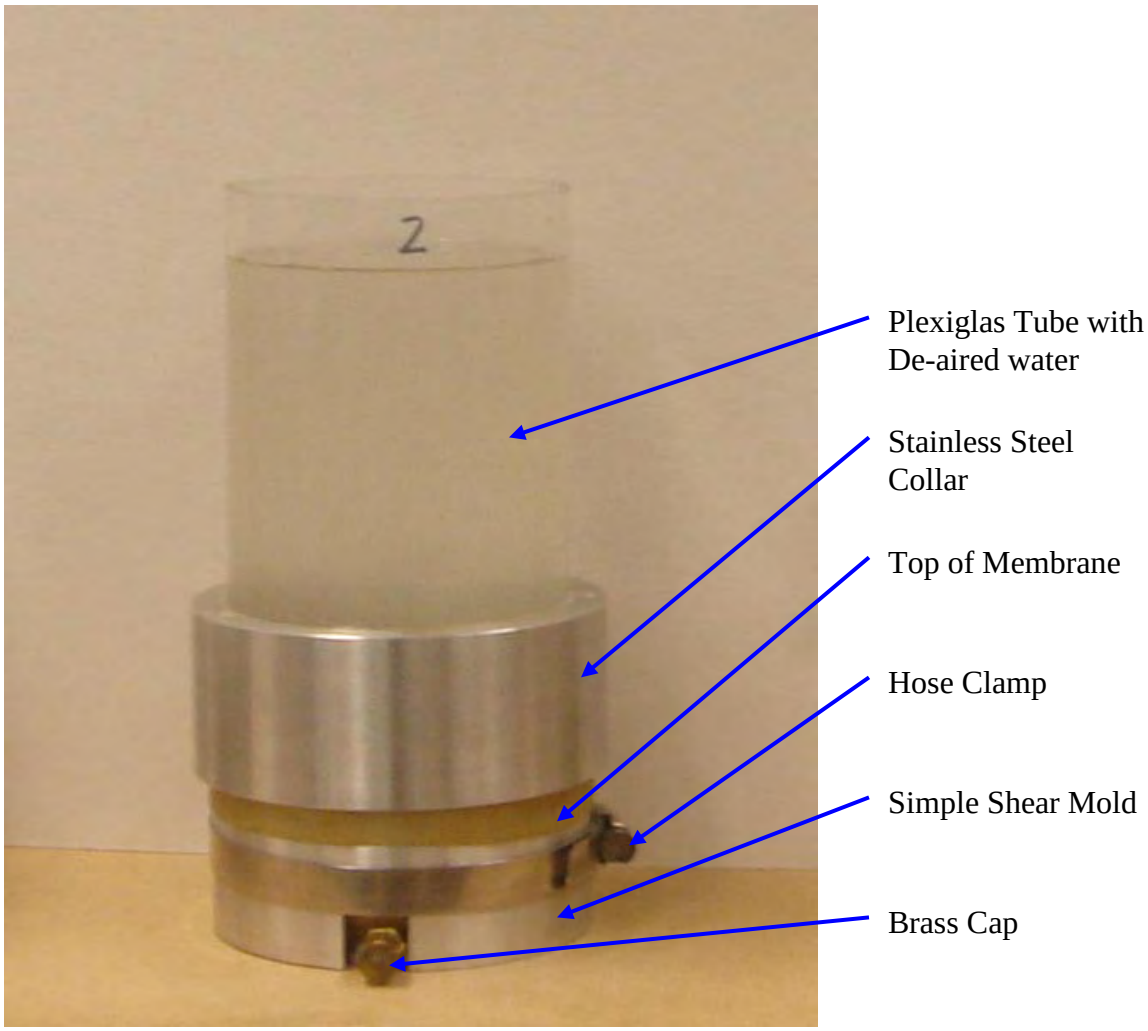

Figure 3.11 Fully assembled In-Place Wet Pluviated specimen.

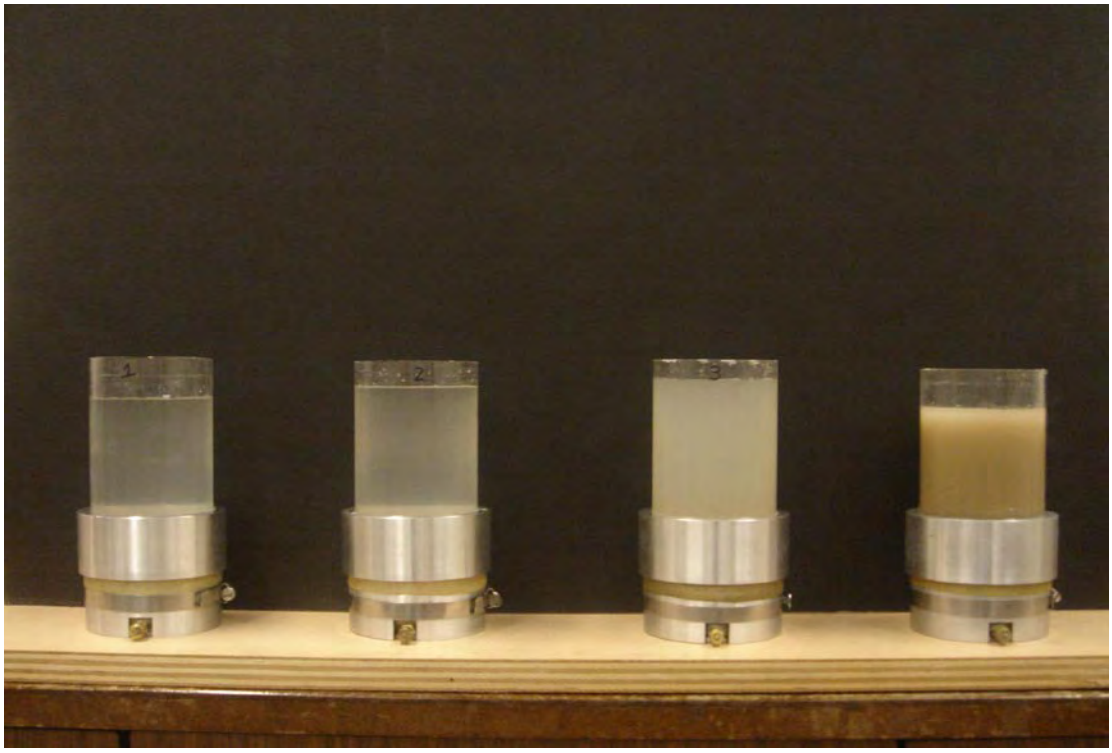

Figure 3.12 Four In-Place Wet Pluviation Specimens at different stages of sedimentation.

Chapter 4 TESTING PROCEDURES

4.1 Introduction

The experiments performed during this research to assess the liquefaction resistance and susceptibility of the reconstituted fine-grained soils from Adapazari, Turkey included the Constant Rate of Strain Consolidation, grain size distribution, undrained triaxial and undrained simple shear tests. These experiments allowed for the determination of the consolidation and gradation characteristics, and the static and the cyclic strength response of the specimens. This chapter describes the testing procedures performed.

4.2 Constant Rate of Strain Consolidation Tests

One-dimensional consolidation tests using controlled-strain loading at a constant rate were performed as per ASTM D4186 on Slurry Deposition Method specimens. The objective of the constant rate of strain consolidation test is to simulate the compression of the soil under given external loads. To establish the relationship between load and deformation in the laboratory specimen, the load is applied and the sample is allowed to consolidate. The compression characteristics of the specimen are then evaluated in order to predict the expected settlement by the soil in the field.

Using the load-deformation data, the void ratio as a function of the effective stress, or e-log P curve is plotted. From this curve, the preconsolidation stress, P'_p, or maximum vertical overburden stress that the particular specimen has sustained in the past is determined. The e-lop P curve can also be used for determining the virgin compression curve, compression index, C_c, and reconsolidation index, C_r, for the soil.

4.2.1 Testing Equipment and Specimen Set-up

The equipment for the one-dimensional constant rate of strain consolidation is comprised of the components of the 1-D consolidation cell and the loading apparatus. The ring used in the 1-D consolidation cell is relatively rigid so that no lateral deformation takes place. The ring used for these tests is a 12.5 cm (4.9") external diameter stainless steel ring with an internal diameter of 10.1 cm (4"). The height of this ring is 2 cm (0.78") and therefore, the diameter to height ratio of the specimen is 5.1. The minimum specimen diameter-thickness ratio is 2.5 as stipulated in the Standard Test Method for One-Dimensional Consolidation Properties of Soils Using Controlled-Strain Loading (ASTM D4186-06).

All specimens were reconstituted using the Slurry Deposition Method. The soil was prepared as per Section 3.3.3 of the previous chapter. A summary of this method is below.

Approximately 160 g (dry weight) of soil is placed directly in the vacuum container and de-aired water is added to increase the specimen's water content to approximately 45%. The specimen is

mixed well and three cycles of vacuum and stirring are typically required. Once the Slurry specimen is sufficiently de-aired, it will not release air or bubble after a stirring cycle. The specimen is ready to be transferred into the 1-D consolidation cell.

The 1-D consolidation cell is a pressure chamber in which the specimen is consolidated as shown in Figure 4.1. In this setup, the rigid ring sits over an inset porous stone that is attached to a drain line that ends to an external valve. A piece of filter paper is placed inside the ring over the porous stone to provide an extra layer of protection against the loss of fines. The slurry is transferred into the ring, ensuring no air pockets are formed during placement, and a second porous stone is placed over the slurry to allow for the drainage of excess pore water pressure. A 1.8 cm (0.72") diameter loading rod is next placed on top of the porous stone. The chamber is attached and filled with de-aired water to cover the ring and specimen. The Slurry specimen will consolidate under the weight of the porous stone and loading rod. Measurements of the height of the specimen are taken after the end of primary consolidation, before the 1-D consolidation cell is taken to the Wykeham Farrance 5 ton loading frame shown in Figure 4.2.

An external 4448N (1000 lbf) load cell is used to measure the vertical force applied to the specimen. Excess pore water pressures at the base of the specimen are measured through a water line attached from the external valve of the 1-D consolidation cell to the differential pore water pressure transducer. The load cell and pore water pressure transducer are connected to a data acquisition system and their output is recorded using the VI Logger, version 4.0.0.3010 software by National Instruments, on a laboratory computer.

4.2.2 Testing Procedures

The tests were performed following the procedures and test recommendations outlined in ASTM D4186-06. After installing the 1-D consolidation cell on the loading frame, a steel ball was placed between the loading rod and the load cell to provide a point-load application. A small seating load of approximately 5 kPa was applied by raising the loading table such that the loading rod/steel ball made contact with the load cell. An initial chamber pressure of 100 kPa was then applied with an equal value of backpressure applied through the drain line to the specimen. These conditions were maintained for a period of over 1 hour to ensure full saturation of the specimen. Before each test began, the "A" valve of the differential pore water pressure transducer was closed to prevent drainage and to measure changes in excess pore water pressure at the base of the specimen.

Specimens were compressed at a rate of 0.03048 mm/min (0.0012 in/min) and unloaded at a rate of 0.006096 mm/min (0.00024 in/min). Specimens were first loaded to approximately 100 kPa and then unloaded to 50 kPa. They were then reloaded to over 400 kPa, and unloaded to 50 kPa. The loading rates were chosen to be sufficiently slow such that pore water pressure equalization occurred throughout the test and thus no significant or measurable excess pore water pressures could be measured. The excess pore water pressure measurements did not exceed 3 kPa and therefore the coefficient of consolidation, c_v, was not calculated as per ASTM guidelines. The unloading of the specimen was performed to obtain the slope of the recompression line.

After the testing was completed, the 1-D consolidation cell was removed from the loading frame and quickly disassembled. The specimen was removed from the ring, weighed, placed in the oven to dry for 24 hours and then re-weighed to calculate the water content and dry mass.

4.3 Grain Size Distribution Tests

Particle size distribution is obtained through gradation testing in the form of sieve analysis for particles greater than 75 μm, and hydrometer analysis for particles less than 75 μm. Both tests were performed as outlined in the Standard Test Method for Particle-Size Analysis of Soils (ASTM D422-63(2002)e1).

Hydrometer analysis is based on Stoke's Law. A sphere falling freely through a liquid of infinite extent will accelerate rapidly to a certain maximum velocity and will continue at that velocity as long as conditions remain the same. The grain diameter can thus be calculated from knowledge of the distance and time of the fall. The results of the hydrometer analysis are valid if the equivalent grain diameter is considered, rather than actual grain diameter. Under the assumptions of Stoke's Law, inaccuracies in the hydrometer testing occur due to the following:

- Soil particles are not spheres,
- The fluid is not of infinite extent,
- The specific gravity of individual particles may vary,
- Turbulence caused by larger particles falling,
- Brownian movement of smaller particles, and
- Disturbance due to insertion and removal of hydrometer

These inaccuracies cannot be controlled or minimized by proper testing techniques.

There are many testing errors which can be avoided during hydrometer analysis. These errors occur due to the following:

- Variance in temperature over the course of the test,
- Loss of sample during agitation,
- Accumulation of soil on the hydrometer bulb,
- Evaporation, and
- Misreading the meniscus

By proper sampling and laboratory techniques, these testing errors can be controlled or minimized so that the resulting inaccuracies listed above can be accounted for during testing.

4.3.1 Testing Equipment

Grain size analysis testing requires only a few essential pieces of equipment. The ASTM hydrometer, graduated to read in specific gravity of the suspension and conforming to the requirements of hydrometers 151H in Specification E100 was used. The dispersion cup, or stirring apparatus, conformed to the "Apparatus A" from the ASTM standard and the sedimentation cylinders were marked for a volume of 1000 mL.

For this testing series, the following sieves were used: #30 (0.59 mm), #50 (0.295 mm), #60 (0.25 mm), #80 (0.1778 mm), #100 (0.15 mm), #140 (0.106 mm), and #200 (0.075 mm).

4.3.2 Testing Procedures

The hydrometer test is performed by initially placing approximately 50 g (dry weight) of material in a dispersion cup. Distilled water is added along with 40 g/L of the dispersant, sodium hexametaphosphate, and then the mixture is blended for at least 5 minutes.

The slurry is transferred to a glass sedimentation cylinder and distilled water is added until the total volume is 1000 mL. The slurry is agitated by turning the cylinder upside-down and back for 1 min. The cylinder is set down and hydrometer readings are taken at 30 seconds and at intervals of 1, 2, 4, 8, 15, 30, 60, 120 (2 hours), 240 (4 hours), 480 (8 hours), 960 (16 hours), 1440 (24 hours), and 2880 (48 hours). To do this, insert the hydrometer 20 seconds before the reading is needed to the predicted depth. Readings are to be taken at the top of the meniscus, not at the bottom. The temperature is to be taken at each recording.

Once the hydrometer testing is completed, wet sieve all material through the #200 sieve. Dry and weigh both the materials passing and not passing the #200 sieve. Dry sieve the materials not passing #200 through the series of sieves listed in Section 4.3.1.

4.4 Undrained Triaxial Tests

Prior to testing, specimens were prepared as stated in Section 3.3.2 of the previous chapter. Only Slurry Deposition Method specimens were tested monotonically and cyclically on the triaxial device.

4.4.1 Testing Equipment

All triaxial tests in this study were performed on the CKC electropneumatic cyclic triaxial testing system described by Chan (1982). The instrumentation of this equipment includes five sensors: external load cell, external LVDT, and three differential pressure transducers. The external load cell records the deviatoric load applied to the specimen and the external LVDT monitors vertical displacement. The three differential pressure transducers measure the chamber pressure, the effective stress, and volume change. The layout of the equipment is shown in Figure 4.3. The system is controlled by a laboratory computer using the Georobot Triaxial Testing System software. This system allows for both closed and open-loop stress-controlled loading. For the triaxial tests, the 50 mm air piston with a rod diameter of 9.53 mm was used.

A series of cyclic triaxial tests were first performed on Monterey sand following the methodology described by Silver et al. (1976) to verify adequate calibration of the system. This procedure consists of performing tests at an effective confining stress of 100 kPa on saturated specimens of Monterey #0 sand prepared to a relative density of 60% using the moist tamping technique. The number of cycles applied to reach initial liquefaction ($\sigma'_3 = 0$) and 10% double amplitude strain for a given cyclic deviator stress should plot within the bounds indentified in the method. The results from a test performed for this study is compared to the results by Silver et al. (1976), in Figure 4.4. The testing equipment and procedure produced consistent results with Silver et al. (1976).

Table 4.1 Characteristics and results of the test performed on Monterey #0 sand

Test Name	D_r (%)	CSR	Number of Cycles to reach Lateral Effective Stress = 0	Number of Cycles to reach 10% DA Axial Strain
Cyc Sand 5-1	58	0.36	14	18

4.4.2 Triaxial Testing Preparation

The fine-grained triaxial specimens were prepared using the Slurry Deposition Method described in Chapter 3. The testing preparation of the triaxial specimens is described in this section.

The triaxial cell is assembled and filled with de-aired water for triaxial testing as per Section 3.3.2 of the previous chapter. Even though the specimens were de-aired in the vacuum container and the triaxial cell is filled with de-aired water, full saturation of the specimens may not have been achieved. Full saturation is required for accurate and reliable measurement of excess pore water pressure response during an undrained triaxial test. Two procedures that will increase the saturation level of a specimen, differential vacuum and backpressure saturation, are described below.

Step 1: Differential Vacuum

Differential vacuum is first used to extract air from the specimen. Once the triaxial cell was mounted on the CKC triaxial device, two vacuum chambers were attached to the triaxial cell: one to the top drain line, and the other to the bottom drain line. A third vacuum line was attached directly to the triaxial cell to apply vacuum to the exterior of the specimen. Differential vacuum saturation occurs when a vacuum is applied to the exterior of the specimen within the triaxial cell and to the interior of the specimen through the drain lines. The difference in vacuum between the exterior and interior of the cell is the effective stress of the specimen and this difference must always be greater than zero and smaller than a limiting value. For this testing series, the limiting value was 10 in-Hg (33 kPa), which is less than the level of effective confining stress at which the specimens were subsequently monotonically or cyclically tested, σ'_{test}. The vacuum is incrementally applied to the exterior and interior until the interior of the specimen has reached full vacuum (1 atm or 100 kPa).

To assist in the extraction of air and increase the flow of the de-aired water through the specimen, the vacuum to the top drain line was always kept at 3 to 4 in-Hg (13 kPa) greater than the vacuum applied to the bottom of the specimen. The vacuum chamber connected to the bottom drain line was filled with de-aired water, which was pulled through the specimen to the top drain line by the difference in vacuum between the top and bottom vacuum chambers.

After approximately 1 hour of differential vacuuming, the vacuums applied to the interior and exterior of the specimen are slowly lowered in increments until only 7 in-Hg (24 kPa) remained in the interior and no vacuum is applied to the exterior of the specimen.

The saturated triaxial specimen was now ready to be connected to the triaxial device. The following procedure is done to keep the effective confining stress lower than the testing level of effective stress, σ'_{test}.

Attach the pressure line to the top of the triaxial chamber and apply the chamber pressure (which is approximately 25 kPa). Reduce the vacuum chamber slowly to zero and attached the drain lines to the volume change device. Open valves "A" and "B" to the volume change device and increase the backpressure to 20 kPa, then wait approximately 10 minutes for the specimen to equilibrate. During the startup of the Georobot program, the pneumatic system will automatically apply a chamber pressure of approximately 50 kPa to the specimen. With the backpressure already set at 20 kPa, the effective stress will be 30 kPa.

Step 2: Back Pressure Saturation

Following the differential vacuum and start-up of the system, the specimen is ready for backpressure saturation. In backpressure saturation, the saturation level is increased by reducing or dissolving any remaining air in the voids. To backpressure saturate, the chamber pressure and backpressure are simultaneously increased so that the effective stress remains constant.

The specimens are saturated at an isotropic confining stress of at least 5 kPa smaller than the final testing effective stress, σ'_{test}, to avoid exceeding σ'_{test} during the B-value measurements. After the backpressure had been applied and a sufficient time had elapsed, the degree of saturation is measured using Skempton's B-value, which is the ratio of the increase in excess pore water pressure, Δu_e, resulting from an undrained increase in chamber pressure, ΔCP:

$$\mathbf{B} = \frac{\Delta u_e}{\Delta CP} \qquad \mathbf{4.1}$$

The "A" valve to the volume change device is closed, the cell pressure is increased, and the changes in excess pore water pressures are monitored. Because the compressibility of the soil structure used in this study was not known, the minimum acceptable B-value determined for this study was chosen based on the work done by Black and Lee (1973). Black and Lee (1973) determined the correlation between B-value and saturation for a number of soil types and according to their study, a B-value of 0.97 corresponds to a level of saturation of at least 99% for a soft soil, as shown in Figure 4.5.

Step 3: Consolidation

After achieving satisfactory B-values of at least 0.97, the specimens were isotropically consolidated to the final effective stress for testing, σ'_{test}. For the cyclic triaxial tests, the specimens were consolidated for 4 hours. For the monotonic triaxial tests, the consolidation timeframe was increased to 0.8 days, or 19 hours. When the monotonic tests were performed, the effects of the time under confinement had already been investigated, as shown in Chapters 5 and 6, and the baseline duration of 0.8 days was used.

4.4.3 Monotonic Testing Procedures

Monotonic compression tests on Soil A and Soil G were performed by stress control. The stress-controlled loading was performed at $\Delta\sigma'_d$ = 1 kPa/min and the load was increased until the axial strain exceeded 8%. The sampling rate for the monotonic tests was 12 samples/minute.

4.4.4 Dynamic/Cyclic Testing Procedures

All cyclic triaxial tests in this study were performed on Soil G, prepared by the Slurry Deposition Method. Cyclic tests were performed by applying a stress-controlled sinusoidal loading at a

loading frequency of 1 Hz or 0.005 Hz to the Soil G specimen. The sampling rates for tests performed at 1 Hz and 0.005 Hz were 33 samples/second and 12 samples/minute, respectively.

The loading amplitude was characterized in terms of the Cyclic Stress Ratio (CSR), which for the triaxial tests is the ratio of the maximum peak shear stress ($\sigma'_d/2$) to the initial effective consolidation stress (σ'_c or σ'_3). Two CSR values (0.2 and 0.44) were applied to the Soil G specimens during this testing series. These specimens were cyclically loaded until axial strains in excess of 10% double amplitude were reached.

4.5 Simple Shear Tests

Prior to simple shear testing, specimens were prepared as described in Section 3.3.3 and 3.4.2. Both Slurry Deposition Method and In-Place Wet Pluviated specimens were tested monotonically and cyclically using the simple shear device.

Wire-reinforced Membranes

Wire-reinforced latex membranes manufactured by Geonor were used to enforce K_o (coefficient of lateral earth pressure at rest) conditions in the soil by maintaining a nearly constant cross sectional area during consolidation and testing. Two membrane wire-stiffnesses were used in this program of study (c=1.0, 1.25) to replicate the average stiffness properties of soil.

The benefit of using a wire-reinforced membrane is that the appropriate lateral effective stresses are automatically maintained. The use of undrained testing with a wire-reinforced membrane, paired with the Berkeley Bi-directional device, for which full saturation of samples and constant vertical load are possible, allows for reasonably good compliance with the desired boundary conditions: maintaining zero radial strain, constant volume, and constant overburden stress.

A drawback of wire-reinforced membranes is that the use of reinforced membranes prevents direct measurement of the lateral effective confining pressures (σ'_2, σ'_3) because the amount of stress that the wires carry is unknown. Triaxial data is typically plotted in q-p' space for which the stress in all three dimensions (σ'_1, σ'_2, σ'_3) is known. This is not possible for testing with simple shear specimens with wire-reinforced membranes and for this reason, the results for simple shear are presented in terms of the effective vertical stress, σ_v', and effective confining stress, σ_c'. The effective confining stress, σ_c', is calculated as the difference between chamber pressure and backpressure, plus the effective vertical stress.

If non-reinforced membranes are used, lateral forces on the specimen are applied entirely by chamber pressure acting through the membrane. Because lateral stresses under K_o conditions can change substantially during liquefaction (potentially reaching a value of K_o=1) and are not well understood, the use of non-reinforced membranes cause the testing conditions to differ greatly from in situ conditions unless the loading is applied slowly and the testing is carefully performed. Because of these complications, wire-reinforcement was used.

Constant Load

In constant load testing, the vertical load is kept constant while a saturated sample is sheared undrained. Load control was used for both the vertical normal stress and horizontal shear stress. This was possible because the undrained testing was performed on fully saturated samples that

were laterally confined both by NGI-style wire-reinforced membranes and by chamber pressure. This method allows a direct measurement of the excess pore water pressure to be recorded during testing and provides reasonably good compliance with the desired boundary conditions.

More comprehensive descriptions of the advantages and disadvantages of wire-reinforcement and constant load conditions are found in Boulanger (1990) and Kammerer (2002).

4.5.1 Testing Equipment

All simple shear tests performed during this study used the U.C. Berkeley Bi-directional simple shear apparatus, which was designed by Boulanger and Chan (Boulanger, 1990) and later modified by Kammerer (2002). This design was based on three objectives: (1) the capability of uni- and bi-directional monotonic and cyclic loading, (2) low mechanical compliance and (3) a sealable chamber for lateral support and saturation purposes (Boulanger et al., 1991).

Boulanger et al. (1991) presented an extensive review of cyclic simple shear testing and a complete description of the Berkeley Bi-directional simple shear apparatus. Biscontin (2001), Kammerer (2002), Wu (2002), and Anantanavanich (2006) also provided a detailed discussion on the features and capabilities of this apparatus and its subsystems. That information is not repeated herein, and readers who are interested in more details about the Berkeley Bi-Directional Simple Shear apparatus are referred to those documents. A schematic and photograph of the Bi-directional Simple Shear device are shown in Figure 4.6 and Figure 4.7.

4.5.2 Cyclic Simple Shear Preparation

Soil specimens were prepared following procedures in Section 3.3.3 and 3.4.2 of the previous chapter, and the next step was to insert the specimen into the simple shear device. The Cyclic Simple Shear testing preparation is described below.

<u>Step 1: Differential Vacuum</u>

After the initial measurements of specimen height is recorded, a differential vacuum, previously described in Section 0, Step 1, was applied to the specimen. A vacuum chamber attached to the drain lines provided the internal vacuum that was applied directly to the pore water of the specimen. The external vacuum, which was supplied by the house vacuum, was attached to the simple shear chamber and applied to the membrane. The internal vacuum was slowly raised to full vacuum (1 atm or 100 kPa) as the external vacuum was brought up to 50 kPa. The effective stress on the specimen was approximately 50 kPa. This effective stress was erased during consolidation when the mean effective stress was raised to the testing mean effective stress level, σ'_{test}. The differential vacuum is completed when no additional dissolved air is drawn from the specimen into the vacuum chamber. The internal and external vacuums were incrementally lowered until the external vacuum reading was equal to zero and the internal vacuum = 7 in-Hg (24 kPa).

<u>Step 2: Consolidation</u>

Once differential vacuum was completed, the specimen was consolidated by applying a vertical load equivalent to a vertical effective stress, $\sigma'_{v,}$ of 137 kPa. A vertical effective stress of 137 kPa was used to approximate a mean effective stress, $\sigma'_{m,}$ of 100 kPa, which is also σ'_{test} for most simple shear tests. The internal vacuum, provided by the vacuum chamber, is decreased to

zero during the increase in vertical effective stress and the specimen was consolidated for 0.8 days. As previously described, wire-reinforced membranes manufactured by Geonor were used to maintain K_o conditions in the soil during consolidation by enforcing a nearly constant cross-sectional area.

After 0.8 days, the vertical load was reduced and the differential vacuum was once again applied to the specimen as a precaution against the possible loss of saturation that can occur during the extended consolidation phase.

Step 3: Backpressure Saturation

The saturation of a specimen is further increased by backpressure saturation. Backpressure saturation begins after the second differential vacuum following the consolidation phase. The effective stress of the specimen was 7 in-Hg (24 kPa) as applied by the vacuum chamber attached to the drain lines. The next steps will replace the internal vacuum for the external pressure provided by the simple shear device. To begin, 10 kg (12 kPa) of vertical load and 20 kPa of chamber pressure were applied to the specimen. The drain lines to the sample were switched using a T-valve from the vacuum chamber to the volume and differential pore water pressure transducer. The specimen should come to equilibrium before proceeding.

To bring the specimen up to the proper effective stress for backpressure saturation, the vertical load is increased to 20 kg (24 kPa), and the chamber pressure and the backpressure are slowly, simultaneously increased to approximately 40 kPa and 25 kPa, respectively. The difference in pressure that occurs between the chamber pressure and backpressure is called the differential, σ'_{dif}. Combining the differential, σ'_{dif}, with the vertical load, gives the vertical effective stress, σ'_v, of the specimen. During backpressure saturation, σ'_{dif} should remain within a range of 15 to 20 kPa, because when combined with the vertical load (24 kPa), the resulting effective stress must be less than the testing level mean effective stress, σ'_{test}. See Section 0, Step 2 for more detailed information on this procedure.

Following backpressure saturation, the specimen was reloaded to a vertical effective stress of 137 kPa. To achieve a 137 kPa vertical effective stress in the specimen, the vertical load was increased to 75 kg (92 kPa) and the differential, σ'_{dif}, was increased to 45 kPa. The high differential was specifically chosen because of the increases in excess pore water pressure that occur during undrained testing. During undrained testing, the pore water pressure inside the membrane increases, causing the effective stresses within the specimen to decrease, and the differential to become negative. If the differential is too low at the onset of the test, when the pore water pressure increases, the membrane may rupture or blister because the lateral constraint provided by the chamber pressure is not large enough.

The specimens were reconsolidated to the vertical effective stress of 137 kPa, which is equivalent to $\sigma'_{test} = \sigma'_m$ = 100 kPa, for at least 30 minutes prior to testing under undrained conditions.

4.5.3 Monotonic Testing Procedures

Monotonic shear tests on Soil A, Soil D and Soil G were performed by both strain and stress control. The strain-controlled loading rate applied was 0.40 mm/min and the stress-controlled loading rate applied was $\Delta\sigma'_d$ = 2.5 kPa/min. Load was increased until the shear strains exceeded 15%. The sampling rate for the monotonic tests was 3 samples/second.

4.5.4 Dynamic/Cyclic Testing Procedures

Cyclic tests were performed by applying a stress-controlled sinusoidal loading to the soil specimens at a loading frequency of 0.005 Hz for the majority of the tests, and a faster loading frequency of 1 Hz for loading rate comparisons. Sampling rates were chosen for 50 samples per cycle. The sampling rates for tests performed at loading frequencies 0.005 Hz and 1 Hz were 15 samples/min and 50 samples/second, respectively.

The loading amplitude was characterized in terms of the Cyclic Stress Ratio (CSR) which for the simple shear tests is the ratio of the horizontal shear stress, τ_h, to the initial vertical effective stress, σ'_{vi}. The soil specimens were cyclically loaded until shear strains in excess of 10% single amplitude were reached.

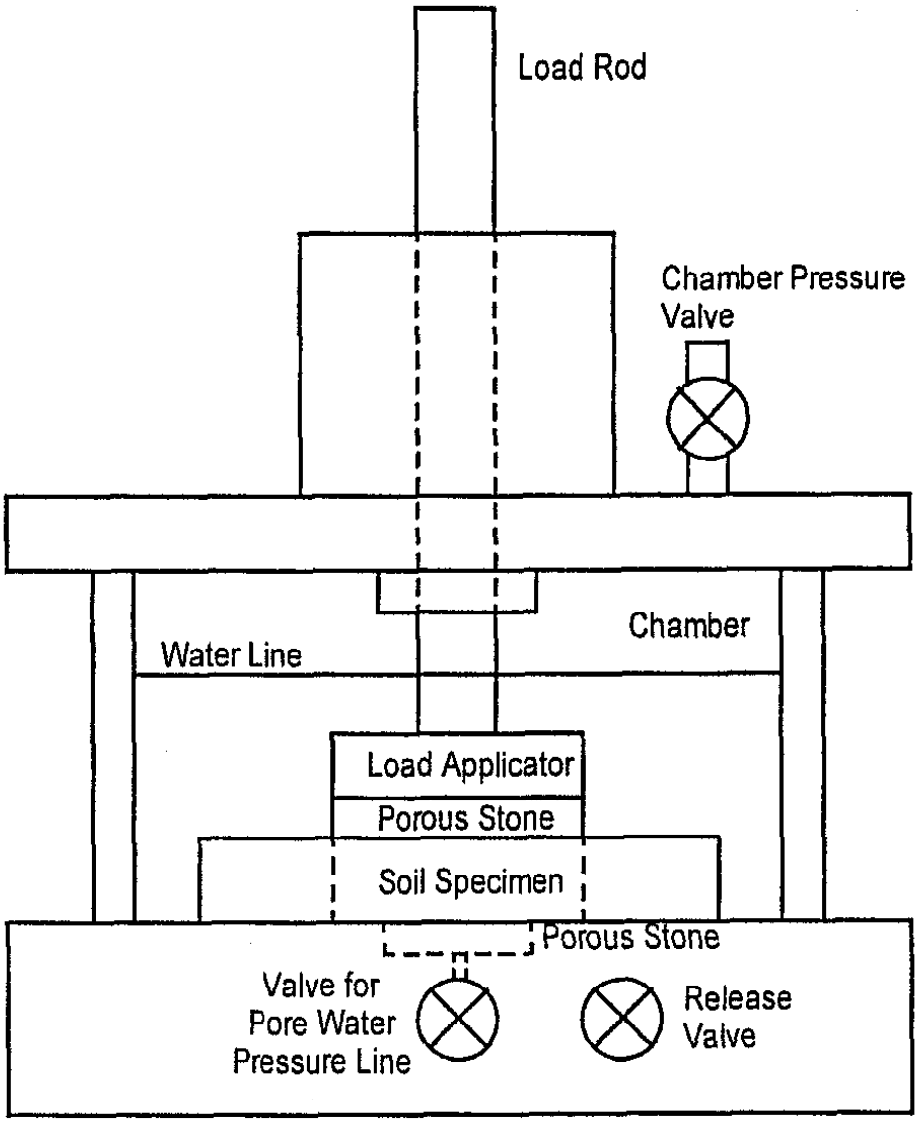

Figure 4.1 Front elevation of the cell used for constant rate of strain consolidation (from Sancio 2003).

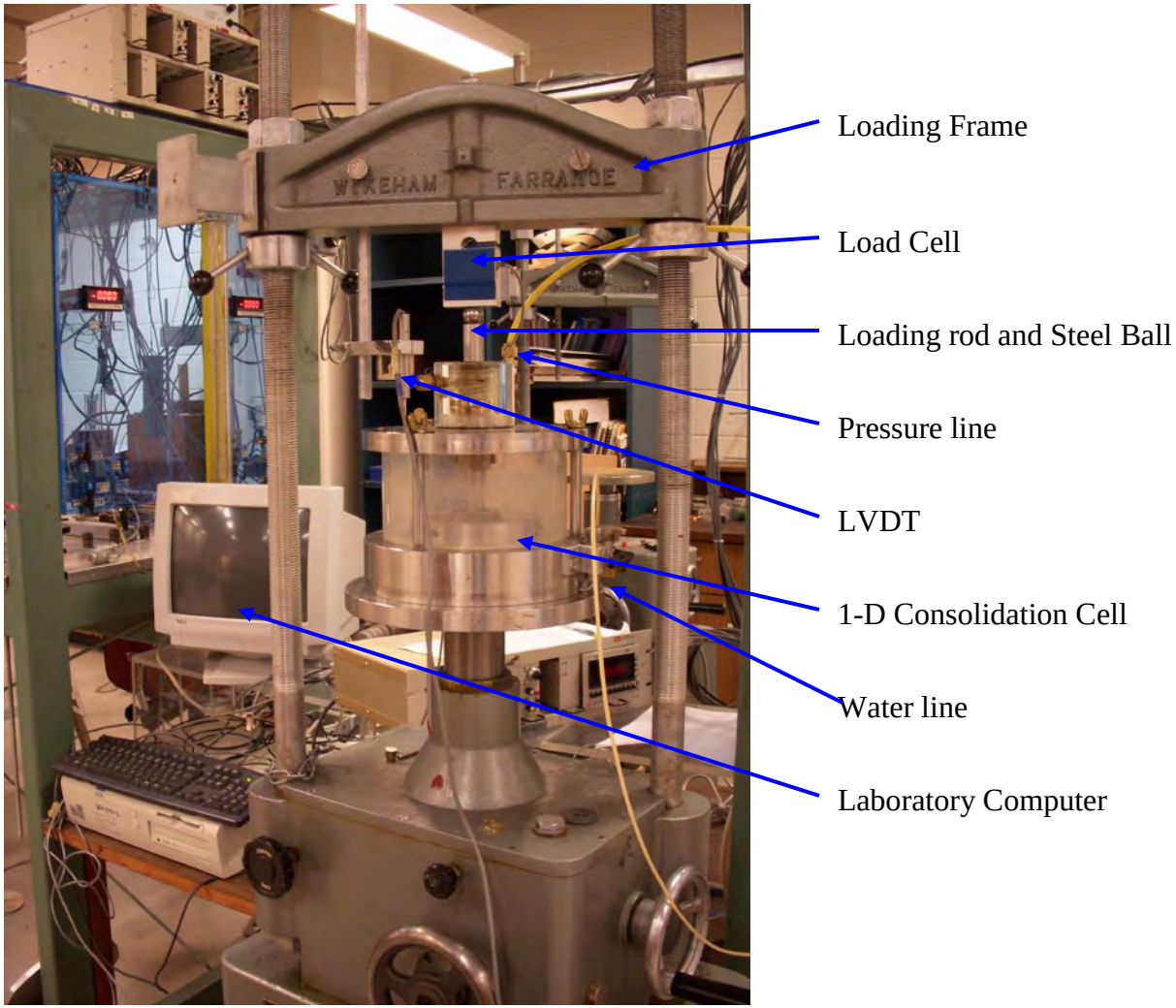

Figure 4.2 Layout for the constant rate of strain consolidation test.

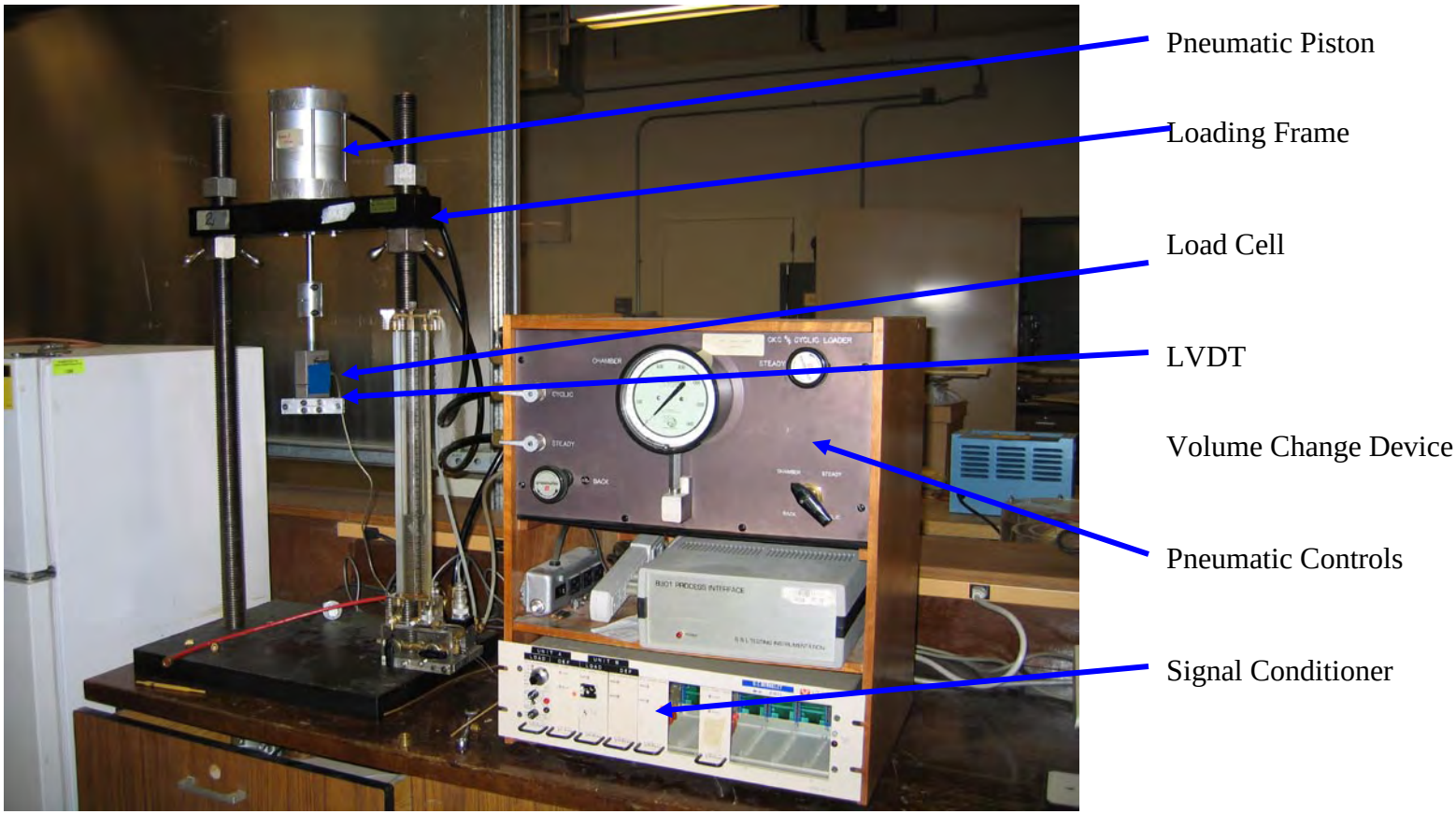

Figure 4.3 Automated Triaxial Testing System.

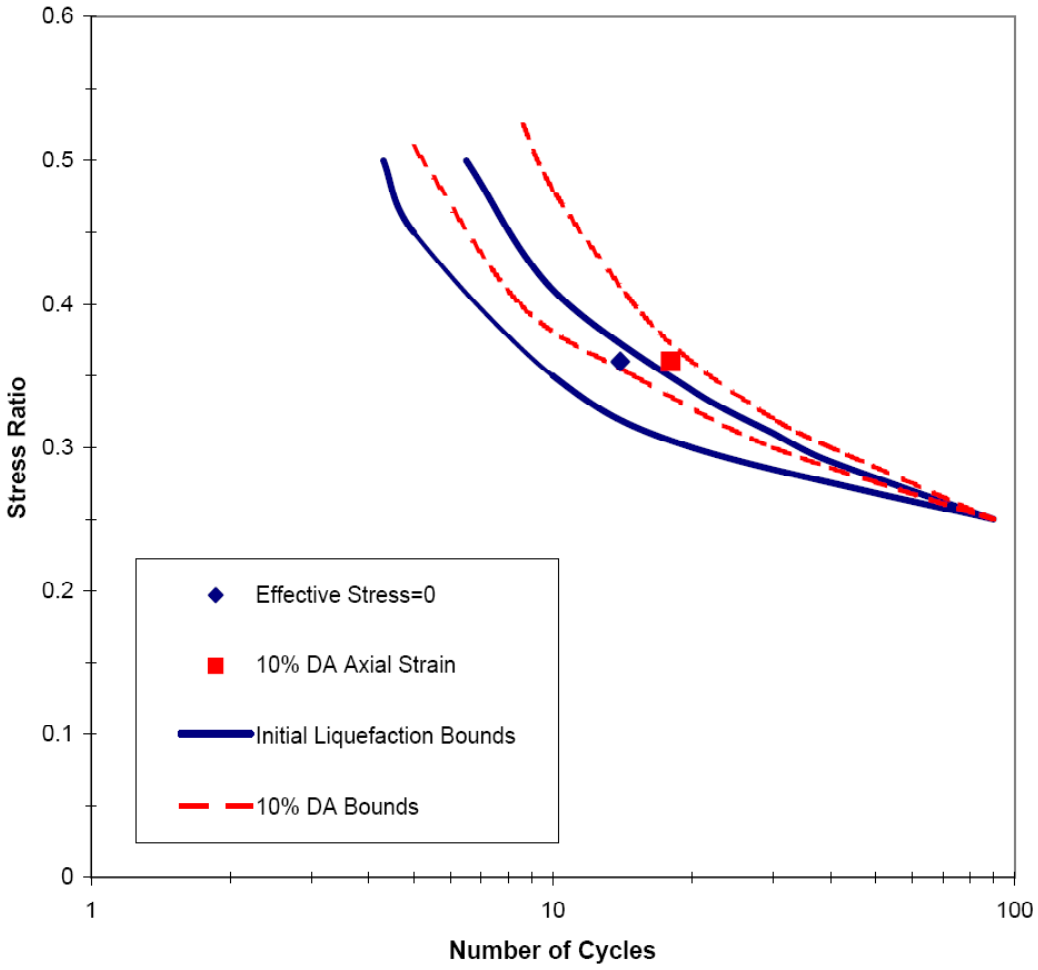

Figure 4.4 Comparison of the results obtained by through this research and the trends found by Silver et al. (1976) for cyclic triaxial tests on Dr = 60% specimens of Monterey #0 sand tested at a confining stress of 100 kPa.

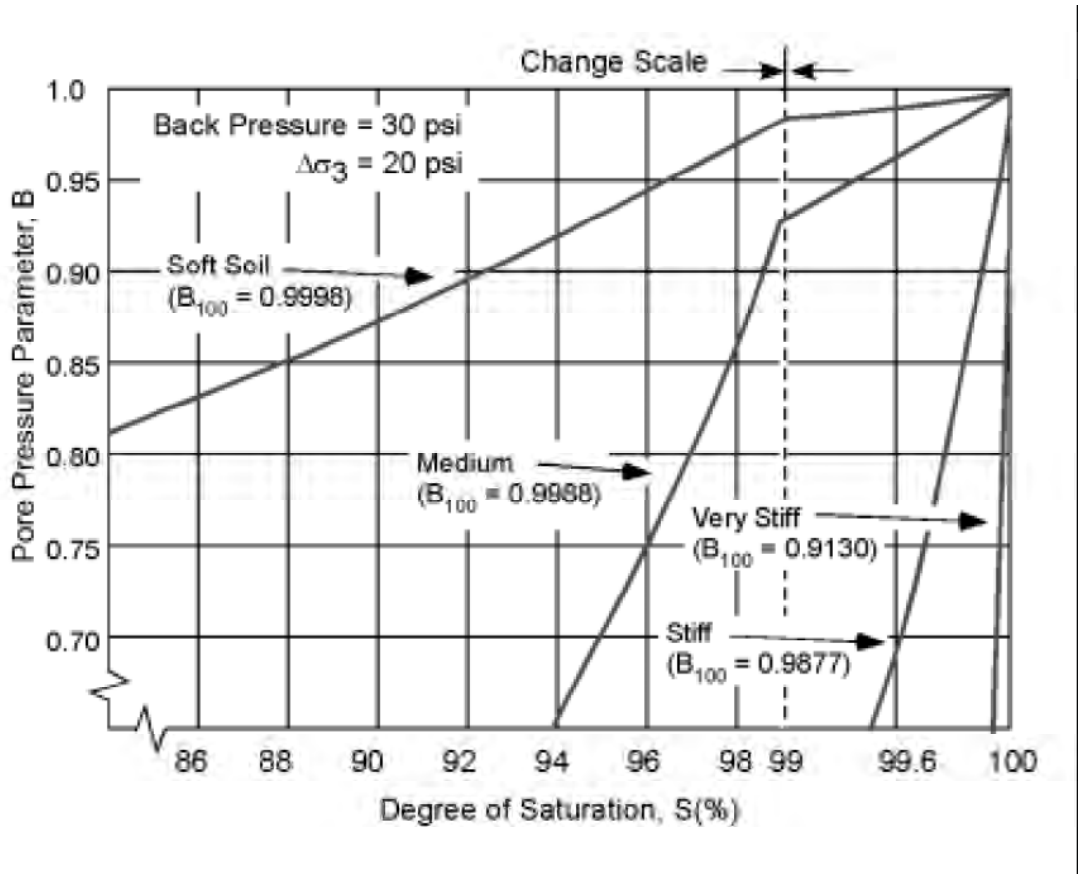

Figure 4.5 Relationship between B-values and degree of saturation, after Black and Lee (1973).

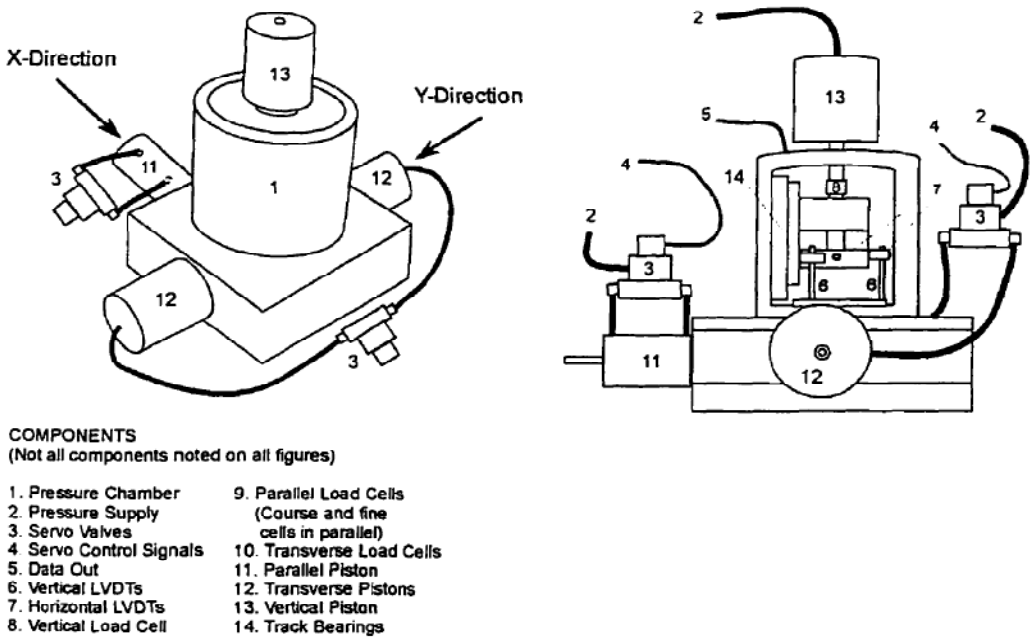

Figure 4.6 Schematic of the Bi-directional simple shear device (from Biscontin 2001).

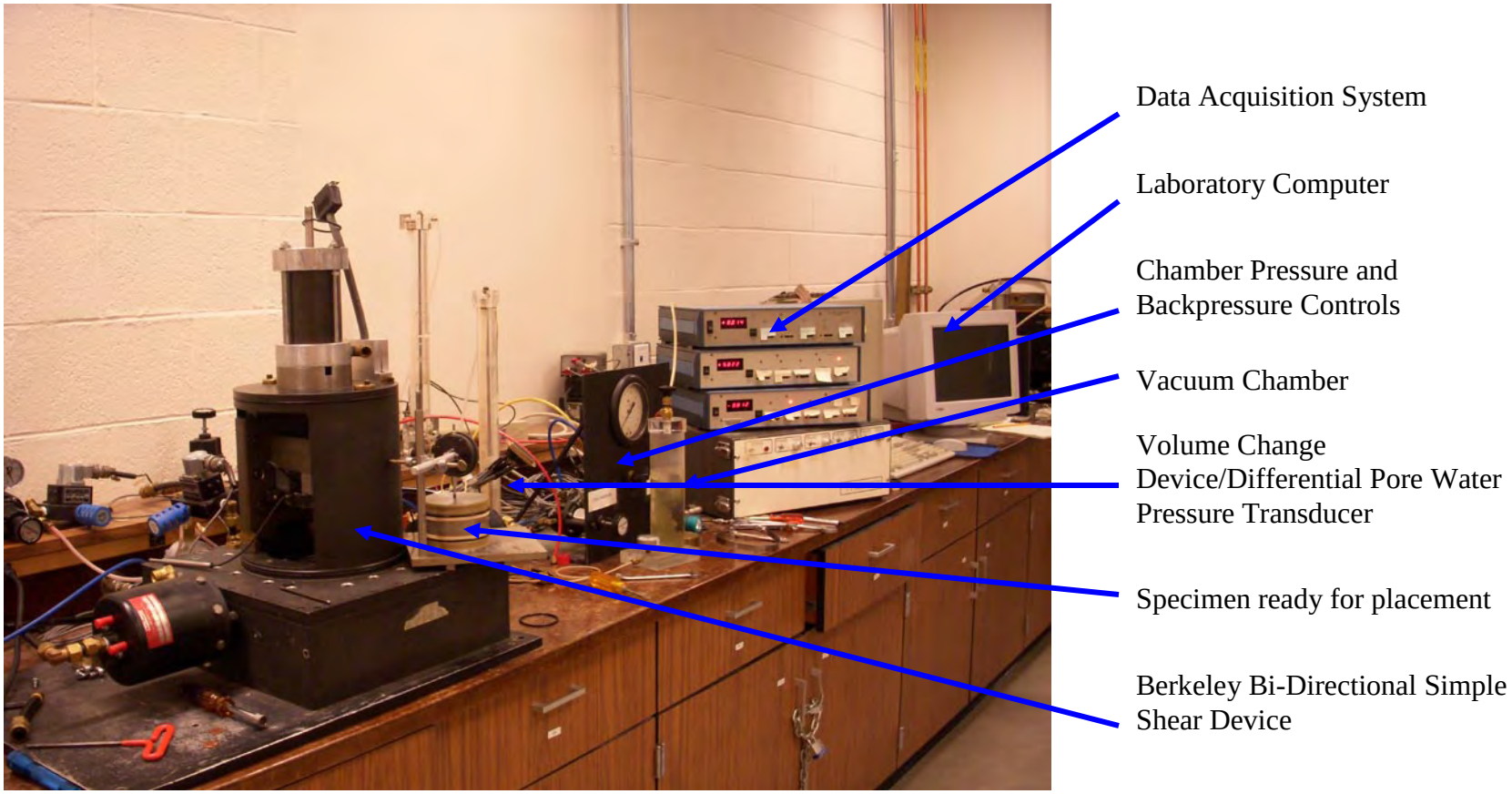

Figure 4.7 The UC Berkeley Bi-directional simple shear device.

Chapter 5 SOIL CHARACTERIZATION AND STATIC SOIL RESPONSE

5.1 Introduction

In this chapter, the laboratory tests performed at the UC Berkeley geotechnical laboratory are presented to investigate the static stress-strain relationships of the reconstituted fine-grained soils from Adapazari, Turkey. The laboratory testing program was designed so that a number of variables, such as reconstitution method, effective confining stress, soil index properties, loading rate, and time under confinement could be studied. The results are interpreted and discussed to develop the context for the cyclic experiments described in Chapter 6.

5.2 Grain Size Analysis

Characterization tests were performed on each of the seven batched soils. The samples were taken from the batched material as described in Chapter 2 and subjected to hydrometer and sieve analysis. Using the criteria for sand, these soils would be classified as well graded as seen in Figure 5.1. Some of the gradation curves do cross each other indicating that each soil has an independent composition. This means that the percentage of clay content, or particles finer than 2 μm, is not solely dependent on the Fines Content, commonly referred to as the particles finer than 75 μm. The ratio of particles finer than 75 μm to 2 μm is different for each of the materials. This relationship also appears independent of Plasticity Index (PI). Although Soils B through F all share ratios between 6.1 and 7.7, Soils A and G exhibit values on the extreme ends of the spectrum at 13.1 and 5.1, respectively. These differences in gradation may explain systematic differences between the two soils during monotonic and cyclic testing.

Table 5.1 Index Properties for Soils A through G from grain size analysis and Atterberg Limits

Soil Name	PI	LL	D_{10} (μm)	D_{30} (μm)	D_{60} (μm)	C_u	C_c	% of Particles < 75 μm	% of Particles < 2 μm	Ratio 75 μm / 2 μm
A	2	31	2.8	21.8	62.7	22.6	2.72	72%	5.5%	13.1
B	5	32	2.0	21.0	48.5	24.2	4.53	77%	10.0%	7.7
C	5	32	1.3	15.4	30.0	22.4	5.90	88%	13.5%	6.5
D	11	38	1.8	8.4	21.5	11.9	1.81	94%	12.0%	7.8
E	14	39	1.1	6.5	21.1	19.2	1.82	95%	15.5%	6.1
F	7	28	4.4	32.9	80.0	18.3	3.10	57%	7.5%	7.6
G	10	31	1.3	12.3	42.6	31.7	2.66	77%	15.0%	5.1

PI = Plasticity Index; LL = Liquid Limit

D_{10} = diameter for 10% finer by weight

C_u = coefficient of uniformity; C_c = coefficient of curvature

These results place the soils firmly in the "high fines content" category. Few researchers have thoroughly studied liquefaction in soils with a fines content higher than 60%. A majority of the research has centered on studying the effects of adding 0 to 45% fines to clean sands. Recently more researchers have begun studying the effects of soils primarily composed of high fines contents (e.g., Romero, 1995; Yasuhara et al., 2003; Sancio, 2003; Bray and Sancio, 2004a, 2004b, 2006; Wijewickreme and Sanin, 2004; Wijewickreme, Sanin, and Greenway, 2005; Boulanger and Idriss, 2004, 2006).

5.3 Constant Rate of Strain Consolidation Tests

Constant rate of strain consolidation tests were performed on each of the seven soils to obtain continuous curves of one-dimensional consolidation. These curves plot void ratio as a function of vertical effective stress, otherwise known as "e – log P" curves. All samples were constructed using the Slurry Deposition Method.

All tests were performed with loading and unloading rates to allow for pore water pressure dissipation as per ASTM D 4186. The loading rate was 0.03048 mm/min and unloading rate was 0.006096 mm/min. Given the slow nature of the tests, the coefficient of consolidation, c_v, could not be determined.

Figure 5.2 presents the e – log P relationship for a test performed on Soil G (PI = 10, LL = 31). As described in Section 4.2, the e – log P curve is typically used to find the preconsolidation pressure, P'_P, of the field specimen. Since all specimens were constructed using the Slurry Deposition Method, all specimens were in virgin compression at the start of the test sequence. There was minimal initial reconsolidation, which is atypical of what is observed for field specimens. For this reason, each specimen was subjected to two unloading cycles in order to evaluate the recompression index, C_r.

Table 5.2 lists the void ratio and consolidation characteristics of each of the soil samples. From the test results, the initial void ratio roughly increases with increasing PI. Soil E has the highest initial void ratio, 1.31, while Soil A has the lowest void ratio, 0.90.

Interestingly, some soils, such as Soil A and Soil G have similar initial void ratios, yet different PIs. This may be explained by the lower fines content (both finer than 75 μm and 2 μm) of Soil A relative to Soil G. It is certainly possible that the clay particles in Soil G are largely infilling what would otherwise be voids in the silt fabric. This may be particularly true for a totally remolded and dispersed soil fabric.

Table 5.2 Index properties and consolidation parameters as a result of the interpretation of constant rate of consolidation test.

Specimen	PI	LL	% of Particles < 75 μm	% of Particles < 2 μm	e_o	C_c	C_r	C_c/C_r
A	2	31	72%	6%	0.90	0.103	0.025	4.2
B	5	32	77%	10%	1.01	0.116	0.017	6.7
C	5	32	88%	14%	1.08	0.143	0.017	8.5

D	11	38	94%	12%	1.19	0.179	0.013	14.0
E	14	39	95%	16%	1.31	0.215	0.023	9.2
F	7	28	57%	8%	0.97	0.087	0.017	5.2
G	10	31	77%	15%	0.94	0.127	0.011	11.3

PI = Plasticity Index; LL = Liquid Limit; e_o = initial void ratio;
C_c = compression index; C_r = recompression index

There is a direct correlation between the compression index, C_c and the percentage of particles finer than 75 μm. As the particles finer than 75 μm increases, so does C_c. Interestingly, there does not appear to be a relationship between C_c and the particles finer than 2 μm.

Likewise, there does not appear to be a direct relation between the recompression index, C_r and the other index properties. A loose correlation is seen between the ratio of C_c to C_r and the percentage of particles finer than 2 μm. As the percentage of particles finer than 2 μm increases, the C_c/C_r ratio roughly increases.

The above-described relationships between each of the soils are shown in Figure 5.3 and Figure 5.4. Soils are grouped in increasing order of PI. From Figure 5.3, although Soil C has a low PI, it has a considerably higher Fines Content (percentage of particles finer than 75 μm) when compared to the other soils in this group. The PIs of Soils B and C are the same, and from the relationship of PI to void ratio previously discussed, the two soils have similar initial void ratios. However, Soil C has a higher percentage of particles finer than 75 μm, and from previously drawn relationships, a higher compression index, C_c. This explains why the shape of the consolidation curve for Soil C is different from the other three curves.

5.4 Consolidation Tests

The main purpose of consolidation tests is to gain insight into primary consolidation, secondary consolidation, and settlement characteristics. Using these characteristics will lead to valuable information needed for future monotonic and cyclic tests. For instance, the parameter "$4t_{50}$", or four times the time required for 50% consolidation, is used to define the minimum time to failure needed for proper pore water pressure equilibration during a monotonic test. This same parameter was used in cyclic testing to identify the time needed for each ¼ cycle of a cyclic test. Thorough consolidation testing is required to ensure future monotonic and cyclic tests reliably measure the pore water pressures and effective pressures.

Measuring the coefficient of consolidation, c_v, is critical for monotonic and cyclic testing. The coefficient of consolidation, c_v, was calculated using Equation 5.1.

$$\mathbf{c_v} = \frac{T_{50} * D^2}{t_{50}} \qquad \mathbf{5.1}$$

where T_{50} = time factor for 50% consolidation and is equal to 0.196, D = length of the drainage path, or H/2 for doubly drained specimens, and t_{50} is found using Casagrande's Logarithm of Time Fitting Method.

Another form of evaluating the coefficient of consolidation is the Taylor's Square Root of Time Fitting Method (1948). After evaluating a few specimens, it was found that the values of c_v were similar for each method. As an example, the consolidation curve for specimen Pluv A13 was evaluated using both methods. Figure 5.5 illustrates the differences in the two methods. In the Casagrande method, t_{50} was found to be 15 seconds resulting in a c_v of 0.016 cm^2/sec. Using the Taylor method, t_{90} was 8.2 seconds and a c_v was calculated to be 0.016 cm^2/sec. For this research, the Casagrande Logarithm of Time Fitting Method proved to be more straightforward and expedient. In addition, the term t_{50} is regularly used in other applications, so calculating this value up front proved convenient.

5.4.1 Triaxial Tests

Prior to each triaxial test, either monotonic or cyclic, specimens were consolidated from an initial state to the final effective isotropic stress. Table 5.3 lists the consolidation properties of each triaxial test. Table 5.3 and all future tables will be color-coded for ease in comparing the separate soils types. For instance, all Soil A tests will be light yellow in color.

Table 5.3 Summary of index properties and characteristics of consolidation for triaxial tests

Test Name	Type of Consol	PI	LL	σ'_i (kPa)	σ'_f (kPa)	e_f	Vol. Strain (%)	t_{50} (sec)	c_v (cm^2/s)
Mono A	Initial	2	31	30	100	0.76	1.7	18	0.438
Mono G	Initial	10	31	31	100	0.58	1.6	200	0.036
Triax G 3	Initial	10	31	37	50	0.69	0.3	600	0.014
Triax G 5-1	Initial	10	31	37	50	0.74	0.5	1000	0.021
Triax G 5-2	Post-cyclic	10	31	50	50	0.71	2.8	250	0.082
Triax G 5-3	Post-cyclic	10	31	50	50	0.68	4.8	410	0.050

PI = Plasticity Index; LL = Liquid Limit;
σ'_i = initial isotropic effective stress; σ'_f = final isotropic effective stress;
e_f = final void ratio; Vol. Strain = maximum Volumetric Strain
t_{50} = time required for 50% consolidation; c_v = coefficient of consolidation

5.4.1.1 Effects of Soil Index Properties

From Table 5.3, it is evident that large differences exist in consolidation properties between Soil A and Soil G. Though the maximum volumetric strains are similar between the two monotonic tests, Mono A and Mono G, the shape of the volumetric curves, shown in Figure 5.6, are quite different. This means the parameter, t_{50}, will be different and thus, the parameter, c_v. The coefficient of consolidation, c_v, for initial consolidation is 19 times greater for Soil A than for Soil G.

5.4.1.2 Post-Cyclic Reconsolidation to Initial Stress State

Tests Triax G 5-1, Triax G 5-2 and Triax G 5-3 were cyclic tests in which the specimens were loaded to 10% double amplitude axial strain, then allowed to reconsolidate to the initial stress state prior to the next phase of cyclic testing. Reconsolidation results from Triax G 5-2 and Triax G 5-3 show greater volumetric and axial strains than any of the other tests performed on Soil G. Figure 5.7 illustrates the differences in volumetric strain between these tests and the initial consolidation.

The volumetric strain in the first post-cyclic consolidation is nearly 7 times greater than the average initial consolidation strain. The maximum volumetric strain between the first and second post-cyclic consolidation increases by nearly 2 times. The coefficient of consolidation, c_v, for post-cyclic consolidation is also 3-5 times larger than the initial consolidation.

5.4.2 Simple Shear

Consolidation data was gathered on each soil and each reconstitution method prior to simple shear cyclic or monotonic testing.

Table 5.4 represents the consolidation characteristics of specimens reconstituted using the Slurry Deposition Method, or SDM. The consolidation characteristics of SDM B1 are not presented below due to an error at the beginning of consolidation.

Table 5.4 Summary of index properties and consolidation characteristics for specimens built using the Slurry Deposition Method

Test Name	PI	LL	σ'_{vi} (kPa)	σ'_{vf} (kPa)	e_f	ε_a (%)	t_{50} (sec)	c_v (cm^2/s)
SDM A1	2	31	65	139	0.69	1.08	4.5	0.040
SDM A2	2	31	63	132	0.70	0.94	7.5	0.027
SDM C1	5	32	65	142	0.70	0.85	12	0.019
SDM D1	11	38	66	138	0.76	1.46	18	0.012
SDM E1	14	39	63	142	0.80	2.46	50	0.004
SDM F1	7	28	62	138	0.81	0.88	4	0.064
SDM G1	10	31	51	141	0.63	1.67	5	0.035
SDM G2	10	31	44	143	0.65	1.12	12	0.018
SDM G3	10	31	62	134	0.65	1.12	13	0.016
SDM G4	10	31	66	137	0.66	0.90	7.5	0.023

PI = Plasticity Index; LL = Liquid Limit; σ'_{vi} = initial vertical effective stress;
σ'_{vf} = final vertical effective stress; e_f = final void ratio
ε_a = maximum axial strain; t_{50} = time required for 50% consolidation;
c_v = coefficient of consolidation

Table 5.5 represents the consolidation characteristics of specimens reconstituted using the In-Place Wet Pluviation method.

In Table 5.4 and Table 5.5, axial strain, not volumetric strain, is reported. Initially, the small tube on the volumetric device was split and at a medium to high backpressure, the tube would leak. For this reason, the volumetric data for many of the early tests are not reliable. Corrections have been made to simulate the correct volumetric strain, but these are approximations only. In addition, as seen in Appendix A2.2, volumetric measurements were also complicated by the spike in volumetric strain commonly seen at the beginning of consolidation. Once the "A valve" was opened, several seconds were needed for the volumetric transducer to equilibrate. For the reasons given above, the axial strain, not the volumetric strain, is presented in the tables above.

Table 5.5 Summary of index properties and consolidation characteristics for specimens built using In-Place Wet Pluviation

Test Name	PI	LL	σ'_{vi} (kPa)	σ'_{vf} (kPa)	e_f	ε_a (%)	t_{50} (sec)	c_v (cm^2/s)
Pluv A1	2	31	66	140	0.94	1.85	6.5	0.042
Pluv A5	2	31	66	138	0.95	2.12	5.7	0.048
Pluv A7	2	31	59	139	0.93	1.53	8	0.034
Pluv A13	2	31	64	136	0.91	1.07	15	0.016
Pluv A16	2	31	66	133	0.96	1.83	6.5	0.040
Pluv D2	11	38	63	138	0.97	2.9	22	0.013
Pluv D7	11	38	66	136	0.96	2.99	15	0.019
Pluv F1	7	28	66	139	1.02	1.44	2.7	0.104
Pluv G1	10	31	65	142	0.73	1.54	11	0.035
Pluv G2	10	31	67	139	0.85	1.78	6	0.039
Pluv G3	10	31	65	136	0.78	2.68	5.2	0.043
Pluv G4	10	31	64	135	0.82	2.19	12	0.021
Pluv G8	10	31	63	138	0.81	2.27	10	0.024

PI = Plasticity Index; LL = Liquid Limit; σ'_{vi} = initial vertical effective stress;
σ'_{vf} = final vertical effective stress; e_f = final void ratio;
ε_a = maximum axial strain; t_{50} = time required for 50% consolidation;
c_v = coefficient of consolidation

For the case of simple shear specimens tested with wire-reinforced membranes, the volumetric and axial strains are correlated. The use of wire-reinforcement limits increases in lateral dimensions meaning that the area is held constant. If the area is held constant, changes in volume caused by an increase in vertical load can only be represented as changes in height. For this reason, the volumetric strain and axial strain are comparable. More information on testing with constant volume is found in Section 4.5.1.

5.4.2.1 Effects of Reconstitution Method

As reported in Table 5.4 and Table 5.5, the amount of axial strain between the two methods is quite different. The In-Place Wet Pluviated specimens tend to strain, on average, 1.7 times more than the Slurry Deposition Method specimens, over the same change in stress.

The coefficient of consolidation, c_v, is slightly greater in the In-Place Wet Pluviated specimens as compared to the Slurry Deposition specimens. This is shown in Table 5.6 below.

Table 5.6 Comparison of c_v (cm^2/sec) for Slurry Deposition Method and In-Place Wet Pluviation

	Mean c_v (cm^2/sec)	St Dev
SDM A	0.034	0.009
Pluv A	0.036	0.012
SDM D	0.012	-
Pluv D	0.016	0.004
SDM F	0.064	-
Pluv F	0.104	-
SDM G	0.023	0.008
Pluv G	0.033	0.010

The results of these tests indicate that the dispersed fabric of the Slurry Deposition Method may account for the lower initial void ratios and lower coefficient of consolidation. The In-Place Wet Pluviated specimens, with higher void ratios, and striated fabric have the means for greater coefficients of consolidation.

In Table 5.6, the mean and the standard deviations are both shown. Although repeatability and consistency are the goals in making each specimen, variance does exist between specimens within a set.

5.4.2.2 Effects of Soil Index Properties

The index properties directly influence the consolidation response of the soil. This is true regardless of the reconstitution method. As the PI increases, the coefficient of consolidation, c_v, decreases as shown in Figure 5.8. This is true for all soils, except for Soil F (PI = 7, LL = 28). The c_v for Soil F is much greater than all other soils. This trend may be explained by the considerably lower fines content (particles finer than 75 μm) which is equal to 57%. Soil F also has the greatest D_{10} (diameter for 10% finer by weight) which is equal to 4.2 μm. All other soils in this investigation have a fines content greater than 72% and a D_{10} less than 2.8 μm.

The axial strains in consolidation also tend to increase as PI increases (Figure 5.9). The exception once again is Soil F. The strains in this soil are much lower than expected given the PI. Again, this may be explained by the low fines content and high D_{10}. The c_v and axial strain characteristics are more representative of a typical sand rather than a silt or clay.

5.5 Triaxial Undrained Monotonic Tests

The purpose of performing triaxial static tests includes the need to study the strength of the soil prior to cyclic loading and to compare these results with static tests performed using the simple shear device.

One important issue that should be addressed when performing triaxial tests on silty and clayey soils is the rate at which the load will be applied. Due to the use of frictional ends, stress concentrations exist at the ends and non-uniformity of strain occurs along the specimen. This deviates from the assumption that the specimen is a simple homogeneous element of soil. Frictional ends may cause an exacerbation of strain rate effects due to non-uniformity of water content throughout the specimen, particularly for dilative soils (Germain and Ladd, 1988). Lee (1977) found that the effect of frictionless ends on the undrained strength of Sacramento River sand at a relative density of 78% was an increase of about 20% in strength. This increase in strength is directly related to the accentuated dilative tendency that is observed in tests performed using frictionless ends.

Given that pore water pressure measurements were taken at the ends of the specimen and that filter paper was not used to reduce the length of the drainage path, equilibration of excess pore water pressures within the specimen was attempted for static tests by performing the tests at a slow rate of loading. As stated in Section 5.4, the proper loading rate to ensure 95% pore water pressure equilibration in an undrained test, the minimum time to failure, t_f, is at least four times greater than t_{50} in undrained tests, where t_{50} is the time needed to reach 50% of consolidation (Germaine and Ladd, 1988, after Bishop and Henkel, 1957).

From Table 5.3, values of t_{50} and c_v are presented for Soils A and G. Although t_{50} values from previous tests are important to establish trends, these values are solely dependent on the dimensions, most importantly, the height of the specimen. The heights for each of the monotonic and cyclic triaxial specimens are slightly different. When testing field specimens, the height and diameter are largely controllable because the specimen is trimmed prior to enveloping in a membrane and testing. For Slurry Deposition Specimens the diameter is relatively fixed due to the mold, but the height will depend on the amount of material placed in the mold, which may vary by a few grams between tests.

For these reasons, it is important to establish t_{50} for each individual consolidation test to calculate c_v. The height of the specimen will change during the course of consolidation, meaning that the parameter D from Equation 5.1 will also change. Using the calculated c_v and new D, a revised t_{50} can be used for monotonic or cyclic testing.

Monotonic triaxial tests were performed on Soils A and G. The monotonic loading was applied by stress control. The mean c_v for Soils A and G are 0.438 cm^2/sec and 0.024 cm^2/sec, respectively. Based on this rate, it was determined that a loading rate of 1 kPa/min would meet the requirements for proper measurement of effective stress and pore water pressures as discussed above.

When possible, the friction angle is also used for comparisons. To evaluate the shear strength of soil, the complete state of stress at failure must be known. For triaxial testing, the Mohr-

Coulomb failure criterion can be expressed in terms of principal stresses at failure and is shown in Equation 5.2.

$$\sin \phi' = \frac{(\sigma'_{1f} - \sigma'_{3f})}{(\sigma'_{1f} + \sigma'_{3f})} \qquad \textbf{5.2}$$

From Equation 5.2, ϕ' is the mobilized friction angle, σ'_{1f} is equal to the deviator stress at failure (q_f) plus the effective confining stress at failure, σ'_{3f}.

Both Soils A and G would exhibit pronounced dilative tendencies if the tests were under drained conditions. For both soils, the excess pore water pressures initially increase up to a given strain, which is followed by the generation of negative pore water pressures accompanied by strain hardening. For Soil A, after ε_a = 0.88% the strength increases linearly with strain at an approximate rate of 2.8 kPa/% strain. The maximum deviator stress (q) of 125 kPa was reached at 11% axial strain. The effective friction angle (assuming c' = 0) is 37°.

For Soil G, after ε_a = 0.5% the strength increases linearly with increasing strain at an approximate rate of 10.3 kPa/% strain. The maximum deviator stress (q) of 244 kPa was reached at 8.2% axial strain. The effective friction angle (assuming c' = 0) is 39°.

Test results are provided in Table 5.7. In the table, the undrained strength, s_u, defined as $s_u = q/2$, is given for axial strains equal to 1%, 3%, 5%, and 10%, respectively. The maximum obliquity (σ'_1/σ'_3-max) and the resulting peak friction angle are also listed.

Table 5.7 Summary of total and effective strength parameters for the undrained monotonic triaxial tests

Test Name	PI	LL	σ'_3 (kPa)	e_o	s_u (1% ε_a) (kPa)	s_u (3% ε_a) (kPa)	s_u (5% ε_a) (kPa)	s_u (10% ε_a) (kPa)	σ'_1/σ'_3	ϕ' (○)
Mono A	2	31	100	0.76	35	41	46	60	4.04	37
Mono G	10	31	100	0.58	46	67	88	-	4.65	39

PI = Plasticity Index; LL = Liquid Limit; σ'_3 = initial isotropic effective stress;
e_o = initial void ratio; s_u (1% ε_a) = undrained shear strength at 1% axial strain;
σ'_1/σ'_3 = maximum obliquity; ϕ' = mobilized friction angle

It should be noted that the initial void ratio for Soil G during this monotonic test is much lower than for specimens created for cyclic triaxial tests on this material. During construction of the specimen, the top cap and porous stone where caught in the mold and the specimen did not properly consolidate at first. The top cap and porous stones were repositioned and the specimen was allowed to consolidate once again. This sequence has lead to a lower void ratio in comparison to the cyclic triaxial tests. This may also explain the increased friction angle and strength profile in relation to Soil A. Figure 5.10 illustrates these points.

It is recommended that additional monotonic tests are performed on both soils to gain further insight into the static strength characteristics. These additional tests should be performed at different densities and different loading rates. The loading rate of each test was 1 kPa/min, as previously stated. Given the strength profiles and c_v for the material, the loading rates could be significantly increased. Sancio (2003) found that the rate of loading directly affects the stress-strain relationship. He found that increasing the loading rate from 0.02% strain/min to 1% strain/min could increase the strength by up to 21% at $\varepsilon_a = 1\%$. Although rate dependency is not expected to significantly affect low PI materials, additional testing may be required. In addition, Soils B through F should also be tested for a full range of strength profiles.

5.6 Simple Shear Undrained Monotonic Tests

A laboratory testing program for monotonic tests performed on the simple shear device was developed to assess the strengths of Soils A and G. The testing program was designed to first establish a baseline condition. Subsequent tests had systematically different testing conditions to observe possible variations in response. These conditions include changes in time under confinement, density, overconsolidation ratio (OCR), and effective confining pressure. The shear stress on the horizontal plane at 1%, 3%, 5%, 10%, and 15% shear strain (γ) are used in comparing results from different tests.

In most simple shear testing devices, only the vertical normal stress and horizontal shear stress can be effectively measured if wire-reinforced membranes are used to ensure K_o conditions. The complete state of stress on the specimen is unknown and assumptions must be made to calculate values of principal stresses, and related parameters such as the mobilized friction angle. There are at least three different methods of interpreting the effective friction angle for such simple shear results:

1) the horizontal plane is the plane of maximum obliquity,
2) the horizontal plane is the plane of maximum shear stress, or
3) the vertical plane is the plane of maximum obliquity

For this research, the first method will be used to evaluate the friction angle. This method was chosen because it is an accepted technique first published by Ladd and Edgers (1972) and popularized by Wroth (1984). In a simple shear test using wire-reinforced membranes, only the effective stresses on the horizontal plane can be effectively measured. This method of determining the friction angle assumes the failure occurs along the horizontal plane, not a vertical or angled plane. Previous researcher (e.g., Biscontin, 2001; Kammerer, 2002; Wu, 2002; Anantanavanich, 2006) have used this method of determining the friction angle when using the Berkeley Bi-directional simple shear device with NGI-type wire-reinforced membranes.

The resulting Mohr's circle depiction of the state of stress at failure is shown in Figure 5.11. As stated above, for this method, the horizontal plane is assumed to be the failure plane. The Mohr-Coulomb failure envelope is tangent to the Mohr circle at τ_f, where τ_f is the shear stress at failure. In the equation below, σ'_{vf} is the vertical effective stress at failure. Calculation of ϕ' based on the assumption that the horizontal plane is the failure plane, results in a lower estimate of the effective friction angle of the soil than some other plausible assumptions. The mobilized friction angle, ϕ', is given in Equation 5.3.

$$\tan \phi' = \frac{\tau_f}{\sigma'_{vf}} \qquad \textbf{5.3}$$

In many of the tests, the specimens did not develop negative excess pore water pressures, or proceed along the failure envelope. The lack of a distinct failure state made the determination of the friction angle difficult to find, especially for the In-Place Wet Pluviated specimens. For these cases, the friction angle is evaluated using the measured shear stress at a limiting strain of γ = 20%, $\tau_{\gamma = 20\%}$, not τ_f. The friction angles found using this method are denoted with an "*" in Table 5.8 and Table 5.12.

Most tests were consolidated and then tested once the specimen was adequately saturated to a B-value of at least 0.96. The loading rate of the undrained monotonic test is as important in the simple shear tests as in the triaxial tests. For this reason, the determination of the coefficient of consolidation, c_v, by the methods described in Section 5.4, is crucial to applying the correct loading rate.

In the following tables, both σ'_{vo} and σ'_m will be presented. σ'_m is calculated as:

$$\sigma'_m = \frac{(\sigma'_1+\sigma'_2+\sigma'_3)}{3} = \frac{(\sigma'_v+2K_o*\sigma'_v)}{3} \qquad \textbf{5.4}$$

where σ'_1, σ'_2, σ'_3, are the effective stresses on the principal axes, σ'_v is the vertical effective stress and K_o is the coefficient of lateral earth pressure at rest. K_o was assumed to equal 0.6 from previous work by Sancio (2003) on similar soils.

To date, few monotonic tests have been performed on low plasticity silts and clays. For this reason, it is difficult to compare the results of this body of work to others. The intention of these tests is to lay a framework not only for the pending cyclic tests, but also to develop a database of experimental results upon which to characterize silty soils.

5.6.1 Slurry Deposition Method

Six specimens were prepared for monotonic testing using the Slurry Deposition Method. The strength parameters of the six specimens are shown in Table 5.8 These specimens varied by soil type, time under confinement and method of loading.

5.6.1.1 Effects of Soil Index Properties

From Table 5.8, it is clear that SDM A specimens exhibit greater strength characteristics than SDM G specimens based on maximum shear stress on the horizontal plane, τ_h, and friction angle, ϕ'.

To compare the effects of soil index properties, two specimens, one Soil A and one Soil G, were tested in an identical manner, i.e., same time under confinement, effective confining pressure, and B-value. Both specimens were tested using strain control. Parameters of the specimens tested are listed in Table 5.9.

Table 5.8 Summary of total and effective strength parameters for the monotonic undrained simple shear tests on Slurry Deposition Method specimens

Test Name	PI	LL	σ'_{vo} (kPa)	σ'_{m} (kPa)	e_o	τ_h (1% γ) (kPa)	τ_h (3% γ) (kPa)	τ_h (5% γ) (kPa)	τ_h (10% γ) (kPa)	τ_h (15% γ) (kPa)	ϕ' (○)
SDM A2	2	31	132	97	0.70	25	34	40	48	54	28*
SDM A3	2	31	137	101	0.70	31	37	43	58	72	31
SDM A9	2	31	137	100	0.72	29	36	40	52	65	31
SDM G2	10	31	142	104	0.65	26	35	40	48	52	26*
SDM G3	10	31	134	98	0.65	26	35	40	47	53	27
SDM G4	10	31	137	100	0.66	26	31	34	41	46	26*

PI = Plasticity Index; LL = Liquid Limit; σ'_{vo} = initial vertical effective stress;
σ'_{m} = mean effective stress ($\sigma'_{m} = (\sigma'_{1} + \sigma'_{2} + \sigma'_{3})/3$); e_o = initial void ratio;
τ_h (1% γ) = shear stress on the horizontal plane at 1% shear strain;
ϕ' = mobilized friction angle; "*" = mobilized friction angle using shear stress at a limiting strain of 20%

Table 5.9 Specimen parameters and monotonic testing conditions for Soils A and G prepared using the Slurry Deposition Method

Test Name	PI	LL	FC (%)	σ'_{vo} (kPa)	σ'_m (kPa)	e_o	B-Value	w_c (%)	w_c/LL	Days
SDM A2	2	31	72	132	97	0.70	0.99	25.99	0.84	0.04
SDM G3	10	31	77	134	98	0.65	0.99	24.21	0.78	0.04

PI = Plasticity Index; LL = Liquid Limit;
FC (%) = Percentage of particles finer than 75 μm; σ'_{vo} = vertical effective stress;
σ'_m = mean effective stress ($\sigma'_m = (\sigma'_1 + \sigma'_2 + \sigma'_3)/3$); e_o = initial void ratio;
B-Value = Black and Lee (1973) saturation relationship, w_c (%) = water content;
w_c/LL = ratio of water content to Liquid Limit; Days = time under confinement

Figure 5.12 represents graphically the two aforementioned tests. The two tests are strikingly similar. Note however that the void ratios given in Table 5.9 are quite different. Again, the void ratio of Soil G is much lower than Soil A, yet the results for the monotonic test under a short duration in time under confinement, yield comparable results.

Unlike Soil A, Soil G was never monotonically tested at a confinement time of 0.8 days. It is believed that this would be a better time under confinement condition in which to do a comparison between the two soils.

5.6.1.2 Effects of Time Under Confinement

Soil A was subjected to monotonic testing at different times of confinement. All other parameters such as initial vertical effective stress and overconsolidation ratio (OCR) were held constant. Both specimens were tested using strain control. Table 5.10 and Figure 5.13 give the numerical and graphical details of these tests.

Table 5.10 Specimen parameters and monotonic testing conditions of Soil A prepared using the Slurry Deposition Method and tested at different times under confinement

Test Name	PI	LL	FC (%)	σ'_{vo} (kPa)	σ'_m (kPa)	e_o	B-Value	w_c (%)	w_c/LL	Days
SDM A2	2	31	72	132	97	0.70	0.99	25.99	0.84	0.04
SDM A3	2	31	72	137	101	0.70	0.96	26.21	0.85	0.88

By increasing the time under confinement by greater than an order of magnitude, the maximum shear stress increases by 38%. However, the void ratio and water content tend to be nearly the same between the tests.

Seed (1979) found that identical sand samples subjected to sustained loads for periods ranging from 0.1 day to 100 days prior to testing exhibited increases in cyclic mobility resistance. The results from Figure 5.13 imply that for increases in the period of sustained loading for silty soils there is also an increase in static strength. Although these tests were not cyclic tests, the strength characteristics from the monotonic testing give valuable insight into the cyclic testing results.

As stated in the previous section, Soil G was never monotonically tested at different times under confinement. Future testing on Slurry Deposition Method specimens may include Soils B through F into the study and increasing the time under confinement to 10 and 100 days.

5.6.1.3 Effects of Stress Control vs. Strain Control

Many of the In-Place Wet Pluviated specimens tested under strain control were found to have a "goose neck" shape on the effective stress path; yet the Slurry Deposition Method specimens did not. A "goose neck" shape, illustrated in Figure 5.14, begins as a typical stress path with increasing normalized shear stress and decreasing normalized vertical effective stress. The curve begins to flatten as the specimen nears what could be the failure envelope. Abruptly, the normalized shear stress increases with little decrease in the normalized vertical effective stress. At some point, the normalized vertical effective stress begins to decrease again with little change in shear stress.

It was not known if this phenomenon is internal to the soil and the method of reconstitution by using the In-Place Wet Pluviation Method. One hypothesis for this unusual shape is that the soil fails along a weaker seam in the specimen until a given point. After this, the shear transfers to a stronger layer within the specimen until failure. Another hypothesis is that this is a reflection of a failure in the simple shear device when testing using strain control. For this reason, the Slurry Deposition Method and In-Place Wet Pluviation specimens were subjected to stress-controlled testing. Care was given to ensure the rate of loading conformed to the specifications that failure would occur after $4t_{50}$.

Properties of the Slurry Deposition Method specimens tested are listed in Table 5.11 and both are comparable. Figure 5.15 visually depicts the comparison between the two tests. Both SDM A3 and SDM A9 exhibit only a very minor "goose neck" at the very end of the tests. This occurs at approximately 17% shear strain when the slope of the shear stress begins to decrease or level off.

Table 5.11 Summary of specimen properties and monotonic test parameters for Slurry Deposition Method specimens tested at different loading rates

Test Name	σ'_{vo} (kPa)	σ'_m (kPa)	e_o	Loading Type	Loading Rate	B-Value	w_c (%)	w_c/LL	Days
SDM A3	137	101	0.70	Strain	0.4 mm/min	0.96	26.2	0.85	0.88
SDM A9	137	100	0.72	Stress	2.50 kg/min	0.97	26.8	0.87	0.83

The effective stress path and shear stress – shear strain curves for SDM A3 and SDM A9 are similar. Although the strain-controlled test generated higher ultimate strength than the stress-controlled test, the maximum shear stress on the horizontal plane, τ_h, is very similar at 1%, 3%, and 5% strain, which are important in this study regarding liquefaction. For this reason, it is concluded that for this material, and using this reconstitution method, the loading types, whether strain-controlled or stress-controlled, are interchangeable. Additional tests on Soil G are recommended to determine if the same trends in strength between strain control and stress control are found.

5.6.2 In-Place Wet Pluviation Method

Fifteen specimens were prepared for monotonic testing using the In-Place Wet Pluviation Method. The strength parameters of the fifteen specimens are shown in Table 5.12. These specimens varied by soil type, time under confinement, and method of loading.

To evaluate if the In-Place Wet Pluviation Method is a repeatable and consistent method of reconstitution, two specimens, Pluv A4 and Pluv A4val, were prepared using the same techniques and monotonically tested using strain control in the simple shear device.

From Table 5.12, the shear stress on the horizontal plane for these two specimens from the beginning of the test through 10% shear strain (γ), are quite similar. After 10% strain, the maximum shear stress varies by 10%. However, a majority of studies on liquefaction are not concerned with shear strains greater than 10%, because most failure criterion for silty and clayey soils is generally 5% single amplitude strain using cyclic simple shear.

Although the effective stress paths for specimens Pluv A4 and Pluv A4val from Figure 5.16 are not identical, they are nearly identical through 80% of the initial vertical effective stress. After 80%, the curves diverge in their responses, but they remain similar.

Table 5.12 Summary of total and effective strength parameters for the monotonic undrained simple shear tests on In-Place Wet Pluviated specimens

Test Name	PI	LL	σ'_{vo} (kPa)	σ'_{m} (kPa)	e_o	τ_h (1% γ) (kPa)	τ_h (3% γ) (kPa)	τ_h (5% γ) (kPa)	τ_h (10% γ) (kPa)	τ_h (15% γ) (kPa)	ϕ' (○)
Pluv A2	2	31	212	156	0.93	35	42	47	53	52	23
Pluv A4	2	31	138	101	0.90	26	29	31	34	35	25*
Pluv A4val	2	31	137	101	0.94	27	29	31	35	37	25*
Pluv A5	2	31	141	103	0.95	22	24	25	26	25	24*
Pluv A6	2	31	140	103	0.96	27	28	29	32	34	21*
Pluv A17	2	31	139	102	0.92	30	36	39	44	47	23
Pluv D2	11	38	135	99	0.97	20	23	25	28	30	22*
Pluv D3	11	38	138	101	0.95	27	31	33	34	34	24
Pluv D4	11	38	140	103	0.90	25	33	36	37	38	26*
Pluv G2	10	31	140	103	1.09	22	26	28	28	29	19*
Pluv G3	10	31	136	100	0.78	21	23	23	22	20	19
Pluv G4	10	31	135	99	0.82	22	24	26	30	33	24*
Pluv G5	10	31	138	102	0.76	25	28	29	32	30	22
Pluv G6	10	31	138	101	0.81	23	31	34	37	28	22

PI = Plasticity Index; LL = Liquid Limit; σ'_{vo} = initial vertical effective stress;
σ'_{m} = mean effective stress ($\sigma'_{m} = (\sigma'_{1} + \sigma'_{2} + \sigma'_{3})/3$); e_o = initial void ratio;
τ_h (1% γ) = shear stress on the horizontal plane at 1% shear strain;
ϕ' = mobilized friction angle; "*" = mobilized friction angle using shear stress at a limiting strain of 20%

Table 5.13 Summary of specimen properties and monotonic testing parameters for Pluv A4 and Pluv A4Validation

Test Name	σ'_{vo} (kPa)	σ'_m (kPa)	e_o	B-Value	w_c (%)	w_c/LL	Days
Pluv A4	138	101	0.90	0.96	33.33	1.08	1.10
Pluv A4val	137	101	0.94	0.96	34.80	1.12	1.19

Table 5.13 also lists the specimen properties prior to monotonic testing. The void ratios are not the same for the tests; however, results from the monotonic test prove that these two void ratios will give similar results. From the cyclic testing in Chapter 6, differences in void ratios of this magnitude for normally consolidated Pluviated A specimens do not produce large differences in the responses of the similar soils.

5.6.2.1 Effects of Soil Index Properties

Representative specimens of Soils A, D, and G were subjected to monotonic testing at 0.8 days confinement, using the same preparation technique and same effective confining pressure, $\sigma'_m \approx$ 101 kPa. All tests were performed under strain-controlled loading. The specimen properties are given in Table 5.14 and shown graphically in Figure 5.17.

Table 5.14 Summary of specimen properties and monotonic testing parameters for Soils A, D, and G constructed by the In-Place Wet Pluviated Method

Test Name	PI	LL	FC (%)	σ'_{vo} (kPa)	σ'_m (kPa)	e_o	B-Value	w_c (%)	w_c/LL	Days
Pluv A4	2	31	72%	138	101	0.90	0.96	33.33	1.08	1.10
Pluv D3	11	38	94%	138	101	0.95	0.94	35.41	0.93	1.04
Pluv G5	10	31	77%	138	102	0.76	0.95	28.17	0.91	1.06

As shown in the table above, Pluviated G soils consistently have lower void ratios and w_c/LL ratios than either Pluviated A or D soils, regardless of the PI. This was previously explained by the Constant Rate of Strain Consolidation relationships presented in Section 5.3.

The effective stress paths of these three soils are very interesting and complicated. Pluv A4 and Pluv D3 follow the same effective stress path to 90% of the initial vertical effective stress; whereas the slope of Pluv G5 is considerably higher. At 90%, all three slopes converge and the slope of Pluv A4 and Pluv G5 begin to level off and follow the same path until approximately 75% of the initial vertical effective stress. In the end, each soil begins to bend toward their own failure envelope. The friction angles from Table 5.12 indicate that Pluv G5 has a friction angle of 22°, compared to the friction angle of 24° for Pluv D3 and 25° for Pluv A4.

The stress-strain curves of the three soils are similar, yet Soils A and D prove to have a higher maximum shear stress on the horizontal plane than Soil G. These same trends are repeated in the cyclic tests, which will be examined in the following chapter.

5.6.2.2 Effects of Time Under Confinement

Like the Slurry Deposition Method specimens, the In-Place Wet Pluviated specimens were subjected to monotonic testing using strain control at different times under confinement. The objective was to subject the specimens to confined loading of 0.1 Day, 1 Day, and 10 Days, or roughly over three log cycles. Table 5.15 lists the specimen properties for each of the aforementioned tests.

Table 5.15 Summary of specimen properties and monotonic testing parameters for Soils A, D, and G constructed by the In-Place Wet Pluviated Method tested under different times under confinement.

Test Name	PI	LL	FC (%)	σ'_{vo} (kPa)	σ'_m (kPa)	e_o	B-Value	w_c (%)	w_c/LL	Days
Pluv A5	2	31	72%	141	103	0.95	0.98	35.23	1.14	0.11
Pluv A4	2	31	72%	138	101	0.90	0.96	33.33	1.08	1.10
Pluv A6	2	31	72%	140	103	0.96	0.96	35.63	1.15	14.1
Pluv D2	11	38	94%	135	99	0.97	0.94	35.96	0.95	0.13
Pluv D3	11	38	94%	138	101	0.95	0.94	35.41	0.93	1.04
Pluv D4	11	38	94%	140	103	0.90	0.95	33.44	0.88	17.4
Pluv G3	10	31	77%	136	100	0.78	0.97	28.83	0.93	0.04
Pluv G4	10	31	77%	135	99	0.82	0.97	30.38	0.98	0.11
Pluv G5	10	31	77%	138	102	0.76	0.95	28.17	0.91	1.06
Pluv G6	10	31	77%	138	101	0.81	0.99	30.08	0.97	10.6

To simulate time under confinement for greater than 0.8 days, specimens were prepared as all other specimens. Once the mold had been removed and initial consolidation was complete, as described in Section 3.4.2, the specimen was ready for long-term loading. Instead of placing the specimen in the simple shear device, the specimen was placed on a horizontal surface with the drain lines attached to a water-filled vacuum chamber. No vacuum was applied, but the vacuum chamber served as a reservoir and was always located above the specimen to provide a positive head of water.

The specimens were slowly loaded vertically with weights until approximately 114 kg was applied. Figure 5.18 shows specimen Pluv A6 loaded with 114 kg. Given the area of the specimen, this is roughly 137 kPa vertical effective stress. Using K_o = 0.6, the mean effective stress, σ'_m, is 100 kPa. As stated earlier, the specimens must be loaded very slowly, taking as much as 4 to 5 hours to load. This allowed the specimen to consolidate under each load increment before the next load was applied. The specimens were freestanding, so keeping the stack of weights level was imperative.

As illustrated in Figure 5.19, for Soil A there is a great deal of strength gain between 0.1 days and 10 days. The maximum shear stress on the horizontal plane increased 34% for this increment in time. The difference in strength between 1 day and 10 days is not immediately obvious. Though each of the specimens achieves $\tau_{h\text{-}max}$ of approximately 35 kPa, the difference lies in the stress-strain curves. Pluv A4 reaches a $\tau_{h\text{-}max}$ at approximately 10% shear strain then

begins to decline. Conversely, Pluv A6 continues to increase in strength throughout the test. This strain hardening is possibly an indicator of the increased strength with increased time under confinement.

For Soil D, as shown in Figure 5.20, all specimens tend to follow the same effective stress path to approximately 90% of the initial vertical effective stress. After this point, the time under confinement determines the ultimate strength. With greater time under confinement comes greater strength. From the stress – strain diagram, at 5% shear strain, the increase in the shear stress increases by 12% from 0.1 days to 1 day and 13% from 1 day to 17 days. It is also important to point out that for Pluv D4 (17 Days), like Pluv A6 (14 Days), the strength of the material increases as the test continues. This is in contrast to Pluv D2 (0.13 Days) and Pluv D3 (1.04 Days), which both seem to reach their peak strength at approximately 13% strain then decline.

Finally, for Soil G, Figure 5.21 shows a different response among the specimens tested. Pluv G3 shows a classic failure for a loose material subjected to monotonic loading. Notice the curvature of the effective stress path towards the origin, indicating the failure envelope. Pluv G4 and Pluv G5, although separated by one log cycle of time, have somewhat similar $\tau_{h\text{-}max}$. However, the effective stress path between Pluv G3, Pluv G4, and Pluv G5 shows a steady increase in strength due to time under confinement from the start of the test through 80% of the initial vertical effective stress.

Pluv G6 has the highest shear stress on the horizontal plane among the tests; however, Pluv G6 (10 Days) clearly "breaks" at a shear strain of 9%. This was puzzling until similar results are seen in Pluv G15, a cyclic test with a time under confinement of 18 days. After 15% shear strain, the specimen strained uncontrollably to failure. This was also true for Pluv G24, a cyclic test which was under confinement for 50 days. Once Pluv G24 reached 5% shear strain, it also strained uncontrollably. Initial inspection concludes that the additional time under confinement increases the strength, as in the other specimens, yet the strength cannot be sustained and the specimen "breaks", looses strength rapidly, and exhibits large strains.

Figure 5.22 graphically depicts the relationships between the maximum shear stress on the horizontal plane and time under confinement for Soils A, D, and G. The shear stress used for this graph is the maximum shear recorded, regardless of the strain. As seen from this figure, time under confinement has a greater influence on Soil G, with the least effect on Soil D.

5.6.2.3 Effects of Stress Control vs. Strain Control

The "goose neck" phenomenon was more pronounced in the Pluviated specimens than the Slurry specimens. This was the main reason to test an In-Place Pluviated specimen via stress control.

Table 5.16 Summary of specimen properties and monotonic testing parameters for stress and strain controlled materials

Test Name	σ'_{vo} (kPa)	σ'_m (kPa)	e_o	Loading Type	Loading Rate	B-Value	w_c (%)	w_c/LL	Days
Pluv A4 val	137	101	0.94	Strain	0.4 mm/min	0.96	34.80	1.12	1.19
Pluv A17	139	102	0.92	Stress	2.24 kg/min	0.96	34.24	1.10	0.82

Figure 5.23 illustrates the difference in response for the two loading methods and

Table 5.16 shows the similarities between the specimens tested. The effective stress path for Pluv A17 is more similar to the effective stress paths of the Slurry Deposition Method specimens mentioned earlier in the chapter, than the Pluviated specimens. The effective stress path for Pluv A17 eventually increases in vertical effective stress with increased shear stress. This is in contrast to most Pluviated specimens which continue to decrease in vertical effective stress with only slight increases in shear stress. The maximum shear stress on the horizontal plane of the stress-controlled specimen is also much greater. The $\tau_{h\text{-}max}$ of Pluv A17 is 27% greater than that of Pluv A4val. The "goose neck" phenomenon also seems to disappear from the Pluv A17 test. It is recommended that more stress-controlled testing takes place to better define the differences between the two test methods.

5.6.2.4 Effects of Effective Confining Pressure

The effect of effective confining stress on the $\tau_{h\text{-}max}$ and liquefaction resistance has been shown by previous researchers to be a significant factor. For example, Hynes and Olsen (1999) found that in similar soils, the soil with greater effective confining stress has a lower Cyclic Resistance Ratio (CRR). When the applied deviator stress is normalized by the initial effective confining stress, an increase of effective confining stress causes a decrease of the normalized strength. More information on testing at different effective confining stresses and K_σ effects can be found in Section 6.3.4.

Specimen Pluv A2 was loaded and allowed to consolidate for 17 day then tested at an effective confining pressure of 150 kPa. This was later compared to Pluv A6, which has a time under confinement for 14 days and tested at 100 kPa under strain control. The soil characteristics prior to testing are given in Table 5.17.

Table 5.17 Summary of specimen properties and monotonic testing parameters for Soil A tested at different effective confining pressures

Test Name	σ'_{vo} (kPa)	σ'_m (kPa)	e_o	B-Value	w_c (%)	w_c/LL	Days
Pluv A2	212	156	0.93	0.95	34.44	1.11	17
Pluv A6	140	103	0.96	0.96	35.63	1.15	14.1

In Figure 5.24b, it is apparent that the $\tau_{h\text{-}max}$ in much greater given the higher effective confining pressure. The maximum shear stress on the horizontal plane of Pluv A2 is 56% greater than Pluv A6. However, at approximately 7% shear strain, the shear stress for Pluv A2 peaks then begins to decline. By contrast, the shear stress of Pluv A6 continues to rise until the test concludes at 20% shear strain.

The difference lies in the effective stress paths, Figure 5.24a. At all times, the effective stress path for Pluv A6 is greater than Pluv A2. Because the effective stress path is normalized by the initial effective vertical stress, Pluv A6 clearly has greater normalized strength. This conforms to the work by Hynes and Olsen mentioned previously.

5.6.3 Effects of Specimen Preparation

Seed (1979) illustrated the importance of different soil formation procedures, given a constant density, on cyclic resistance. Although constant density is not possible between the Slurry Deposition Method and the In-Place Wet Pluviation Method, the results of monotonic testing indicate that the two methods do not give identical results. Table 5.18 compares monotonic strength characteristics between the two reconstitution methods.

Table 5.18 Comparison of total and effective strength parameters for the monotonic undrained simple shear tests prepared using the Slurry Deposition Method and In-Place Wet Pluviation Method

Test Name	PI	LL	σ'_{vo} (kPa)	σ'_{vo} (kPa)	e_o	τ_h (1% γ) (kPa)	τ_h (3% γ) (kPa)	τ_h (5% γ) (kPa)	τ_h (10% γ) (kPa)	τ_h (15% γ) (kPa)	ϕ' (○)
Pluv A4	2	31	138	101	0.90	26	29	31	34	35	25*
SDM A3	2	31	137	101	0.70	31	37	43	58	72	31
Pluv G4	10	31	135	99	0.82	22	24	26	30	33	24*
SDM G4	10	31	137	100	0.66	26	31	34	41	46	26*

In Figure 5.25, Pluv A4 and SDM A3 are compared. Each is tested at about 1 day under confinement, at σ'_m = 100 kPa, and under strain control. The maximum shear stress of SDM A3 at γ = 5% is twice that of Pluv A4 at the same shear strain. Each of the specimens initially follows the same stress path to 90% of the initial vertical effective stress. At this point, the effective stress path of the Pluviated specimen begins to level off; meaning that for decreases in vertical effective stress there is little increase in shear stress. However, the Slurry Deposition specimen exhibits pronounced decreases in excess pore water pressures and the strength increases linearly with increasing strain.

In Figure 5.26, Pluv G4 and SDM G4 are compared. Each is tested at 0.1 Days under confinement, at σ'_m = 100 kPa, and under strain control. The maximum shear stress at γ = 15% for SDM G4 is 40% greater than Pluv G4 at the same shear strain. Each of the soils initially follow the same stress path up to 80% of the initial vertical effective stress. At this point, the effective stress path of the Pluviated specimen begins to level off while the shear stress for the Slurry specimen increases sharply with little decrease in vertical effective stress.

When comparing the Pluviated specimens to the Slurry Deposition specimens, it has already been noted that the Slurry Deposition specimens are more dense and have a lower void ratio. The Slurry specimens would have a dilative tendency if tested under drained conditions. In the undrained monotonic tests performed on Slurry specimens, each specimen has a contractive response at the beginning of the test when excess pore water pressures increase. The specimens then have a dilative response, which translates into the development of negative excess pore water pressures, or at least a decrease in excess pore water pressure after an initial contractive response. SDM A3 (0.9 Days) developed significant negative excess pore water pressures and SDM A9 (0.8 Days) had almost developed negative pore water pressures by the end of testing. SDM A2 and all SDM G specimens were relatively "young" in that their time under confinement was less than 0.1 days and none of these specimens developed negative pore water pressures; however, the excess pore water pressure did begin to decrease before the end of testing.

The Pluviated specimens, on the other hand, are more loose and have higher void ratios. The Pluviated specimens would have a tendency to contract if tested under drained conditions. In the undrained monotonic tests performed on the Pluviated specimens, the specimen's excess pore water pressures continued to increase throughout the tests or increase to a point then remain constant. There is a tendency for the excess pore water pressures to level off after approximately 70% of the initial vertical effective stress, but the excess pore water pressures eventually begin to increase again and the stress path develops a "goose neck" shape. For this reason, it is believed that Slurry Deposition specimens fall below the steady state line and Pluviated specimens are above the steady state line.

From Figure 5.27, consider two soils that have the conditions noted as Points C and D. Soils lying above and to the right of the steady-state line are loose with a contractive tendency, and thus are expected to develop large positive excess pore water pressures, soften, and eventually move to Point A. This applies to both monotonic and cyclic testing. Point C on the diagram corresponds to most of the In-Place Wet Pluviation specimens.

Point D will move to the steady state line during monotonic testing. During a cyclic test, the tendency of Point D is to move to Point B, a condition of zero effective stress, with large strains, and considerable softening. In these cases, the Slurry Deposition Method specimens are embodied by Point D.

5.7 Summary and Principal Findings

Characterization of a soil's response to monotonic loadings is a critical element in developing a framework for understanding a soil's liquefaction susceptibility and resistance. Without the background information of consolidation characteristics, grain size, and static strength, it may be difficult to draw sound insights for cyclic testing. Improper testing, such as using an improper rate of loading, or inappropriate generalizations of the soils based on only one characteristic, such as PI, could lead to misinterpretation and erroneous findings.

The grain size analysis determines the percentage of particles finer than 75 μm and 2μm. These soil characteristics have direct relationships to the Plasticity Index, PI, the void ratio, e, and the compression index, C_c, as described in Section 5.3.

The results of the grain size analysis and constant rate of strain consolidation testing tie into the consolidation tests. The properties defined by grain size analysis and the CRS testing define the initial soil properties and the response during the tests. In the end, the coefficient of consolidation, c_v, is found graphically from the shape of the consolidation curve (affected by PI, fines content, and compression index). This coefficient is then used for all monotonic and cyclic tests to ensure that the rate of loading is slow enough to ensure proper excess pore water pressure measurement to reliably calculate the effective stress.

The monotonic tests are not only crucial for interpreting the upcoming cyclic tests, but they ultimately define the static strength of the materials. Based on the monotonic tests performed as part of this study, the following findings are drawn:

- The method of reconstitution, either by Slurry Deposition or by In-Place Wet Pluviation, plays a significant role in the consolidation parameters as well as the shear strength. The coefficient of consolation, c_v, was always greater for In-Place Wet Pluviated specimens than for Slurry Deposition specimens. The maximum shear stress on the horizontal plane during simple shear monotonic testing was consistently greater for the Slurry Deposition Method specimens. The void ratios were also consistently lower for the Slurry specimens, and this is believed to be the reason behind the differences in response during shearing.

- A change in index properties of the material affects all consolidation and monotonic parameters tested. For instance, the coefficient of consolidation, c_v, decreased with increasing PI, except for Soil F that has a low Fines Content and high D_{10}. The axial strains in consolidation increased with increasing PI, except for Soil F for the reasons given above. The maximum shear stress on the horizontal plane also varied according to the index properties with Soils A and D generating greater strengths than Soil G. The exception to this is soil that is tested with a short time under confinement. Figure 5.12 is a prime example of testing "young" soils and the similarity in response.

- The increase in time under confinement for each soil is shown to increase strength. Soil D is a prime example with an increase in the maximum shear stress on the horizontal plane of approximately 10% per time log cycle.

- Loading using strain-control or stress-control requires more experimentation. No change in response was seen between the Slurry Deposition Method specimens up to 5% shear strain. On the other hand, the In-Place Wet Pluviated specimens were dissimilar.

- Lastly, the effective confining pressure acting on a material has been shown to dictate the maximum shear stress on the horizontal plane of the material. However, an increase in effective confining pressure results in a lower normalized strength (i.e., when normalized by initial effective confining stress).

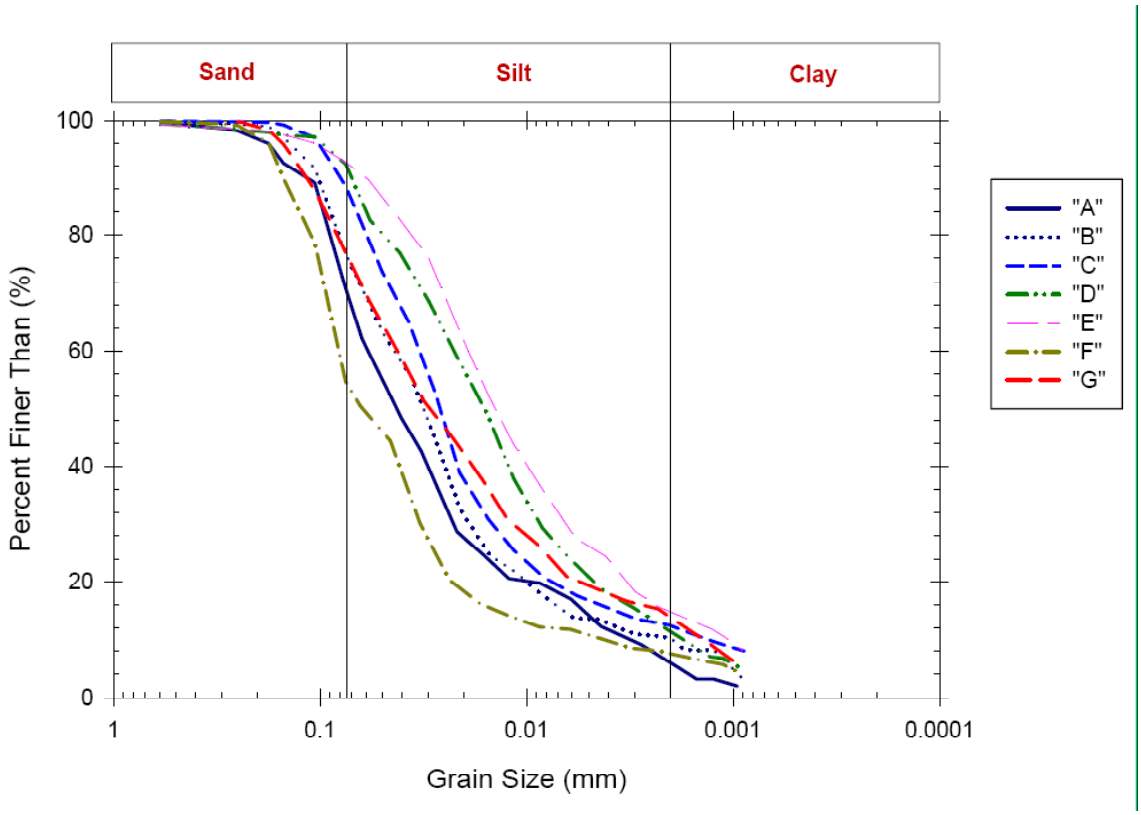

Figure 5.1 Gradation Information for seven soils.

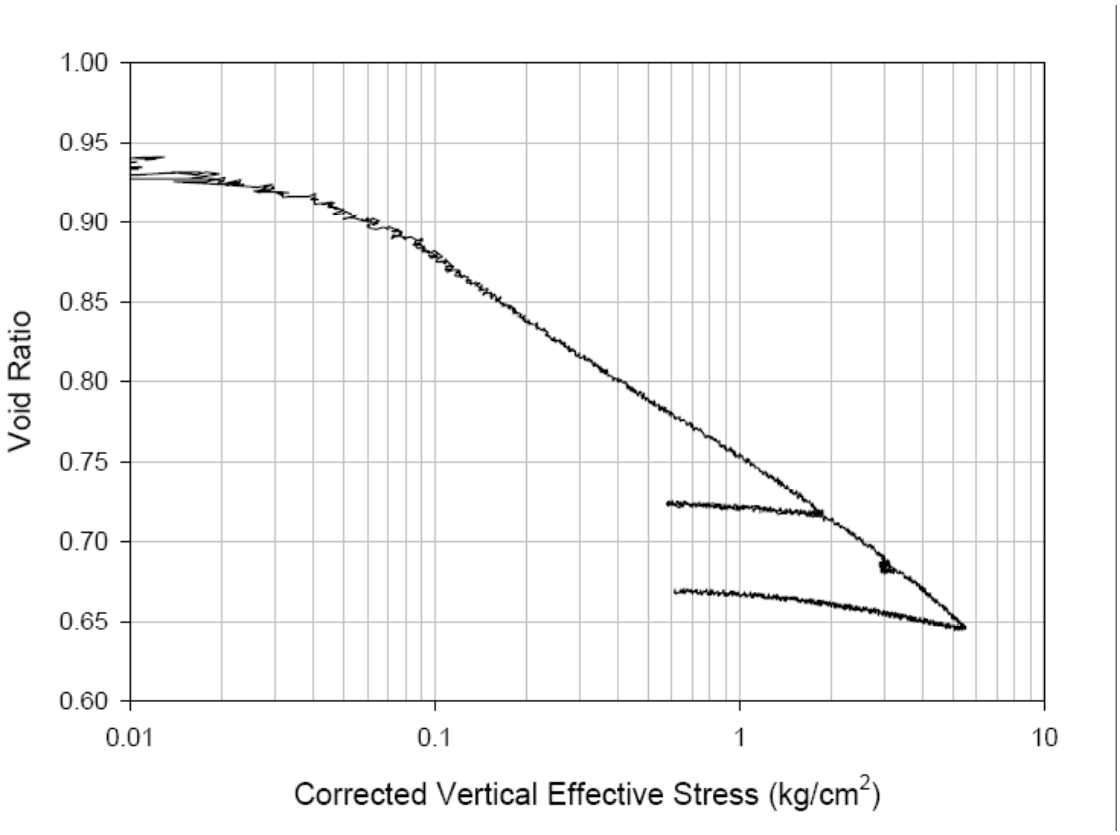

Figure 5.2 One dimensional void ratio - vertical stress curve for the constant rate of strain consolidation test performed on G Soil (PI = 10, LL = 31).

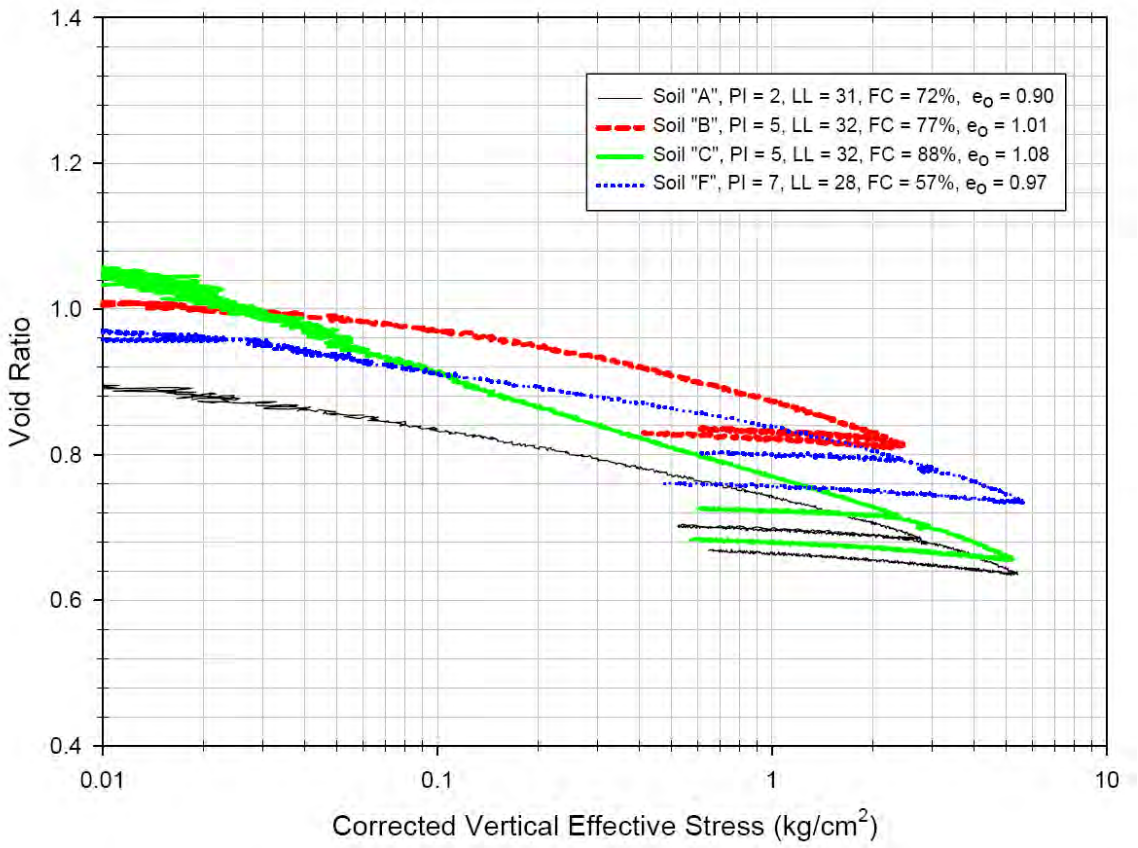

Figure 5.3 One-dimensional void ratio to vertical stress curve for the constant rate of strain consolidation test performed on Soils A, B, C and F.

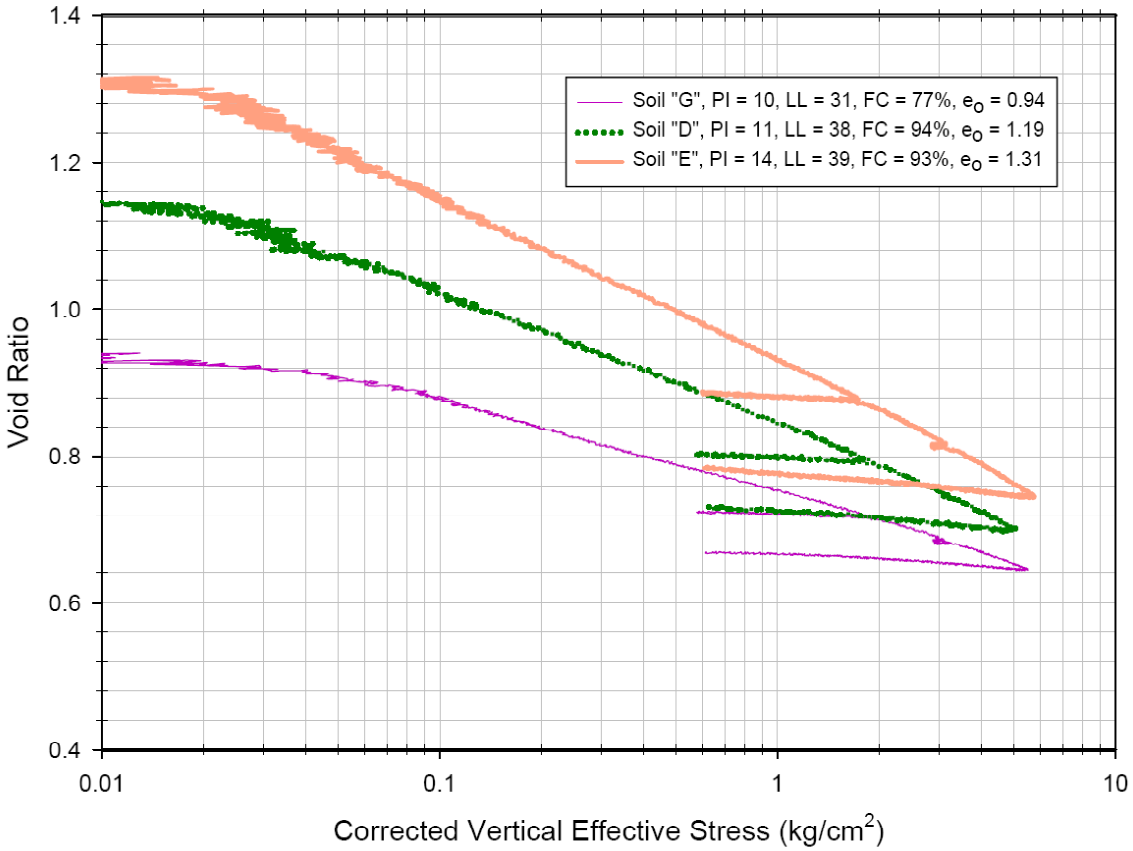

Figure 5.4 One-dimensional void ratio – vertical stress curve for the constant rate of strain consolidation test performed on Soils G, D and E.

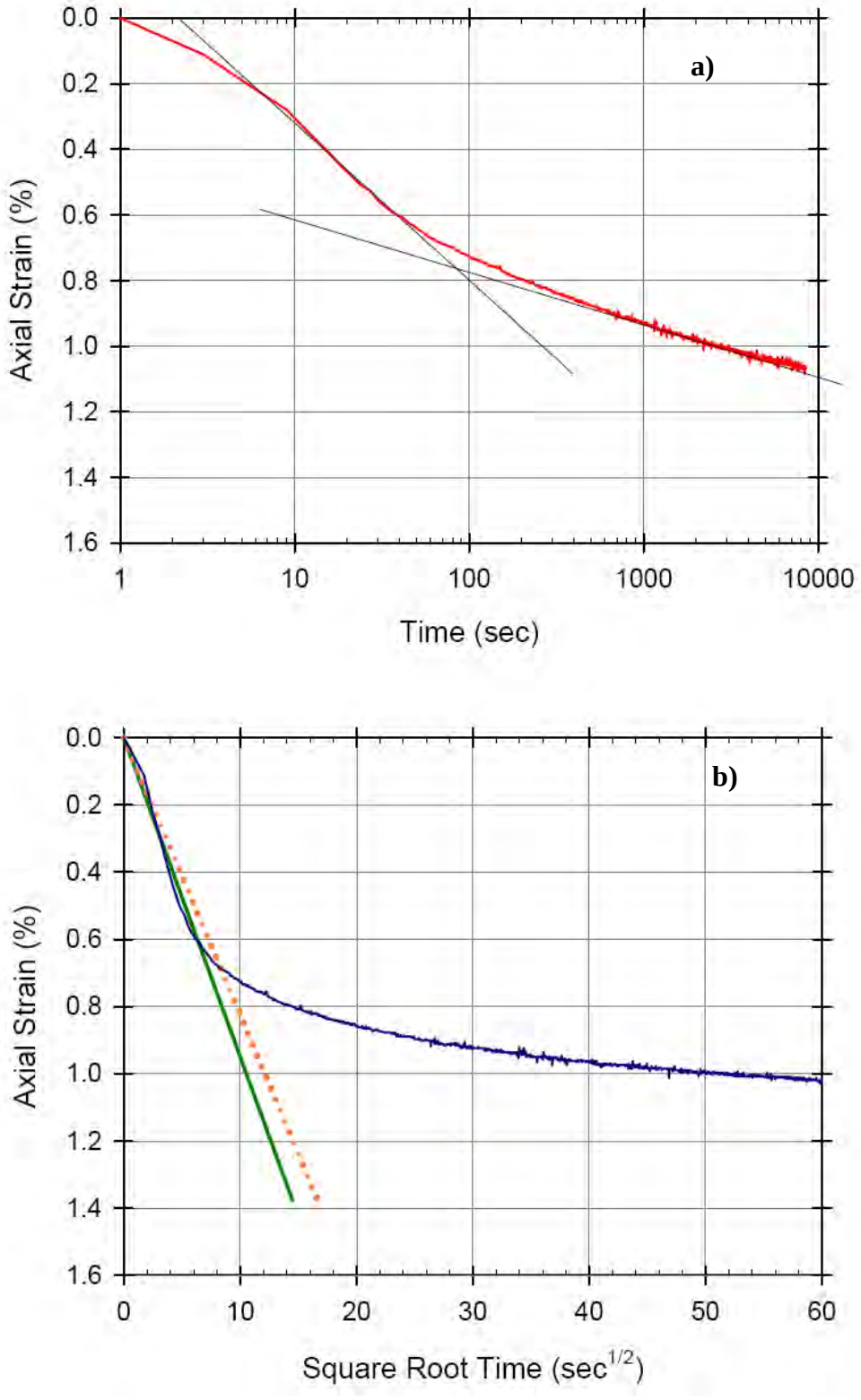

Figure 5.5 Determination of the end of primary consolidation for Pluv A13 using a) Casagrande logarithm of time method, and b) the square root of time method (Taylor, 1948).

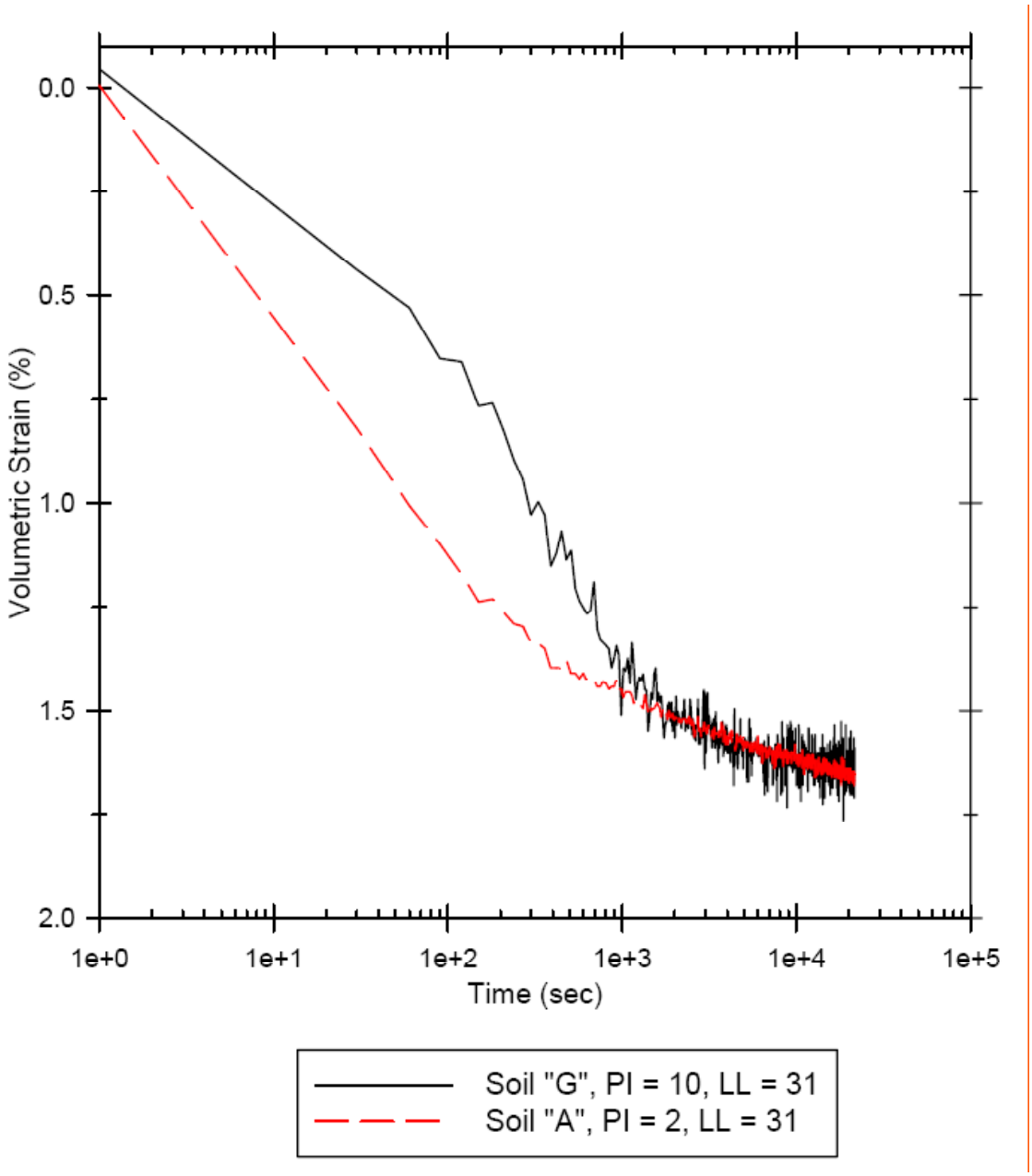

Figure 5.6 Comparison of Triaxial Consolidation Curves for Soil G and Soils A, σ'_3 = 100 kPa.

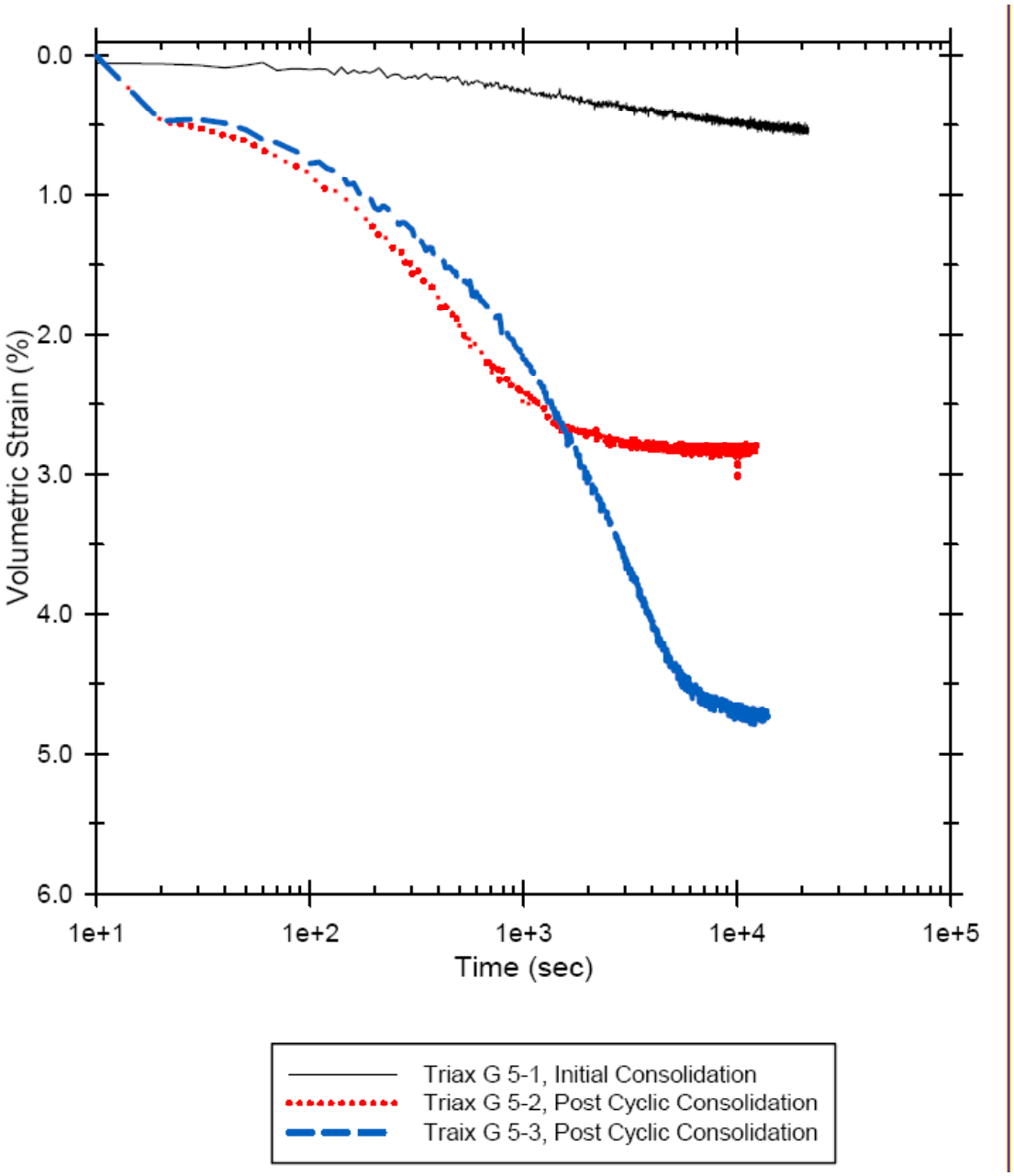

Figure 5.7 Initial Consolidation and Two Post-cyclic Consolidations performed on Soil G (PI = 10, LL = 31), σ'_3 = 100 kPa.

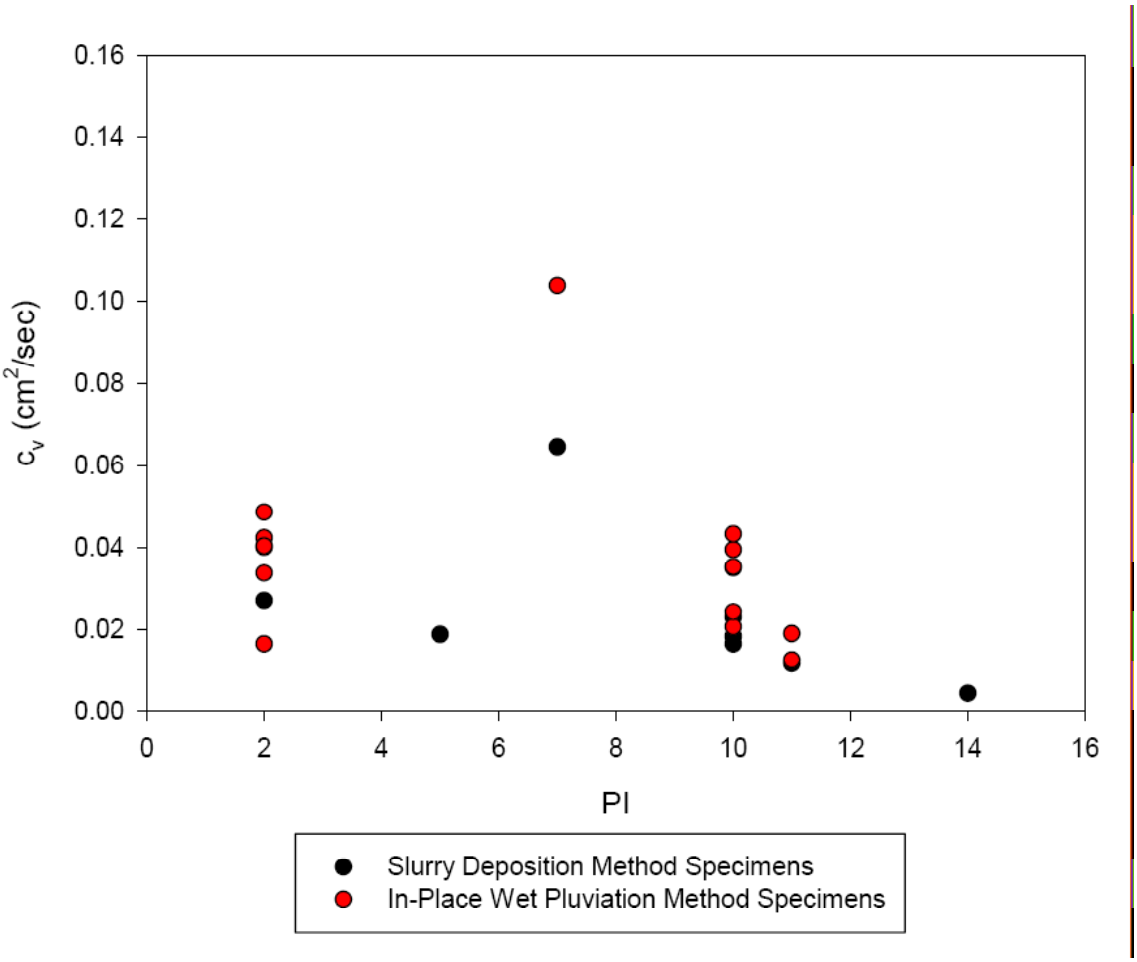

Figure 5.8 Relationship of Plasticity Index to the coefficient of consolidation, c_v, for both reconstitution methods.

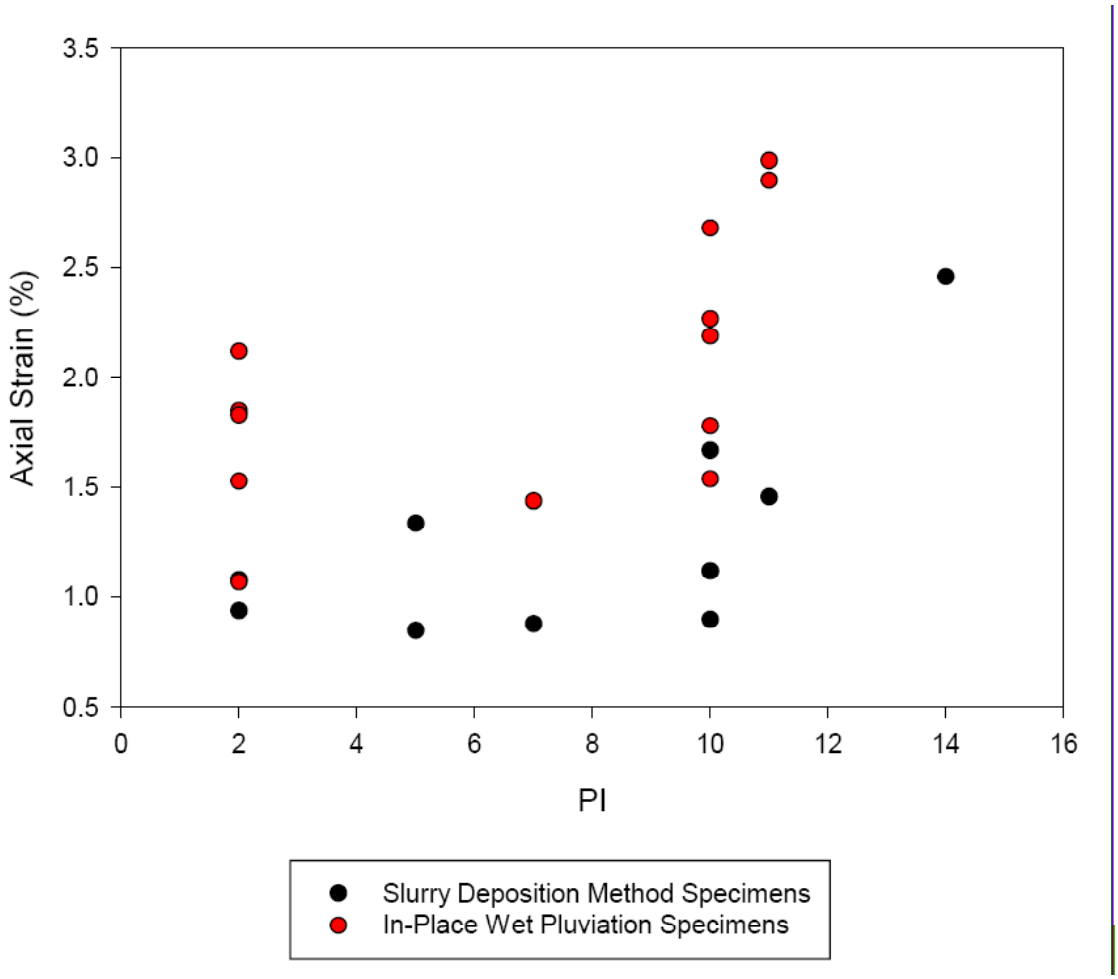

Figure 5.9 Relationship of Plasticity Index to Axial Strain for both reconstitution methods.

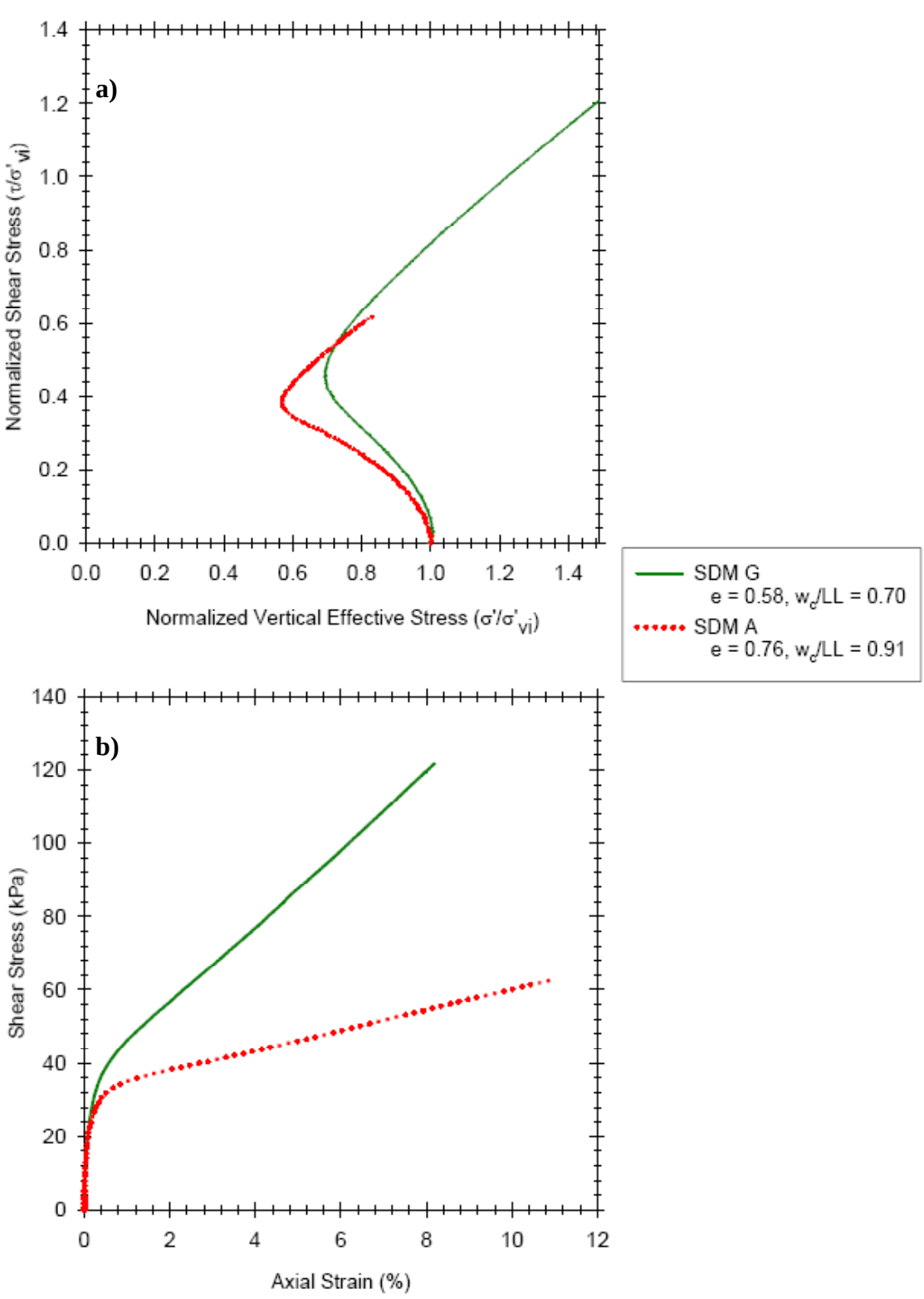

Figure 5.10 Two examples of triaxial compression, stress-controlled tests on Soils A and G, σ'_3 = 100 kPa: a) effective stress path, and b) shear stress - strain response.

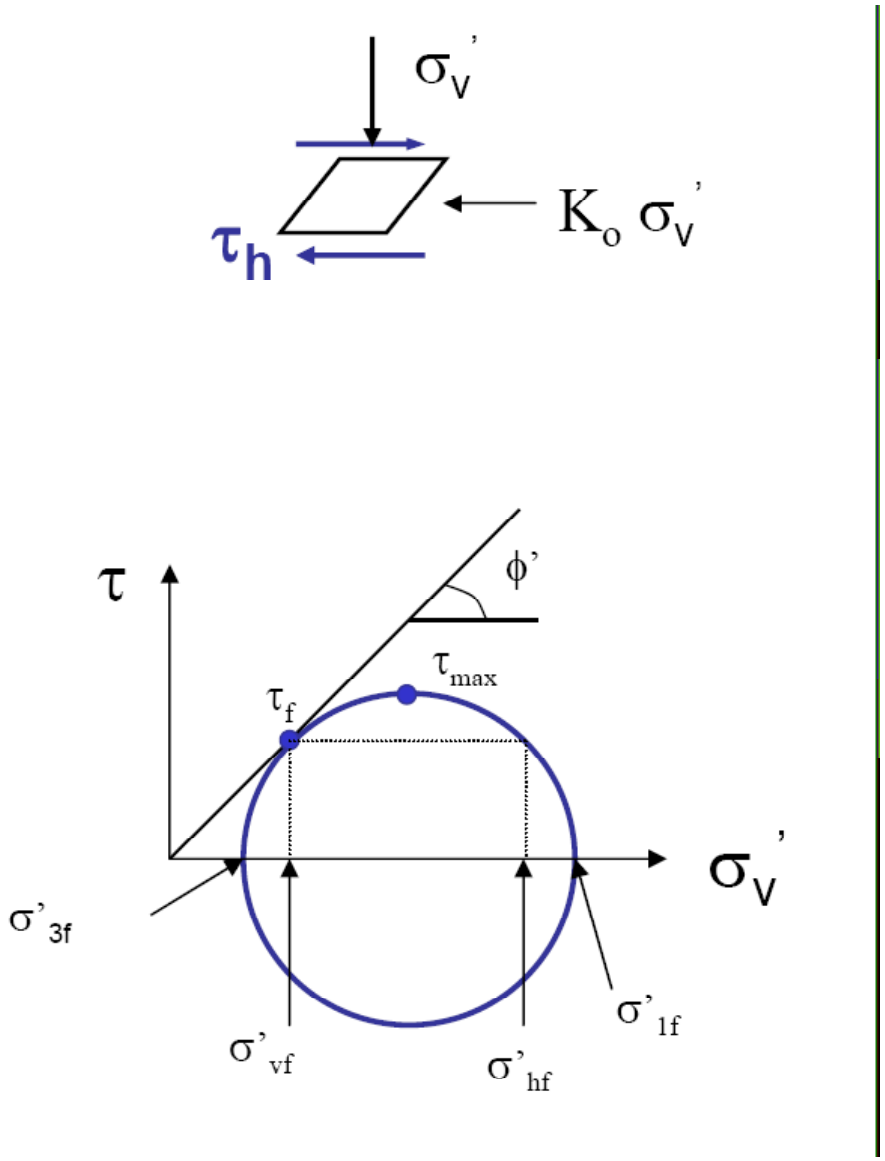

Figure 5.11 Interpreted state of effective stress for simple shear tests with wire-reinforced membranes.

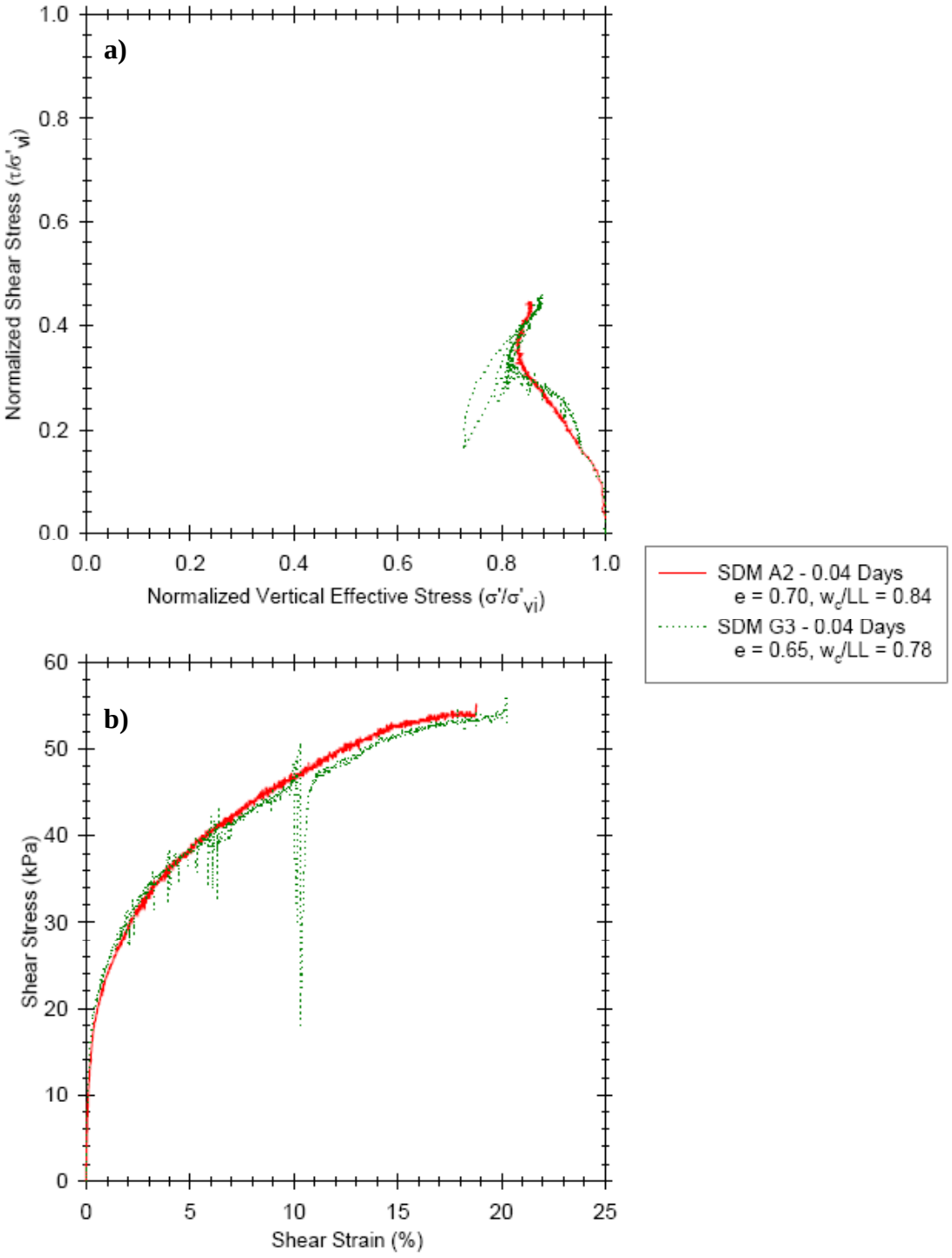

Figure 5.12 Comparison of Soils A and G prepared using the Slurry Deposition Method and subjected to simple shear monotonic, strain-controlled testing, σ'_{vi} = 132 and 134 kPa, respectively: a) effective stress path, and b) shear stress - strain response.

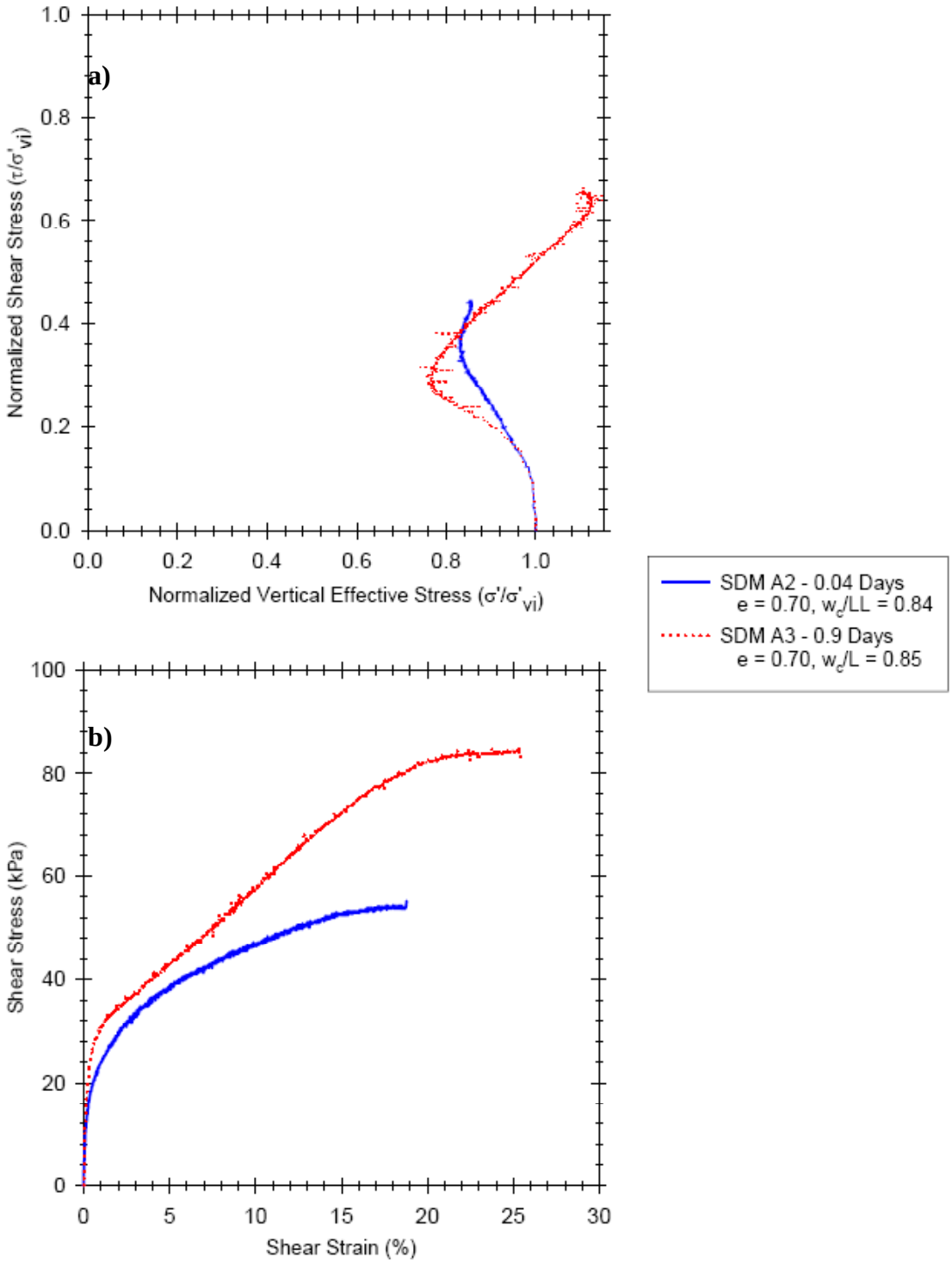

Figure 5.13 Comparison of Soil A constructed using the Slurry Deposition Method subjected to simple shear monotonic, strain-controlled testing under different times of confinement, σ'_{vi} = 132 and 137 kPa, respectively: a) effective stress path, and b) shear stress - strain response.

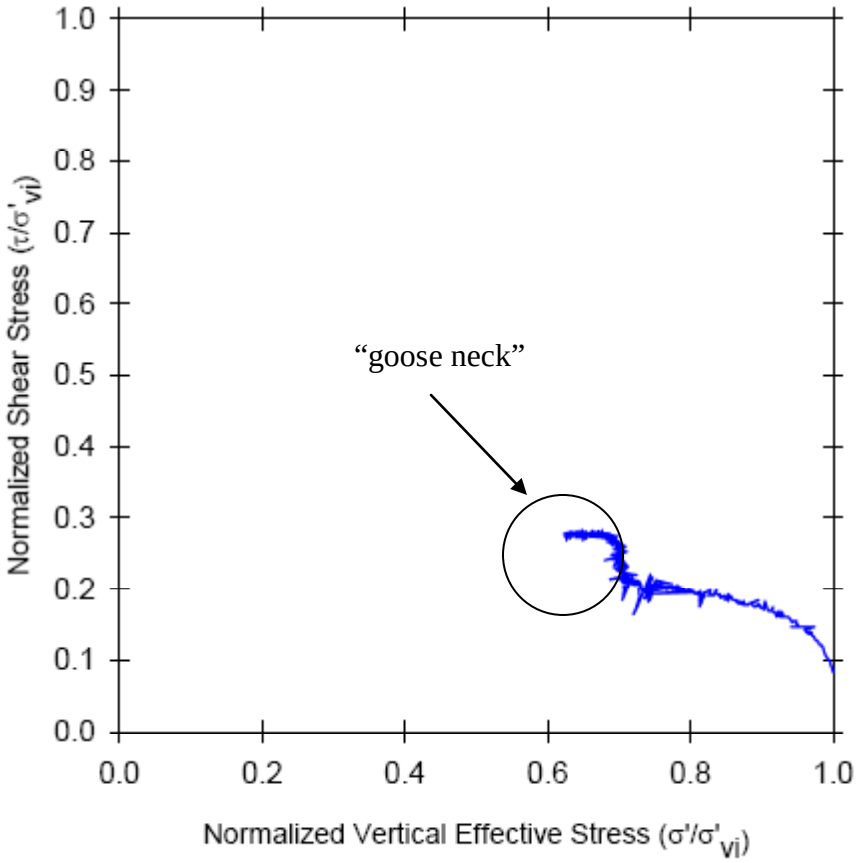

Figure 5.14 Example of simple shear monotonic effective stress path with "goose neck" response, performed by strain-control at σ'_{vi} = 140 kPa. Specimen is Pluv D2, PI = 11, LL = 38, Fines Content = 94%.

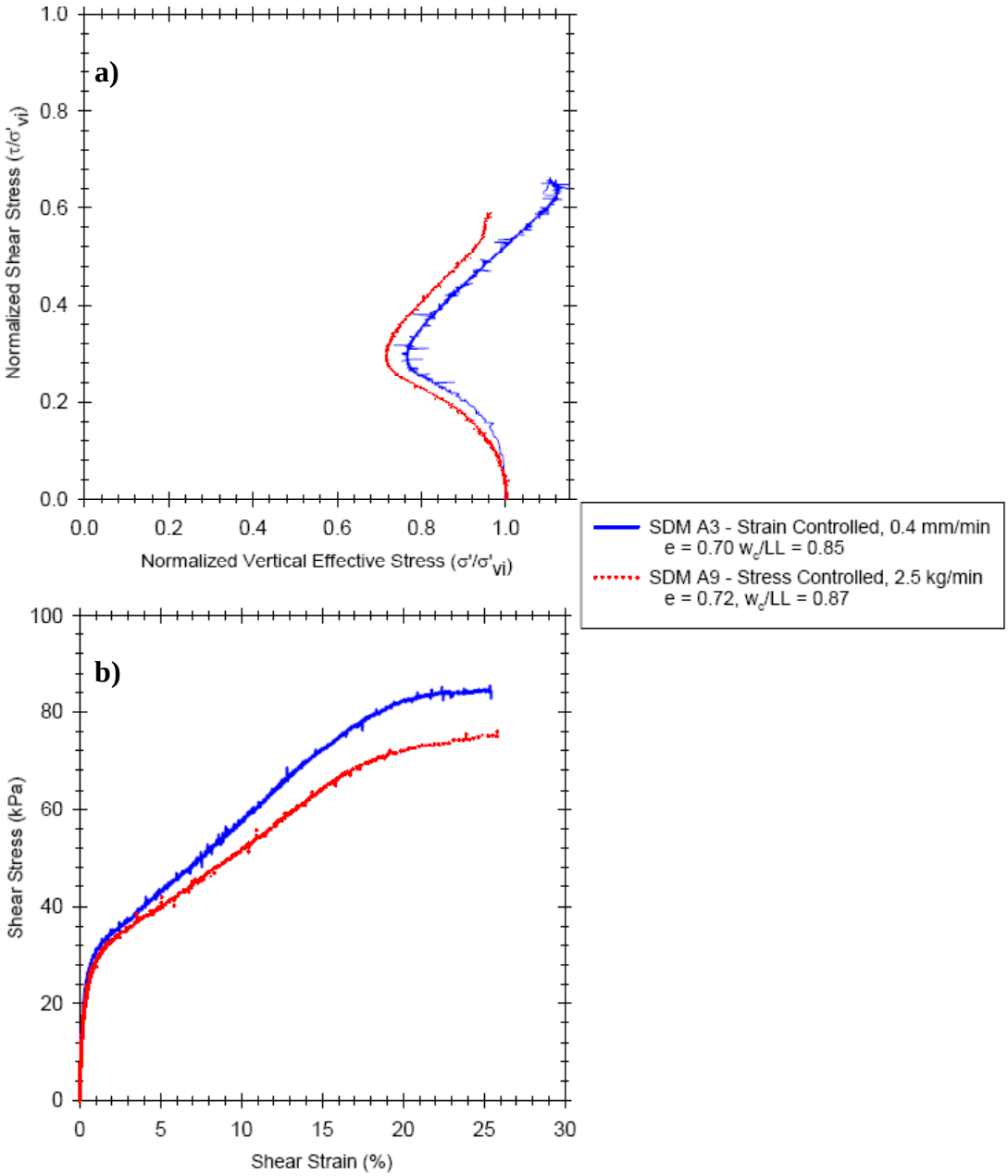

Figure 5.15 Simple Shear monotonic test results for Slurry Deposition Method specimens tested by strain-control and stress-control, σ'_{vi} = 137 kPa: a) effective stress path, and b) shear stress - strain response.

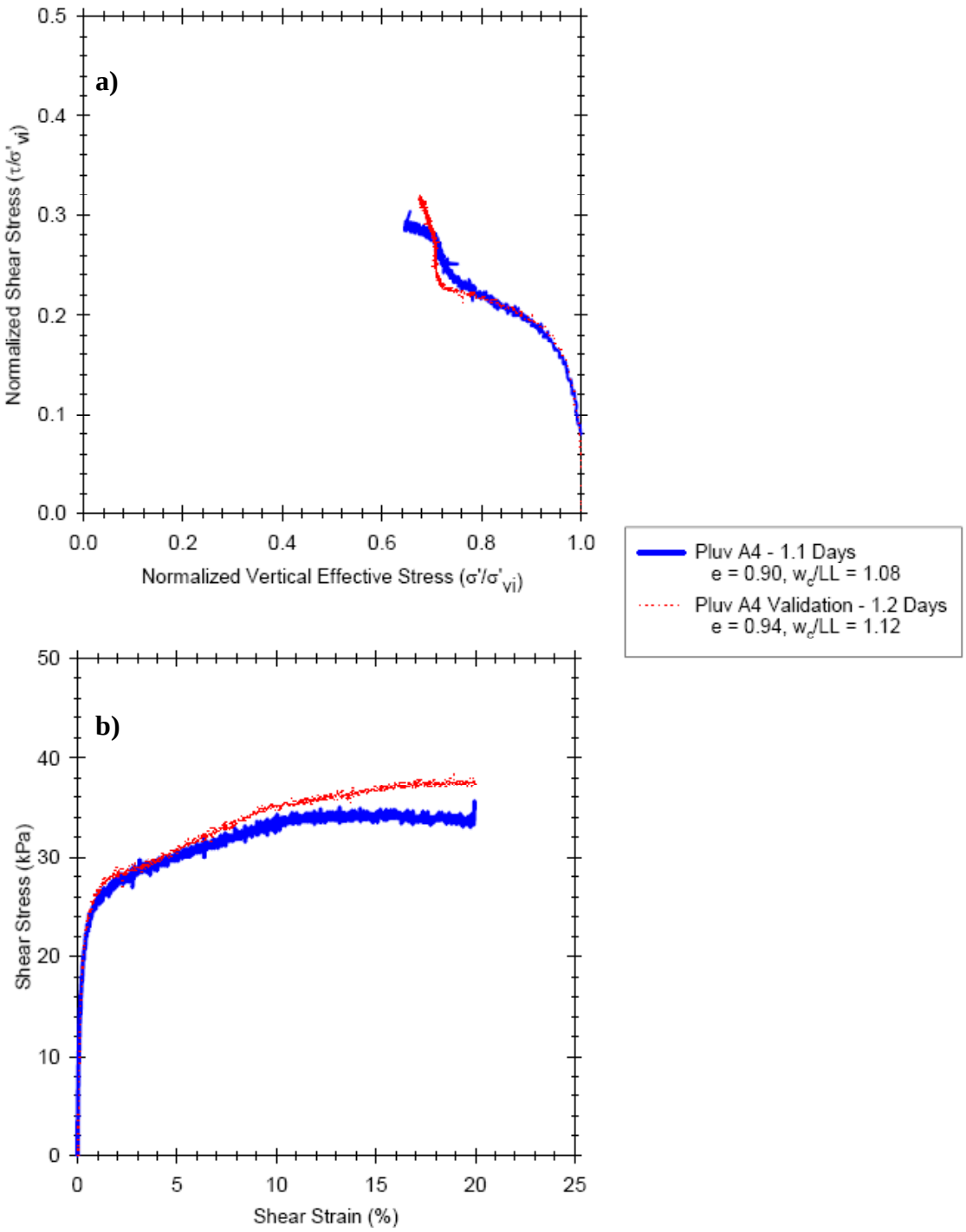

Figure 5.16 Validation of the repeatability of Soil A using the In-Place Wet Pluviation Method subjected to monotonic simple shear, strain-controlled testing, σ'_{vi} = 138 and 137 kPa, respectively: a) effective stress path, and b) shear stress - strain response.

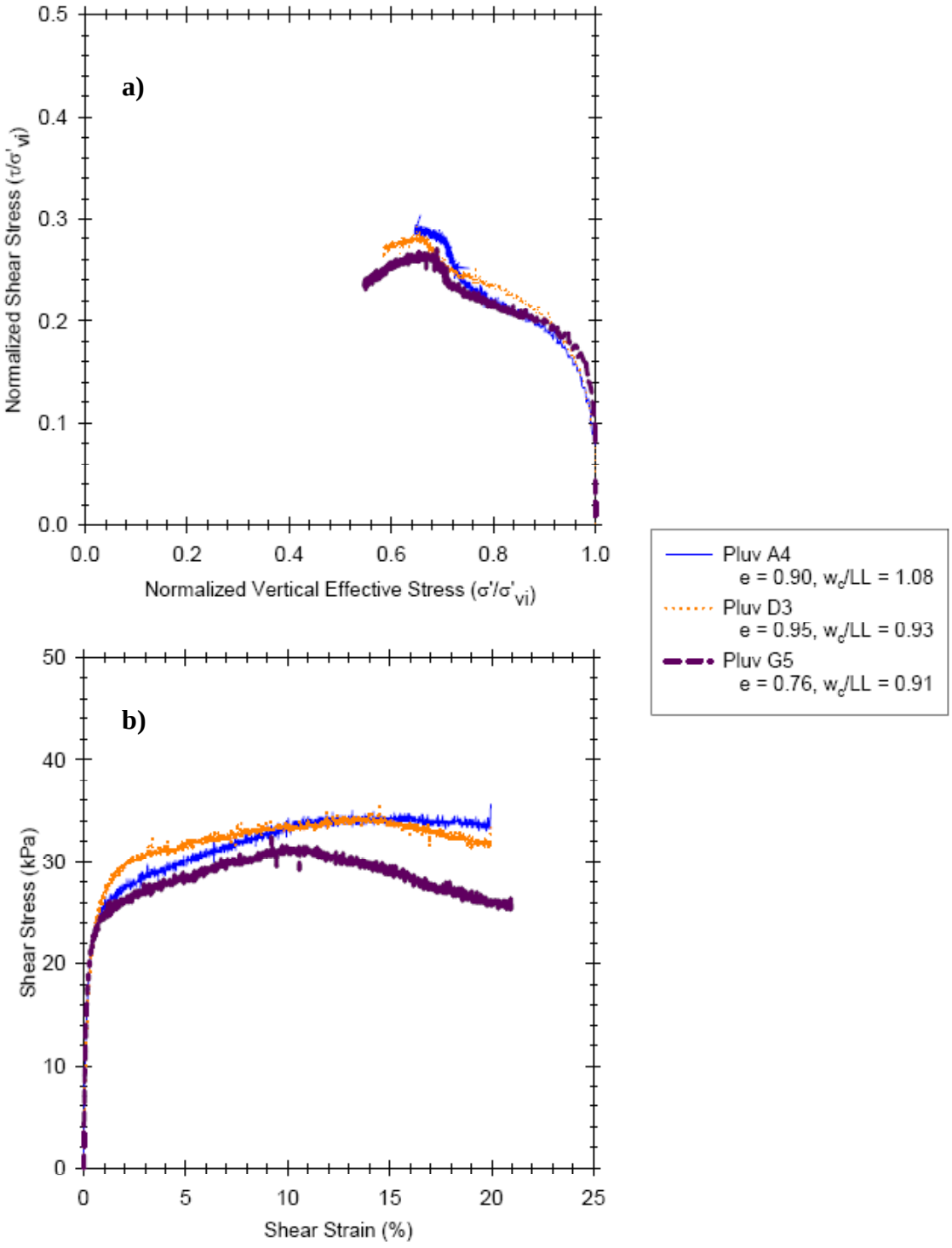

Figure 5.17 Simple Shear monotonic, strain-controlled test results for Soils A, D and G constructed by In-Place Pluviation, σ'_{vi} = 138, 138, and 139 kPa, respectively: a) effective stress path, and b) shear stress - strain response.

a)

b)

Figure 5.18 Pluv A6 under 114 kg simulating time under confinement for 14 days: a) Specimen under full load, and b) the specimen is freestanding and not propped in any fashion.

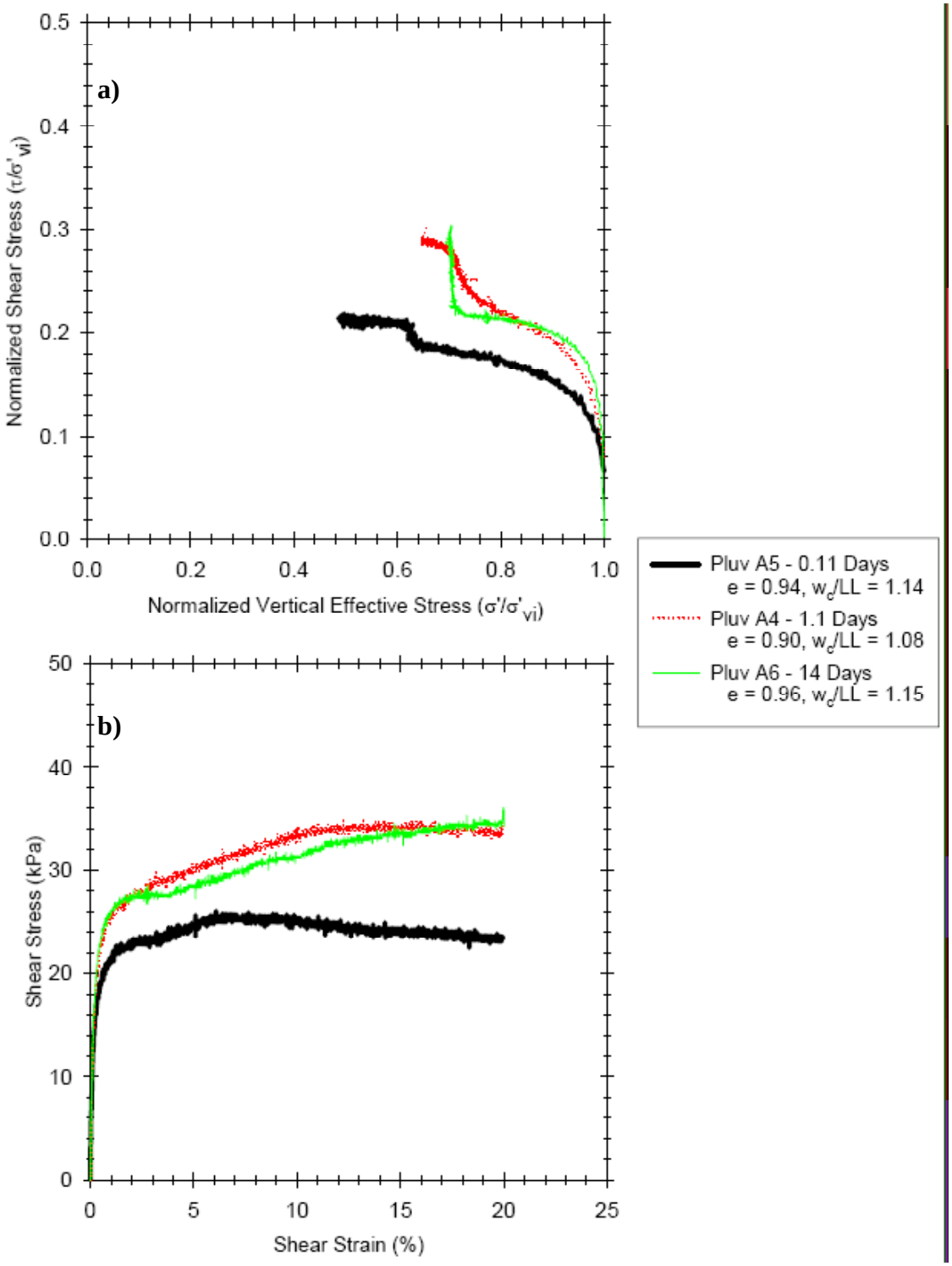

Figure 5.19 Simple Shear monotonic, strain-controlled testing comparing Soil A constructed by In-Place Wet Pluviation under different times under confinement, σ'_{vi} = 141, 138 and 140 kPa, respectively: a) effective stress path, and b) shear stress - strain response.

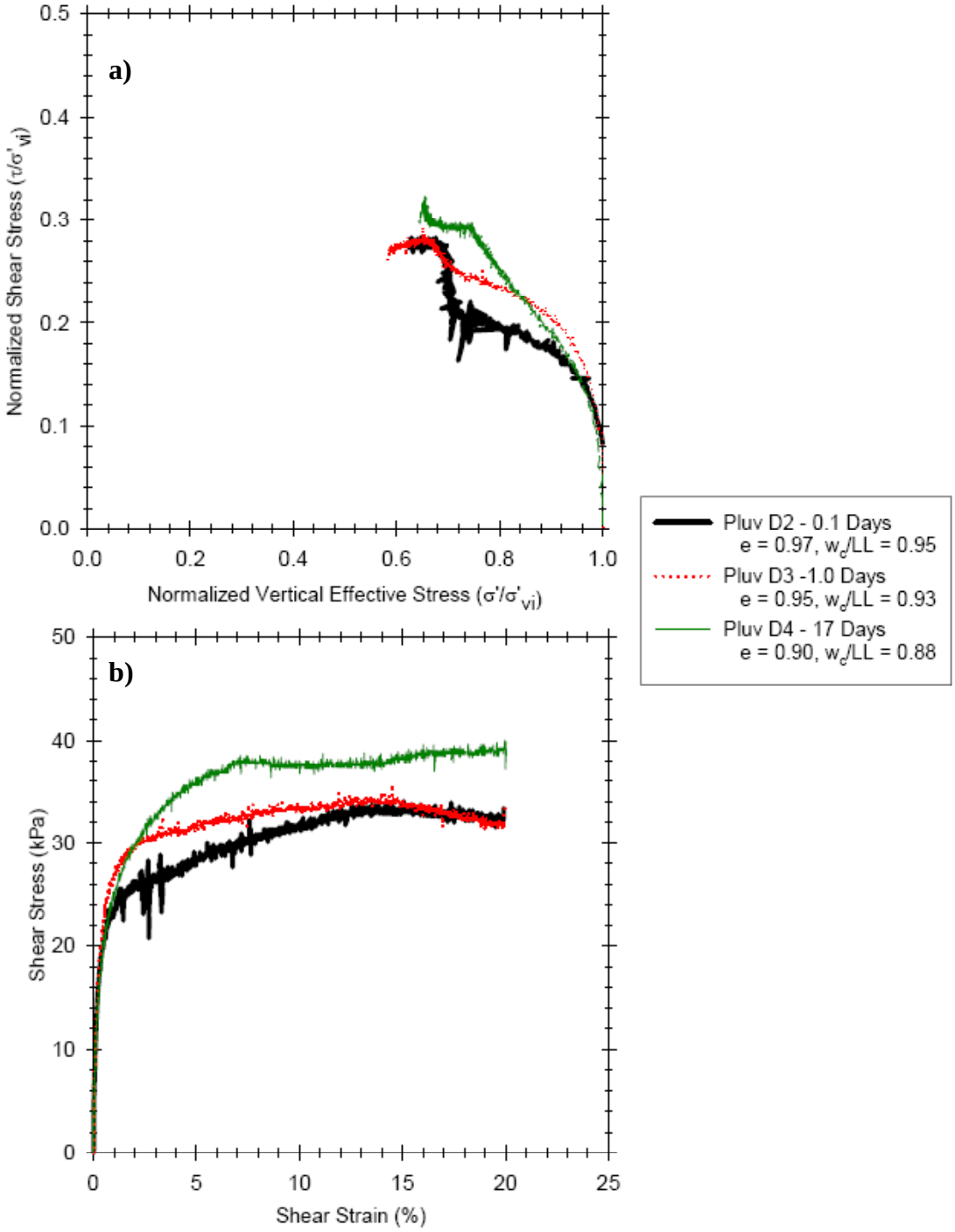

Figure 5.20 Simple Shear monotonic, strain-controlled testing comparing Soil D constructed by In-Place Wet Pluviation under different times under confinement, σ'_{vi} = 135, 138 and 140 kPa, respectively: a) effective stress path, and b) shear stress - strain response.

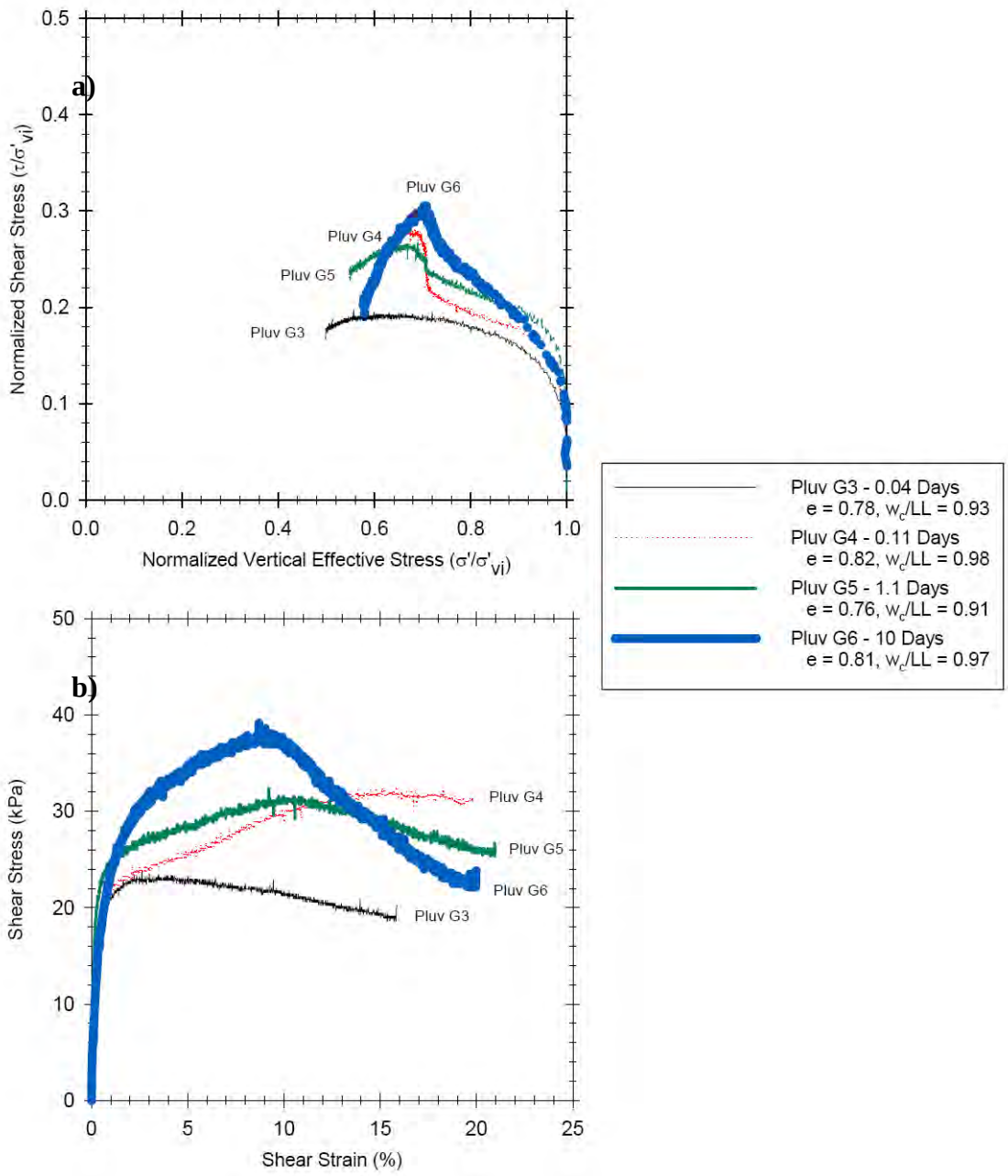

Figure 5.21 Simple Shear monotonic, strain-controlled testing comparing Soil G constructed by In-Place Wet Pluviation under different times under confinement, σ'_{vi} = 136, 135, 139 and 138 kPa, respectively: a) effective stress path, and b) shear stress - strain response.

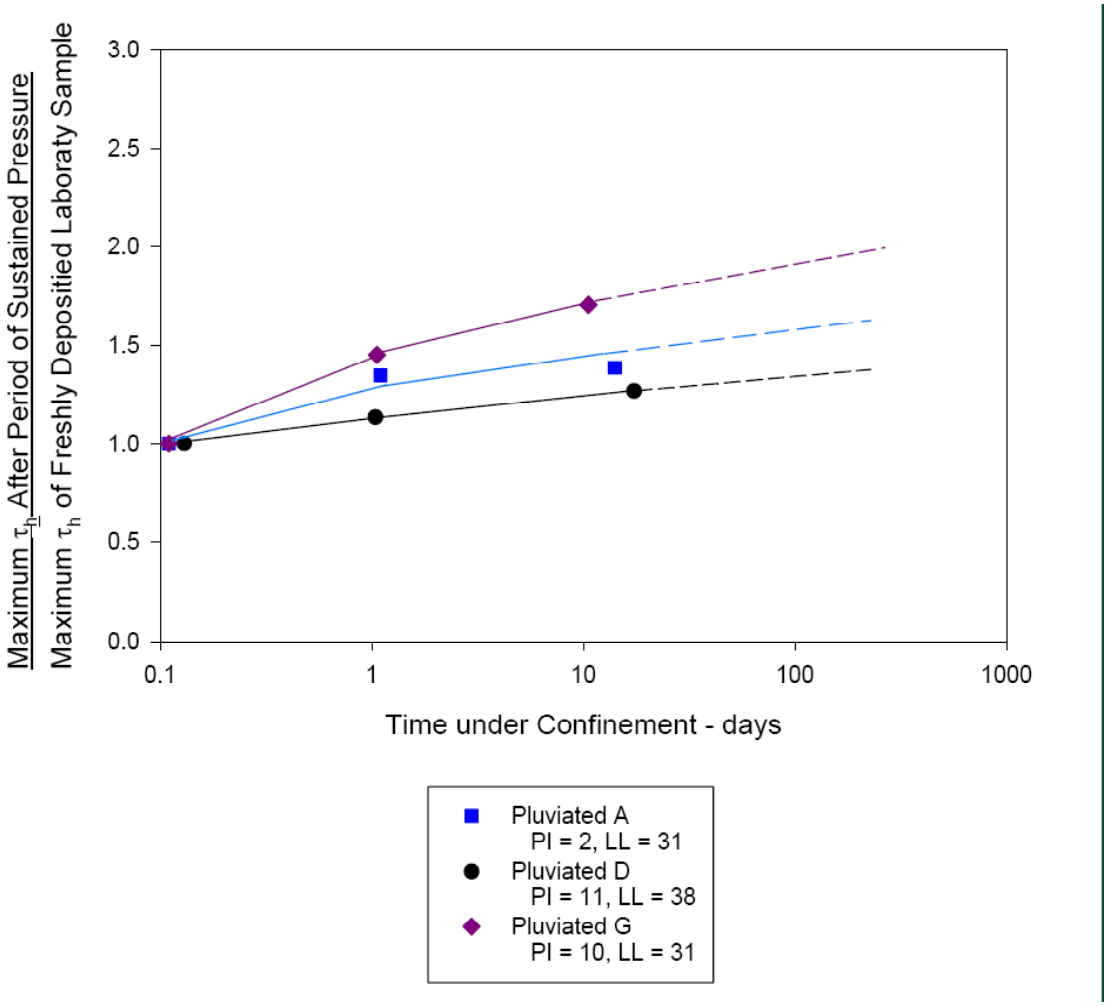

Figure 5.22 Influence of time under confinement on maximum shear stress on the horizontal plane.

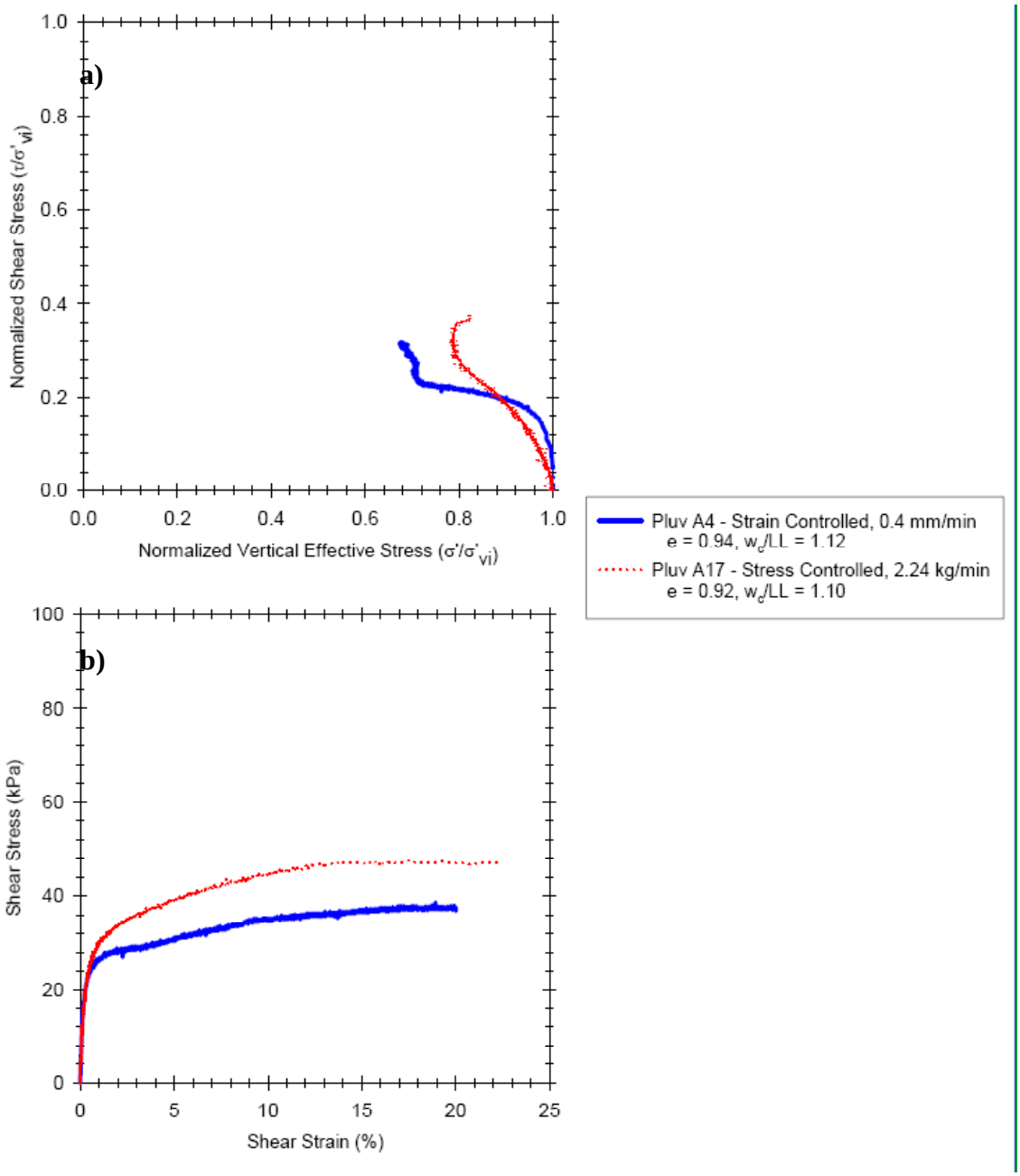

Figure 5.23 Simple Shear monotonic test results for In-Place Pluviated specimens tested by strain-control and stress-control, σ'_{vi} = 138 and 139 kPa, respectively: a) effective stress path, and b) shear stress - strain response.

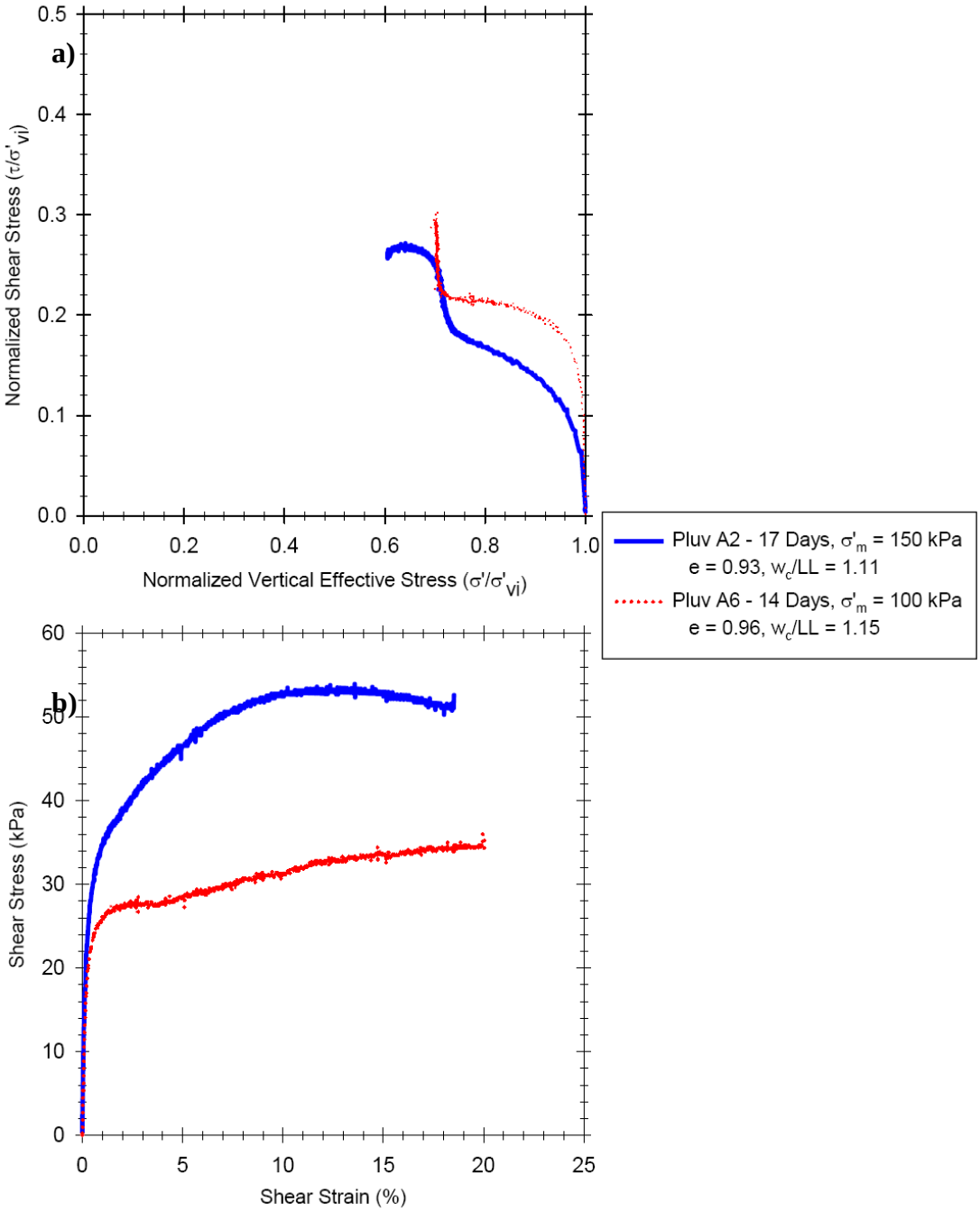

Figure 5.24 Simple Shear monotonic, strain-controlled test results for In-Place Pluviated specimens tested by under different effective confining pressures, σ'_{vi} = 212 and 140 kPa, respectively: a) effective stress path, and b) shear stress - strain response.

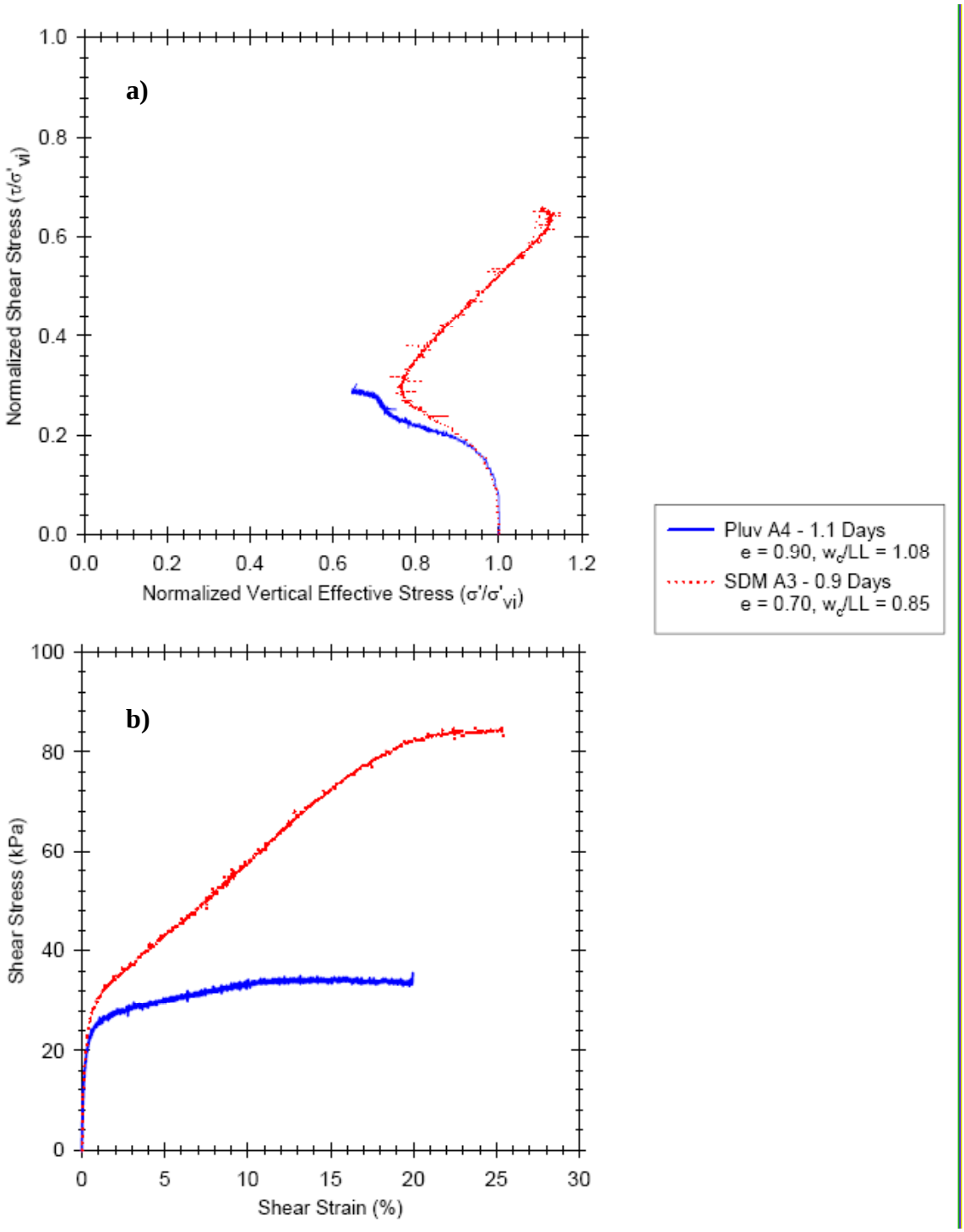

Figure 5.25 Simple Shear monotonic, strain-controlled testing comparing Soil A prepared using the In-Place Pluviated Method and Slurry Deposition Method, σ'_{vi} = 138 and 137 kPa, respectively: a) effective stress path, and b) shear stress - strain response.

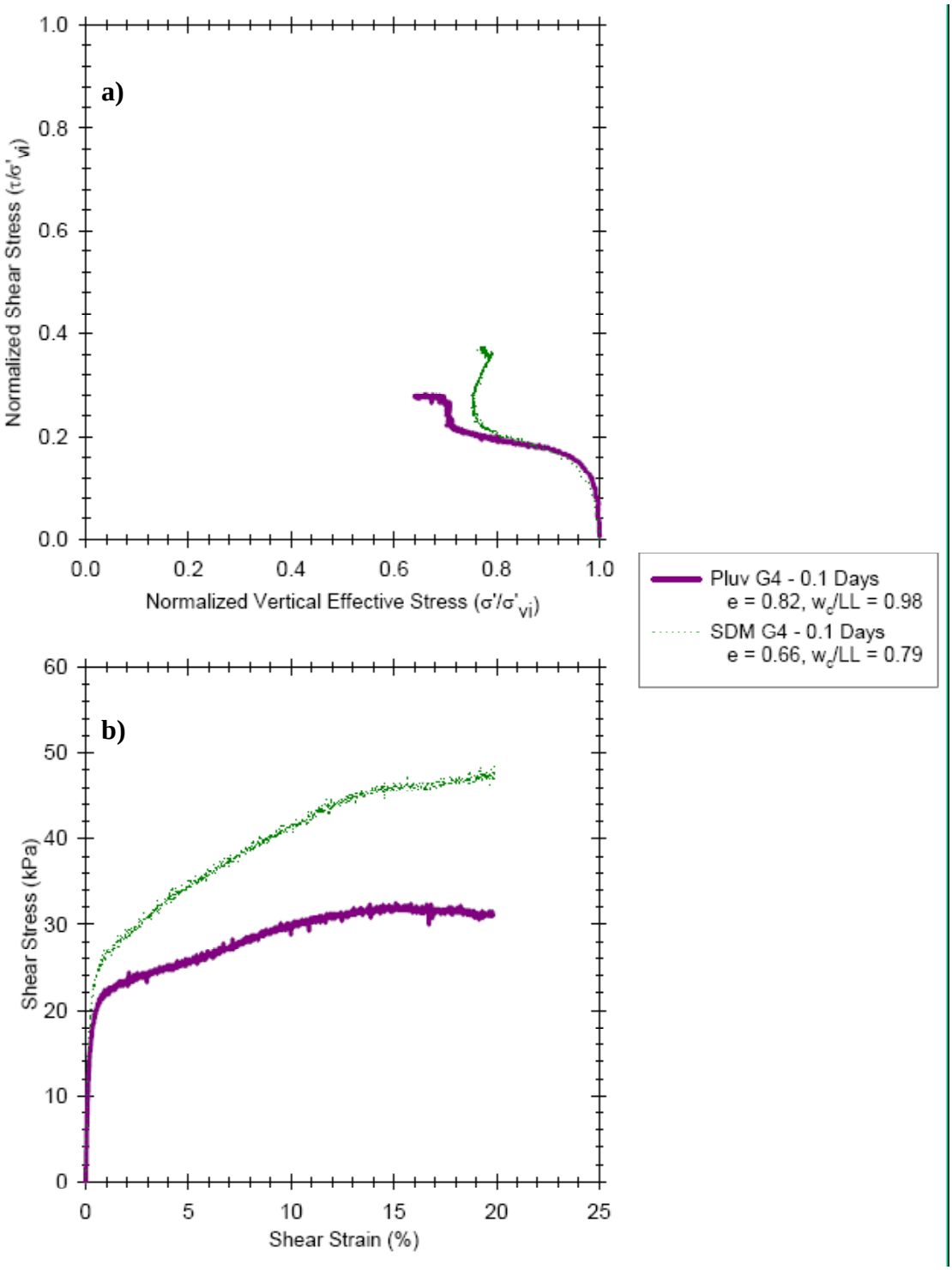

Figure 5.26 Simple Shear monotonic, strain-controlled testing comparing Soil G prepared using the In-Place Pluviated Method and Slurry Deposition Method, σ'_{vi} = 135 and 137 kPa, respectively: a) effective stress path, and b) shear stress - strain response.

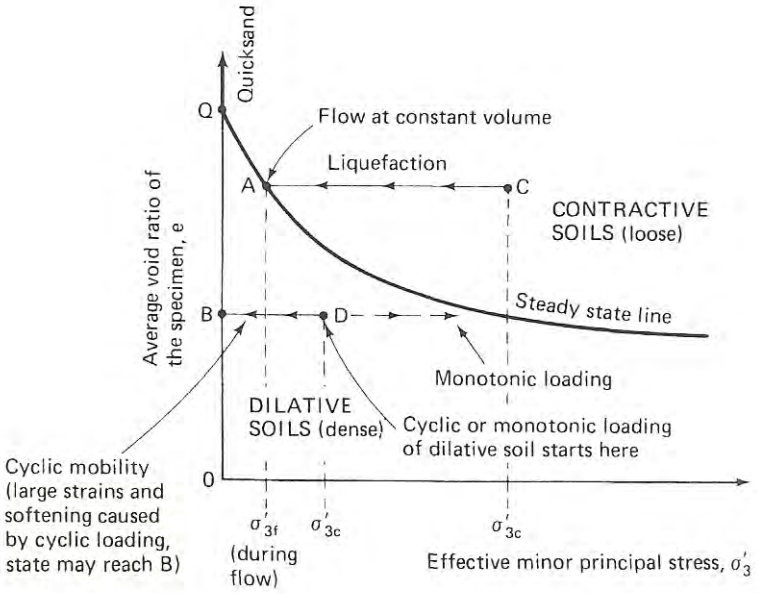

Figure 5.27 Example of state diagram showing liquefaction potential based on undrained tests on saturated sands (after Castro and Poulos, 1977).

Chapter 6 CYCLIC SOIL RESPONSE

6.1 Introduction

This chapter describes the laboratory tests that were performed to investigate the cyclic response of the reconstituted fine-grained soils from Adapazari, Turkey. The objective of this testing program is to evaluate the cyclic response of fine-grained soils using the cyclic triaxial and cyclic simple shear devices. This was accomplished by initially testing the reconstituted soil specimens at specified baseline conditions described in the following sections, and then retesting these soils after varying these seven parameters:

- specimen preparation method,
- time under confinement,
- void ratio (e),
- overconsolidation ratio (OCR),
- effective confining pressure (σ'_m),
- rate of loading, and
- initial static shear stress (α)

There were 82 tests performed on the soils as part of this program. Individual test results are provided in Appendix C1 and C2. Results are presented in a 4-way plot that shows the response of the soil during testing as a function of stress and strain. An example of the 4-way plot is shown in Figure 6.1. The first plot, Figure 6.1a, is a plot of the normalized shear stress (τ/σ'_{vi}) versus the normalized vertical effective stress (σ'_v/σ'_{vi}), which shows the effective stress path of the material during testing. The second plot, Figure 6.1b, is a plot of the shear stress (τ) versus the axial strain (ε_a) or horizontal shear strain (γ), hereafter described as the stress-strain plot. The third plot, Figure 6.1c, is a plot of the number of cycles of loading that the soil underwent before the initiation of liquefaction, or in some cases before the test was terminated, versus the normalized vertical effective stress. Figure 6.1c shows the time history of effective stress. The last plot, Figure 6.1d, is a plot of the number of cycles of loading that the soil underwent before the initiation of liquefaction, or in some cases before the test was terminated, versus the axial (ε_a) or shear (γ) strain. Figure 6.1d shows the time history of axial or shear strain.

One of the goals of this research is to evaluate the cyclic susceptibility and resistance of soils with different properties under varied loading conditions. The Cyclic Stress Ratio (CSR) versus the number of cycles to liquefaction initiation (N) plot is a useful tool for this purpose and it is an accepted graphical representation that quantifies this response. The Cyclic Stress Ratio (CSR) is the ratio of the shear stress, τ, to the initial effective confining stress, σ'_c, or

$$\mathbf{CSR} = \frac{\tau}{\sigma'_c} \qquad \mathbf{6.1}$$

The CSR is a fixed input parameter in each test that represents the intensity of the cyclic loading applied to the soil and is represented on the Y-axis in arithmetic units. The test's result, the

number of cycles of loading the soil experienced before liquefaction at the respective CSR, is represented on the X-axis, a logarithmic scale. The liquefaction criterion used in this research will be described in detail in Section 6.1.2. CSR vs. log N plots are developed by testing many specimens at a range of CSR values under the same baseline conditions (e.g., time under confinement, effective confining pressure, overconsolidation ratio (OCR), and initial static shear stress) and then compiling these results to develop a curve for the respective material.

Once the CSR vs. log N baseline curve is established, additional tests are performed that systematically vary one of the seven previously mentioned soil testing parameters. Differences between these tests and the baseline curve can then be interpreted as increases or decreases in the cyclic resistance of the soil.

6.1.1 Cyclic Triaxial and Simple Shear Descriptions and Comparisons

Cyclic triaxial testing

Laboratory liquefaction testing is often performed using cyclic triaxial equipment (e.g., some initial testing was performed by Seed and Lee, 1967; and Lee and Seed, 1967). In a triaxial test, a cylinder of soil with an un-reinforced membrane is isotropically consolidated to a specified effective confining stress. The specimen is cyclically loaded in the vertical direction and the axial strain and effective stress measurements are used to assess any trends in the cyclic response of the specimen.

In the past 40 years, the majority of all liquefaction testing of sands, silts, and even low plasticity clays has been performed using the triaxial equipment. This has accumulated a large database of information that has benefited the engineering community by improving the ability to draw rational conclusions on the cyclic response of an untested material by comparing responses of other soils within the database.

A major drawback to the triaxial test is that it does not reflect actual field conditions. The replication of an earthquake motion in laboratory testing is better represented by vertically propagating horizontal shear waves, not by a cyclic vertical loading. Additionally, laboratory triaxial specimens are typically isotropically consolidated, while in the field, the soil is typically anisotropically consolidated. The rotation of the principal stresses during loading is also different. In a triaxial test, the direction of the major principal stress will instantaneously rotate 90°, from vertical to horizontal and then back. In the field, the major principal stress will rotate smoothly and remain nearly vertical.

Another drawback of the triaxial test is the limit to which specimens may be tested. Care should be taken when high cyclic stress ratios are tested. A very large CSR may lift the top cap off of the specimen during the extension phase of loading. If this occurred, the accuracy of the results would be affected because the caps must remain in contact with the specimen for proper stress and strain measurements to be taken. The occurrence of “necking” during the extension phase of loading can also be a problem. “Necking” is a local decrease in cross-sectional area, which induces significant stress concentrations. If significant stresses are induced, the experimental stress–strain measurements are also affected because global volume is not consistent throughout

the specimen. These advantages and disadvantages of cyclic triaxial testing are summarized in Table 6.1.

Table 6.1 Advantages and Disadvantages of Cyclic Triaxial Testing

Advantages	Disadvantages
▪ **Commonly used, widely available** ▪ **Large international database** • Tests of almost all soil types in different conditions available	▪ **Does not replicate field conditions** • Horizontal loading in field conditions vs. vertical axial loading in the laboratory • Anisotropic field conditions vs. isotropic lab conditions • Principal rotation of stress to ~40° for field conditions vs. 90° instantaneous transitions for lab conditions ▪ **Limited testing capability** • End cap displacement at high CSR • Necking possible

Cyclic simple shear testing

The simple shear test is another test that was used for this research to evaluate the cyclic strength of soils. The cyclic simple shear (CSS) testing device is superior to the cyclic triaxial (CTX) testing device because it better replicates field conditions. Unlike the CTX device in which the major principal stress axis instantaneously rotates 90°, in the CSS test the major principle stress axis will undergo a smooth rotation during cyclic loading.

Another advantage to the CSS device is that the specimens have a relatively uniform stress field and minimum pore water pressure redistribution. Unlike triaxial specimens, which are relatively tall (13 cm) and thin (7 cm diameter), simple shear specimens have small heights (2 cm) and large diameters (10 cm). The diameter to height ratio (D/H) is relatively large, D/H > 5, allowing for more uniformity of the stresses throughout the specimen.

The CSS device can also load soils in two horizontal directions, which is an advantage because it betters resembles actual earthquake motions. Bi-directional loadings were not applied in this research program; however, the UC Berkeley Bi-directional CSS device has been utilized previously to test in this manner. Seed et al. (1975), Ishihara and Yamazaki (1980), and Kammerer (2002) found that materials loaded under multi-directional shear conditions exhibit much larger shear strains than with one-directional loading.

There are also several disadvantages to the CSS test. Simple shear testing has been available for many decades, yet standardization and lack of ability to saturate specimens have limited the availability for a large database of reliable results. This situation is improving. More researchers are able to produce saturated specimens to test in robust cyclic simple shear devices such as the ones at the University of California, Davis, and the University of British Columbia.

Secondly, the specimens tested using CSS lack imposed complementary shear stresses. This disadvantage was not of major concern for this research because the D/H ratio for the specimens used in this study was approximately 5. Numerical studies (e.g., Duncan and Chang, 1970) have suggested for samples with D/H ratios greater than 4, the lack of complementary shear stresses will influence only a relatively small portion of the sample. Additionally, Franke et al. (1979) found no differences in the loading resistance of samples tested with diameter to height (D/H) ratios between 3.75 and 7.5.

A third disadvantage of the CSS is the propensity to rock or pinch the specimen during testing, however this too was not an issue in this research. The UC Berkeley Bi-directional CSS, which was used for this research, is robustly designed to minimize the potential for rocking and pinching because it is nearly rigid. More information on the testing device can be found in Section 4.5.1. These advantages and disadvantages of CSS testing are summarized in Table 6.2.

Table 6.2 Advantages and Disadvantages of Cyclic Simple Shear Testing

Advantages	Disadvantages
▪ **Replicates field conditions well**	▪ **Relatively small reliable database**
▪ **Mostly uniform stresses over specimen**	▪ **Lack of complementary shear stresses**
▪ **Loading in 2 horizontal directions to better simulate 2-D testing**	▪ **Rocking of specimen possible**

6.1.2 Liquefaction Criteria

A clear definition of "liquefaction" is required to compare results with other studies. Several different thresholds of stress and strain have been used in the past. In the laboratory, liquefaction is often defined as the point at which the pore water pressure has increased to a level that nearly equals the initial total confining stress (i.e., the effective stress is zero, which is synonymous to the pore water pressure ratio, $r_u = \Delta u/\sigma_{co}' \approx 1.0$). Quantifying liquefaction is difficult using this definition because the point of $r_u \approx 1.0$ is often difficult to discern precisely and may not be reached in all cases. Alternatively, 3% single amplitude axial strain (typically in extension), or 5% double amplitude (DA) axial strain have been used to define the initiation of liquefaction in CTX testing. For the CSS test, liquefaction is typically defined using a single-amplitude horizontal shear strain threshold. Wijewickreme and Sanin (2004) defined it as 3.75% single amplitude shear strain; whereas Bray and Sancio (2006), Kammerer (2002), and Wu (2002) defined it as 5% single amplitude shear strain. For a stress-based definition, Boulanger (1998)

reports that an effective stress equal to 20% of the initial effective stress, or r_u=80%, is sufficient to cause significant shear strains leading to large deformations.

For this research, initiation of liquefaction is defined as 3% single amplitude axial strain (ε_a), or 5% double amplitude axial strain for the CTX testing. For CSS testing, the 5% single amplitude shear strain (γ) criterion will be used. An illustration of the terms single amplitude strain and double amplitude strain are shown in Figure 6.2. When testing using the CSS device during the course of the research, the effective stress never reached zero, or r_u = 100%. Instead, most soils had a minimum normalized effective stress of 20%, or r_u = 80%. For this reason, the less traditional r_u=80% criteria is also used as a definition of the onset of liquefaction in the stress-based comparison between the different specimens in cyclic simple shear.

Liquefaction has also been defined using the term cyclic mobility. For this research, cyclic mobility has been divided into two distinct responses, i.e., cyclic mobility with limited strain potential and cyclic mobility with large shear strain potential. A graphical depiction of the two modes of cyclic mobility is shown in Figure 6.3. For specimens that exhibit cyclic mobility with limited shear strain potential, shear strains usually increase in a linear fashion with each loading cycle. For specimens that exhibit cyclic mobility with unlimited shear strain potential, the shear strains per cycle are typically small at the beginning of the cyclic test. After a point, the cyclic-induced strains increase significantly and reach 5% shear strain or greater within 1 to 2 more cycles of loading.

6.2 Cyclic Triaxial Tests

The cyclic triaxial test is widely used for the measurement of pore water pressure response and strain potential of saturated soils subjected to cyclic loading (e.g., Seed and Lee, 1966; Seed et al., 1969; Lee and Roth, 1977; Andersen et al., 1988; Zergoun and Vaid, 1995; Boulanger et al., 1998; Naeini and Baziar, 2003; Yasuhara et al., 2003; Yilmaz et al., 2004). In this test the specimen is usually isotropically consolidated to an initial effective confining stress equal to σ'_c, ($\sigma'_c = \sigma'_1 = \sigma'_3$). The vertical load is subsequently cycled symmetrically (using a sine wave) at constant amplitude and at a loading frequency equal to 0.005 Hz (1 cycle per 200 seconds) or 1 Hz (1 cycle per second) until a predetermined axial strain is reached, or a given number of cycles has been applied. The predetermined value for this research is 3% single amplitude axial strain in extension, or 5% double amplitude axial strain. A summary of the cyclic triaxial tests performed in this study is listed in Table 6.3.

For CTX conditions, the CSR is defined as the ratio of one-half of the deviator stress, σ'_d, to the effective confining stress, σ'_c or σ'_3. This can be expressed as Equation 6.2.

$$\textbf{CSR} = \frac{\sigma'_d}{2\sigma'_3} \qquad \textbf{6.2}$$

The response of a soil during a cyclic triaxial test can be depicted using a Mohr's circle representation, and an example of the Mohr's circle is shown in Figure 6.4. In this figure the specimen begins in an isotropic state, σ'_c. The Mohr's circle then expands to the right and then back to the left in the compression and extension phases, respectively, when the cyclic deviatoric stress, or σ'_d, is applied to the specimen.

Table 6.3 Summary of index properties and results of cyclic triaxial tests performed on specimens isotropically consolidated

Test Name	PI	LL	FC (%)	σ'_m (kPa)	e_o	σ'_d (kPa)	CSR	r_u = 100%	freq (Hz)	+1% ε_a	+2% ε_a	+3% ε_a	+4% ε_a	+5% ε_a	-1% ε_a	-2% ε_a	-3% ε_a	-4% ε_a	-5% ε_a	5% (DA) ε_a
Triax G1	10	31	77	50	0.71	22	0.23	73	1	66	68	69	70	71	65	67.5	69	70	71.5	68
Triax G2	10	31	77	50	0.72	44	0.44	4	1	2	2	3	3	3	1	1.5	1.5	2	2	2
Triax G3	10	31	77	50	0.69	44	0.44	-	0.005	0.5	0.5	-	-	-	0.5	1	1	1	1	1
Triax G5-1	10	31	77	50	0.74	20	0.20	-	0.005	-	-	-	-	-	5	5	5	5	5	5
Triax G5-2	10	31	77	50	0.71	22	0.22	-	1	45	55	59	63	66	52	59	64	67	72	61
Triax G5-3	10	31	77	50	0.68	20	0.20	-	0.005	-	-	-	-	-	-	-	-	-	-	-

PI = Plasticity Index; LL = Liquid Limit; FC (%) = Percentage of particles finer than 75 μm;
σ'_m = Mean effective stress ($\sigma'_m = (\sigma'_1 + \sigma'_2 + \sigma'_3)/3$); e_o = void ratio; σ'_d = peak deviator stress applied;
CSR = Cyclic Stress Ratio ($\sigma'_d/2\sigma'_3$); r_u = 100% = Number of cycles to required to reach 100% pore water pressure ratio;
freq = Frequency of Loading, in Hz; +1% ε_a = number of cycles required to reach 1% single amplitude axial strain;
+5 % (DA) ε_a = number of cycles required to reach 5% double amplitude axial strain

6.2.1 Isotropically Consolidated Cyclic Triaxial Tests

The two tests, Triax G-1 (CSR = 0.225) and Triax G-2 (CSR = 0.44), were prepared using the Slurry Deposition Method and were tested at an effective confining stress, σ'_c = 50 kPa and at a loading frequency of 1 Hz. The index properties and test parameters are listed in Table 6.4.

Table 6.4 Specimen index properties and test parameters for cyclic triaxial testing

Test Name	PI	LL	FC (%)	e_o	freq (Hz)	B-Value	w_c (%)	w_c/LL	CSR	5% (DA) ε_a
Triax G1	10	31	77	0.71	1	0.92	26.15	0.84	0.225	68
Triax G2	10	31	77	0.72	1	0.98	25.18	0.81	0.44	2

The results of the two tests are shown in Figure 6.5. As previously mentioned in Chapter 5 and in greater depth in Section 6.2.1.1, this loading rate is too high to properly measure pore water pressures and report effective stresses. Only plot (b) and plot (d) of the 4-way plot are shown because the effective stresses in (a) and (c) cannot be accurately reported at this loading rate.

Triax G1 reached 5% double amplitude (DA) axial strain in 68 cycles compared to Triax G2 that reached 5% DA axial strain in 2 cycles. Using these results, the CSR Chart, shown in Figure 6.6, was developed.

6.2.1.1 Effects of the Rate of Loading

Four tests were performed using the Cyclic Triaxial testing device to evaluate the effects of the rate of loading. Specimens Triax G1, G2, G3, and G5-1, were prepared by the Slurry Deposition Method and were tested at an effective confining stress, σ'_c = 50 kPa. Two CSR levels: 0.2 and 0.44 were tested in combination with loading frequencies of 0.005 and 1 Hz. The index properties and test conditions for these tests are listed in Table 6.5.

Table 6.5 Index properties and test conditions for cyclic triaxial testing at different loading rates

Test Name	PI	LL	FC (%)	e_o	freq (Hz)	B-Value	w_c (%)	w_c/LL	CSR	5% (DA) ε_a
Triax G1	10	31	77	0.71	1	0.92	26.15	0.84	0.225	68
Triax G2	10	31	77	0.72	1	0.98	25.18	0.81	0.44	2
Triax G3	10	31	77	0.69	0.005	0.97	25.49	0.82	0.44	1
Triax G5-1	10	31	77	0.74	0.005	0.99	27.25	0.88	0.2	5

The loading rate was shown in each test to significantly affect the number of cycles to the initiation of liquefaction. Testing at a CSR = 0.22, the specimens reached 5% DA axial strain in 68 cycles for a loading frequency of 1 Hz and at 5 cycles for a loading frequency of 0.005 Hz. An example of the stress-strain curves developed from the tests is shown in Figure 6.7a. Likewise, testing at a CSR = 0.44, the specimens reached 5% double amplitude axial strain at 2

cycles and 1 cycle with loading frequencies of 1 Hz and 0.005 Hz, respectively. This is consistent, but not as dramatic as the test results for tests performed at lower CSR values.

These results are consistent with the findings of Zergoun and Vaid (1994) and Boulanger et al. (1998), in which they found that nearly identical specimens with similar void ratios have an order of magnitude difference in the number of cycles of loading to the initiation of liquefaction when testing at low and high cyclic loading frequencies.

These results were crosschecked with the Triax G-5 test series. Specimen Triax G5-1 was tested at a CSR = 0.2 and at a loading frequency of 0.005 Hz; and it liquefied in 5 cycles. The specimen was reconsolidated, renamed Triax G5-2, and retested at a CSR = 0.2 and at a loading frequency of 1 Hz; and it liquefied in 61 cycles. The specimen was again reconsolidated, renamed Triax G5-3, and retested at a CSR = 0.2 and a loading frequency of 0.005 Hz; and this test liquefied in less than 1 cycle.

The specimens exhibited significantly different responses at these two loading frequencies. Notice in Figure 6.7b that relatively little axial strain develops in the early cycles. It is possible that the specimen preparation method of Slurry Deposition creates a sensitive material, which is relatively brittle under sustained loads. During the rapid cyclic loading, the material is more compliant, and thus it requires more cycles to cause liquefaction. The CSR vs. log N plot comparing the 0.005 Hz test results to the baseline of 1 Hz tests is given in Figure 6.8.

For these triaxial tests, pore water pressure measurements were made at the top and bottom of the specimen. These measurements do not accurately represent the pore water pressure response of the entire specimen unless the test is performed at a rate that is slow enough to allow for pore water pressure equilibration throughout the specimen.

As explained in Chapter 5, the loading rate of a cyclic test should be based on the duration such that ¼ cycle is greater than or equal to $4t_{50}$, or four times the time to 50% consolidation. This is equivalent to $16t_{50}$ for one cycle. Equation 5.1 is used to find the appropriate t_{50} of cyclic testing. From the results of Section 5.4.1, the coefficient of consolidation, c_v, for Soil G is approximately 0.021 cm^2/sec. Most specimens were approximately 13 cm in height and double drained (D = 13/2). From these dimensions, t_{50} is approximately 400 seconds, meaning the frequency of loading to properly measure pore water pressures is 0.00016 Hz (or 1 cycle every 105 minutes). This means that pore water pressures measurements taken even at the slower loading frequency of 0.005 Hz are not accurate and should not be relied upon.

6.3 Cyclic Simple Shear Tests

The cyclic simple shear test is superior to the cyclic triaxial tests in that it better replicates field conditions and earthquake loading (e.g., Boulanger, 1993, 2004, 2006, 2007; Biscontin, 2001; Kammerer, 2002; Wu, 2002; Sancio, 2003; Anantanavanich, 2006; Bray, 2004a, 2004b: Bray and Sancio, 2006; Wijewickreme, 2004, 2006). In simple shear testing, the specimen is initially anisotropically consolidated to a mean effective confining stress of σ'_m; which is calculated as:

$$\sigma'_m = \frac{(\sigma'_1+\sigma'_2+\sigma'_3)}{3} = \frac{(\sigma'_v+2K_o*\sigma'_v)}{3} \qquad \textbf{6.3}$$

where σ'_1, σ'_2, σ'_3, are the effective stresses on the principal axes, σ'_v is the vertical effective stress and K_o is the coefficient of lateral earth pressure at rest. K_o was assumed equal to 0.6 from previous work by Sancio (2003) on similar soils. In cyclic simple shear tests, the horizontal shear load is cycled symmetrically (using a sine wave) at constant amplitude and at a loading frequency equal to 0.005 Hz (1 cycle per 200 seconds) or 1 Hz (1 cycle per second) until a predetermined shear strain is reached, or a given number of cycles of loading have been applied. The predetermined shear strain, as stated in Section 6.1, is 5% single amplitude shear strain (γ), which is considered the initiation of liquefaction.

For cyclic simple shear conditions, CSR is the ratio of the shear stress, τ, to the initial vertical effective stress σ'_{vi}. The CSR can be expressed through Equation 6.4.

$$\mathbf{CSR} = \frac{\tau_{\max}}{\sigma'_{vi}} \qquad \mathbf{6.4}$$

Figure 6.9 depicts a generalized Mohr's circle of a cyclic simple shear test. In this figure, the specimen is initially in an anisotropic state with the coordinates of σ'_v and $K_o * \sigma'_v$. The Mohr's circle expands and contracts radially as the specimen is cycled by the shear stress, τ_{cyc}, to accommodate the increase and decrease in shear stress.

The parameter τ_{max} was determined by using the average of the maximum and minimum shear stresses over the first 6 cycles of loading, when six cycles were available. This averaging gave a stable calculation for computing the CSR and it smoothed over any noise that may have been in the system. A full description of laboratory corrections and data reductions for the UC Berkeley Bi-Directional Simple Shear Device can be found in Kammerer (2002) and Wu (2002).

6.3.1 Effects of Soil Index Properties

The soil index properties, as discussed in Chapter 5, affect the static strength and the response of the material. A number of previous researchers have identified the soil index property PI as the primary parameter describing a material's liquefaction susceptibility.

6.3.1.1 Slurry Deposition Method

Thirty-three cyclic simple shear samples were prepared using the Slurry Deposition Method. The Slurry Deposition Method was shown to be a useful method of preparing consistent and repeatable specimens for determining cyclic strengths. The specimen index properties and the cyclic simple shear test results are listed in Table 6.6 and

Table 6.7.

The soil batches, Soil A, Soil B, Soil C, Soil D, Soil E, Soil F, and Soil G, were tested at a constant CSR = 0.21, σ'_m = 100 kPa, OCR = 1, and a loading frequency of 0.005 Hz. This frequency met the requirements for proper pore water pressure measurements due to the reduced drainage length in the shorter CSS test specimens. Using the tests results, comparisons were made of the first cycle and 5% shear strain cycle between Soil G and Soil A, Soil C, Soil D, Soil E, and Soil F. Soil B was not included in these comparisons because it was tested at an OCR = 1.6. The specimen index properties for Soil A, Soil C, Soil D, Soil E, Soil F, and Soil G are listed in Table 6.8.

Table 6.6 Summary of index properties and results of cyclic simple shear tests performed on Soils A through F reconstituted using the Slurry Deposition Method

Test Name	PI	LL	FC (%)	σ'_v (kPa)	σ'_m (kPa)	e_o	CSR	freq (Hz)	+1% γ	+2% γ	+3% γ	+4% γ	+5% γ	-1% γ	-2% γ	-3% γ	-4% γ	-5% γ
SDM A1	2	31	72%	138	101	0.69	0.210	0.005	1	1	1	2	2	1	1	1	2	2
SDM A4	2	31	72%	139	102	0.74	0.199	0.005	1	2	2	2	3	1	1	2	2	2
SDM A5	2	31	72%	136	100	0.67	0.145	0.005	(did not produce at least 1% shear strain after 60 loading cycles)									
SDM A6	2	31	72%	140	103	0.67	0.173	0.005	3	4	5	6	6	3	4	5	6	6
SDM A7	2	31	72%	137	101	0.66	0.164	0.005	7	14	16	18	19	12	15	17	18	19
SDM A8	2	31	72%	138	101	0.69	0.209	0.005	2	3	4	5	5	2	3	4	4	5
SDM A10	2	31	72%	138	101	0.70	0.210	1	4	7	8	9	9	5	7	8	9	9
SDM A11	2	31	72%	138	101	0.68	0.210	0.005	2	3	4	4	4	2	3	3	4	4
SDM A12	2	31	72%	70	51	0.69	0.174	0.005	8	15	18	20	21	19	21	22	23	24
SDM A13	2	31	72%	273	200	0.64	0.162	0.005	5	8	9	10	10	5	8	9	10	10
SDM A14	2	31	72%	135	99	0.66	0.211	0.005	20	26	28	29	30	23	26	28	29	30
SDM A15	2	31	72%	137	101	0.66	0.250	0.005	6	12	14	15	16	9	13	14	15	16
SDM A16	2	31	72%	139	102	0.69	0.101	0.005	5	15	23	34	46	-	-	-	-	-
SDM B1	5	32	77%	138	102	0.73	0.216	0.005	1	1	4	5	6	1	4	5	6	6
SDM C1	5	32	88%	142	104	0.70	0.213	0.005	1	1	1	3	3	1	2	4	4	5
SDM D1	11	38	94%	139	102	0.76	0.210	0.005	1	1	2	2	3	1	1	2	2	3
SDM E1	14	39	95%	144	106	0.80	0.210	0.005	1	1	1	1	1	1	1	3	3	4
SDM F1	7	28	57%	136	100	0.81	0.209	0.005	1	1	1	2	3	1	2	2	2	3

PI = Plasticity Index; LL = Liquid Limit; FC (%) = Percentage of particles finer than 75 μm; σ'_v: initial vertical effective stress
σ'_m = Mean effective stress ($\sigma'_m = (\sigma'_1 + \sigma'_2 + \sigma'_3)/3$); e_o = void ratio; CSR = Cyclic Stress Ratio (τ_{cyc}/σ'_{vi});
freq = Frequency of Loading, in Hz; +1% γ = number of cycles required to reach 1% shear strain

Table 6.7 Summary of index properties and results of cyclic simple shear tests performed on Soil G reconstituted using the Slurry Deposition Method

Test Name	PI	LL	FC (%)	σ'_v (kPa)	σ'_m (kPa)	e_o	CSR	freq (Hz)	+1% γ	+2% γ	+3% γ	+4% γ	+5% γ	-1% γ	-2% γ	-3% γ	-4% γ	-5% γ
SDM G1	10	31	77%	140	103	0.63	0.216	0.005	1	1	4	5	6	1	4	5	6	7
SDM G5	10	31	77%	135	99	0.60	0.198	0.005	6	12	15	16	17	8	13	15	16	17
SDM G6	10	31	77%	138	101	0.64	0.145	0.005	12	16	18	19	20	17	20	20	21	22
SDM G7	10	31	77%	138	101	0.64	0.240	0.005	1	1	2	2	2	1	1	1	1	1
SDM G8	10	31	77%	145	106	0.68	0.215	1	1	2	3	3	3	1	2	2	3	3
SDM G9	10	31	77%	138	101	0.65	0.193	0.005	2	2	3	3	3	2	2	2	3	3
SDM G10	10	31	77%	138	101	0.62	0.176	0.005	2	4	5	6	7	4	5	6	7	8
SDM G11	10	31	77%	137	100	0.66	0.176	1	7	10	11	12	12	9	11	11	12	12
SDM G12	10	31	77%	68	50	0.67	0.177	0.005	6	10	11	12	13	11	12	13	13	14
SDM G13	10	31	77%	274	201	0.63	0.171	0.005	2	3	4	4	4	2	3	3	4	4
SDM G14	10	31	77%	68	50	0.68	0.177	0.005	3	5	7	7	8	6	7	8	8	9
SDM G15	10	31	77%	137	101	0.67	0.175	0.005	2	2	2	2	3	2	2	2	2	3
SDM G16	10	31	77%	137	101	0.60	0.178	0.005	(did not produce at least 1% shear strain after 60 loading cycles)									
SDM G17	10	31	77%	141	103	0.65	0.172	0.005	51	63	67	69	71	67	70	72	74	-
SDM G18	10	31	77%	138	101	0.61	0.176	0.005	2	4	4	5	5	3	4	4	5	5

PI = Plasticity Index; LL = Liquid Limit; FC (%) = Percentage of particles finer than 75 μm; σ'_v: initial vertical effective stress
σ'_m = Mean effective stress ($\sigma'_m = (\sigma'_1 + \sigma'_2 + \sigma'_3)/3$); e_o = void ratio; CSR = Cyclic Stress Ratio (τ_{cyc}/σ'_{vi});
freq = Frequency of Loading, in Hz; +1% γ = number of cycles required to reach 1% shear strain

The void ratios in Table 6.8 are not the same for all the materials. These initial void ratios were found to be consistent for a given material at a given level of stress. The term "formation void ratio" was adopted following multiple Constant Rate of Strain Consolidation tests on Soil G prepared using the Slurry Deposition Method. The results showed that the same void ratio was achieved at a given level of stress for each test. Thus, each of the soils tested had a unique stress-dependent formation void ratio when prepared using the Slurry Deposition Method.

Table 6.8 Soil properties and cyclic simple shear testing conditions for specimens reconstituted by the Slurry Deposition Method

Test Name	PI	LL	FC (%)	e_o	B-Value	w_c (%)	w_c/LL	Days	OCR	CSR	5% γ
SDM A1	2	31	72%	0.69	0.97	25.84	0.83	0.04	1.0	0.210	2
SDM C1	5	32	88%	0.70	0.97	25.97	0.81	0.03	1.1	0.213	3
SDM D1	11	38	94%	0.76	0.99	28.44	0.75	0.04	1.0	0.210	3
SDM E1	14	39	95%	0.80	0.99	29.63	0.76	0.05	1.0	0.210	1
SDM F1	7	28	57%	0.81	0.98	29.96	1.07	0.05	1.0	0.209	3
SDM G1	10	31	77%	0.63	0.99	23.53	0.76	0.08	1.0	0.216	7

The results for the cyclic simple shear tests as a function of PI are shown in Figure 6.10. In this figure, the PI ranges between 2 and 14. As shown in the middle plot of Figure 6.10, Soil G (PI = 10) and Soil D (PI = 11) have very similar stress-strain curves, i.e. "banana loops," but reached 5% shear strain in a different numbers of cycles of loading, 7 cycles and 3 cycles, respectively. These results suggest that the PI of soil, by itself, may be insufficient as an indicator of liquefaction susceptibility.

The shapes of the stress-strain curves at 5% shear strain are commonly described as "football shapes" and "banana loops." The "football shape," shown in Figure 6.11a, is representative of materials with a contractive tendency under drained conditions, such as Pluv F1 (PI = 7, LL = 28, FC = 57%), which did not fail during testing, but exhibits the quintessential "football shape." "Banana loops," shown in Figure 6.12a, are representative of materials with a dilative tendency under drained conditions, such as SDM A6 (PI = 2, LL = 31, FC = 72%).

In the case of a cyclic test on a contractive material, the first quarter cycle (point A to point B) begins with an increase in stress. Small strains occur during this part of the loading, which is shown in Figure 6.11b and Figure 6.11c. The material then moves back to the original stress in the next quarter cycle (point B to point C), as the strains return to the origin. In the third quarter cycle (point C to point D), only slight negative pore water pressures develop, even though strains are increasing. In the last quarter cycle (point D to point E), the strains have reversed and a slight increase in excess pore water pressure occurs as the specimen heads back to the original stress.

In the case where the soil exhibit a dilative tendency, in the first quarter of a cycle (point A to point B) large strains as well as significant negative excess pore water pressures are shown in Figure 6.12b and Figure 6.12c. The shear stress increases, pore water pressures decrease, and the effective stress increases. From point B to C, the material "collapses" and develops positive pore

water pressures and the effective stress decreases. Following the collapse after point B, the material begins to develop negative excess pore water pressures as it proceeds through point C. From point C to D, strains are increasing and the material continues to produce negative excess pore water pressures. At point D, the strains reverse causing the material to develops positive pore water pressures again, as in point B, until the a new cycle begins.

The shear strain time histories for Soil A, Soil C, Soil D, Soil E, Soil F, and Soil G are shown in Figure 6.13. This figure shows the cyclic mobility of the soils and their different responses within the initial four cycles of loading. By the fourth cycle, most soils have already developed substantial pore water pressures (r_u > 70%), and the 5% single amplitude strain level has been reached or nearly reached.

Despite the lower void ratios, all specimens reconstituted by the Slurry Deposition Method developed large strains in a smaller number of cycles when compared to the natural samples of Adapazari silts with the same PI and LL. Strains in the reconstituted soils developed considerably faster than in field specimens. As an example, one specimen, A5-P9B-3 (PI = 11, LL = 38), from Sancio (2003) tested at a CSR = 0.27, developed 5% shear strain in 12 cycles of loading. Test SDM D1 (PI = 11, LL = 38), tested at a CSR = 0.21, developed 5% strain after 3 loading cycles. Specimen SDM D1 was a relatively young soil (i.e., time under confinement of 0.04 days) which may have influenced its response. The effects of the time under confinement are likely a reason for the observed differences in the responses of reconstituted and natural soil specimens. These effects are discussed further in Section 6.3.2. The large strains that develop at relatively low formation void ratios in the reconstituted soils prepared by Slurry Deposition were a prime motivation to switch to the In-Place Wet Pluviation Method. The results from the Slurry Deposition Method remain useful in that they allow for a systematic investigation of the key factors of liquefaction susceptibility and resistance because of their specimen uniformity and lack of particle segregation.

After the seven soils were tested, a comprehensive testing program was instituted for Soils A and G with baseline conditions of: σ'_m = 100 kPa, 0.8 days under confinement, a loading frequency of 0.005 Hz, and OCR = 1. The CSR was then varied for each test and CSR vs. log N plots were developed.

To develop the CSR baseline curve for Soil A prepared by the Slurry Deposition Method, four tests with properties listed in Table 6.9 were performed. The mean void ratio was 0.67 and the w_c/LL was approximately 0.81.

Table 6.9 Specimen properties and cyclic simple shear testing conditions for Soil A reconstituted by the Slurry Deposition Method for CSR comparison

Test Name	PI	LL	FC (%)	e_o	B-Value	w_c (%)	w_c/LL	CSR	5% γ
SDM A5	2	31	72%	0.67	0.96	24.9	0.80	0.145	-
SDM A6	2	31	72%	0.67	0.96	25.1	0.81	0.173	6
SDM A7	2	31	72%	0.66	0.97	24.5	0.79	0.164	19
SDM A11	2	31	72%	0.68	0.96	25.4	0.82	0.210	21

Figure 6.14 shows the results of these tests. In Figure 6.14b, the stress strain curves for the first cycle and cycle at 5% single amplitude shear strain are given. The stress-strain curves of SDM A6 and SDM A7 are nearly identical, but SDM A6 reached 5% shear strain in 6 cycles and SDM A7 reached 5% shear strain in 19 cycles. The hollow point on the CSR Chart, Figure 6.15, represents SDM A5 which did not reach 5% shear strain at the given CSR.

The functional form of the CSR curve for Soil A prepared using the Slurry Deposition Method was found to be CSR = a + b/N, where N represents the cycles to liquefaction initiation. This form was determined by doing a best fit using a least-squares regression to solve for the coefficients a and b, which are 0.147 and 0.226, respectively. The standard error term is 0.0145 and $R^2 = 0.83$. SDM A5 was not included in the regression.

Four tests, with the properties listed in Table 6.10, were also performed on Soil G prepared by the Slurry Deposition Method to construct a baseline CSR curve. The mean void ratio was 0.65 and the w_c/LL ratio was approximately 0.78. As with the CRS consolidation, monotonic, and triaxial tests, the void ratio for Soil G is lower than Soil A.

The results of these tests are shown in Figure 6.16 and the CSR vs. log N plot is shown in Figure 6.17.

Table 6.10 Specimen properties and cyclic simple shear testing conditions for Soil G reconstituted by the Slurry Deposition Method for CSR comparison

Test Name	PI	LL	FC (%)	e_o	B-Value	w_c (%)	w_c/LL	CSR	5% γ
SDM G6	10	31	77%	0.64	0.97	23.6	0.76	0.145	20
SDM G7	10	31	77%	0.64	0.96	24.0	0.77	0.240	2
SDM G9	10	31	77%	0.65	0.95	24.0	0.78	0.193	3
SDM G18	10	31	77%	0.65	0.96	24.3	0.78	0.176	5

In Figure 6.16b, the stress-strain diagrams for the first cycle of SDM G6, SDM G9, and SDM G18 initially have large shear stress and little shear strain, having a tight "football shape." Negative and positive excess pore water pressures begin to develop and the four specimens exhibit well developed "banana loops" for the final cycle of loading, at approximately 5% shear strain.

From Figure 6.17 the functional form of the CSR curve for Soil G prepared using the Slurry Deposition Method was found to be CSR = a + b/N, where N represents the cycles to 5% shear strain. The coefficients a and b, are 0.133 and 0.204, respectively. The standard error term is 0.0072 and $R^2 = 0.98$.

In both Figure 6.16 and Figure 6.17, the differences in the responses of specimens with CSR = 0.145 to 0.176, is greater than the differences between specimens with CSR = 0.176 to 0.240. Specimens SDM G6 (CSR = 0.145), SDM G18 (CSR = 0.176) and SDM 7 (CSR = 0.240), failed in 20, 5 and 2 cycles, respectively. The distribution of the number of cycles to 5% shear strain,

suggests that it is logarithmic, making the choice for a logarithmic X-axis for the CSR vs. log N plot appropriate.

To assess the relationship between Soil A (PI = 2, LL = 31) and Soil G (PI = 10, LL = 31) reconstituted by the Slurry Deposition Method, a comparison of the CSR curves is shown in Figure 6.18. As seen in this figure, the cyclic strength of Soil A is greater than Soil G. The two curves for Soil A and G are roughly parallel to each other, with Soil A to the right and above the Soil G curve. This means that for a given level of shaking, say a CSR = 0.175, it would be expected that Soil G would reach 5% shear strain in approximately 5 cycles of loading, and Soil A would require 9 cycles of loading.

Previous research shows a natural progression of CSR curves as up and to the right as the PI increases. Sancio (2003) confirmed this trend of increasing PI as up and to the right for soils of increasing PI between 12 and 20, but for soils with PI less than 12, he did not observe systematic trends in their CSR vs. log N curves. Figure 6.18 also does not show a significant difference between the results for PI=2 and PI=10 soils (i.e., PI<12). Given these results, it is possible that soils with a PI less than 12 do not respond systematically in terms of CRR versus PI.

6.3.1.2 In-Place Wet Pluviation Method

Forty-three cyclic simple shear tests were conducted on specimens prepared by the In-Place Wet Pluviation Method. Table 6.11,

Table 6.12 and
Table 6.13 list the index properties and test results for Pluviated A, D, F, and G specimens.

Soil A and Soil G were the primary soils tested using the In-Place Wet Pluviation Method of specimen preparation. Using this method, specimens typically took twelve days to construct. Most specimens were tested 0.8 days after the application of effective confining stress. This length of time between the start of construction of the specimen and testing limited the number of Pluviated specimens. Soil A and Soil G were chosen out of the seven different batches because they both have a LL = 31, but each has a different PI (i.e., Soil A has PI = 2 and Soil G has PI = 10). The effects of PI could be studied and another key liquefaction parameter, w_c/LL (water content to Liquid Limit ratio) could be assessed.

Table 6.11 Summary of index properties and results of cyclic simple shear tests performed on Soils "A1 – A23" reconstituted using the In-Place Wet Pluviation Method

Test Name	PI	LL	FC (%)	σ'_v (kPa)	σ'_m (kPa)	e_o	CSR	freq (Hz)	+1% γ	+2% γ	+3% γ	+4% γ	+5% γ	-1% γ	-2% γ	-3% γ	-4% γ	-5% γ
Pluv A1	2	31	72%	139	102	0.94	0.126	0.005	30	43	46	47	48	46	48	-	-	-
Pluv A3	2	31	72%	144	105	0.84	0.141	0.005	(did not produce at least 1% shear strain after 15 loading cycles)									
Pluv A7	2	31	72%	141	104	0.93	0.120	0.005	16	(did not produce at least 2% shear strain after 35 loading cycles)								
Pluv A8	2	31	72%	138	101	0.92	0.114	0.005	24	(did not produce at least 2% shear strain after 35 loading cycles)								
Pluv A9	2	31	72%	142	105	0.93	0.188	0.005	1	1	2	2	2	1	1	1	2	2
Pluv A10	2	31	72%	138	101	0.93	0.157	0.005	11	19	21	22	22	19	21	21	21	21
Pluv A11	2	31	72%	138	101	0.96	0.172	0.005	2	2	3	3	4	2	3	3	3	3
Pluv A12	2	31	72%	137	101	0.88	0.160	0.005	14	21	24	26	27	16	22	24	26	27
Pluv A13	2	31	72%	136	100	0.91	0.145	0.005	(did not produce at least 1% shear strain after 60 loading cycles)									
Pluv A14	2	31	72%	135	99	0.94	0.161	0.005	3	4	5	5	5	3	4	4	5	5
Pluv A15	2	31	72%	136	100	0.93	0.150	0.005	24	29	29	30	30	27	29	29	30	30
Pluv A16	2	31	72%	137	100	0.96	0.145	0.005	3	4	4	4	5	2	3	4	4	4
Pluv A18	2	31	72%	139	102	0.93	0.156	0.005	Developed bubble after 20th cycle									
Pluv A19	2	31	72%	139	102	0.92	0.171	0.005	2	6	7	8	8	7	-	-	-	-
Pluv A20	2	31	72%	135	99	0.94	0.161	1	9	11	12	13	13	10	12	12	12	13
Pluv A21	2	31	72%	138	101	0.94	0.165	0.005	6	7	8	9	9	7	8	9	9	9
Pluv A22	2	31	72%	67	50	0.97	0.191	0.005	2	3	3	3	4	2	3	3	3	3
Pluv A23	2	31	72%	272	200	0.92	0.159	0.005	3	4	5	5	5	4	5	5	5	5

PI = Plasticity Index; LL = Liquid Limit; FC (%) = Percentage of particles finer than 75 μm; σ'_v: initial vertical effective stress
σ'_m = Mean effective stress ($\sigma'_m = (\sigma'_1 + \sigma'_2 + \sigma'_3)/3$); e_o = void ratio; CSR = Cyclic Stress Ratio (τ_{cyc}/σ'_{vi});
freq = Frequency of Loading, in Hz; +1% γ = number of cycles required to reach 1% shear strain

Table 6.12 Summary of index properties and results of cyclic simple shear tests performed on Soils "A24 – A28", Soil D, Soil F, and Soil "G1 – G17" reconstituted using the In-Place Wet Pluviation Method

Test Name	PI	LL	FC (%)	σ'_v (kPa)	σ'_m (kPa)	e_o	CSR	freq (Hz)	+1% γ	+2% γ	+3% γ	+4% γ	+5% γ	-1% γ	-2% γ	-3% γ	-4% γ	-5% γ
Pluv A24	2	31	72%	137	100	0.93	0.161	0.005	31	35	36	37	37	34	35	36	36	36
Pluv A25	2	31	72%	137	101	0.91	0.160	0.005	(did not produce at least 1% shear strain after 60 loading cycles)									
Pluv A26	2	31	72%	68	50	1.07	0.175	0.005	1	2	2	3	3	2.5	2.5	2.5	2.5	-
Pluv A27	2	31	72%	137	101	0.90	0.102	0.005	23	-	-	-	-	-	-	-	-	-
Pluv A28	2	31	72%	140	103	0.90	0.186	0.005	3	5	6	7	7	3	5	6	7	7
Pluv D7	11	38	94%	136	100	0.96	0.135	0.005	6	22	36	40	42	43	44	44	44	-
Pluv F1	7	28	57%	137	100	1.02	0.124	0.005	67	(did not produce at least 1% shear strain after 60 loading cycles)								
Pluv G1	10	31	77%	141	103	0.73	0.206	0.005	Initial test, cycled to one side									
Pluv G8	10	31	77%	139	102	0.81	0.142	0.005	5	10	(developed bubble)			10				
Pluv G9	10	31	77%	142	105	0.76	0.141	0.005	5	14	18	19	19	19	20	20	20	20
Pluv G10	10	31	77%	138	101	0.83	0.170	0.005	2	3	4	4	4	2	2	4	4	4
Pluv G11	10	31	77%	142	104	0.78	0.118	0.005	27	41	43	43	44	42	44	44	45	45
Pluv G12	10	31	77%	137	100	0.76	0.151	0.005	7	9	10	10	10	7	9	9	10	10
Pluv G13	10	31	77%	139	102	0.77	0.195	0.005	2	3	4	4	5	3	4	4	4	-
Pluv G14	10	31	77%	139	102	0.73	0.148	0.005	25	33	35	36	37	32	35	36	37	38
Pluv G15	10	31	77%	138	101	0.74	0.147	0.005	8	12	13	14	15	12	13	14	15	15
Pluv G16	10	31	77%	137	100	0.83	0.193	1	2	4	4	4	5	2	3	4	4	4
Pluv G17	10	31	77%	70	51	0.85	0.147	0.005	5	7	8	8	9	7	8	8	-	-

PI = Plasticity Index; LL = Liquid Limit; FC (%) = Percentage of particles finer than 75 μm; σ'_v: initial vertical effective stress
σ'_m = Mean effective stress ($\sigma'_m = (\sigma'_1 + \sigma'_2 + \sigma'_3)/3$); e_o = void ratio; CSR = Cyclic Stress Ratio (τ_{cyc}/σ'_{vi});
freq = Frequency of Loading, in Hz; +1% γ = number of cycles required to reach 1% shear strain

Table 6.13 Summary of index properties and results of cyclic simple shear tests performed on Soils "G28 – G25" reconstituted using the In-Place Wet Pluviation Method

Test Name	PI	LL	FC (%)	σ'_v (kPa)	σ'_m (kPa)	e_o	CSR	freq (Hz)	+1% γ	+2% γ	+3% γ	+4% γ	+5% γ	-1% γ	-2% γ	-3% γ	-4% γ	-5% γ
Pluv G18	10	31	77%	68	50	0.84	0.149	0.005	2	4	5	6	6	5	-	-	-	-
Pluv G19	10	31	77%	270	198	0.80	0.140	0.005	8	11	12	12	12	9	11	11	12	12
Pluv G20	10	31	77%	137	101	0.77	0.199	0.005	8	10	11	11	12	8	10	11	11	11
Pluv G21	10	31	77%	139	102	0.80	0.176	0.005	13	15	16	16	16	14	15	15	16	16
Pluv G22	10	31	77%	138	102	0.83	0.192	0.005	1	1	2	2	2	1.5	1.5	1.5	-	-
Pluv G24	10	31	77%	138	101	0.69	0.198	0.005	5	13	17	18	19	14	18	19	-	-
Pluv G25	10	31	77%	137	101	0.87	0.124	0.005	16	18	18	19	19	17	18	18	19	19

PI = Plasticity Index; LL = Liquid Limit; FC (%) = Percentage of particles finer than 75 μm; σ'_v: initial vertical effective stress
σ'_m = Mean effective stress ($\sigma'_m = (\sigma'_1 + \sigma'_2 + \sigma'_3)/3$); e_o = void ratio; CSR = Cyclic Stress Ratio (τ_{cyc}/σ'_{vi});
freq = Frequency of Loading, in Hz; +1% γ = number of cycles required to reach 1% shear strain

To examine the effects of soil index properties, four cyclic simple shear tests, summarized in Table 6.14, were prepared using the In-Place Wet Pluviation Method on Soil A, Soil D, Soil F, and Soil G. The test conditions for this test series were σ'_m = 100 kPa, less than 0.12 days under confinement, a loading frequency = 0.005 Hz, and OCR = 1. Once again, Soil G has the lowest void ratio (0.81), and Soil F has the highest (1.02) at this mean effective confining stress of 100 kPa.

Table 6.14 Index properties and cyclic simple shear testing conditions for reconstituted by the Slurry Deposition Method

Test Name	PI	LL	FC (%)	e_o	B-Value	w_c (%)	w_c/LL	Days	CSR	5% γ
Pluv A1	2	31	72%	0.94	0.98	35.07	1.13	0.05	0.126	48
Pluv D7	11	38	94%	0.96	0.99	35.53	0.93	0.12	0.135	42
Pluv F1	7	28	57%	1.02	0.99	37.93	1.35	0.03	0.124	-
Pluv G8	10	31	77%	0.81	0.93	30.22	0.97	0.12	0.142	-

Figure 6.19 shows the stress-strain curves for the four different soils. The specimens were confined for 0.12 days or less, thus are relatively "young." Increasing the time under confinement for each specimen to a period of 0.8 days or greater is recommended. An increase in confinement from 0.12 days to 0.8 days (which was later selected as the baseline) results in an increase in cyclic strength, which is discussed further in Section 6.3.2.2.

The stress strain plots shown in Figure 6.19 for Pluv A1, Pluv D7, and Pluv G8 have the familiar "football shapes." As seen in this figure, the "young" Pluviated specimens do not develop large positive excess pore water pressures as they each pass through the origin, unlike the specimens prepared using the Slurry Deposition Method. The stress-strain curves for Pluv A1 and Pluv D7 remains a "football shaped" even though they begin to cycle primarily to one side. Pluv F1 did not liquefy with 100 cycles of loading.

Figure 6.20 shows the strain time histories of SDM A1, SDM D7, SDM F1, and SDM G8. Except for Pluv F1, which does not liquefy, in each of the other specimens as they approach liquefaction, the rate of increase in strain per cycle is quite high. This high rate of increase is typical of normally consolidated In-Place Wet Pluviated specimens and will be discussed more in Section 6.3.1.3.

Specimens Pluv A1 and Pluv F1 both had CSR ≈ 0.12, yet their cyclic responses differed significantly. Specimen Pluv A1 reached the 5% strain threshold after 48 cycles of loading; whereas, Pluv F1 still cycled at less than 5% strain at the 100th loading cycle. The cyclic strength of Pluv F1 was greater than Pluv A1, despite its higher void ratio, lower fines content, and higher water content to liquid limit ratio (w_c/LL). Typically, one would expect that a fine-grained soil with a higher void ratio, lower fines content, and higher w_c/LL would have a lower cyclic strength. This increase in cyclic strength may have been because Pluv F1 has a larger PI value, which may negate the contribution of the other soil parameters mentioned. Once again, testing at a time under confinement of 0.8 days or more is recommended to explore the responses of Soils A and F.

To construct the CSR vs. log N curve for Pluviated specimens from Soil A, seven tests with properties listed in Table 6.15 were performed on Soil A. The test conditions for this test series were: σ'_m = 100 kPa, 0.8 days under confinement, a loading frequency of 0.005 Hz, and OCR = 1. Of these seven tests, the mean void ratio was 0.94 and the w_c/LL was approximately 1.12. Results from the cyclic testing on these seven Soil A specimens are shown in Figure 6.21.

Table 6.15 Specimen properties and cyclic simple shear testing conditions for Soil A reconstituted by In-Place Wet Pluviation for CSR comparison

Test Name	PI	LL	FC (%)	e_o	B-Value	w_c (%)	w_c/LL	CSR	5% γ
Pluv A8	2	31	72%	0.92	0.97	34.28	1.11	0.114	-
Pluv A9	2	31	72%	0.93	0.97	34.39	1.11	0.188	2
Pluv A10	2	31	72%	0.93	0.95	34.64	1.12	0.157	22
Pluv A11	2	31	72%	0.96	0.97	35.57	1.15	0.172	4
Pluv A14	2	31	72%	0.94	0.98	35.13	1.13	0.161	5
Pluv A15	2	31	72%	0.93	0.98	34.58	1.12	0.150	30
Pluv A21	2	31	72%	0.94	0.95	35.06	1.13	0.165	9

The results from Figure 6.21d showed that over a small range of CSR values (0.157 to 0.161) the number of cycles of loading to the initiation of liquefaction differs significantly. Specimens that had a CSR value less than 0.157 reached 5% shear strain in 20 or more cycles, while specimens that had a CSR value greater than 0.161 reached 5% shear strain in 9 cycles or less. The CSR for Pluv A8 was too low to induce liquefaction in the specimen.

The CSR vs. log N plot for Soil A for this test series is shown in Figure 6.22, and shows that for a small range in CSR (0.15 to 0.19) the number of cycles to 5% shear strain is large (2 to 30 cycles). The "flatness" of the curve for Soil A was confirmed through extensive testing using similar test conditions.

The functional form of the CSR vs. log N curve for Soil A constructed by the In-Place Wet Pluviation method was found to be CSR = a + b/N. This form was determined by doing a best fit using a least-squares regression to solve for the coefficients a (0.152) and b (0.071). The standard error term is 0.0044 and R^2 = 0.91.

From Chapter 5, the monotonic tests have a loading that is equivalent to ¼ of a cyclic test. Using the ratio of the maximum horizontal shear stress on the horizontal plane, τ_h, and the initial effective vertical stress, the static stress ratio (SSR) can be determined. For the specimen Pluv A4 (1.1 days under confinement, σ'_v = 138 kPa, and OCR = 1), the SSR was 0.26. Extrapolating the CRR curve shown in Figure 6.22 for Soil A to 0.25 cycles, the CSR would be 0.44. This apparent discrepancy between the SSR and CSR at one quarter of a load cycle is due to loading rate effects. For the monotonic test, τ_h occurs at approximately 11% shear strain and 15 minutes of testing. In the cyclic test, ¼ of a cycle occurs at less than 1% shear strain and 50 seconds.

The repeatability of the In-Place Wet Pluviation Method was evaluated by preparing and testing two nearly identical test specimens, (i.e., Pluv A10 and Pluv A18) using the CSS device. The specimen properties prior to cyclic testing are listed in Table 6.16. From the results shown in this table, the two specimens have equal void ratio and water contents.

Table 6.16 Specimen properties and cyclic simple shear testing conditions for Soil A reconstituted by In-Place Wet Pluviation for repeatability testing

Test Name	PI	LL	FC (%)	σ'_v (kPa)	σ'_m (kPa)	e_o	B-Value	w_c (%)	w_c/LL	Days	OCR	CSR	5% γ
Pluv A10	2	31	72%	138	101	0.93	0.95	34.64	1.12	0.79	1.00	0.157	22
Pluv A18	2	31	72%	139	102	0.93	0.98	34.50	1.11	0.80	1.00	0.156	-

Pluv A10 and Pluv A18 test results are shown in Figure 6.23. From this figure, in all four plots, the effective stress path, stress-strain curves, and time histories for stress and strain are nearly identical. Unfortunately, the Pluv A18 test was terminated prematurely after a small tear developed in the membrane. Judging from the soil properties and the time histories, the In-Place Wet Pluviation process can provide consistent results for similar specimens.

Three tests with properties listed in Table 6.17 were performed on Soil G, prepared using the In-Place Wet Pluviation Method, to construct a CSR baseline curve. The tests conditions for this test series were: σ'_m = 100 kPa, 0.8 days under confinement, a loading frequency of 0.005 Hz, and OCR = 1. Of these three tests, the mean void ratio was 0.84 and the w_c/LL was approximately 1.01. Results from the cyclic testing on these Soil G specimens are shown in Figure 6.24.

Table 6.17 Specimen properties and cyclic simple shear testing conditions for Soil "G-Loose" reconstituted by In-Place Wet Pluviation for CSR comparison

Test Name	PI	LL	FC (%)	e_o	B-Value	w_c (%)	w_c/LL	CSR	5% γ
Pluv G10	10	31	77%	0.83	0.99	30.69	0.99	0.170	4
Pluv G22	10	31	77%	0.83	0.97	30.96	1.00	0.192	2
Pluv G25	10	31	77%	0.87	0.95	32.25	1.04	0.124	19

The CSR vs. log N curve resulting from using the In-Place Wet Pluviated Method for Soil G is shown in Figure 6.25. The CSR curve in this figure shows that for a wider range of CSR values (0.124 to 0.192), there is a narrower range of cycles to liquefaction (2 to 19 cycles). The CSRs were chosen so that two data points on the CSR curve would fall in the range of 10 cycles or less where the CSR vs. log N relationship is significantly curved, and another point would fall in the range between 20 and 30 cycles, where the CSR vs. log N relationship is less curved.

The functional form of the CSR curve for Soil G prepared by the In-Place Wet Pluviation Method was found to be CSR = a + b/N. The coefficients a and b are 0.1205 and 0.1527, respectively. The standard error term is 0.0138 and R^2 = 0.92.

A comparison of the cyclic resistances of Soil A (PI = 2, LL = 31) and Soil G (PI = 10, LL = 31), both of which were prepared by In-Place Wet Pluviation, is shown in Figure 6.26. Unlike the previous comparisons of these soils when prepared by the Slurry Deposition Method (Figure 6.18), where the curves are parallel, the CSR vs. log N curves of the Pluviated specimens intersect at a CSR of 0.175. The Pluv G CSR vs. log N curve exhibits typical curvature, but the Pluv A CSR vs. log N curve is relatively flat, which leads to an eventual crossing. At CSRs lower than 0.175, Soil A has more cyclic strength than Soil G. However, at CSRs higher than 0.175, Soil G has more strength than Soil A during cyclic loading.

6.3.1.3 Effects of Specimen Preparation

As shown in Chapter 5, the method of specimen preparation has a major influence on the response of soils and the effects of test parameters, such as void ratio. Two methods of specimen preparation were explored in this research. They are the Slurry Deposition Method and the In-Place Wet Pluviation Method, and detailed information concerning their construction is covered in Chapter 4. There are significant differences in the specimens produced by these preparation methods.

The stress-strain curves are different. The stress-strain curves for the In-Place Wet Pluviation specimens shown in Figure 6.21b do not exhibit the distinctive "banana loop" shape that is shown for the Slurry Deposition Method specimens in Figure 6.14b. The shape of the stress-strain curves for the In-Place Wet Pluviation specimens is instead a hybrid between the "banana-shaped" and "football-shaped" forms, indicating that the specimen is not undergoing significant phases of positive and negative excess pore water pressures during cyclic testing.

The shapes of the effective stress time histories are also different. Specimens prepared by the Slurry Deposition Method typically have a normalized vertical effective stress response that decreases linearly to approximately 40% of their initial value (i.e., r_u = 60%), at which point large variations in excess pore water pressures occur until the initiation of liquefaction (Figure 6.14c and Figure 6.16c). Conversely, specimens reconstituted by the In-Place Wet Pluviation Method have backwards S-shaped effective stress curves, which may be seen in results for Soil A (Figure 6.21c) and Soil G specimens (Figure 6.24c). The variations in excess pore water pressures in these specimens remain small compared to those that develop in the Slurry specimens.

Additional differences are apparent in the shear-strain time history plots, i.e., Figure 6.14d and Figure 6.21d, of soils prepared by each method. Slurry Deposition specimens have a nearly linear increase in strain per cycle beyond the threshold of r_u = 70% until 5% shear strain, i.e., cyclic mobility with limited shear strain potential. This contrasts with the rapid increase in strain per load cycle observed in the Pluviated specimens, i.e., cyclic mobility with large shear strain potential. Typically, specimens reach 5% shear strain within 2-3 cycles after reaching a threshold of r_u = 60%.

The CSR vs. log N plot comparing Soil A prepared using the Slurry Deposition and the In-Place Wet Pluviation Method, and tested under the same test conditions, is shown in Figure 6.27. As previously noted, Pluviated Soil A has a "flatter" CSR vs. log N curve. Small changes in CSR

result in large changes in the number of cycles to the initiation of liquefaction. The Slurry Soil A exhibits more typical curvature, which is relatively less sensitive to CSR.

Both CSR vs. log N curves converge at a CSR of approximately 0.15. Although the curves are extrapolated beyond this point, there appears to be little or no difference between the two methods for a CSR less than 0.15. At CSR values higher than 0.15, however, the Slurry Deposition Method specimens have higher cyclic strength than their Pluviated counterparts.

Potential effects of the specimen preparation methods on Soil G were also explored; and a comparison of the responses from the two specimens, SDM G22 and Pluv G24, prepared using the Slurry Deposition Method and In-Place Wet Pluviation Methods, respectively, are shown in Figure 6.28. Each specimen was tested at an effective confining stress of 100 kPa, a loading frequency of 0.005 Hz, and the same CSR.

Although Pluv G22 reaches 5% single amplitude shear strain in the second cycle of loading and SDM G9 reaches 5% shear strain in the third, the stress and strain relationship between the two specimens is very different. Pluv G22 has a "football shape" stress-strain curve typical of loose materials, compared to the classic "banana loops" displayed by SDM G9, typical of a denser material (Figure 6.28b). Pluv G22 fails almost immediately into the second cycle with very large strains and a rapid decrease in effective stress while SDM G9 continues cycling until at least 10% single amplitude strain (Figure 6.28d).

The CSR vs. log N plot for Soil G, prepared using the Slurry Deposition and the In-Place Wet Pluviation Methods tested under the same baseline conditions, is given in Figure 6.29. Curves for the Pluviated Soil G and Slurry Soil G specimens are roughly parallel to each other, with the Slurry Soil G curve above and to the right of Pluviated Soil G. The Slurry specimens have a higher cyclic strength than the Pluviated specimens possibly due to their lower void ratios and w_c/LL ratios.

6.3.2 Effects of Time under Confinement

As seen in Sections 5.6.1.1 and 5.6.2.2, as the time under confinement increases, the static shear strength increases. This increase in strength over time is also manifested during cyclic loading.

To date, there has been no consensus on the amount of time a specimen should remain under confinement prior to testing, and regardless of the preparation method, this parameter has varied largely between researchers. Yamamuro (2001) tests immediately after deposition. Carraro (2003) uses 30 to 240 minutes of time under confinement depending on the amount of silt added to the sand mixture. Yasuhara (2003) waits 24 hours between slurry deposition and testing. For this body of research, 0.8 days or 19 hours, was used as the baseline time under confinement, because a stable response was generally observed if the time of confinement exceeds 12 hours or so. The time under confinement begins after the specimen is prepared, placed in the simple shear device, backpressure saturated and consolidated to the level of stress at which the specimen will be tested.

6.3.2.1 Slurry Deposition Method

Two cyclic simple shear specimens of Soil A, created using the Slurry Deposition Method, were compared to examine time under confinement effects. The difference in time under confinement is greater than one log cycle of time. The index properties of the two specimens are shown in Table 6.18. Both specimens were tested at the same CSR, a loading frequency of 0.005 Hz, an effective confining pressure of σ'_m = 100 kPa, and OCR = 1. Soil G was not tested under different times under confinement.

Table 6.18 Specimen properties and cyclic simple shear testing conditions for Soil A reconstituted by the Slurry Deposition Method for different times under confinement

Test Name	PI	LL	FC (%)	e_o	B-Value	w_c (%)	w_c/LL	Days	CSR	5% γ
SDM A1	2	31	72%	0.69	0.97	25.84	0.83	0.04	0.210	2
SDM A11	2	31	72%	0.68	0.96	25.39	0.82	0.95	0.210	4

The void ratio and water contents are only slightly smaller for the specimen loaded for a longer time under confinement.

Test results comparing specimens with different amounts of time under confinement are plotted in Figure 6.30 and show that the "younger" specimen, SDM A1, reaches the onset of liquefaction in half of the cycles of loading necessary to produce liquefaction in the "older" SDM A11 specimen. The time history of the effective stress and shear strains from Figure 6.30c and Figure 6.30d show that SDM A1 reaches an r_u = 80% (or 20% of the normalized vertical effective stress) within the first two cycles of loading, while SDM A11 does not reach r_u = 80% until the 5^{th} loading cycle. It is also evident that much greater shear strains are exhibited in SDM A1 than SDM A11. Clearly, the additional time under confinement has increased the soil's cyclic resistance, while the specimen properties (shown in Table 6.18) have remained the same.

Extrapolation of the CSR line in Figure 6.31 shows that Soil A should fail in 2 cycles with a CSR = 0.264, assuming it had been under confinement for at least 0.8 days. SDM A1 reached 5% shear strain in 2 cycles with a CSR = 0.21. This indicates a 21% decrease in cyclic strength by testing in 0.04 days instead of 1 day.

6.3.2.2 In-Place Wet Pluviation

A more thorough analysis of the time under confinement for specimens created using the In-Place Wet Pluviation Method was conducted for Soil A and Soil G, with the objective of determining a relationship between increasing cyclic strength and log of time. For preparation techniques for the specimens with periods of confinement longer than 0.8 days, readers should refer to Section 5.6.2.2.

Four specimens of Soil A were subjected to different times under confinement. The index properties of the specimens are shown in Table 6.19. All were tested at a loading frequency of 0.005 Hz, an effective confining pressure of σ'_m = 100 kPa, and OCR = 1.

Table 6.19 Specimen properties and cyclic simple shear testing conditions for Soil A reconstituted by In-Place Wet Pluviation for different times under confinement

Test Name	PI	LL	FC (%)	e_o	B-Value	w_c (%)	w_c/LL	Days	CSR	5% γ
Pluv A1	2	31	72%	0.94	0.98	35.07	1.13	0.05	0.126	48
Pluv A10*	2	31	72%	0.93	0.97	34.64	1.12	0.79	0.157	22
Pluv A12	2	31	72%	0.88	0.96	32.88	1.06	11	0.160	27
Pluv A28	2	31	72%	0.90	0.97	33.48	1.08	50	0.186	7
Pluv A3	2	31	72%	0.84	0.94	31.25	1.01	101	0.141	-

*Denotes baseline soil for comparison

The void ratio and water content decline as the time under confinement increases (Table 6.19). The CSR of Pluv A3 was too small to generate significant excess pore water pressures given the long time under confinement, but the specimen's response was still useful to examine.

Figure 6.32 and Figure 6.33 demonstrate that increasing the time under confinement increases the cyclic strength. One key result is that the stress-strain curves in Figure 6.32b and Figure 6.33b for the older specimens now show the typical "banana loops" and not the "football shape." It is possible that with the increase in time under confinement, additional benefits besides the decrease in void ratio and water content have occurred. Secondary compression, bonding between the soil particles, and a more stable soil fabric for specimens tested after 10 days may be responsible for the added strength of these specimens.

The time history of the normalized effective stress response for Pluv A12 (11 Days), shown in Figure 6.32c, has a similar response to the Slurry specimens and does not have the backwards S-shape of the younger Pluv A10 (0.8 days). This also holds true in Figure 6.33c. Similarities in pore water generation per cycle are seen in each of the older specimens.

Older specimens also appear to have more stable shear strain curves. From Figure 6.32d and Figure 6.33d, the older specimens have a steady increase in strain per cycle compared to the younger specimens which strain to 5% rapidly after the r_u = 60% threshold has been reached.

Extra care is required for specimens under long times of confinement such as Pluv A3 (100 Days). Specimens chosen for long-term consolidation have the likelihood of the membrane drying, cracking, or developing holes around the cap/soil interface. Other possible issues such as the loss of saturation, growth of mold, and blockage in the cap or drain lines caused by stagnation should be resolved prior to testing.

The CSR vs. log N plot for specimens with different times under confinement compared to the baseline conditions of 0.8 days in shown Figure 6.34. Increases and decreases in cyclic strength are found by comparing the CSR of a non-baseline test to the CSR curve at the same cycles to 5% shear strain. The difference between the two quantities is an increase or decrease in strength. From Figure 6.34, by decreasing the time under confinement from 0.8 days to 0.05 days, the cyclic strength decreases by 22%. By increasing the time under confinement from 0.8 days to 11 days, and then to 50 days, the cyclic strength increases by 3% and 13%, respectively. This

increase in strength may be a small percentage given the length of time under confinement, but the stress and strain histories show that the specimens have become more stable with increasing time under confinement. The increased cyclic strength from the specimen confined for 100 days was not included in this analysis because it did not reach 5% shear strain within a reasonable number of cycles.

Three specimens of Soil G, prepared using the In-Place Wet Pluviation Method, were subjected to different times under confinement. The index properties of the three specimens are listed in Table 6.20. The three specimens were tested at a loading frequency of 0.005 Hz, σ'_m = 100 kPa, and OCR = 1.

Table 6.20 Specimen properties and cyclic simple shear testing conditions for Soil G reconstituted by In-Place Wet Pluviation for different times under confinement

Test Name	PI	LL	FC (%)	e_o	B-Value	w_c (%)	w_c/LL	Days	CSR	5% γ
Pluv G8	10	31	77%	0.81	0.93	30.22	0.97	0.12	0.142	-
Pluv G22*	10	31	77%	0.83	0.97	30.96	1.00	0.83	0.170	2
Pluv G15	10	31	77%	0.74	0.97	27.42	0.88	18.02	0.147	15
Pluv G24	10	31	77%	0.69	0.96	25.59	0.83	50.14	0.198	19

*Denotes baseline soil for comparison

The time under confinement has a direct effect on the void ratio and water content. As seen in Table 6.20 as the time under confinement increases, these parameters decrease. Pluv G8 (0.12 days) is only shown in the above table for void ratio and water content analysis. This test was terminated prematurely after a tear developed in the membrane.

Similar to Pluviated A soils, Figure 6.35 shows the added benefit of increased time under confinement. In addition to the increase in cyclic strength at a given CSR, the stress-strain curves in the older specimens in Figure 6.35b are now forming "banana loops."

The only exception to the above-mentioned trends is Pluv G24 (50 days). The specimen appears to "break" as shown in Figure 6.35d. The test proceeded up to a 5% single amplitude shear strain, and then the specimen strains immediately to 15% single amplitude shear strain. No sudden losses of effective stress or increases in excess pore water pressure are seen in Figure 6.35c. This "breaking" in Soil G with increased time under confinement is similar to the reaction of Pluv G6, a monotonic test with 10 days time under confinement. The information on the strength characteristics of Pluv G6 can be found in Section 5.6.2.2. The reason for "breaking" response is not fully understood and additional testing may be required.

The CSR vs. log N plot for effects of time under confinement for Pluviated Soil G is given in Figure 6.36. From this chart, it can be seen that an increase in the time under confinement from 0.8 days to 18 days equals an increase of 8% in cyclic strength. Increasing the time under confinement from 0.8 days to 50 days increases the cyclic strength by 33%. Each of these specimens show a dramatic increase in cyclic strength over the same durations in time under confinement when compared to the Pluviated A specimens.

Seed (1979) published results for the influence of time under confinement prior to cyclic testing for sands. From Figure 17 of this paper, an increase in time under confinement for laboratory specimens from 1 day to 10 days leads to a 5% increase in cyclic strength and an increase to 100 days was an increase in cyclic strength of approximately 25%. Figure 6.37 is a recreation of Figure 17 from the Seed (1979) paper, updated for soils with a PI. Based on the results from tests conducted to assess the effects of time under confinement on Soils A (PI = 2) and G (PI = 10), soils with higher PI are more affected by time under confinement.

6.3.3 Effects of Changes in Density

For liquefaction susceptibility and resistance, one of the most important index properties to consider is the density of a soil. For two specimens with the same PI, LL, and fines content, the response to cyclic loading will be different given the densities of the specimens. Generally the less dense the material, the lower its resistance to liquefaction will be.

For this testing series, the parameter e_o, or void ratio, represents a soil's density. Density is a function of volume and mass. Determining the true volume of a specimen is more difficult than the mass; and finding a reconstituted specimen's density is more complicated than finding a field specimen's density. For a field specimen, the diameter and height can be measured with some confidence using a pi tape and calipers before covering with a membrane. When reconstituting, the specimen is prepared within a wire-reinforced membrane surrounded by a mold. Small variations in the diameter and thickness of the wire membrane equate to large differences in the area of the specimen. Sensitivity tests proved that a change in the diameter of a wire-reinforced membrane of 0.1 centimeter would change the density by 0.4 g/cm^3. In addition, the true diameter of the specimen cannot be measured unless the wire reinforcement is fully engaged. This can only be done when the specimen is vertically loaded to a level of stress large enough to induce K_o conditions, which will fully engage the wires. A drawback to this configuration is that measurements are more difficult to take, because the specimen is either in the simple shear device, or loaded with 114 kg. Because the void ratio is a function of the mass of the specimen and because it is easier to measure, the void ratio proved to be a more stable parameter to represent the soil's density.

6.3.3.1 Slurry Deposition Method

To compare the effects of changes in density of Soils A and G, prepared by the Slurry Deposition Method, specimens were prepared more loose and more dense than the baseline soils. These soils were tested at the same testing conditions: loading frequency of 0.005 Hz, σ'_m = 100 kPa, an OCR = 1, and 0.8 days of confinement. The tests SDM A4 and SDM A11, which were performed to compare the effects of changes in density, were tested at different CSRs and are compared using the CSR vs. log N plot, Figure 6.38. A comparison using a 4-way plot is not useful for this purpose because the 4-way plot can only compare the effects of one parameter at a time, versus two parameters (density and CSR) which was needed here.

Table 6.21 Specimen properties and cyclic simple shear testing conditions for Soils A and G reconstituted by the Slurry Deposition Method at different densities

Test Name	PI	LL	FC (%)	e_o	B-Value	w_c (%)	w_c/LL	CSR	5% γ
SDM A11*	2	31	72%	0.68	0.96	25.39	0.82	0.210	4
SDM A4	2	31	72%	0.74	0.98	27.42	0.88	0.199	3
SDM G10	10	31	77%	0.62	0.95	23.18	0.75	0.176	7
SDM G18*	10	31	77%	0.65	0.96	24.30	0.78	0.176	5
SDM G15	10	31	77%	0.67	0.98	24.98	0.81	0.175	3

* Denotes baseline soil for comparison

From

Table 6.21, the specimen SDM A4 had a higher void ratio and water content than the baseline soils. Based on the CSR vs. log N plot, Figure 6.38, this increase in void ratio of 10% from the baseline average of 0.67 to the higher void ratio of 0.74, decreased the cyclic strength of the material by 11%. For Soil A, creating a denser specimen using the Slurry Deposition Method proved difficult and was not successfully accomplished.

The 4-way plots showing the shear stress, strain, and effective stress time histories for Soil G, prepared by the Slurry Deposition Method, are given in Figure 6.39. From Figure 6.39b, during the first loading cycle of Soil G, the stress-strain curves are identical, regardless of the density tested. After the first cycle, excess pore water pressures begin to generate at different rates between the three specimens. SDM G10 (Dense) had greater cyclic strength characteristics as shown from the number of cycles to 5% shear strain when compared to SDM G18 (baseline), and SDM G15 (loose) at the same CSR.

The CSR vs. log N plot comparing the effects of changes in void ratio for Soil G, prepared by the Slurry Deposition Method, is shown in Figure 6.40. For the same CSR, a decrease in void ratio by 5% from 0.65 to 0.62 increases the overall cyclic strength of the material by 13%. Conversely, an increase in the void ratio by 3% from 0.65 to 0.67 decreases the strength by 8%. A key point to this testing series is that cyclic response for the three specimens with the same PI, LL, and Fines Content also varies greatly.

6.3.3.2 In Place Wet Pluviation

To assess the effects of changes in density for the In-Place Wet Pluviated specimens from Soil A, one specimen at a high density (low void ratio) and one specimen at a low density (high void ratio) were prepared. All other testing conditions such as OCR (OCR = 1), rate of loading (0.005 Hz), and time under confinement (0.8 Days) were held constant. The specimen parameters and

testing conditions are listed in Table 6.22.

Table 6.22 Specimen properties and cyclic simple shear testing conditions for Soil "G-Dense" reconstituted by In-Place Wet Pluviation for CSR comparison

Test Name	PI	LL	FC (%)	σ'_v (kPa)	σ'_m (kPa)	e_o	B-Value	w_c (%)	w_c/LL	CSR	5% γ
Pluv A11*	2	31	72%	138	101	0.96	0.97	35.57	1.15	0.172	4
Pluv A19	2	31	72%	139	102	0.92	0.96	34.24	1.10	0.171	9
Pluv A22*	2	31	72%	68	50	0.97	0.97	36.16	1.17	0.191	4
Pluv A26	2	31	72%	68	50	1.07	0.97	39.82	1.28	0.175	3

*Denotes baseline soil for comparison

Specimen Pluv A19 was pluviated and prepared using the same techniques as Pluv A11. Prior to placing the top cap on the assembly of Pluv A19, the sides of the mold were tapped at least three times on each side. This forced the specimen to consolidate and excess water to rise to the surface. This excess water was removed and the top cap was placed. All other testing procedures remained the same. The results of the cyclic testing on Pluv A11 and Pluv A19 are shown in Figure 6.41.

The cyclic response for Pluv A19 is different from all the other Pluv A specimens. This dense specimen provided more cycles of loading at the same CSR as Pluv A11, but "broke" in the seventh cycle, and rapidly strained past 5% shear strain. Sudden increases in pore water pressure or decreases in effective stress are not shown in Figure 6.41c. This same "breaking" response is seen in Pluv G6 and Pluv G24, which both have higher densities than other Pluv G specimens. These results imply that for a higher density material, a catastrophic, brittle failure is possible if the material does not undergo strain softening. For these reasons, additional testing at higher densities is recommended.

The CSR vs. log N plot comparing the response to changes in void ratio to the baseline specimens for Pluviated Soil A is shown in Figure 6.42. As seen in this figure, a 2% decrease in void ratio from 0.94 to 0.92 equates to an increase in cyclic strength of 6%.

The comparison of a specimen Pluv A22 and Pluv A26 (loose), tested at an effective confining stress of 50 kPa is presented in Figure 6.43. Pluv A22 was tested at a higher CSR (0.191) than Pluv A26 (0.175), yet Pluv A26 reached 5% shear strain before Pluv A22. These results show that the large difference in CSR is not enough to overcome the difference in void ratios between the two soils. In this case, the density has greater implications to cyclic response than CSR.

After the testing on Pluviated Soil A was mostly completed, testing began on Pluviated Soil G. A baseline for Soil G was established based on an effective confining stress of 100 kPa, loading rate of 0.005 Hz, and OCR = 1, and 0.8 days under confinement. Four specimens: Pluv G9, Pluv G11, Pluv G12, and Pluv G13 composed the baseline. Shortly after these four tests were completed, a change occurred in the chemical composition in the laboratory water used for pluviation. After this point, all other specimens were found to be considerably more loose. (The specimen Pluv A26, mentioned in the previous paragraph, was one of the Pluv A specimens

affected by this change in the water chemistry.) The specimens remained loose after several attempts were made to flush the laboratory water system. The soils were oven dried and reconstituted, yet, considerably higher void ratios remained, meaning that the change in water chemistry had adhered to the soil and could not be removed.

The soils retained their original PI, LL, and fines contents allowing a new baseline to be established using the altered Soil G. This baseline has been presented as the baseline for Pluv G in Section 6.3.1.2. These circumstances were advantageous in that two formation densities of the same soil are possible given different water chemistries. This is another example why a liquefaction assessment based on key index parameters, such as PI and LL are not conclusive.

The original set of specimens for CSR comparisons, hereafter known as the dense baseline specimens, shown in Table 6.23, comprise a denser set of data for which assessments may still be drawn. One additional test, Pluv G14, was purposely created more dense than all other Pluv G specimens. The specimen properties and testing conditions are listed in Table 6.23 below.

Table 6.23 Specimen properties and cyclic simple shear testing conditions for Soil "G-Dense" reconstituted by In-Place Wet Pluviation for CSR comparison

Test Name	PI	LL	FC (%)	e_o	B-Value	w_c (%)	w_c/LL	CSR	5% γ
Pluv G9	10	31	77%	0.76	0.94	28.19	0.91	0.141	19
Pluv G11	10	31	77%	0.78	0.97	28.87	0.93	0.118	44
Pluv G12	10	31	77%	0.76	0.95	28.37	0.92	0.151	10
Pluv G13	10	31	77%	0.77	0.96	28.68	0.93	0.195	5
Pluv G14	10	31	77%	0.73	0.95	27.27	0.88	0.148	37

The top four tests from Table 6.23, which composed the dense baseline for Soil G, have an average void ratio of 0.77 and a w_c/LL average of 0.92. These results are very different from the new baseline for Soil G, which has a void ratio of 0.84 and a w_c/LL average of 1.01. These four dense specimens are compared in a 4-way plot given in Figure 6.44. Like the looser Pluv G specimens mentioned in Section 6.3.1.2, the specimens exhibit the same backwards S-shape for the normalized vertical effective stress path and the same shear strains that increased rapidly to past 5% shear strain after the threshold of r_u = 60%.

The cyclic response of Pluv G13 is compared to the looser specimen Pluv G22 in Figure 6.45. From this figure, the CSRs that were achieved are comparable for the two specimens as well as all other testing conditions. The higher void ratio of Pluv G22 may have caused this material to liquefy immediately after the first cycle at high CSR, while the denser Pluv G13 liquefied after 5 cycles.

In Figure 6.46, the dense specimen Pluv G14 is compared to one of the dense baseline specimens (Pluv G12). The stress-strain curves of both materials have a definite "banana loop" shape, typical in more dense specimens. In this figure, the normalized vertical effective stress curve of Pluv G14 is more similar to the Slurry specimens, Figure 6.16c, and does not show the

backwards S-shape configuration seen in Figure 6.24c. In addition, the increase in the strains per cycle is more gradual and not as rapid as either of the specimens from the loose or dense baselines.

The four dense baseline specimens for Pluviated Soil G were combined and compared to the looser Pluviated Soil G CSR curve and Pluv G14 in Figure 6.47. The functional form of the CSR curve for Soil G_{Dense} constructed by the In-Place Wet Pluviation method was found to be CSR = a + b/N, where N represents the cycles to 5% shear strain. This form was determined by doing a best fit using a least-squares regression to solve for the coefficients a (0.114) and b (0.382). The standard error term is 0.0058 and $R^2 = 0.98$.

As shown in Figure 6.47, Pluv G14 reached 5% shear strain in 37 cycles at a CSR of 0.148. At a CSR = 0.122 and 37 cycles to 5% shear strain, the cyclic strength for the higher density specimen increased by 16% over the loose baseline materials due to the decrease in void ratio.

6.3.4 Effects of Initial Effective Confining Stress

The effects of changes to the effective confining stress were previously introduced in Section 5.6.2.4. Historically, (e.g., Castro and Poulos, 1977; Seed, 1983; Harder 1988; Seed and Harder, 1990) research has focused on effective confining pressures equal to or greater than 100 kPa that simulate effects under a building or deep within large earth dams. In these studies, it is common to see fewer cycles to the initiation of liquefaction for specimens tested at a higher effective confining stress, than those tested at a lower or moderate effective stress, given the same CSR. In recent years, testing at an effective confining stress of 50 kPa found that a smaller effective confining pressure often leads to more cycles before the initiation of liquefaction (e.g., Hynes and Olsen; 1999, Sancio, 2003; Bray 2004a). Testing at the lower effective confining stress simulates effects on shallower specimens.

Figure 6.48 gives the Mohr's circle for specimens with increased and decreased effective confining stress. From Figure 6.48a, the Mohr's circle depicts specimens with a lower effective confining pressure than the baseline. The lower overall effective stress causes the Mohr's circle to be smaller and closer to the origin than Figure 6.48b and Figure 6.48c. In this program of experimentation, specimens were consolidated to a vertical effective stress of 68 kPa, or σ'_m = 50 kPa, to simulate lower effective confining pressures.

Larger effective confining pressures are from greater overburden stress caused by greater depths or from being located under a heavy object, such as a building. The parameter, q_c, in Figure 6.48c represents the additional effective confining stress. The larger effective stresses cause the Mohr's circle in this plot to be further from the origin than Figure 6.48a or Figure 6.48b. In this testing series, specimens were consolidated to a vertical effective stress of 270 kPa, or σ'_m of 200 kPa, to simulate the additional effective confining pressure.

6.3.4.1 Slurry Deposition Method

To study the effects of changes in the effective confining pressure on Soils A and G, specimens reconstituted by the Slurry Deposition Method were made at a higher effective confining pressure (200 kPa) and at a lower effective confining pressure (50 kPa) to compare to the

baseline soils (100 kPa). All other testing conditions: loading frequency of 0.005 Hz, OCR = 1, and 0.8 days of confinement were held constant.

Table 6.24 Specimen properties and cyclic simple shear testing conditions for Soils A and G reconstituted by the Slurry Deposition Method at different effective confining pressures

Test Name	PI	LL	FC (%)	σ'_v (kPa)	σ'_m (kPa)	e_o	w_c (%)	w_c/LL	τ (kPa)	CSR	5% γ
SDM A12	2	31	72%	70	51	0.69	25.55	0.82	24.3	0.174	21
SDM A7*	2	31	72%	137	101	0.66	24.46	0.79	45.0	0.164	19
SDM A13	2	31	72%	273	200	0.64	23.97	0.77	88.7	0.162	10
SDM G14	10	31	77%	68	50	0.68	25.36	0.82	24.1	0.177	8
SDM G18*	10	31	77%	138	101	0.65	24.30	0.78	48.5	0.176	5
SDM G13	10	31	77%	274	201	0.63	23.28	0.75	93.8	0.171	4

* Denotes baseline specimen for comparison

The results of these tests, listed in Table 6.24, show that the void ratio is correlated to the effective confining pressure, as predicted in Section 5.3. As the effective confining pressure increases, the void ratio decreases. Also from Table 6.24, for a consistent CSR level, the shear, τ, required for a specimen at 200 kPa is four times greater than that required for a specimen at 50 kPa, because the CSR is calculated as τ/σ'_{vi} (Equation 6.4).

Figure 6.49 compares a Slurry Deposition Method Soil A baseline, σ'_m = 100 kPa, specimen to a Slurry Deposition Method Soil A at a lower mean effective confining pressure, σ'_m = 50 kPa. This comparison was specifically done to compare the shear strain relationship of SDM A6 (100 kPa) and SDM A12 (50 kPa) in Figure 6.49d. SDM A6 exhibits a linear increase in shear strain per cycle, shown by the light gray lines in the figure, until 5% shear strain. In contrast, SDM A12 shows a constant strain per cycle until the threshold of r_u = 70%, or 30% of the initial vertical effective stress. After this threshold, the rate of increase in strains per cycle is similar to SDM A6 until 5% shear strain. This linear increase in strains per cycle is characteristics of materials that undergo cyclic mobility with limited strain potential.

The specimen consolidated to the higher mean effective confining stress, σ'_m = 200 kPa is compared to a specimen consolidated to a mean effective confining stress, σ'_m = 100 kPa in Figure 6.50. The shear strain time histories for SDM A7 (100 kPa) and SDM A13 (200 kPa) are the same through the first 5-6 cycles. After this point, the strains per cycle in SDM A13 increase more rapidly to 5% shear strain than SDM A7.

The normalized vertical effective stress time histories from Figure 6.49c and Figure 6.50c show that in each case, the specimen with the lower effective confining stress also has the greater effective stress build-up per cycle throughout the test. This means that the normalized effective stress of SDM A12 (50 kPa) was always greater than SDM A6 (100 kPa), and SDM A7 (100 kPa) was always greater than SDM A13 (200 kPa). This further supports that once specimens are normalized by the vertical effective stress, specimens under higher effective confining pressure exhibit less cyclic strength that those at lower effective confining pressures.

The CSR vs. log N plot comparing the baseline (100 kPa) to results from tests performed at different effective confining pressures is shown in Figure 6.51. Here, decreasing the effective confining pressure from 100 kPa to 50 kPa (SDM A12), increases the cyclic strength by 9%, and conversely, doubling the effective confining pressure from 100 kPa to 200 kPa (SDM A13), decreases the cyclic strength by 5%.

Figure 6.52, compares Soil G specimens prepared by the Slurry Deposition Method for at effective confining pressures of 50 kPa, 100 kPa, and 200 kPa. From this graph, the specimen with the lowest effective confining pressure reach the threshold of 5% shear strain in a larger number of cycles of loading, 8, when compared to specimens with greater effective confining pressures of 100 kPa and 200 kPa, 5 and 4 cycles of loading, respectively. In the normalized effective stress plot, Figure 6.52c, SDM G14 (50 kPa) consistently has a higher normalized effective stress when compared to specimens SDM G18 (100 kPa) and SDM G13 (200 kPa).

In Figure 6.53, the stress-strain curves from Figure 6.52b are enlarged. The slope of the shear modulus, G, is shown for each of the specimens during the cycle at which 5% single amplitude shear strain is reached. Although it is atypical to describe the shear modulus, G, at 5% shear strain because of soil non-linearity at this high strain, the figure does well in depicting the relationship for changes in effective confining pressure. As predicted by Assimaki (2000) and Zhang (2005), as well as others, the effective confining pressure has a direct influence on the shear modulus. As the effective confining pressure increases, the slope of the secant increases as well. The secants of the shear modulus are given below:

- $G_{sec\ 200\ kPa} = 7.2$ (kPa/%)
- $G_{sec\ 100\ kPa} = 3.7$ (kPa/%)
- $G_{sec\ 50\ kPa} = 2.0$ (kPa/%)

Although the study of small strains and G_{max} are not part of this body of research, results presented here supports previous research on the effects of effective confining pressure and shear modulus relationships.

The CSR vs. log N plot for the comparison of the results from changes in effective confining stress compared to the baseline is shown in Figure 6.54. By decreasing the effective confining pressure from 100 kPa to 50 kPa, the cyclic strength increases by 10%. In contrast, increasing the effective confining pressure from 100 kPa to 200 kPa decreases the cyclic strength by 7%. These results are comparable to the increases and decreases found in the Soil A Slurry Deposition Method testing series on effects of changes in effective confining pressures. Additional tests to develop full curves will better define the degree of the effects observed.

From Castro and Poulos (1977), the relationship between cyclic strength and effective confining pressure will vary depending on the relative densities. For this reason, it is suggested that further testing of Soils A and G specimens at various densities be performed.

6.3.4.2 In-Place Wet Pluviation

To study the effects of effective confining pressure on Soil A and Soil G reconstituted by the In-Place Wet Pluviation Method, specimens were tested at a higher effective confining stress (200 kPa) and at a lower effective confining stress (50 kPa) to compare to the baseline soils (100 kPa).

All other testing conditions: loading frequency of 0.005 Hz, OCR = 1, and 0.8 days of confinement were held constant. From Table 6.25, results from testing on Soil A and Soil G show that the void ratios and water contents decrease with increasing effective confining pressures.

Table 6.25 Specimen properties and cyclic simple shear testing conditions for Soils A and G reconstituted by In-Place Wet Pluviation at different effective confining pressures

Test Name	PI	LL	FC (%)	σ'_v (kPa)	σ'_m (kPa)	e_o	w_c (%)	w_c/LL	τ (kPa)	CSR	5% γ
Pluv A22	2	31	72%	67	50	0.97	36.16	1.17	25.7	0.191	4
Pluv A14*	2	31	72%	135	99	0.94	35.13	1.13	43.4	0.161	5
Pluv A23	2	31	72%	272	200	0.92	34.20	1.10	86.6	0.159	5
Pluv G17	10	31	77%	70	51	0.85	31.50	1.02	20.6	0.147	9
Pluv G10*	10	31	77%	138	101	0.83	30.69	0.99	46.8	0.170	4
Pluv G19	10	31	77%	270	198	0.80	29.66	0.96	75.5	0.140	12

*Denotes baseline specimen for comparison

The comparison between the specimen Pluv A9 (σ'_m = 100 kPa) and specimen Pluv A22 (σ'_m = 50 kPa) is shown in Figure 6.55. Pluv A22 was tested at a higher CSR than Pluv A9, yet Pluv A22 required more cycles of loading before the initiation of liquefaction. Given the high CSR, the baseline specimen, Pluv A9, liquefies before completing the second cycle, whereas Pluv A22 liquefies in the fourth cycle. From the CSR vs. log N plot in Figure 6.57, by decreasing the effective confining pressure to 50 kPa, the cyclic strength increases by 11%.

In contrast, by consolidating specimens to an effective confining stress of 200 kPa (Pluv A23) the cyclic strength decreased as shown in Figure 6.56. The CSR of Pluv A14 (100 kPa, CSR = 0.161) is higher than Pluv A23 (200 kPa, CSR = 0.159). As described in Section 6.3.1.2, Pluviated A specimens are sensitive to small changes in CSR. For instance, when comparing two baseline specimens, Pluv A14 (CSR = 0.161) liquefied in 5 cycles while Pluv A10 (CSR = 0.157) liquefied in 22 cycles. Pluv A23 was tested at a higher effective confining pressure and liquefied in 5 cycles, the same number as Pluv A14. If Pluv A23 had been tested at an effective confining pressure of 100 kPa vice 200 kPa, it would be expected that it would liquefy near 10 cycles. From the CSR curve, Figure 6.57, which compares the changes in effective confining pressure to the baseline, by doubling the effective confining pressure to 200 kPa, the cyclic strength decreases by 5%.

A comparison of the Pluviated Soil G specimens tested at 50 kPa and 200 kPa using a 4-way plot were not done because there were no baseline specimens tested at those CSRs. Each of the individual test responses can found in Appendix C2.2.

The comparison of the effects of effective confining pressure for Pluv G17 (50 kPa) and Pluv G19 (200 kPa) when compared to the baseline of 100 kPa are given on the CSR vs. log N plot, Figure 6.58. As expected from the results of the three previously mentioned test series (Slurry Deposition Method Soils A and G and the Pluviated Soil A), the specimen consolidated to the

lower effective confining stress, Pluv G17, lies above the CSR curve. Decreasing the effective confining stress to 50 kPa from 100 kPa increased the cyclic strength by 7%.

The results of Pluv G19 are inconsistent with the three previous series of tests performed using the higher effective confining stress. These previous test shows that specimens with the higher effective confining stress fall below the CSR curve, but Pluv G19 does not do this. It is not known if the test material was mistakenly made too dense and requires retesting, or if the Pluv G19 result is an outlier given that all testing conditions were the same. Additional testing to validate the CSR vs. log N curve at lower CSRs and testing at higher effective confining stress are recommended.

The results from the increases and decreases in cyclic strength from the changes in effective confining pressures from the slurry and Pluviated specimens, were plotted against the findings of Hynes and Olsen (1999) and Sancio (2003) on the K_σ chart, Figure 6.59. The K_σ is a correction factor to account for the non-linearity between the cyclic resistance and effective overburden pressure (Seed, 1983). The results from the reconstituted specimens do express similar trends to those observed from the results found by testing on field specimens. However, for effective confining pressures less than 100 kPa, the newly reconstituted specimens tend to underestimate the potential strength. At higher effective confining pressures, the reconstituted specimens tend to overestimate strength. These inconsistencies may be caused by the fact that the specimens are very young compared to those tested by Sancio, Hynes and Olsen. This suggests that aging effects may be more important in the determination of K_σ than expected for testing on reconstituted specimens. A second reason these results may be different is that the three data points composing tests with an effective confining stress less than 100 kPa from the Sancio (2003) testing series may be influenced by OCR, and the cyclic resistance may be higher than expected for a normally consolidated specimen at these effective confining pressures. The third reason is that the findings for this research are only based on one test for each case. Typically, the points for a K_σ graph are determined by comparing the CSR at 10 cycles to 5% shear strain from a curve determined by multiple tests for a given effective confining pressure. For these reasons, testing to formulate CSR curves at higher and lower effective confining pressures should be conducted.

6.3.5 Effects of the Rate of Loading

The rate of loading will directly affect the ability to measure excess pore water pressures accurately and has been shown through monotonic simple shear, Section 5.5, and cyclic triaxial testing, Section 6.2.1.1, to affect the static and cyclic shear strength of soil. The loading rate of a cyclic test should be based on the duration when ¼ cycle is greater than or equal to $4t_{50}$, or four times the time to 50% consolidation. This is equivalent to $16t_{50}$ for one cycle of loading, which is required to measure equilibrated pore water pressures, and therefore representative effective stresses.

The most common loading frequency used by researchers on silt and sand-silt mixtures has been 0.1 Hz (e.g., Wijewickreme, 2004, 2005; Naeini, 2003; Yasuhara, 2003) and 0.5 Hz (e.g., Gratchev, 2006). There is no mention of hydraulic conductivity and consolidation parameters, c_v, of the materials in the previous research to confirm the validity of these loading frequencies.

6.3.5.1 Slurry Deposition Method

To assess the effects of the rate of loading on Soils A and G, testing was performed at a loading frequency of 1 Hz to compare to the baseline loading frequency of 0.005 Hz. All other tests conditions were held constant, i.e., CSR, effective confining stress = 100 kPa, OCR = 1, and 0.8 days of confinement. The characteristics of the specimens are listed in Table 6.26.

Table 6.26 Specimen properties and cyclic simple shear testing conditions for Soils A and G reconstituted by the Slurry Deposition Method at different rates of loading

Test Name	PI	LL	FC (%)	e_o	Freq (Hz)	B-Value	w_c (%)	w_c/LL	CSR	5% γ
SDM A10	2	31	72%	0.70	1	0.96	26.14	0.84	0.210	9
SDM A11*	2	31	72%	0.68	0.005	0.96	25.39	0.82	0.210	4
SDM G11	10	31	77%	0.66	1	0.95	24.47	0.79	0.176	12
SDM G18*	10	31	77%	0.65	0.005	0.96	24.30	0.78	0.176	5

* Denotes baseline soil for comparison

Equation 5.1 was used to find t_{50} to determine the proper rate of loading. The term D equals (2.2/2) =1.1 cm because most cyclic simple shear Slurry Deposition specimens are between 1.8 cm and 2.2 cm in height and double-drained. The parameter c_v from consolidation tests for Soils A and G prepared by the Slurry Deposition Method are presented in Section 5.4, but are approximately 0.034 and 0.021 cm^2/sec, respectively. Using these inputs, t_{50} for Soils A and G are 7.0 and 11 seconds, respectively. As stated in the previous paragraph, the duration of one cycle of loading should be greater than or equal to $16t_{50}$, which is 110 and 180 seconds, respectively. Therefore, the loading frequency of 0.005 Hz, or 200 seconds per cycle, for the cyclic simple shear Slurry Deposition Method specimens is appropriate for the measurement of excess pore water pressures.

For assessing the effects of the rate of loading, baseline specimens (0.005 Hz) were compared to specimens tested at a loading rate of 1 Hz. From the above calculations, testing at 1 Hz would be too fast to accurately measure pore water pressures, and thus the effective stress graphs of the 4-way plot are not presented in Figure 6.60 and Figure 6.62. From these figures, the shear stress and shear strain time histories for the higher loading frequencies are different from the lower loading frequency tests. In Figure 6.60b and Figure 6.62b, the stress-strain curves from both of the 1 Hz tests (SDM A10 and SDM G11) have more-developed "banana loops" that are indicative of dense materials; yet, the void ratios are nearly equal at the beginning of the test. Moreover, the number of loading cycles to 5% shear strain for the higher frequency specimens was two times larger than that for the lower frequency specimens shown in Figure 6.60d and Figure 6.62d.

The results from the higher frequency specimens are plotted on the CSR vs. log N plots for Soil A, Figure 6.61, and Soil G Figure 6.63. For Soil A, by increasing the frequency of loading from 0.005 Hz to 1 Hz, the cyclic strength increases by 22%. Similarly, the increase in cyclic strength for Soil G by increasing the frequency of loading from 0.005 Hz to 1 Hz is 17%.

For nonplastic clean sands, there is minimal loading rate dependency meaning that the rate of loading should not affect the cyclic response. The results from this testing series suggest that there is a rate dependency for these fine-grained soils. For Soil A (PI = 2), the loading cycles to 5% shear strain is doubled and for Soil G (PI = 10), the number of cycles of loading to 5% shear strain increased by 2.4 times when the frequency of loading increased from 0.005 Hz to 1 Hz. This is an "apparent" increase in strength. The term "apparent" is used because pore water pressure equilibration is not occurring during the test and this is a total stress measurement of strength.

6.3.5.2 In-Place Wet Pluviation Method

As discussed in the previous sections, the rate of loading will directly affect the ability to measure excess pore water pressures accurately and may give a different cyclic response. Equation 5.1 was once again used to find t_{50} to determine the proper rate of loading. The term D equals (2.3/2) =1.15 cm because the In-Place Wet Pluviated specimens are between 1.8 cm and 2.3 cm in height and double-drained. The parameter c_v from consolidation tests for Soils A and G prepared by the In-Place Wet Pluviation Method are presented in Section 5.4, but are approximately 0.036 and 0.033 cm^2/sec, respectively. Using these inputs, t_{50} for Soils A and G are 7.2 and 7.9 seconds, respectively. The duration for one cycle of loading should be greater than or equal to $16t_{50}$, which is 120 and 130 seconds, respectively. Loading at a frequency of 0.005 Hz, or 200 seconds per cycle, for the cyclic simple shear In-Place Wet Pluviation Method specimens is appropriate and meets the criteria for accurately measuring excess pore water pressures.

To assess the effects of rate of loading, Pluv A20 and Pluv G16, were tested at a higher frequency of loading (1 Hz) while the other testing conditions, i.e., CSR, σ'_m = 100 kPa, time under confinement (0.8 days), and OCR (OCR = 1) were held constant. The specimen parameters and testing criteria are listed in Table 6.27.

Table 6.27 Specimen properties and cyclic simple shear testing conditions for Soils A and G reconstituted by In-Place Wet Pluviation at different rates of loading

Test Name	PI	LL	FC (%)	e_o	Freq (Hz)	B-Value	w_c (%)	w_c/LL	CSR	5% γ
Pluv A14*	2	31	72%	0.94	0.005	0.98	35.13	1.13	0.161	5
Pluv A20	2	31	72%	0.94	1	0.99	35.06	1.13	0.161	13
Pluv G16	10	31	77%	0.83	1	0.96	30.89	1.00	0.193	5
Pluv G22*	10	31	77%	0.83	0.005	0.97	30.96	1.00	0.192	2

*Denotes baseline specimens for comparison

The effective stress plots in the 4-way plot for Pluv A20 and Pluv G16 are not displayed in Figure 6.64 and Figure 6.66 because the higher loading rate did not allow for proper excess pore water pressures measurements. In the stress-strain plot in Figure 6.64b, the higher loading frequency specimen, Pluv A20, has the characteristic "banana loop" shaped stress-strain curve at the initiation of liquefaction, which is typically seen in a more dense material; yet both Pluv A20 and Pluv A14 specimens have the same void ratio prior to testing. This indicates that similar materials have a cyclic response dependent on the rate of loading. Additionally, from Figure

6.64d, Pluv A14 (0.005 Hz) reached 5% shear strain after 5 loading cycles while the faster loading rate, Pluv A20 (1 Hz), reached 5% shear strain in 2½ times more cycles of loading at the same CSR.

As stated in Section 6.3.1.2, the Pluviated A specimens are sensitive to changes in CSR. A small increase or decrease in the CSR will cause the cyclic response to vary significantly. This has created a relatively flat CSR curve. Comparing the two specimens, Pluv A14 and Pluv A20, tested at the same CSR, as in Figure 6.64, the difference in strength between the two tests is more obvious. When Pluv A20 is plotted and compared on the CSR vs. log N plot (Figure 6.65), there does not appear to be a large contribution of increased cyclic strength by increasing the frequency of loading from 0.005 Hz to 1 Hz. The "apparent" cyclic strength only increases by 3%. As stated in the previous section, the term "apparent" is used because pore water pressure equilibration is not occurring during the test and this is a total stress measurement of strength.

The same trends in cyclic response for Pluviated Soil A are seen in the results for Pluviated Soil G. From Figure 6.66d, Pluv G16 (1 Hz) reached 5% shear strain in the fifth cycle of loading and Pluv G22 (0.005 Hz) in the second cycle. The increase in "apparent" cyclic strength is more noticeable than Soil A as shown in Figure 6.67. By increasing the loading frequency to 1 Hz, the "apparent" cyclic strength increased by 22%.

In summary, increasing the loading frequency from 0.005 Hz to 1 Hz increased the number of cycles to 5% shear strain by approximately 2.5 times for both Soils A and G. This rate dependency, as previously described in Section 6.3.5.1, biases the results by showing the strength of the soil to be greater when testing at a rate of loading too fast to reliably measure effective stress.

6.3.6 Effects of Overconsolidation Ratio (OCR)

Previous research suggests the cyclic strength of sands and clays increase as the overconsolidation ratio (OCR) increases (e.g., Seed and Peacock, 1971; Lee and Focht, 1975; Ishihara et al., 1978; Ishihara and Takatsu, 1979; Dobry et al., 1981; Campenella and Lim, 1981; Stamatopoulos et al., 1995; Nagase et al., 1996). More recently, cyclic testing performed using silt and silty-sand specimens have also correlated the increase in cyclic strength to an increase in OCR (e.g., Ishihara et al., 1978; Lee and Roth, 1977; Sancio, 2003).

To assess the effect of overconsolidation on the cyclic strength of Soils A and G, the specimens were loaded to a higher effective confining stress and consolidated for 0.8 days. The specimens were then unloaded to a specific level of effective stress, which corresponds to a specific OCR, for testing. For example, an OCR = 2 was achieved for specimen SDM A14 by initially apply an effective confining pressure of 200 kPa (σ'_m), allowing it to consolidate for 0.8 days, then reducing the effective confining pressure to 100 kPa (σ'_m) and allowing the material to equilibrate for less than 1 hour before cyclic testing.

6.3.6.1 Slurry Deposition Method

A series of specimens that were prepared using the Slurry Deposition Method were tested at different OCRs to evaluate the effects on cyclic strength. Testing conditions such as mean effective confining stress (σ'_m = 100 kPa), loading frequency (0.005 Hz), and time under

confinement (0.8 days) were held constant. Additionally, SDM G12 (OCR = 1.2) and SDM G14 (OCR = 1) were tested to compare and contrast the effects of OCR at a smaller mean effective confining stress (σ'_m = 50 kPa). The characteristics of the specimens are listed in Table 6.28. As the OCR for Soil A increased from 1 to 3, the void ratio only decreased by a small percentage.

Table 6.28 Specimen properties and cyclic simple shear testing conditions for Soils A and G reconstituted by the Slurry Deposition Method at different OCRs

Test Name	PI	LL	FC (%)	σ'_v (kPa)	σ'_m (kPa)	e_o	B-Value	w_c (%)	w_c/LL	OCR	CSR	5% γ
SDM A11*	2	31	72%	138	101	0.68	0.96	25.39	0.82	1.0	0.210	4
SDM A14	2	31	72%	135	99	0.66	0.95	24.71	0.80	2.0	0.211	30
SDM A15	2	31	72%	137	101	0.66	0.97	24.58	0.79	3.0	0.250	16
SDM G14*	10	31	77%	68	50	0.68	0.97	25.36	0.82	1.0	0.177	8
SDM G12	10	31	77%	68	50	0.67	0.96	24.84	0.80	1.2	0.177	13
SDM G18*	10	31	77%	138	101	0.65	0.96	24.30	0.78	1.0	0.176	5
SDM G17	10	31	77%	141	103	0.60	0.95	22.37	0.72	1.5	0.172	71
SDM G16	10	31	77%	137	101	0.61	0.95	22.52	0.73	2.0	0.178	-

* Denotes baseline specimen for comparison

A comparison SDM A11 (OCR = 1) and SDM A14 (OCR = 2), at the same CSR, is shown in Figure 6.68. In this figure, the higher OCR specimen has 7.5 times more cycles to reach 5% shear strain than the OCR = 1 specimen. The shear strains in Figure 6.68d for SDM A11 increase steadily with each cycle from the onset of the test. For SDM A14, the shear strains are small and consistent until the threshold of 30% of the initial vertical effective stress, or r_u=70%, was reached. After this threshold, the rate of pore water pressure generation increases as seen in Figure 6.68c, and shear strains steadily increase per each successive cycle until 5% shear strain is reached, as seen in Figure 6.68d. A value of r_u=80%, or 20% of the initial vertical effective stress, occurred in the same number of cycles as 5% shear strain, (γ), which is the stress-based definition of liquefaction described in 6.1.2.

In this testing series, SDM A15 (OCR =3) has a larger CSR than any of the Slurry Soil A baseline specimens. If SDM A15 were tested at CSR = 0.21, as SDM A11 and SDM A14, the specimen may continue to cycle and the number of loading cycles to 5% shear strain would be too high to be useful in a liquefaction assessment. The CSR = 0.25 was chosen for SDM A15 so that it would liquefy between 10-20 cycles of loading. This specimen liquefied at 16 cycles.

A comparison of the OCR effects on the cyclic strength of Slurry Soil A specimen is shown in the CSR vs. log N plot in Figure 6.69. The cyclic strength is increased by 36% and 55% when the OCR is increased from 1 to 2 and 1 to 3, respectively.

Two Soil G specimens, prepared by the Slurry Deposition Method, SDM G16 (OCR = 2) and SDM G17 (OCR = 1.5), were compared to a baseline specimen SDM G18 (OCR = 1) and tested near the same CSR. Figure 6.70d shows that the number of loading cycles to 5% shear strain for

SDM G18 (5 cycles) is significantly lower than the number of cycles of loading for SDM G17 (71 cycles). At this CSR, SDM G16 had minimal strains and no significant increases in pore water pressures after 60 cycles, so the test was terminated.

The two tests performed at the lower mean effective confining stress (σ'_m = 50 kPa), shows that a slight increase in OCR will result in more cycles before liquefaction. The OCR of SDM G12 (OCR = 1.2) is only slightly greater than SDM G14 (OCR = 1); yet the cyclic strength of SDM G12 is greater than SDM G14 by five more cycles to 5% shear strain at the same CSR, Figure 6.71d.

A comparison of the results for increases in OCR and the effects on the cyclic strength are shown in the CSR vs. log N plot in Figure 6.72. The cyclic strength is increased by 26% when the OCR is increased from 1 to 1.5. The increase in cyclic strength from OCR = 1 to OCR = 2 was not be assessed because this specimen did not fail at the given CSR. Similarly, any increases in cyclic strength were not assessed from SDM G12, because a baseline curve was not established for the lower effective confining stress (50 kPa).

6.3.6.2 In-Place Wet Pluviation Method

Four specimens, prepared by the In-Place Wet Pluviation Method from Soil A and from Soil G, were tested at different OCRs to assess the effects on cyclic strength. Other testing conditions, i.e., mean effective confining stress (σ'_m = 100 kPa), frequency of loading (0.005 Hz), and time under confinement (0.8 Days) remained the same. The specimen properties are listed in Table 6.29.

In the test series shown in Table 6.29, as the OCR increases, the void ratio and water contents decrease. These effects are less dramatic for Soil A than Soil G, which was also prepared by the In-Place Wet Pluviation Method.

Table 6.29 Specimen properties and cyclic simple shear testing conditions for Soils A and G reconstituted by In-Place Wet Pluviation at different OCRs

Test Name	PI	LL	FC (%)	e_o	B-Value	w_c (%)	w_c/LL	OCR	CSR	5% γ
Pluv A14*	2	31	72%	0.94	0.98	35.13	1.13	1.0	0.161	5
Pluv A24	2	31	72%	0.93	0.95	34.39	1.11	2.0	0.161	37
Pluv A25	2	31	72%	0.91	0.98	33.82	1.09	3.0	0.160	-
Pluv G10*	10	31	77%	0.83	0.99	30.69	0.99	1.0	0.170	4
Pluv G20	10	31	77%	0.77	0.95	28.66	0.92	2.0	0.199	12
Pluv G21	10	31	77%	0.80	0.94	29.59	0.95	2.0	0.176	16

*Denotes baseline specimen for comparison

As previously mentioned in Section 6.3.1.2, Pluviated Soil A is sensitive to changes in CSR. Small changes in CSR result in large differences in the number of cycles to 5% shear strain. For this reason, the results from testing on Pluv A14, Pluv A24, and Pluv A25 are shown in Figure 6.73, using the 4-way plot, are more illustrative than showing the results in Figure 6.74 on the CSR vs. log N plot.

Three specimens, Pluv A14 (OCR = 1), Pluv A24 (OCR = 2), and Pluv A25 (OCR = 3) were tested at the same CSR = 0.161. Pluv A14 reached 5% shear strain at 5 cycles, Pluv A24 reached 5% shear strain in 37 cycles. For Pluv A25, the maximum r_u of 25%, or 75% of the normalized vertical effective stress, was reached after 60 cycles of loading and the test was terminated. From Figure 6.73b, all three specimens have identical first cycles of loading, even though they have different OCRs. After the first cycle, the excess pore water pressures for each specimen begin to generate at different rates. Pluv A24 shown in Figure 6.73c exhibits the same backwards S-shape as many of the normally consolidated specimens in Figure 6.21c, but the rate of increase in strains per cycle near the initiation of liquefaction was more gradual than the normally consolidated specimens. In most normally consolidated tests, after the threshold of r_u = 60% is reached, the specimens will generally liquefy in 2-3 cycles; but for the OCR = 2 test, the specimens liquefied in 5-6 cycles after reaching this same threshold. The final cycle of Pluv A24 resembles a more "banana loop" shape than "football shape," unlike Pluv A14. This is indicative of a more dense material. The CSR chart showing the relationship between OCR and the baseline conditions is shown in Figure 6.74. In this CSR vs. log N plot, an increase in OCR from 1 to 2 only increases the cyclic strength by 4%. However, when comparing the number of cycles to 5% shear strain, the OCR = 2 has six times more cycles of loading than the OCR = 1 specimen.

For the Soil G OCR testing series, two specimens were tested at the same OCR to establish a cyclic resistance curve for the OCR = 2 soil to compare to the OCR = 1 CRR curve.

Pluv G21 (OCR = 2) has a significantly greater cyclic strength than Pluv G10 (OCR = 1) as shown in Figure 6.75. Pluv G21 has 4 times more loading cycles to the initiation of liquefaction than the OCR = 1 specimen, even though the CSR for Pluv G21 is slightly higher. Pluv G21 (OCR = 2) also exhibits many of the same traits as Pluv A24 (OCR = 2), in the shear stress and shear strain time histories, Figure 6.73. The "banana loop" stress-strain curves in Figure 6.75b, and the backwards S-shape normalized vertical effective stress in Figure 6.75c are similar to those in Figure 6.73b and Figure 6.73c.

In Figure 6.76, the CSR vs. log N curve for OCR = 2 is compared to the baseline curve for OCR = 1 specimens. Increasing the OCR from 1 to 2, the cyclic strength increased by at least 26%. This is more dramatic than Pluviated Soil A which increased by 4% over the same range of OCR.

When comparing the effects of OCR on the cyclic strength of sands and clay, clays are more affected by increases in OCR, while the change in the cyclic strength for increases in OCR for sands is negligible. Soil A (PI = 2) has characteristics that are more "sand-like" than Soil G (PI = 10). These characteristics could well account for the differing effect of OCR on cyclic strength for these two soils.

6.3.7 Effects of Initial Static Shear Stress

In previous research, sands have been the primary material tested for the effects of initial static shear stress (e.g., Lee and Seed, 1967; Yoshimi and Oh-oka, 1975; Ishihara et al, 1977; Yoshimi and Tokimatsu, 1978; Rollins and Seed, 1988; Vaid and Finn, 1979; Vaid and Chen, 1983;

Vasquez-Herrera et al, 1988; Boulanger, 1990; Seed and Harder, 1990; Boulanger and Seed, 1995; Harder and Boulanger, 1997; Kammerer, 2002; and Wu, 2002). Results from this research found that the cyclic resistance of the soil in the presence of an initial static shear stress was largely dependent on the specimen's relative density and the magnitude of the initial static shear stress. As an example, for loose soils (soils that are contractive under drained shearing) with an initial static shear stress, cyclic resistance can be significantly reduced. Conversely, for very dense soils (soils that are dilative under drained shearing) the driving shear stresses can lead to a reduction in the generation of pore water pressures during cyclic loading creating an increase in cyclic resistance.

Until recently, only a few researchers have looked at the effects of initial static shear stress on silts and other fine-grained specimens (e.g., Biscontin, 2001; Sancio, 2003; Anantanavanich, 2006). These researchers found that fine-grained specimens tested with an initial static shear stress reached the threshold of 5% shear strain in fewer cycles and had smaller pore water pressure generation than in the tests performed without an initial static shear stress.

The static shear stress ratio, α, is the ratio of the initial static shear stress, τ_o or τ_{static}, to the initial normal stress on the plane, σ'_v, shown in Equation 6.5.

$$\alpha = \frac{\tau_o}{\sigma'_v} \qquad \textbf{6.5}$$

Figure 6.77 illustrates a typical Mohr's circle for a specimen with an initial static shear stress. Soils that are located under slopes or under the edge of a building are examples of cases that have an initial static shear stress. For these examples, the static shear stress (τ_{static}) and the horizontally propagating shear waves (τ_{cyc}) would add to the final diameter of the circle.

Both the Slurry Deposition Method and In-Place Wet Pluviated specimens were tested to assess the effects of initial static shear stress at CSR = 0.1 with the α-value approximately equal to 0.1. Both specimens were tested at the low CSR and α-value to ensure that they would not fail statically or within the first cycle. Future testing with a higher α and CSRs are recommended.

For these values of CSR and α, there is no stress reversal. To simulate stress reversal, the shear stress first cycles to one side then reverses and heads toward the origin. If the shear stress does not cross over the origin before the beginning of the next cycle, there is no stress reversal and the particles within the specimen have little opportunity to move relative to each other. No stress reversal often leads to cyclic densification with each cycle and inhibits the ability of the specimen to liquefy (e.g., Vaid and Finn, 1979; Boulanger and Seed, 1995).

Two tests with an initial static driving shear stress were performed on Soil A, one prepared by the Slurry Deposition Method and the other by the In-Place Wet Pluviation Method, to replicate the initial in situ loading conditions on soil elements under sloping ground conditions and assess its effects on the cyclic strength of the soil. To create a specimen with an initial static shear stress, special measures were taken during the consolidation phase. The specimens were placed

in the simple shear apparatus, vacuum saturated, and vertically loaded to a predetermined effective stress level for testing. During the consolidation process, the horizontal load was increased at the same pace to keep the shear ratio, α, equal to 0.1. The specimens remained under confinement for 0.8 days. All other testing condition such as CSR (0.10), time under confinement (0.8 days), effective confining stress (100 kPa), frequency of loading (0.005 Hz), and OCR (OCR = 1) were held constant. The characteristics of the specimens tested with an initial static shear stress are given in Table 6.30.

Table 6.30 Specimen properties and cyclic simple shear testing conditions for Soil A reconstituted by the Slurry Deposition Method and In-Place Wet Pluviation Method with an initial static shear stress

Test Name	PI	LL	FC (%)	e_o	B-Value	w_c (%)	w_c/LL	α	CSR	5% γ
SDM A16	2	31	72%	0.69	0.95	25.78	0.83	0.13	0.101	46
Pluv A27	2	31	72%	0.90	0.98	33.47	1.08	0.12	0.102	-

The specimen SDM A16, a Soil A specimen prepared by the Slurry Deposition Method, tested at a CSR lower than the Soil A Slurry specimens, reached 5% shear strain in 46 loading cycles. The results of SDM A16 (α = 0.13) are compared to the baseline (α = 0) in the CSR vs. log N plot in Figure 6.78. The reduction in cyclic strength for SDM A16 due to the α-factor was 51%. These results are comparable to the findings by Sancio (2003), which tested similar soils.

Pluv A27, a Soil A specimen prepared by the In-Place Wet Pluviation Method, was also tested at a low CSR, but did not reach 5% shear strain. With each cycle, the strains slowly increased but did not reach 2% shear strain within 60 loading cycles and the test was terminated. Figure 6.79 plots the CSR vs. log N plot for α = 0 results compared to Pluv A27 (α = 0.12).

Figure 6.80 compares the individual test results from the two α-tests, SDM A16 and Pluv A27. The normalized vertical effective stress curves show similar pore water pressure generation similar to all other non-α tests. SDM A16 reached the threshold of r_u = 60%, but unlike the non-α tests, the strains per cycle did not increase rapidly to 5% shear strain. From Figure 6.80d, the magnitude of the double amplitude shear strain for both specimens remained small until the termination of both tests.

A discrepancy needs to be pointed out in regards to α-tests and the definition of liquefaction. For all non-α tests, the specimens are tested to 5% single amplitude strain centered on the origin, which equates to approximately 10% double amplitude strain. The α-tests do reach 5% single amplitude shear strain, but the strains are not centered about the origin. In fact, the double amplitude strain per cycle from this testing series remained less than 1%.

6.4 Effects of Testing Device

Within this laboratory study, two testing devices were used to assess the liquefaction susceptibility and resistance of the soil, i.e., the CTX device and the CSS device. The number of cycles to "liquefaction" between a CTX test (5% double amplitude ε_a) and a CSS test (5%

single amplitude γ) are not equivalent. To convert between the two testing systems, Seed and Peacock (1979) proposed the following equation based on data for clean sands:

$$\mathbf{CSR_{ss} = c_r * CSR_{Tx}} \qquad \mathbf{6.6}$$

where CSR_{ss} is the cyclic stress ratio for cyclic simple shear testing, CSR_{Tx} is the cyclic stress ratio for cyclic triaxial testing, and the term c_r is a conversion factor. Their recommended value of c_r was 0.6 to 0.7 for normally consolidated specimens and depended on the value of the coefficient of earth pressure at rest, K_o. When studying the liquefaction susceptibility of a normally consolidated fine-grained soil deposit after the 1989 Loma Prieta earthquake, Boulanger et al. (1998) used $c_r = 0.7$. Sancio (2003) found that when testing on shallow, fine-grained soils from Adapazari with a PI < 12, at a mean effective of 100 kPa, $c_r = 0.85$.

For this analysis, the Slurry Deposition Method CTX results were compared to a representative Slurry Deposition Method CSS result. All cyclic triaxial testing was performed on Slurry Deposition specimens and at a mean effective confining stress of 50 kPa and a loading frequency of 1 Hz. One Slurry Deposition Method cyclic simple shear test, SDM G12, was performed at an effective confining stress of 50 kPa but at a loading frequency of 0.005 Hz. From Section 6.3.5.1, the cyclic strength increases by approximately 17% when the loading frequency is increased from 0.005 Hz to 1 Hz. The cyclic strength of SDM G12 was first modified to an approximate strength for 1 Hz and then compared to the cyclic triaxial CSR vs. log N curve as shown in Figure 6.81. The cyclic simple shear specimen falls below the triaxial CSR vs. log N curve indicating that the triaxial tests have greater cyclic strength than the simple shear tests. From these few experiments, $c_r = 0.84$ was estimated for the Slurry Deposition Method specimens at an effective confining pressure of 50 kPa.

6.5 Evaluation of the Existing Liquefaction Susceptibility Criteria

Since the 1999 Kocaeli earthquake and the observations of liquefaction and cyclic mobility that were made in Adapazari, Turkey, there has been an increase in testing on fine-grained soils for insight into liquefaction susceptibility and resistance. The proposed susceptibility criteria from these researchers and the results of this laboratory investigation are now compared.

Of the 76 cyclic simple shear specimens tested in this study, the majority of the tests were performed on Soils A and G. Except for 6 tests, the tests reached 5% single amplitude shear strain during cyclic testing and deformed considerably under the applied cyclic stresses. Those that did not reach 5% shear strain were generally tested at a CSR too low to generate significant excess pore water pressures. The results from these 76 tests showed that both Soils A and G were susceptible to cyclic mobility depending on the CSR at which they were tested and not necessarily on their soil characteristics.

The specimens in this testing series are exceptionally young (typically 0.8 days) when compared to field samples that may be centuries older. The cyclic strength results are skewed for the young specimens because aging effects increase the strength of the soil. For this reason, it is more difficult to compare these results to established liquefaction criteria that are typically based on field samples. However, the Slurry Deposition Method and In-Place Wet Pluviation Method test results do give valuable insight into the soil response under cyclic loading.

Prior to the 1999 earthquake, the state of the practice for the engineering community (e.g., Youd et al. 2001) used the "Chinese Criteria" based on Wang (1979) and is shown in Figure 6.82a. From this figure, only Soil A (PI = 2, LL = 31) would be classified as susceptible to liquefaction. Soil D (PI = 11, LL = 38) and G (PI = 10, LL = 31) fall outside of the criteria and would therefore be termed as "not susceptible." The relatively large amount of particles finer than 5μm and the higher LL for Soils D and Soil G would classify these materials as not susceptible to liquefaction according to the "Chinese Criteria." Testing by Sancio (2003) found that soils similar to Soils G and D were susceptible to liquefaction. The results of this testing program agree with Sancio's results, because the soils underwent cyclic mobility after a reasonable number of loading cycles when tested at significant CSRs.

A comparison of the results with the Andrews and Martin (2000) criteria is shown in Figure 6.82b. Using their criteria, of the soils tested, only Soil A would meet their criteria as "susceptible" to liquefaction. Neither Soil D nor Soil G meets the susceptibility criteria regarding the amount of particles finer than 2 μm. In addition, Soil D does not meet the Liquid Limit criteria to be stated as susceptible. Soil G would require "further testing" according to criteria, but Soil D would be "not susceptible".

The Polito and Martin (2001) criteria are compared to the soils within this testing program as shown in Figure 6.83a. Each of the three soils, Soil A, Soil D, and Soil G are labeled as "liquefiable", "susceptible to cyclic mobility", and "potentially liquefiable", respectively. This criterion has better captured the liquefaction potential of Soil A, D, and G than either the "Chinese Criteria" or that of Andrews and Martin (2000). The percentage of clay-sized fines, whether <2 μm or <5 μm, versus the Liquid Limit proposed in the two previous criteria do not capture all aspects of the liquefaction assessment.

The Seed et al. (2003) criteria, which are largely based on the research of Sancio (2003), are compared to the results of this study and can be found in Figure 6.83b. For these criteria, Soils A and G are plotted within the "liquefiable" range, and Soil D is on the line between "liquefiable" and "may be liquefiable." Their criteria have captured the potential of the soils tested within this program.

Using the research of Sancio (2003), Bray and Sancio (2006) developed a new concept for liquefaction criteria which includes the effects of the w_c/LL ratio of the specimen, as well as its PI, which represents the mineralogy of the fine-grained soil. In Figure 6.84a, the results of all In-Place Wet Pluviation specimens are assessed using their criteria. These specimens fall within the "Susceptible" category except for one. This test (Pluv G24, time under confinement of 50 days) falls into the "Test" category. With a high enough CSR, this specimen underwent cyclic mobility within a reasonable number of loading cycles.

Not all specimens within the "Susceptible" category reached 5% shear strain. As stated earlier in this section, the CSR for some of these specimens was too low to produce significant excess pore water pressures and hence did not liquefy. These soils remain susceptible to liquefaction, but they did not liquefy at the CSRs applied in these tests.

The Slurry Deposition Method specimens are not included in this analysis because the densities are greater than both the In-Place Wet Pluviation specimens and field specimens as stated in Section 6.3.1.3. This means the w_c/LL ratios are also lower than for those in situ soils or field specimens. These Slurry specimens would skew the data to the left of the graph and as such are not compared to these criteria.

The w_c/LL criterion appears to be most appropriate for normally consolidated specimens. Specimens Pluv G13 and Pluv G20 both have the same void ratio (0.77) and water content to liquid limit (0.93), but very different cyclic responses. Pluv G20 had an OCR = 2 and Pluv G13 had an OCR = 1. Because of the OCR, Pluv G20 had more cycles of loading before reaching 5% shear strain (12 cycles) than Pluv G13 (5 cycles) and thus greater cyclic strength as seen in Figure 6.85d, regardless of the void ratio and w_c/LL.

In 2004 and 2006, Boulanger and Idriss recommended that soil be categorized as either "sand-like" or "clay-like." From Figure 6.84b, Soil A would be classified as a "sand-like" material, while Soil G would be "clay-like." Soil D is an ML according to Unified Soil Classification System, but it would be classified as "clay-like" according to their criteria. It is this author's contention that soils cannot be categorized into the "black and white" categories of being either sand or clay.

Some researchers have opted for demand-based liquefaction criteria. El Hosri et al. (1984) compare the CSR to the Plasticity Index of undisturbed samples. The data are grouped in categories of number of cycles required to cause initial liquefaction, N_L. Using the chart with these criteria, for a given PI, the number of cycles to liquefaction for a given CSR is estimated. Prakash and Guo (1998) extended this research based on additional testing by Puri (1984) and Sandoval (1989) to include reconstituted silt-clay mixtures. Figure 6.86 depicts the Prakash and Guo (1998) criteria for CSR vs. PI for the number of cycles to liquefaction with Soils A, D, and G overlaid on the figure. For each soil type, numerous tests were performed at different densities, OCRs, frequencies, and times under confinement. However, the Prakash and Guo (1998) demand-based charts over-estimate the number of cycles of loading to failure for Soils A, D, and G. A majority of the tests on the reconstituted fine-grained soils from Adapazari could not sustain CSRs higher than 0.2.

Most recently, Xenaki and Athanasopoulos (2003) have used demand-based liquefaction criteria interrelating the number of cycles to failure, fines content, void ratio, and CSR. However, these criteria are only applicable for FC < 60%, and hence, it was not used for comparison purposes to the fine-grained soils within this research program.

6.6 Insights into the Evaluation of the Liquefaction Susceptibility and Resistance of Fine-Grained Soils

As stated in the previous section, several researchers have proposed criteria for screening for liquefaction susceptibility. Most have used a combination of PI, LL, clay-sized particle amounts, and water content to describe the liquefaction susceptibility of soils based largely on testing of field specimens.

In this research, when testing reconstituted specimens, it was found that the most important factors for consideration of liquefaction susceptibility are the density, parameterized as either

void ratio or w_c/LL, of the material and the intensity of shaking, CSR. The density of the specimen is influenced by three factors: 1) the effective confining pressure, 2) time under confinement, and 3) and whether the specimen was purposefully densified or made loose.

The results from cyclic simple shear testing on In-Place Wet Pluviated specimens have shown that Soil A, D, or G will eventually undergo cyclic mobility if the CSR is sufficiently high.

What differentiates the specimens within the testing program is their density, based on the three factors mentioned above. Similar to the Bray and Sancio (2006) criteria, density is included in this liquefaction criterion. As explained in Section 6.3.3, density and void ratio are related. Void ratio is related to water content through the equation:

$$\mathbf{S * e = w_c * G_s} \qquad \mathbf{6.7}$$

where S is the level of saturation, e is the void ratio, w_c is the water content, and G_s is the Specific Gravity. In this equation, S and G_s are both considered constants. As the void ratio increases, the density decreases, and the water content increases.

The relationship between the water content and LL (w_c/LL) defines where the specimen lies on the water content continuum. Knowing where the water content of the specimen is relative to the Atterberg Limits, such as LL, helps to define the soil's cyclic response. As the water content of the specimen nears the LL, the state of the remolded material changes from a plastic solid towards a viscous liquid. Using the parameter w_c/LL, not only includes the density of the material, but also captures the sensitivity of the soil.

CSR also plays a critical role in determining if a soil will liquefy. This research on fine-grained soils with PI $\leq$ 12 found that if the CSR was sufficiently large, the fine-grained soil specimens would liquefy or be subjected to cyclic mobility.

Using w_c/LL and CSR, Figure 6.87 was developed for Soil A and Figure 6.88 for Soils D and G. These charts are demand-based in that for a given w_c/LL, the CSR required for a range of cycles of loading to 5% shear strain could be estimated for the reconstituted soil specimens. As an example, if a reconstituted specimen similar to Soil A (PI = 2, LL = 31) has a w_c/LL ratio of 1.1, it is expected that at CSRs of 0.18, 0.16, and 0.14, the specimen would reach 5% shear strain in less than 10 cycles, 20 cycles or more, or not at all, respectively.

Additional testing is required to determine if the difference between the two charts (i.e., Soil A has a PI = 2 and Soils D and G have PI = 10 and 11, respectively) is based on PI. These figures do, however, help establish a framework for assessing the effects of the density of the material and cyclic strength.

These charts will only apply to normally consolidated specimens. Pluv G20 (OCR= 2) and Pluv G13 (OCR = 1) have the same void ratio and water content, yet the cycles to the initiation of liquefaction for Pluv G20 is 2.4 times greater than Pluv G13. For this reason, specimens with an OCR greater than 1 have not been included.

In Section 6.3.2, results suggested that the specimens gained strength with time under confinement. Both Soil A and Soil G gained strength, although at different rates, over the same time period under confinement. The in situ cyclic resistance can be estimated by including this important effect. For example, Figure 6.37 could be used to extrapolate the time under confinement factor found on the Y-axis and multiply this factor by the CSR from Figure 6.87 and Figure 6.88.

6.7 Summary and Principal Findings

The results from these CTX and CSS tests bring new insights regarding the cyclic resistance of fine-grained soils for a variety of testing parameters. In this study, the effects of the specimen preparation method, soil index properties, time under confinement, void ratio, effective confining stress, rate of loading, overconsolidation ratio, and initial static shear were explored.

Based on the results from a large number of cyclic triaxial and cyclic simple shear tests performed on reconstituted specimens, the following findings are drawn:

- For soils with a PI < 12, soils with a lower PI will not necessarily have a lower void ratio than those with higher PIs. Whether the specimens were reconstituted using the Slurry Deposition Method or In-Place Wet Pluviation Method, Soil G (PI = 10) consistently had a lower formation void ratio and water content than Soil A (PI = 2).

- For each soil type and reconstitution method, the functional form of the CSR curves was found to be adequately captured by CSR = a + b/N, where N represents the cycles to 5% shear strain. This form was determined by doing a best fit using a least-squares regression to solve for the coefficients a and b. The descriptions of these curves are given in Table 6.31.

Table 6.31 CSR curve properties based on CSR = a + b/N for Soils A and G reconstituted by the Slurry Deposition Method and In-Place Wet Pluviation Method

Specimen Type	a	b	Standard Error	R^2
SDM A	0.1470	0.2261	0.0145	0.83
SDM G	0.1331	0.2040	0.0072	0.98
Pluv A	0.1519	0.0714	0.0044	0.91
Pluv G_{Loose}	0.1205	0.1527	0.0138	0.92
Pluv G_{Dense}	0.1140	0.3820	0.0058	0.98

- For soils with PI < 12, soils with higher PI do not always exhibit higher cyclic resistance. Soil A (PI = 2) has greater cyclic resistance than Soil G whether reconstituted by the Slurry Deposition Method or In-Place Wet Pluviation.

- The failure mechanism of the Pluviated specimens is not fully understood. For the Slurry Deposition Specimens, specimens were shown to be homogeneous and the failure is that of a soil element with a constant PI and water content. For the In-Place

Wet Pluviated specimens, it is not known if the entire specimen failed, or the coarse-grained seams within the specimens caused failure. If these seams are the cause of failure, the lower PI, higher void ratio, and lower fines content within this band may explain the differences in response between the two reconstitution methods.

- The threshold of significant increases in shear strains per cycle is between r_u = 60 to 70% for the specimens tested. Below this threshold, for both Soils A and G, minimal shear strains per cycle are seen. After this point, the shear strains increase with each cycle until liquefaction. For a stress-based definition of liquefaction, 5% shear strain typically coincides with r_u = 80%.

- Soils that did reach 5% shear strain exhibited either cyclic mobility with limited shear strain potential or cyclic mobility with large shear strain potential. All Slurry Deposition specimens, Pluviated soils with very low void ratios, Pluviated soils with a significant time under confinement, and Pluviated Soils tested at 1 Hz exhibited cyclic mobility with limited shear strain potential. Once the threshold of r_u = 60% (for the Pluviated specimens) and r_u = 70% (for the Slurry specimens) was reached, the specimens developed a nearly linear increase in shear strain for each additional cycle. Conversely, all Pluviated A and G soils with OCR = 1, 0.8 days under confinement, tested at a loading frequency of 0.005 Hz, with an average density, regardless of effective confining pressure, exhibited cyclic mobility with large shear strain potential. Once the r_u = 60% threshold was reached, most specimens failed in 1 to 2 more cycles of loading.

- The CSRs resulting in liquefaction of reconstituted specimens are much smaller than those for field specimens. Sancio (2003) was able to test specimens of similar soil up to CSRs as high as 0.5. Previous testing on reconstituted specimens rarely reached a CSR as high as 0.2 (e.g., Xenaki and Athanasopoulos, 2002; Wijewickreme et al., 2005; Wijewickreme and Sanin, 2004; Boulanger and Idriss; 2006). As seen in Section 6.3.2, soils gain strength according to their time under confinement. These aging effects may be responsible for the large discrepancies in cyclic strength between field samples and reconstituted specimens.

- For Soil A and Soil G, using the cyclic simple shear, the loading frequency of 0.005 Hz was chosen to accurately measure excess pore water pressures within the tests specimens. Increases in the loading frequency led to higher cyclic strengths.

- Previous researchers have recommended liquefaction screening criteria based on Liquid Limit, with the amount of particles finer than 5 μm or 2 μm, Plasticity Index, and w_c/LL. From this body of research, it was found that the clay size criterion from the "Chinese Criteria" and Andrews and Martin (2000) did not apply to these fine-grained soils. All of these soils were susceptible to liquefaction, even though some had amounts of clay-size particles that exceeded the thresholds in these criteria. The fine-grained soils within this study were primarily composed of PI < 12 material. Based on the Boulanger and Idriss (2004, 2006) liquefaction screening, the PI < 7 criterion does not adequately capture the liquefaction susceptibility of Soils D (PI =

11) and Soil G (PI = 10). The Ishihara (1996) and Bray and Sancio (2006) criteria, which state that soils with a PI < 10 and PI <12, respectively, are susceptible to cyclic mobility, were found to be more appropriate for the soils represented within this body of research.

- Based on the results from this program of testing on newly formed reconstituted soils, all specimens tested exhibited cyclic mobility at intense CSR levels. Testing on reconstituted specimens should be used to provide insight regarding the trends that result due to changes in time under confinement, density, effective confining stress, and overconsolidation ratios.

- Results from varying each of the testing conditions are presented in the Table 6.32. For many parameters, only one test was performed to examine the effects of variation of the parameter on the cyclic response of these fine-grained soils. This was often insufficient to develop firm conclusions concerning the response of the soil to the varied soil parameters and as such, the increases and decreases in cyclic strength should be considered preliminary.

Table 6.32 Summation of changes to testing parameters and resulting increase and decreases in cyclic strength

Criteria	Specimen Type	Baseline Parameter	Varied Parameter	Increase/ Decrease in Cyclic Strength (%)
Time under Confinement (days)	SDM A	0.8	0.04	-21
	Pluv A	0.8	0.05	-22
		0.8	11	3
		0.8	50	13
	Pluv G	0.8	18	8
		0.8	50	33
Density (Void Ratio)	SDM A	0.67	0.74	-11
	SDM G	0.65	0.67	-8
		0.65	0.62	13
	Pluv A	0.96	0.92	6
	Pluv G	0.84	0.73	16
Effective Confining Pressure (kPa)	SDM A	100	50	9
		100	200	-5
	SDM G	100	50	10
		100	200	-7
	Pluv A	100	50	11
		100	200	-5
	Pluv G	100	50	7
Frequency (Hz)	SDM A	0.005	1	22
	SDM G	0.005	1	17
	Pluv A	0.005	1	3
	Pluv G	0.005	1	22
OCR	SDM A	1	2	36
		1	3	55
	SDM G	1	1.5	26
	Pluv A	1	2	4
	Pluv G	1	2	26
α	SDM A	0	0.13	-51
	Pluv A	0	0.12	-

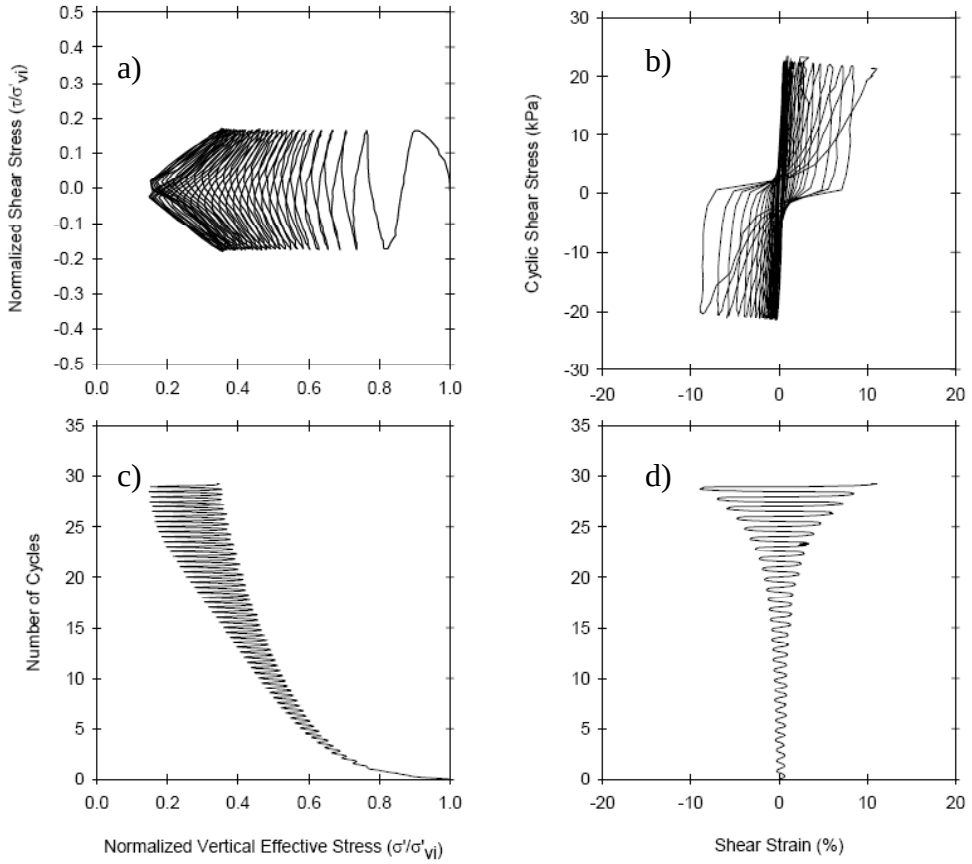

Figure 6.1 Example of a 4-Way plot for a cyclic simple shear test: a) effective stress path, b) stress-strain diagram, c) normalized vertical effective stress to number of cycles, and d) shear strain to the number of cycles of loading.

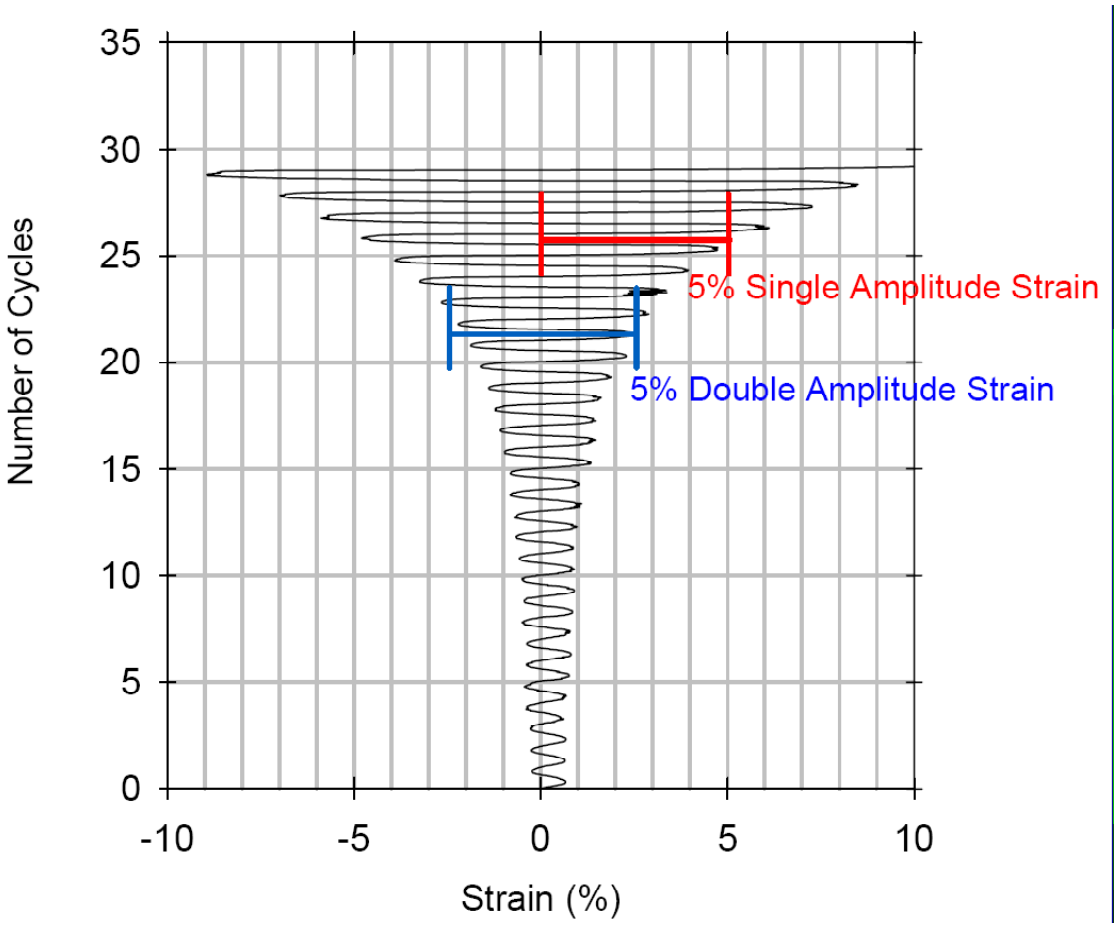

Figure 6.2 Definition of single and double amplitude strain.

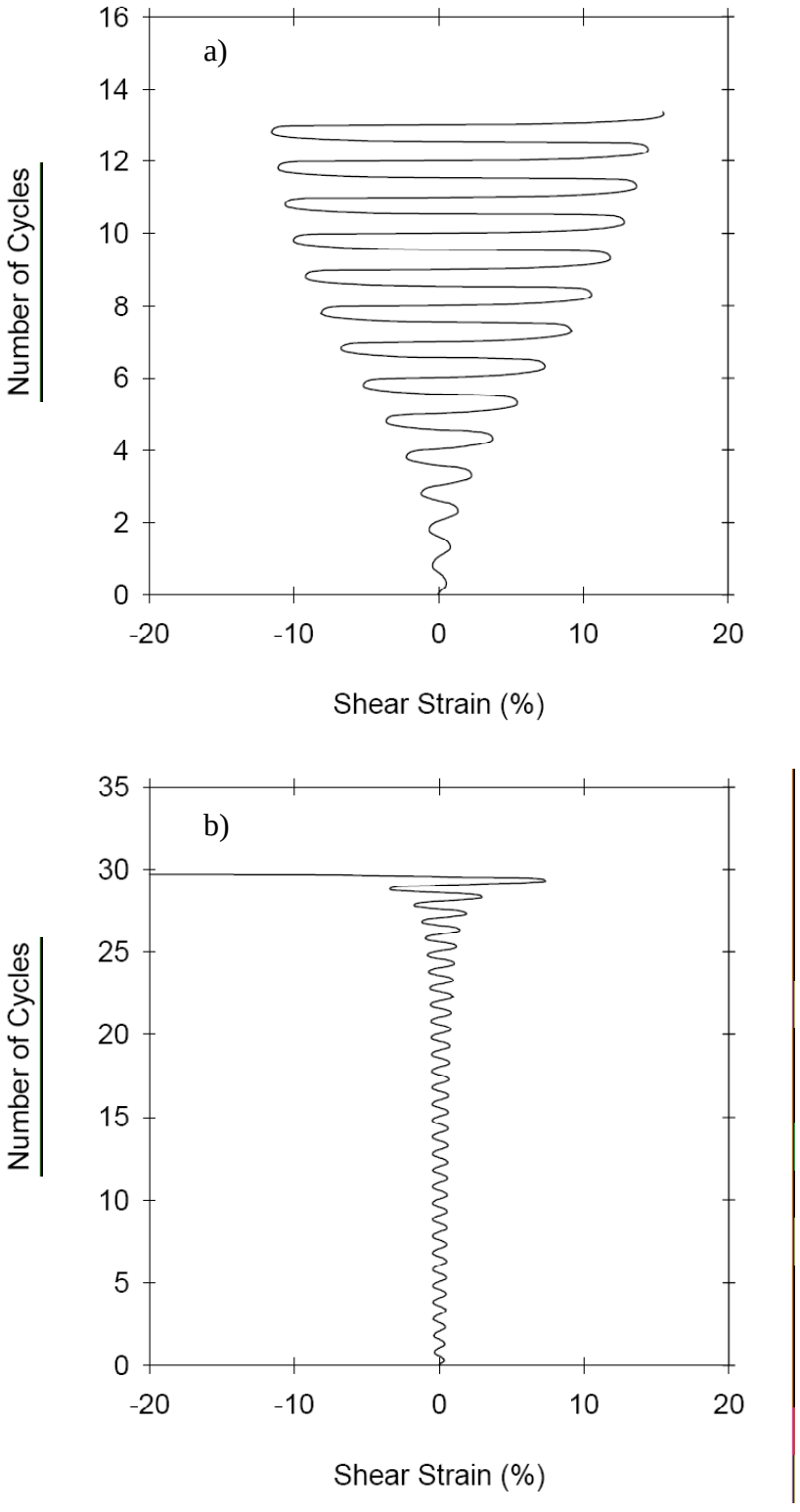

Figure 6.3 Cyclic Mobility: a) cyclic mobility with limited shear strain potential for SDM A6, b) cyclic mobility with large shear strain potential for Pluv A15

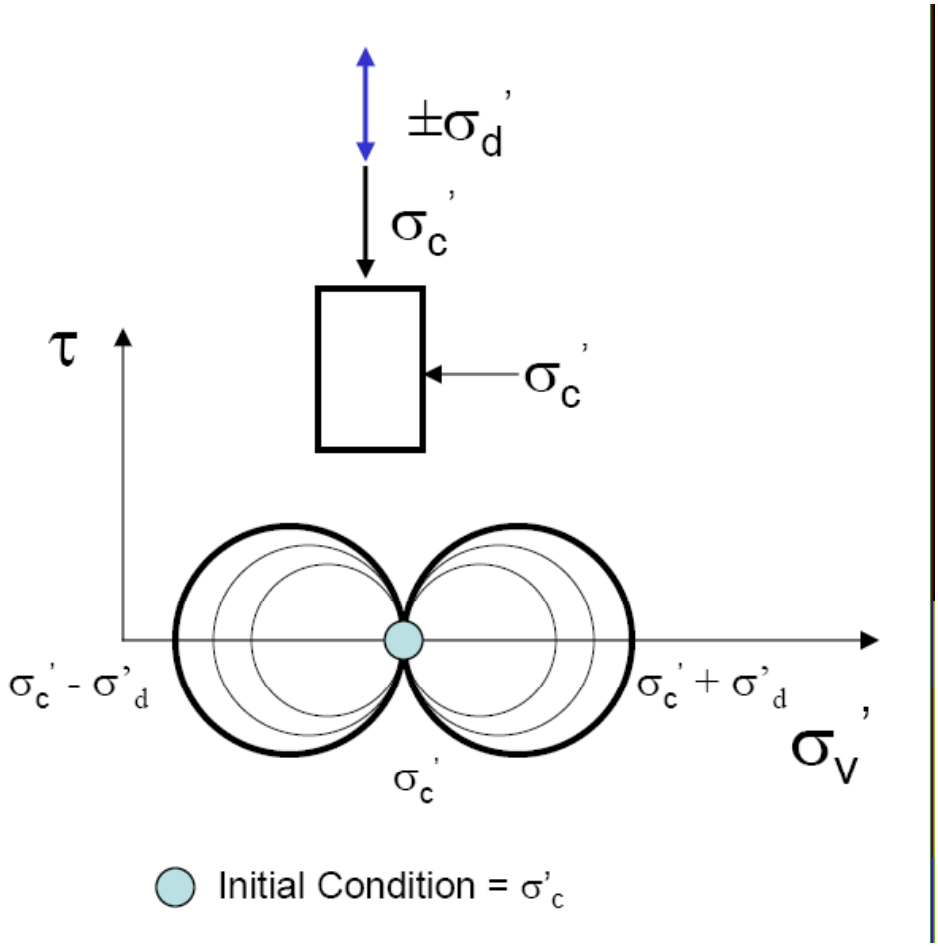

Figure 6.4 Stresses during isotropically consolidated cyclic triaxial testing.

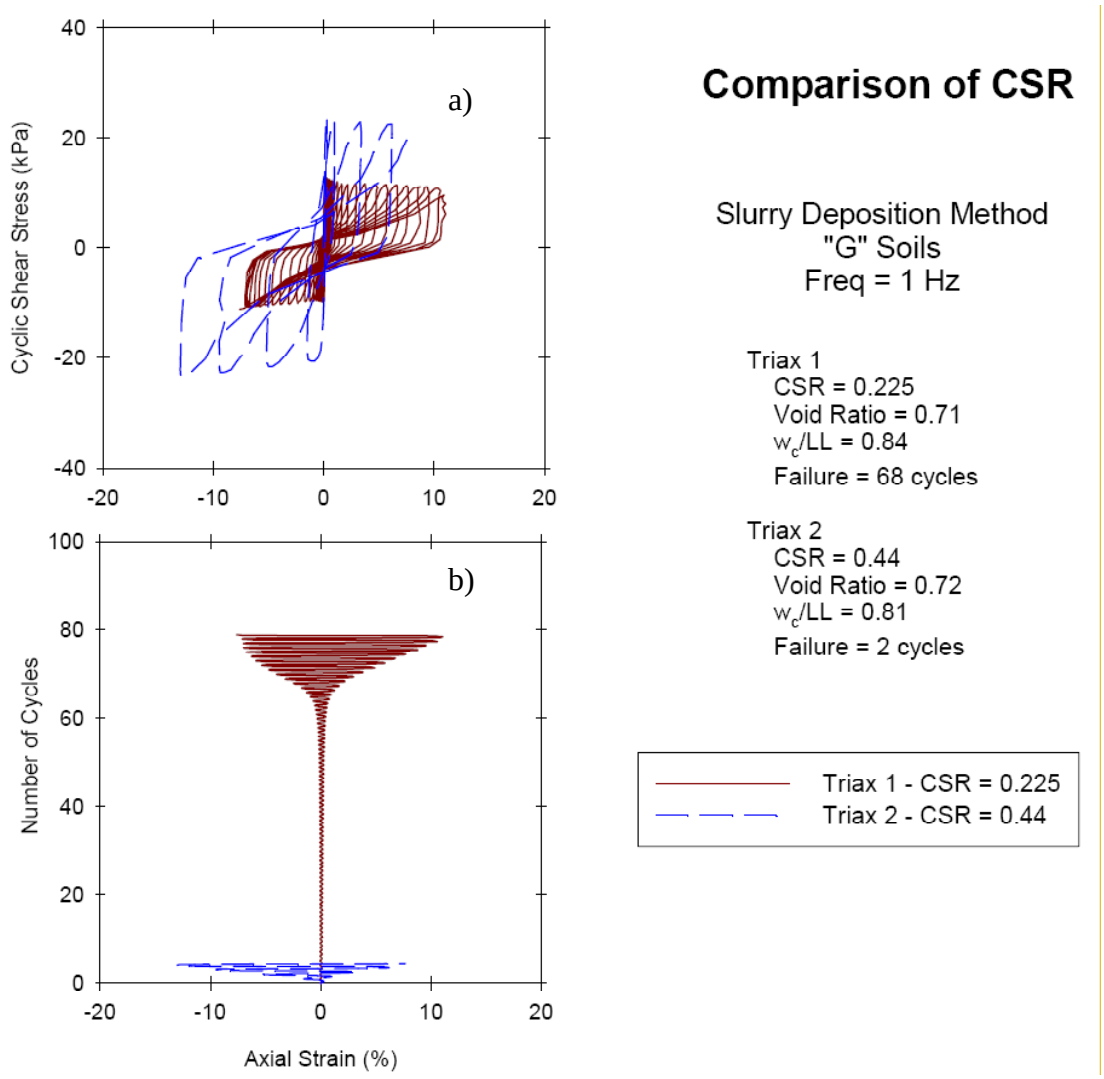

Figure 6.5 2-way plot for cyclic triaxial testing on Soil G using the Slurry Deposition Method, σ'_c = 50 kPa: a) stress – strain diagram, and b) number of cycles versus axial strain.

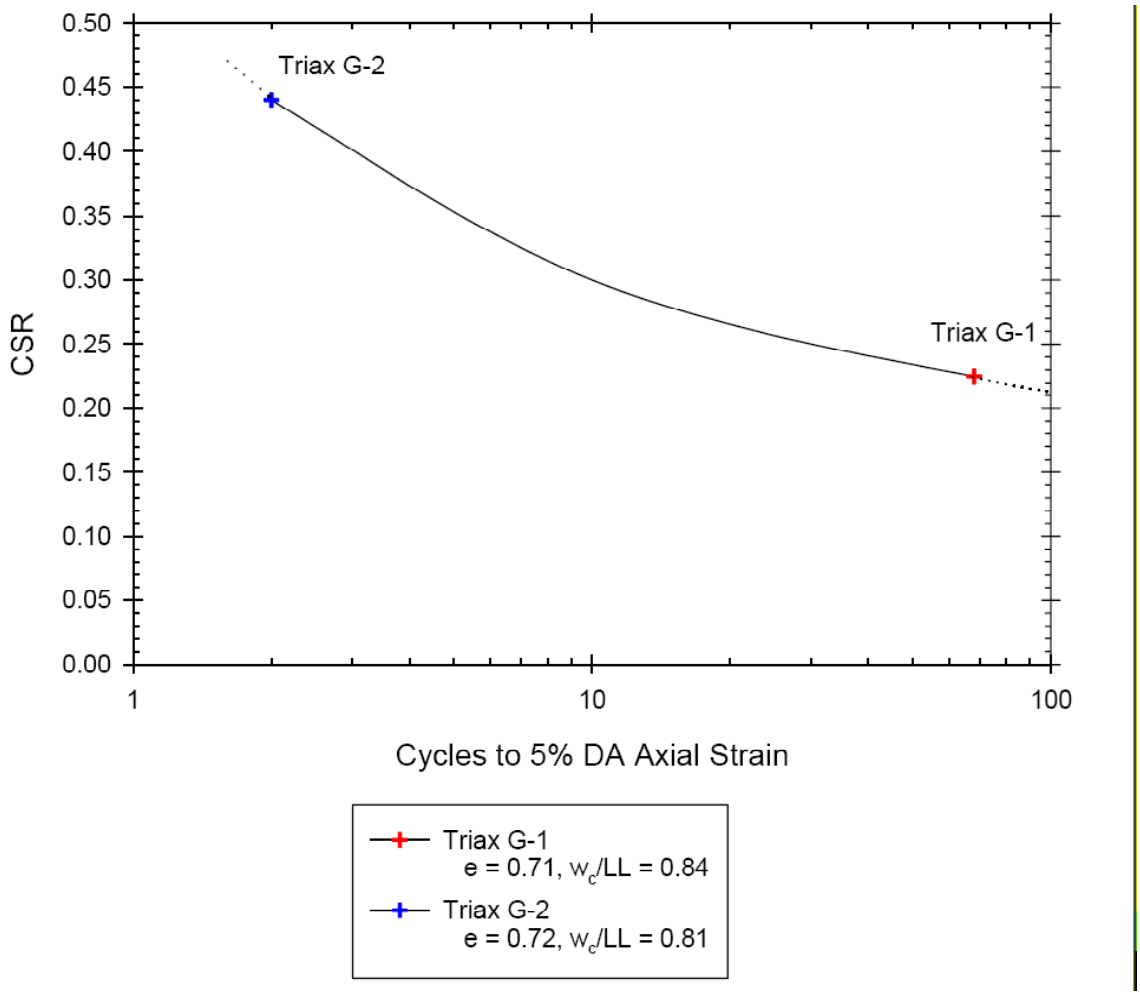

Figure 6.6 CSR Plot of cyclic triaxial testing on Soil G using the Slurry Deposition Method at 1 Hz and σ'_c = 50 kPa.

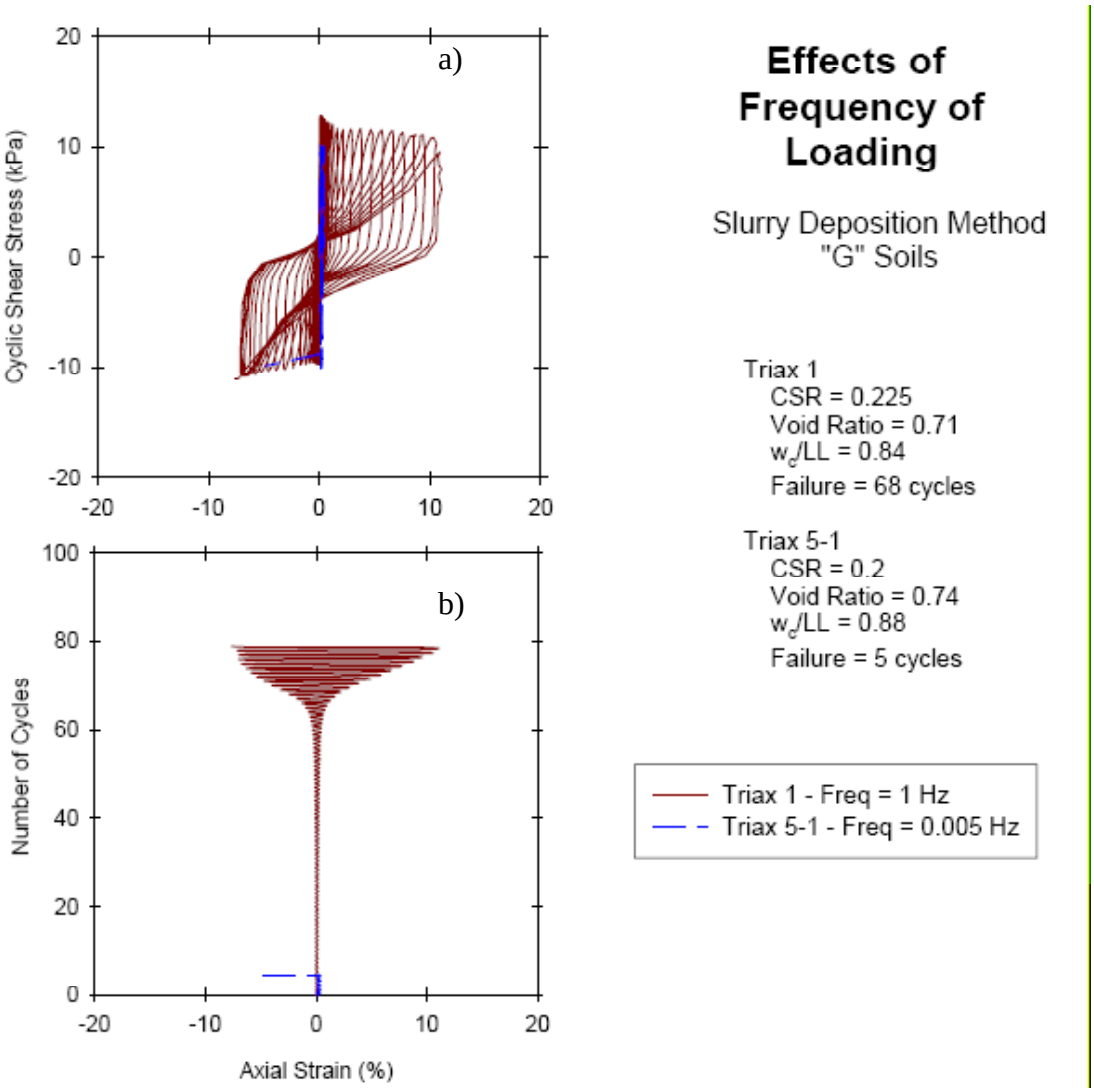

Figure 6.7 2-way plot for cyclic triaxial testing for the effects of frequency of loading for Soil G using the Slurry Deposition Method, σ'_c = 50 kPa: a) stress – strain diagram, and b) number of cycles versus axial strain.

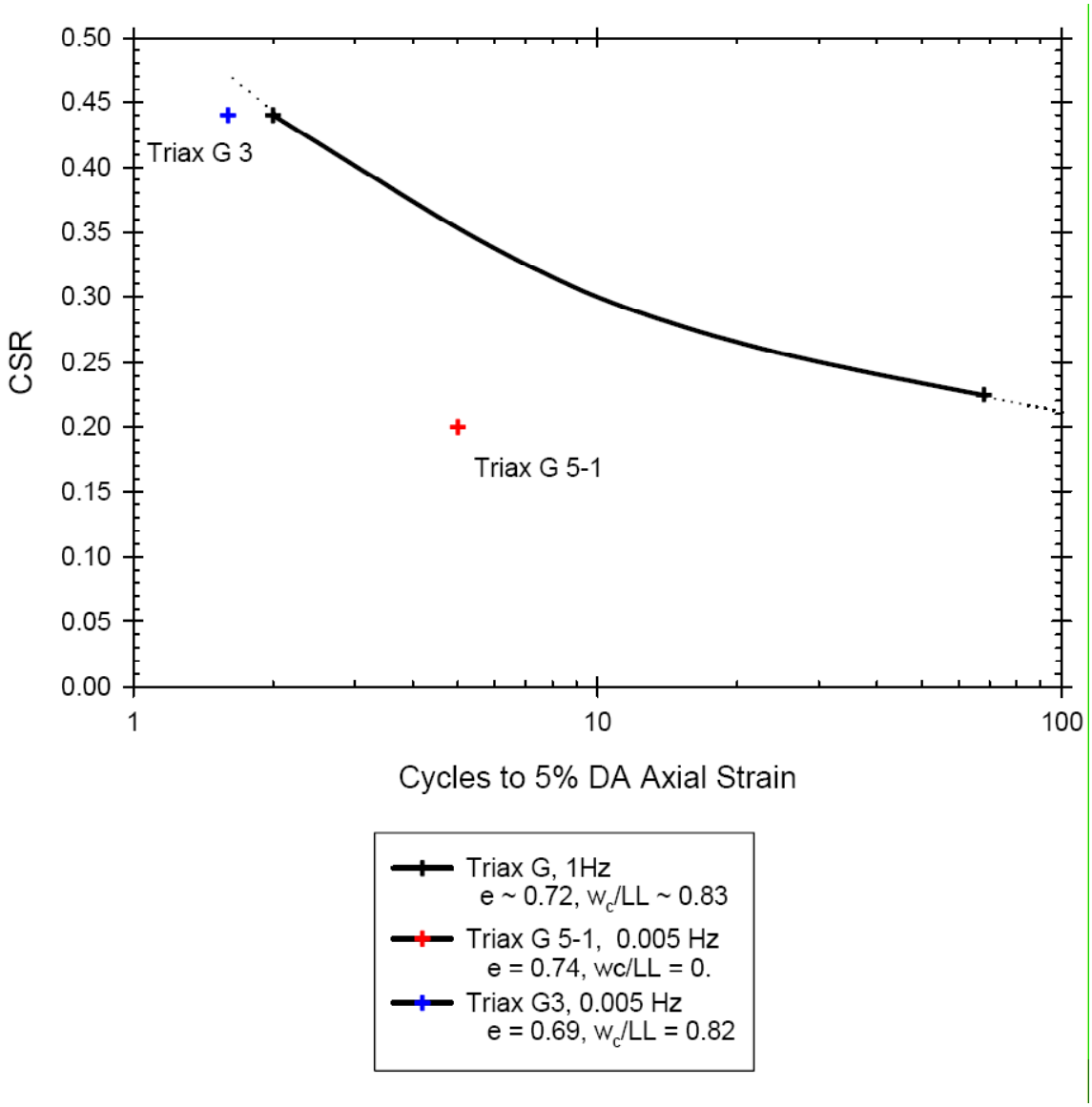

Figure 6.8 CSR Plot for cyclic triaxial testing for the effects of frequency of loading for Soil G using the Slurry Deposition Method. All tests at σ'_c = 50 kPa.

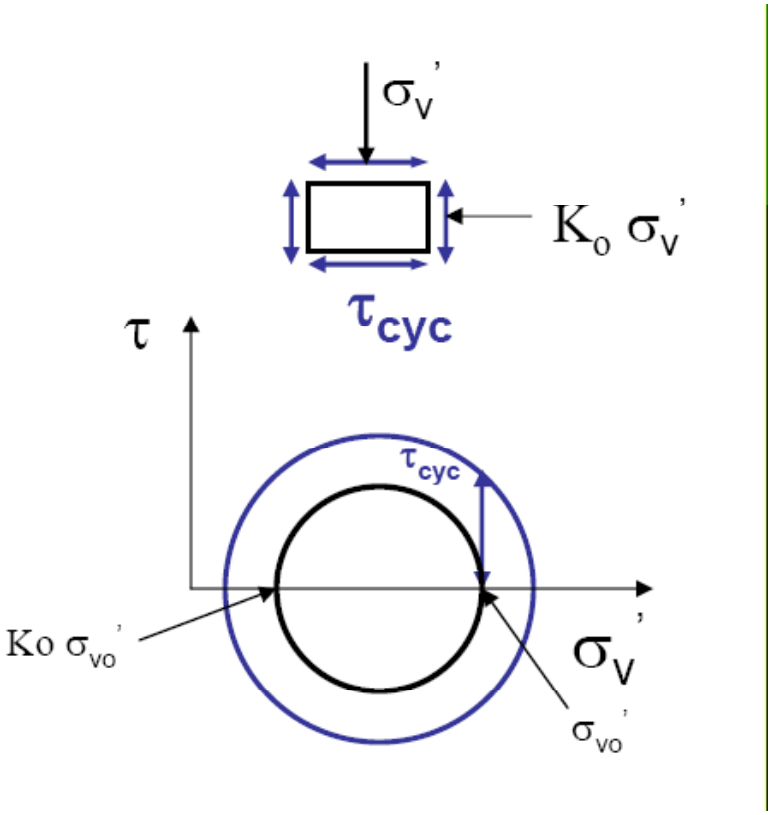

Figure 6.9 Stresses during anisotropically consolidated cyclic simple shear testing.

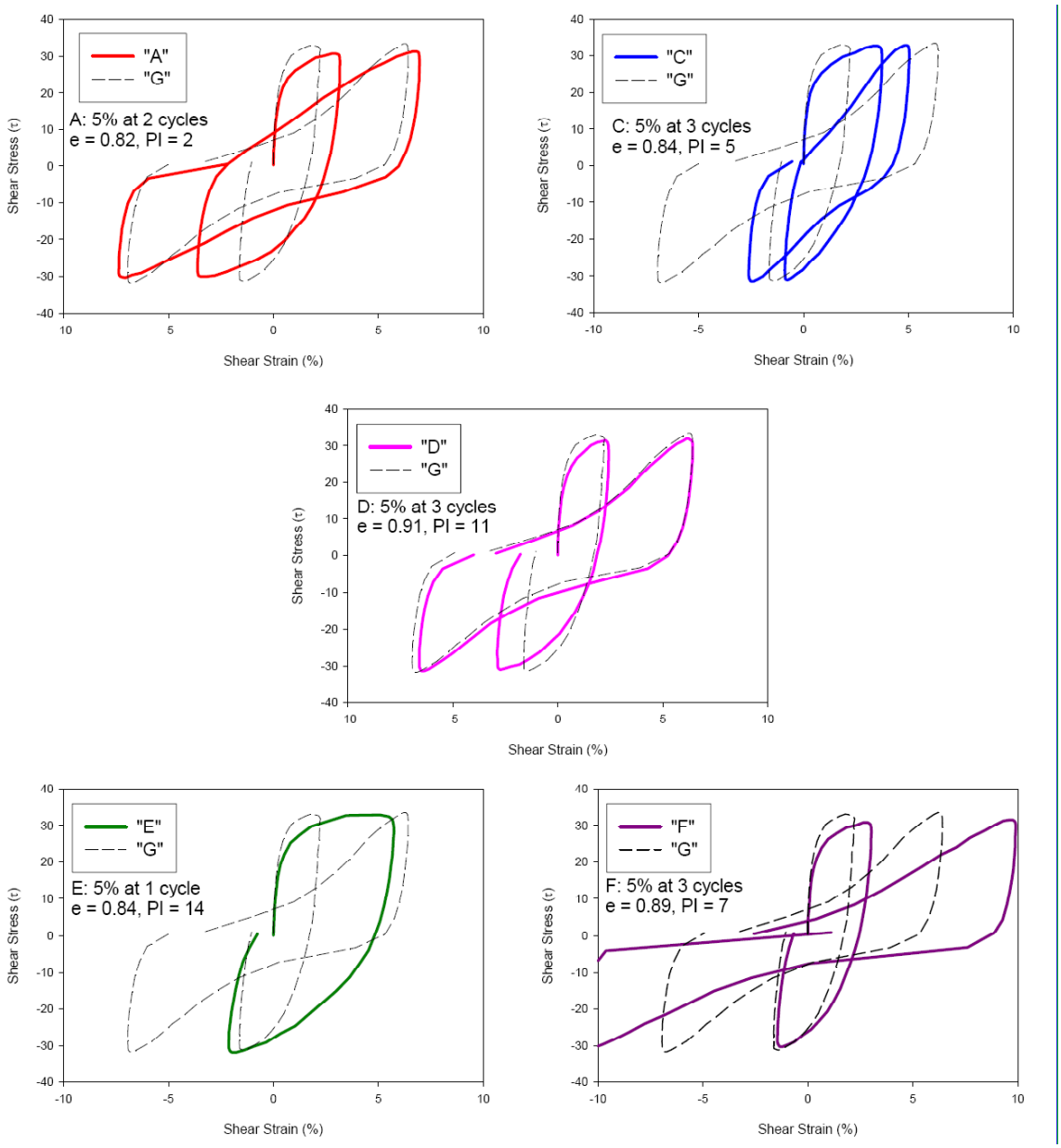

Figure 6.10 Cyclic Simple Shear Results for soils reconstituted using the Slurry Deposition Method. First Cycle and Cycle to reach 5% Shear Strain are compared to Soil G. Soil G reaches 5% Shear Strain at 7 cycles, e = 0.68, PI = 10, $\sigma'_v \approx 137$ kPa, CSR = 0.21.

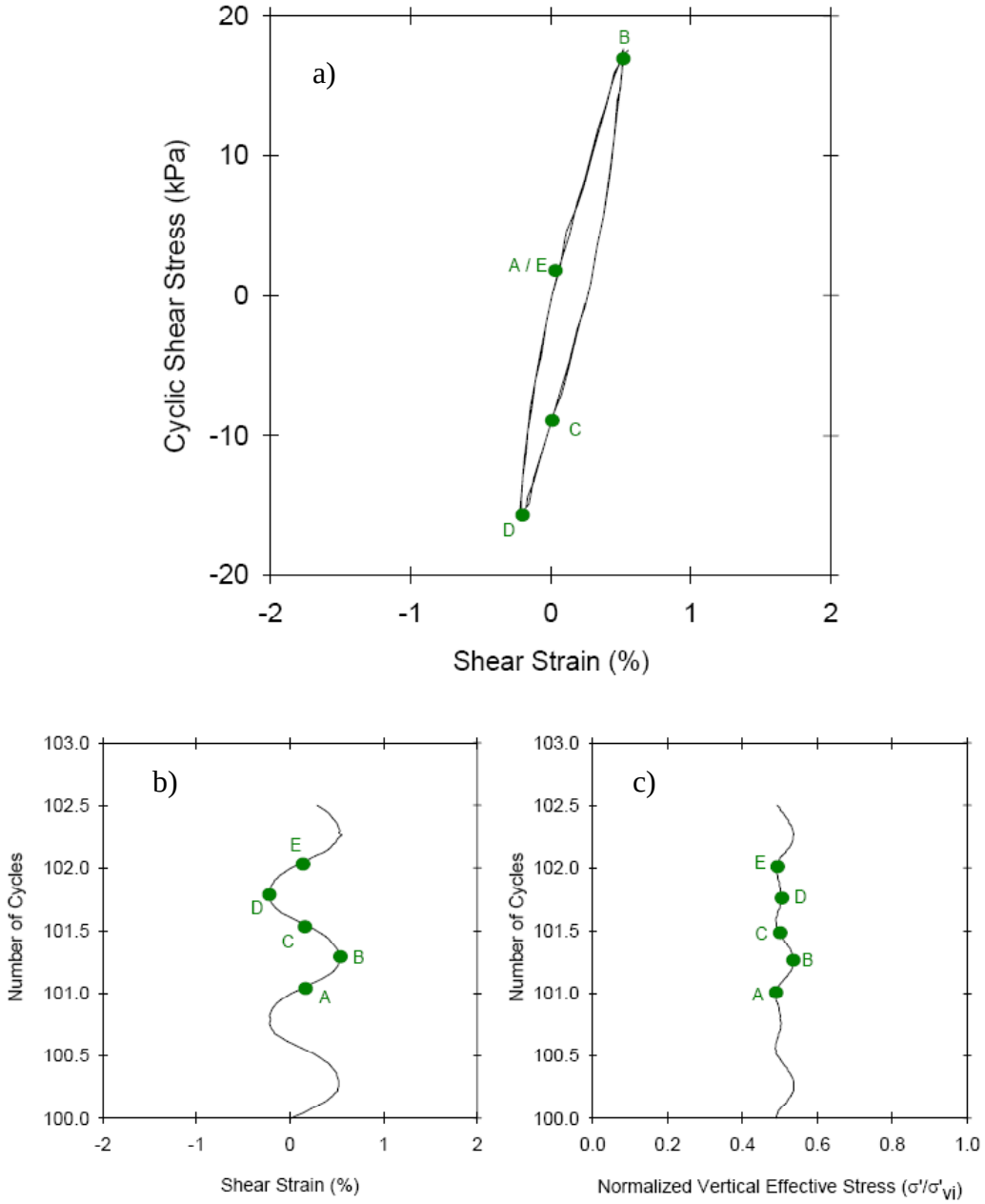

Figure 6.11 Stress-strain relationship of a typical "football shape" for Pluv F1 tested on the cyclic simple shear: a) stress-strain diagram, b) shear strain to number of cycles of loading, and c) normalized vertical effective stress to number of cycles.

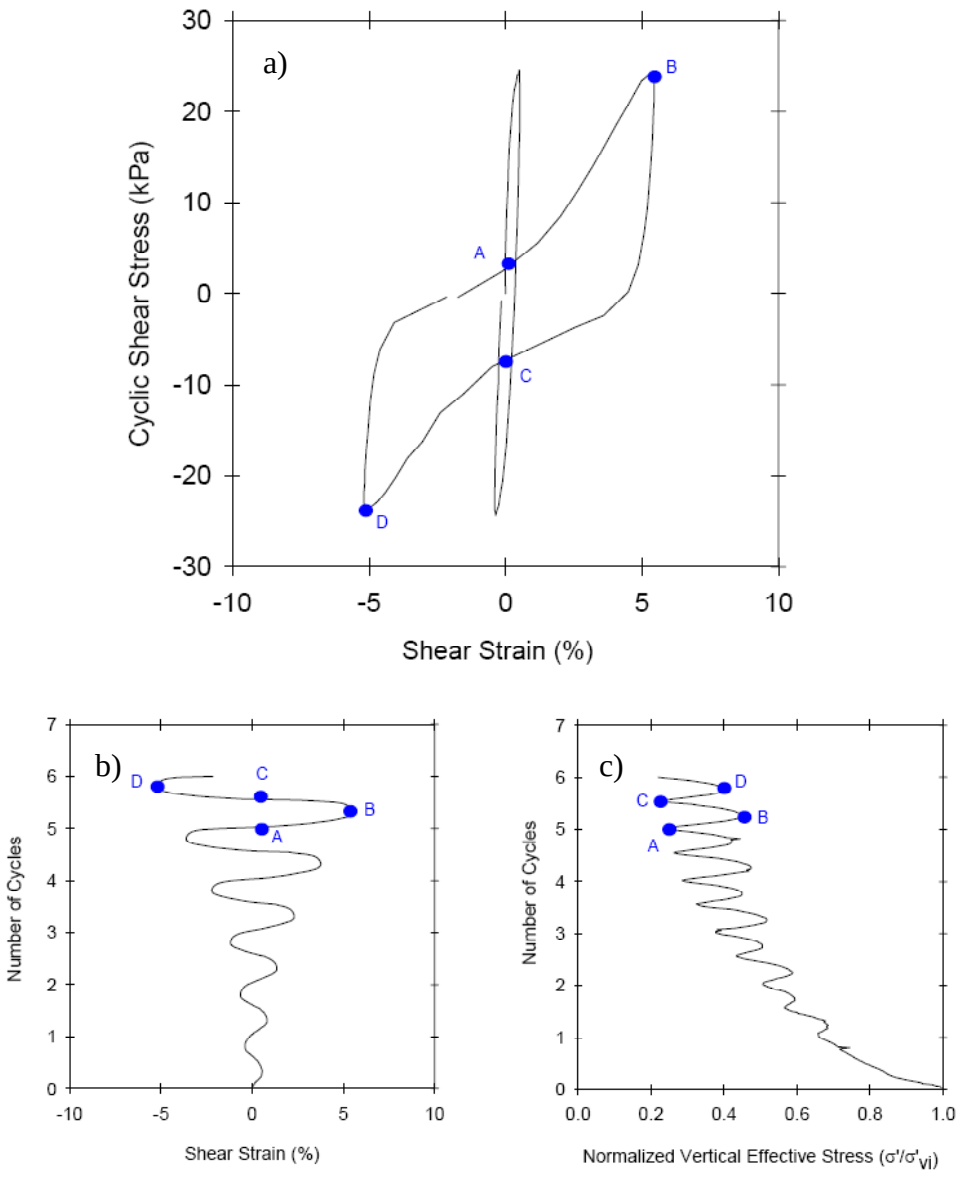

Figure 6.12 Stress-strain relationship of a typical "banana loop" for SDM A6 tested at $\sigma'_v \approx 137$ kPa, on the cyclic simple shear: a) stress-strain diagram, b) shear strain to number of cycles of loading, and c) normalized vertical effective stress to number of cycles.

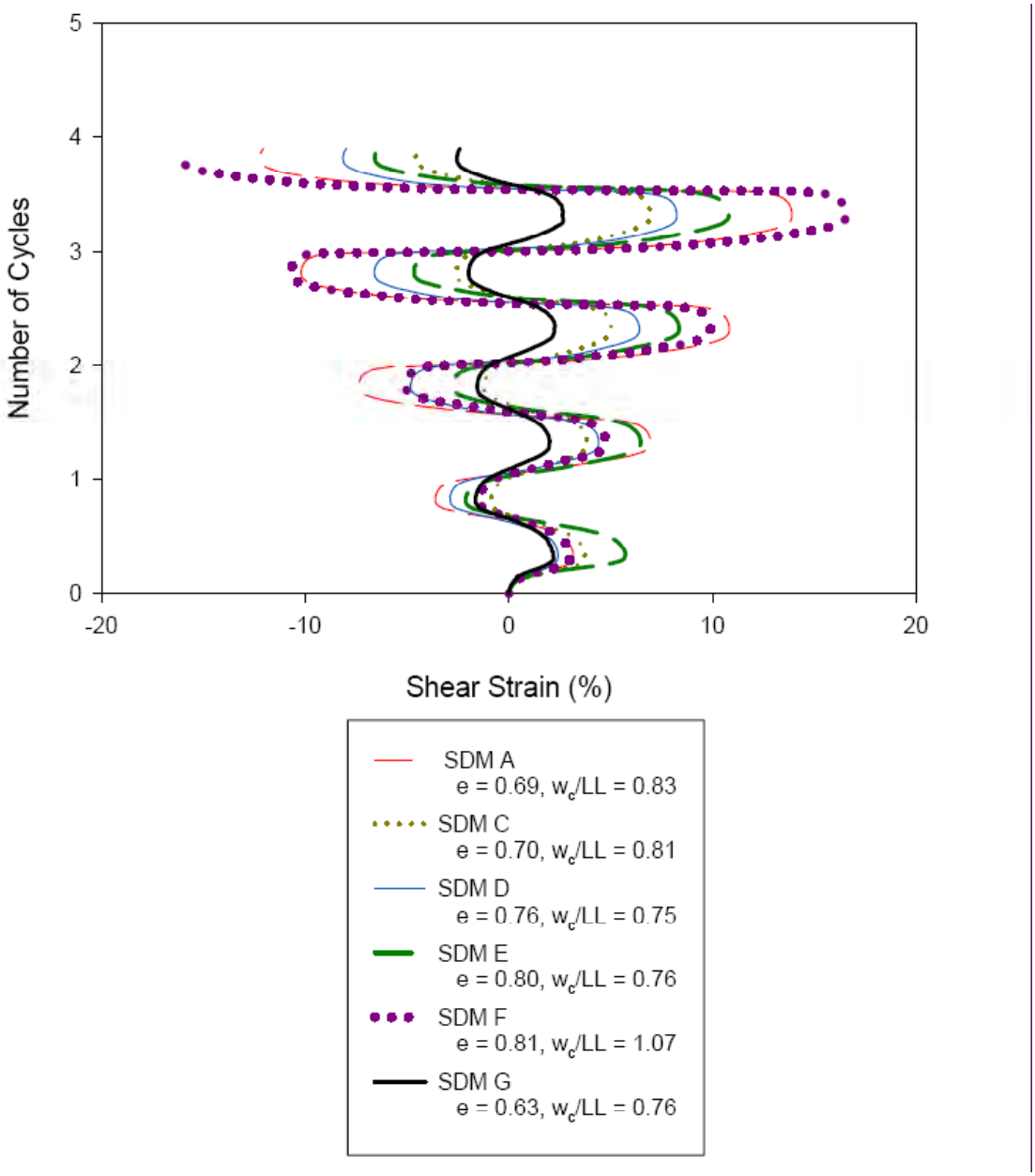

Figure 6.13 Cyclic Simple Shear Results. Shear Strain for Soils A through G reconstituted by the Slurry Deposition Method. $\sigma'_v \approx 137$ kPa, CSR = 0.21.

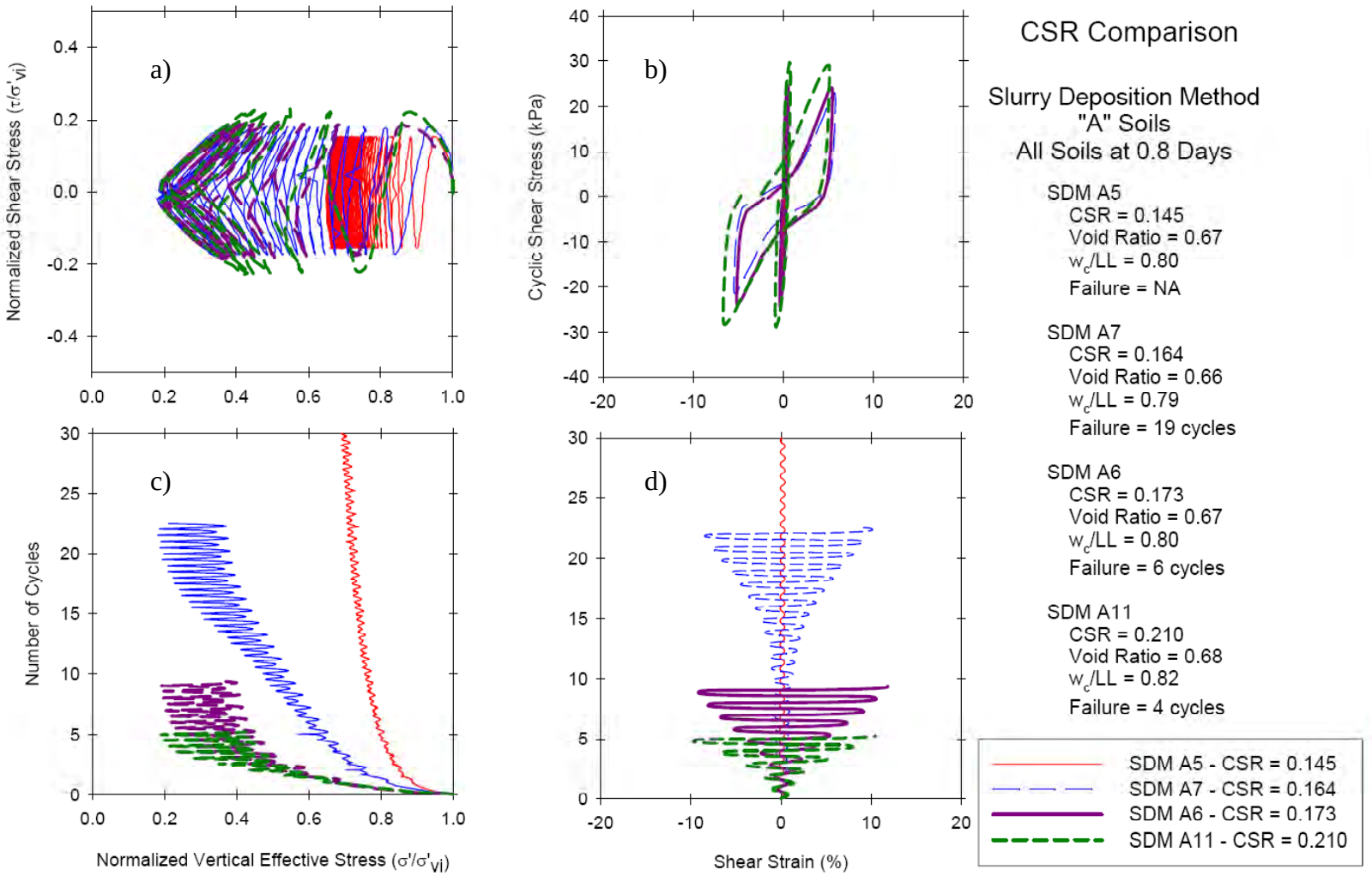

Figure 6.14 4-way Plot, comparison of CSR for Soil A prepared using the Slurry Deposition Method tested by the cyclic simple shear, $\sigma'_v \approx 137$ kPa: a) effective stress path, b) stress-strain diagram, c) normalized vertical effective stress to number of cycles, and d) shear strain to number of cycles of loading.

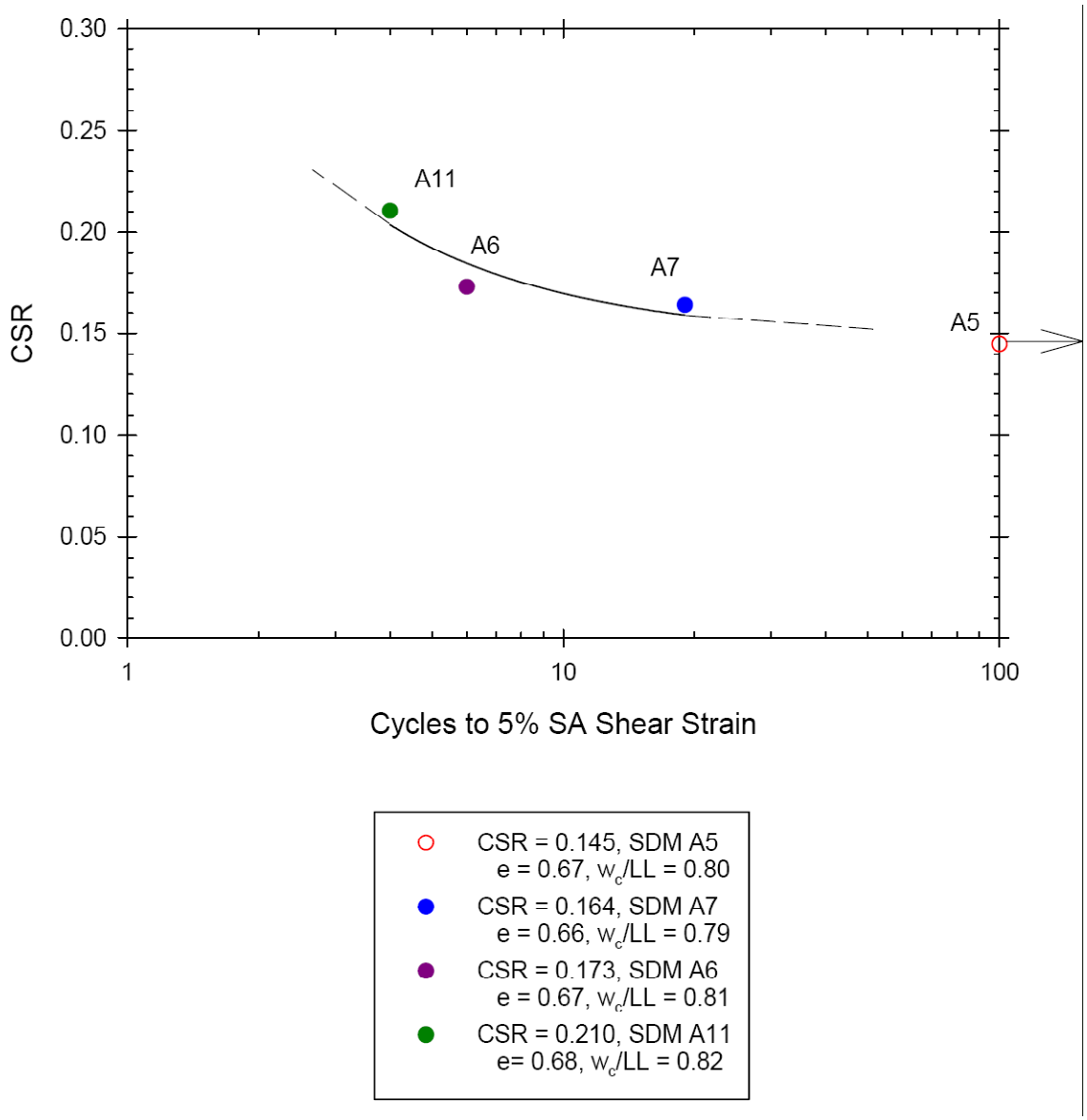

Figure 6.15 CSR Chart of Soil A prepared using the Slurry Deposition Method tested by the cyclic simple shear, all tests at $\sigma'_v \approx 137$ kPa.

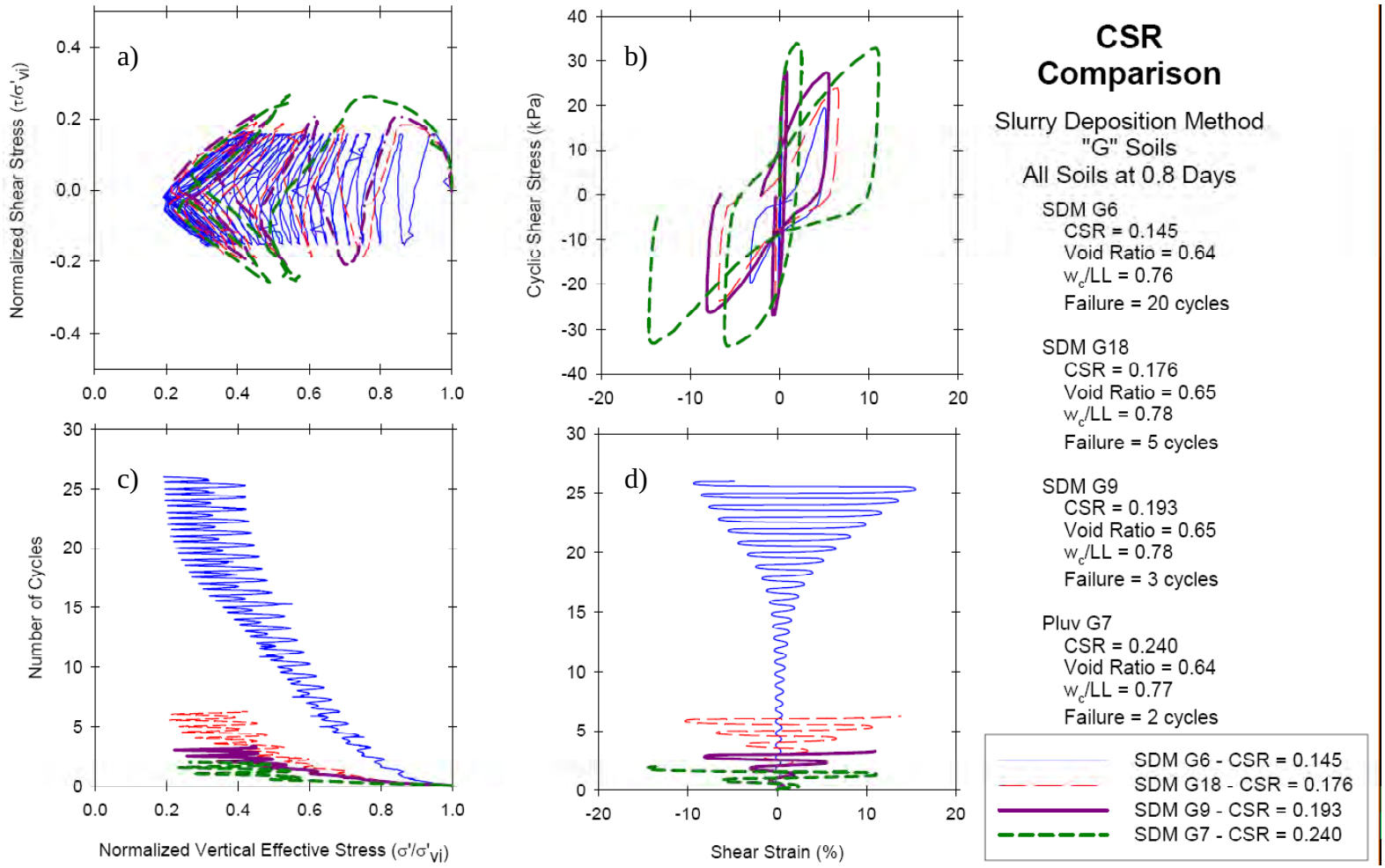

Figure 6.16 4-way plot comparison of CSR for Soil G prepared using the Slurry Deposition Method tested by the cyclic simple shear, $\sigma'_v \approx 137$ kPa: a) effective stress path, b) stress-strain diagram, c) normalized vertical effective stress to number of cycles, and d) shear strain to number of cycles of loading.

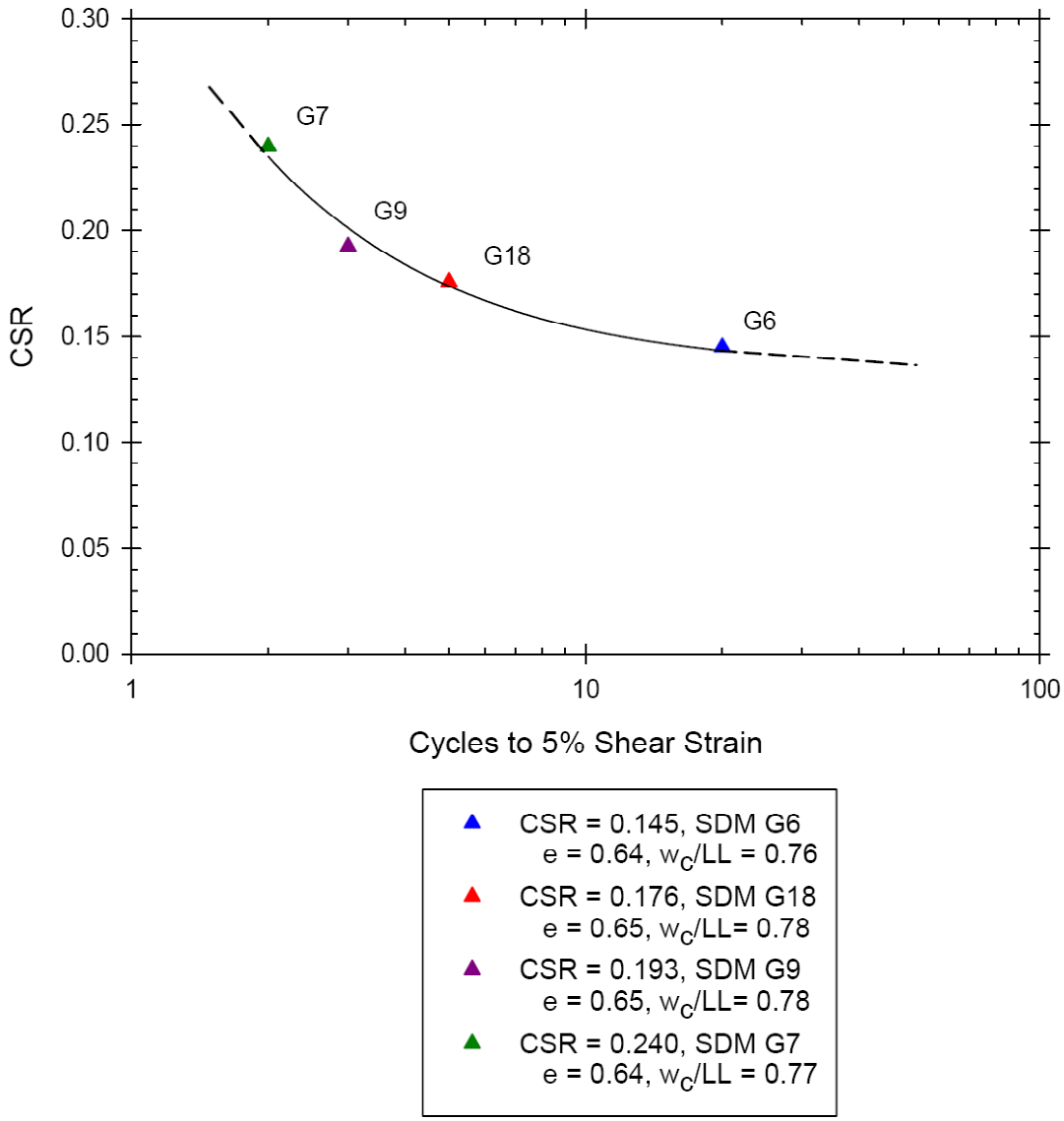

Figure 6.17 CSR Chart of Soil G prepared using the Slurry Deposition Method tested by the cyclic simple shear, all tests at $\sigma'_v \approx 137$ kPa.

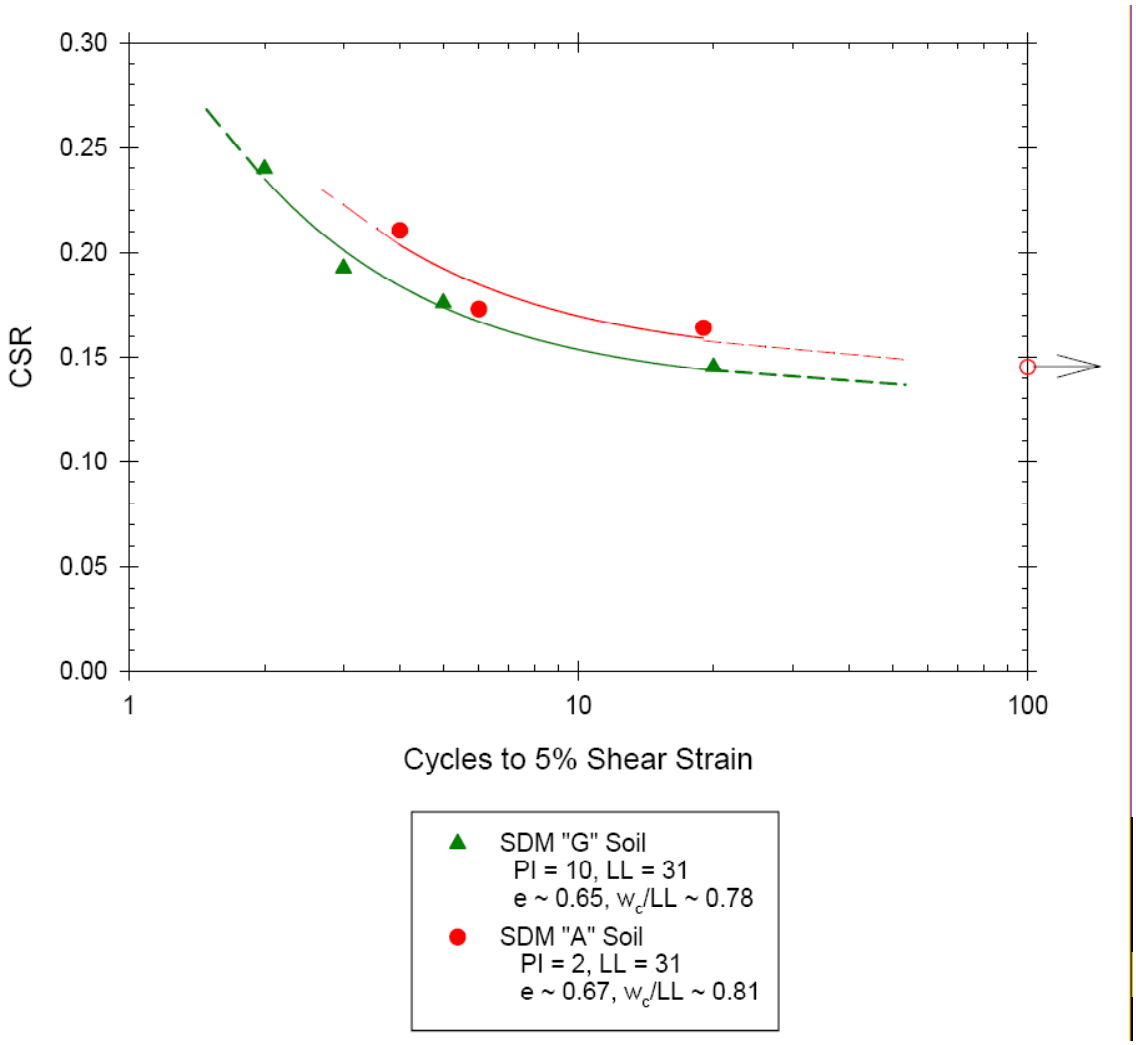

Figure 6.18 CSR Chart comparing Soil A and Soil G prepared using the Slurry Deposition Method tested by the cyclic simple shear, all tests at $\sigma'_v \approx 137$ kPa.

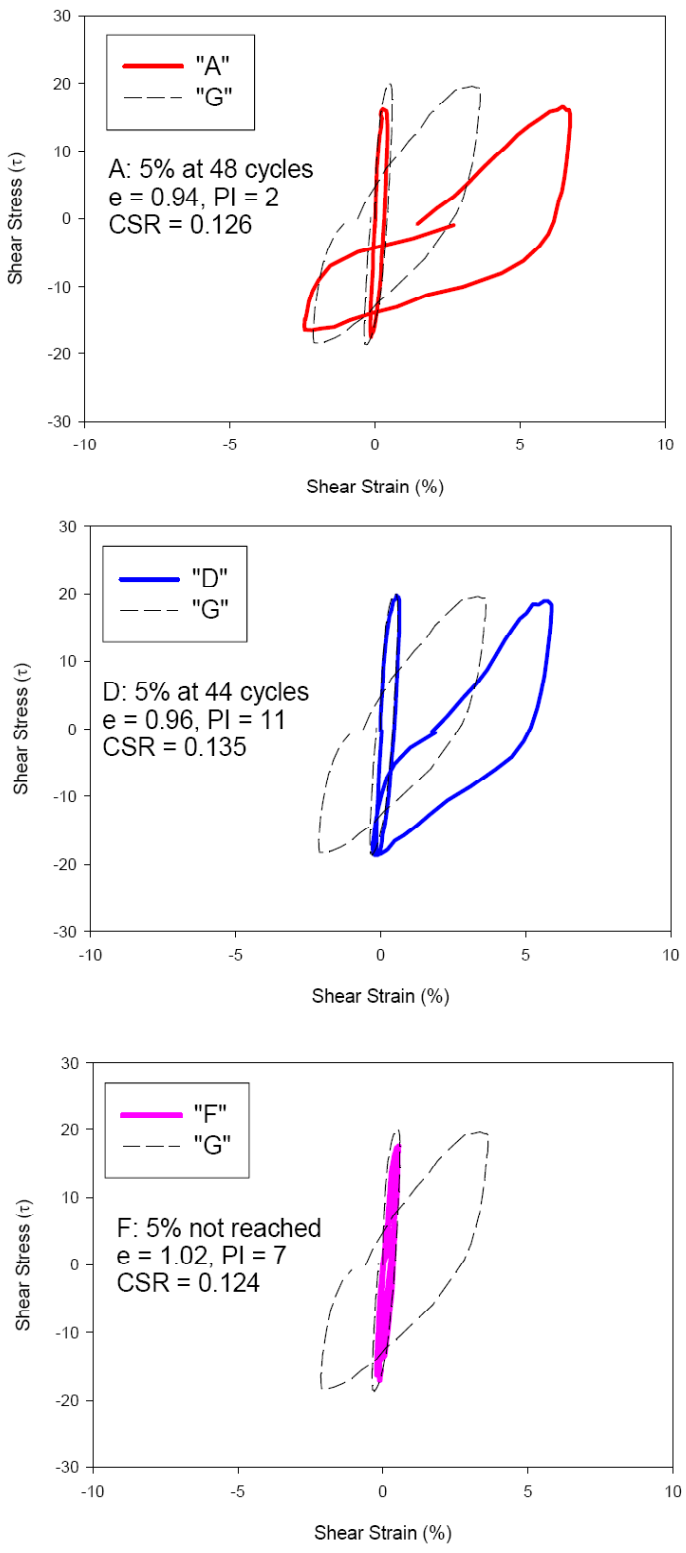

Figure 6.19 Cyclic Simple Shear Results for Soil A, D, F, and G reconstituted using the In-Place Wet Pluviated Method. First cycle and cycle to reach 5% shear strain are compared to Soil G. Soil G: e = 0.81, PI = 10, CSR = 0.142, and $\sigma'_v \approx 137$ kPa.

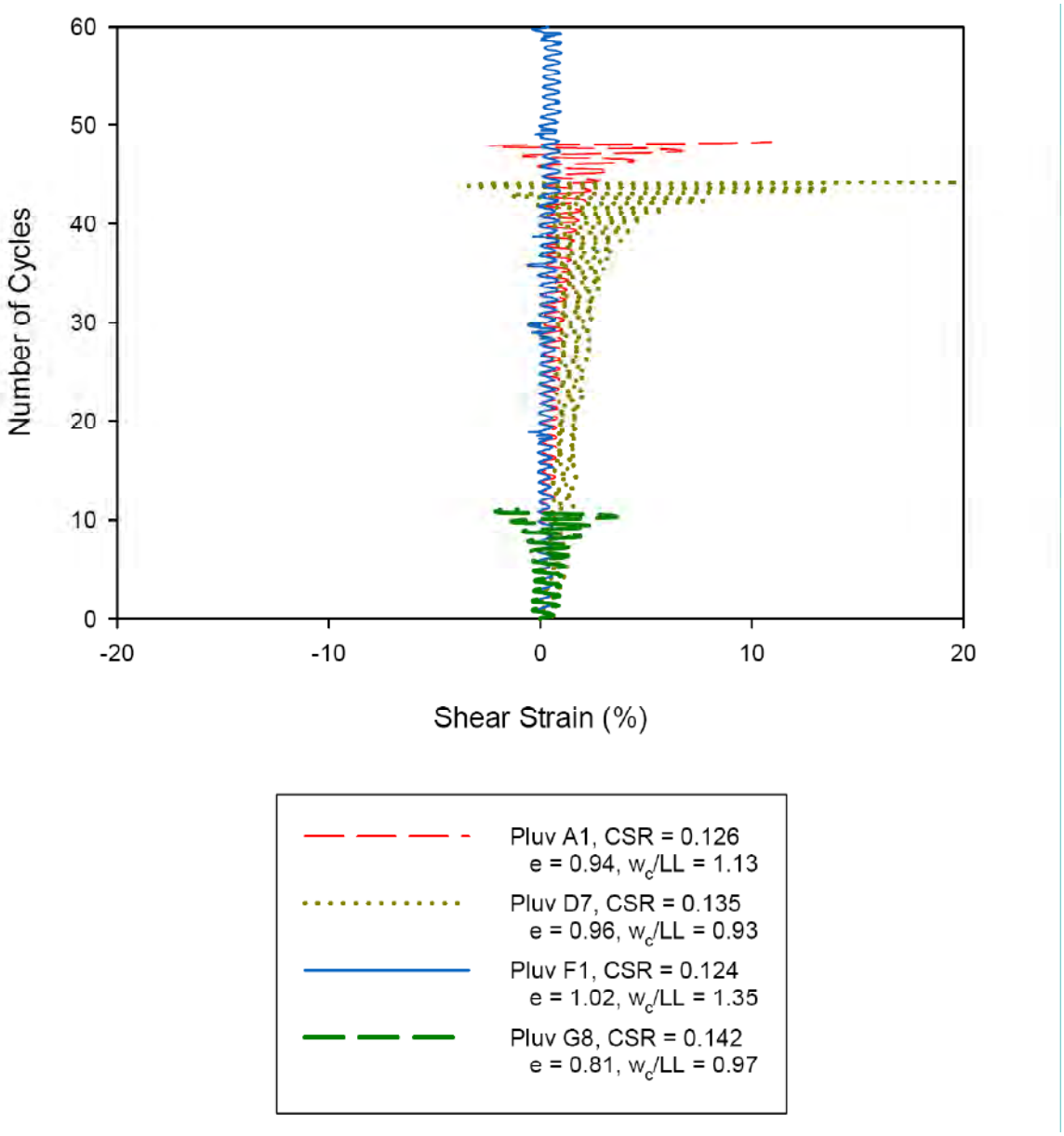

Figure 6.20 Cyclic Simple Shear Results Shear Strain for Soils A through G reconstituted by the In-Place Wet Pluviated Method. All soils tested at $\sigma'_v \approx 137$ kPa.

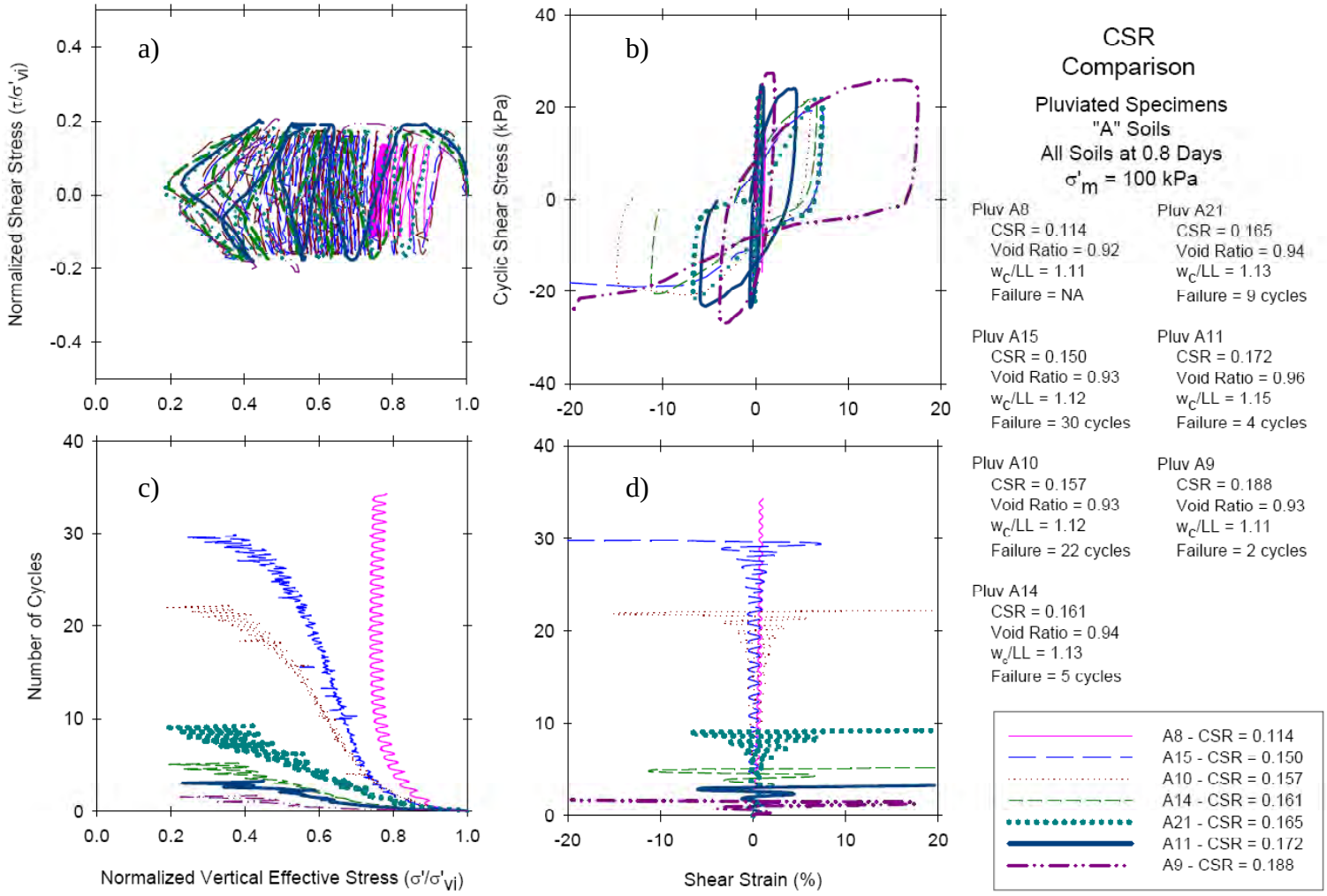

Figure 6.21 4-way plot comparison of CSR for Soil A prepared using In-Place Wet Pluviation tested by the cyclic simple shear: a) effective stress path, b) stress-strain diagram, c) normalized vertical effective stress to number of cycles, and d) shear strain to number of cycles of loading.

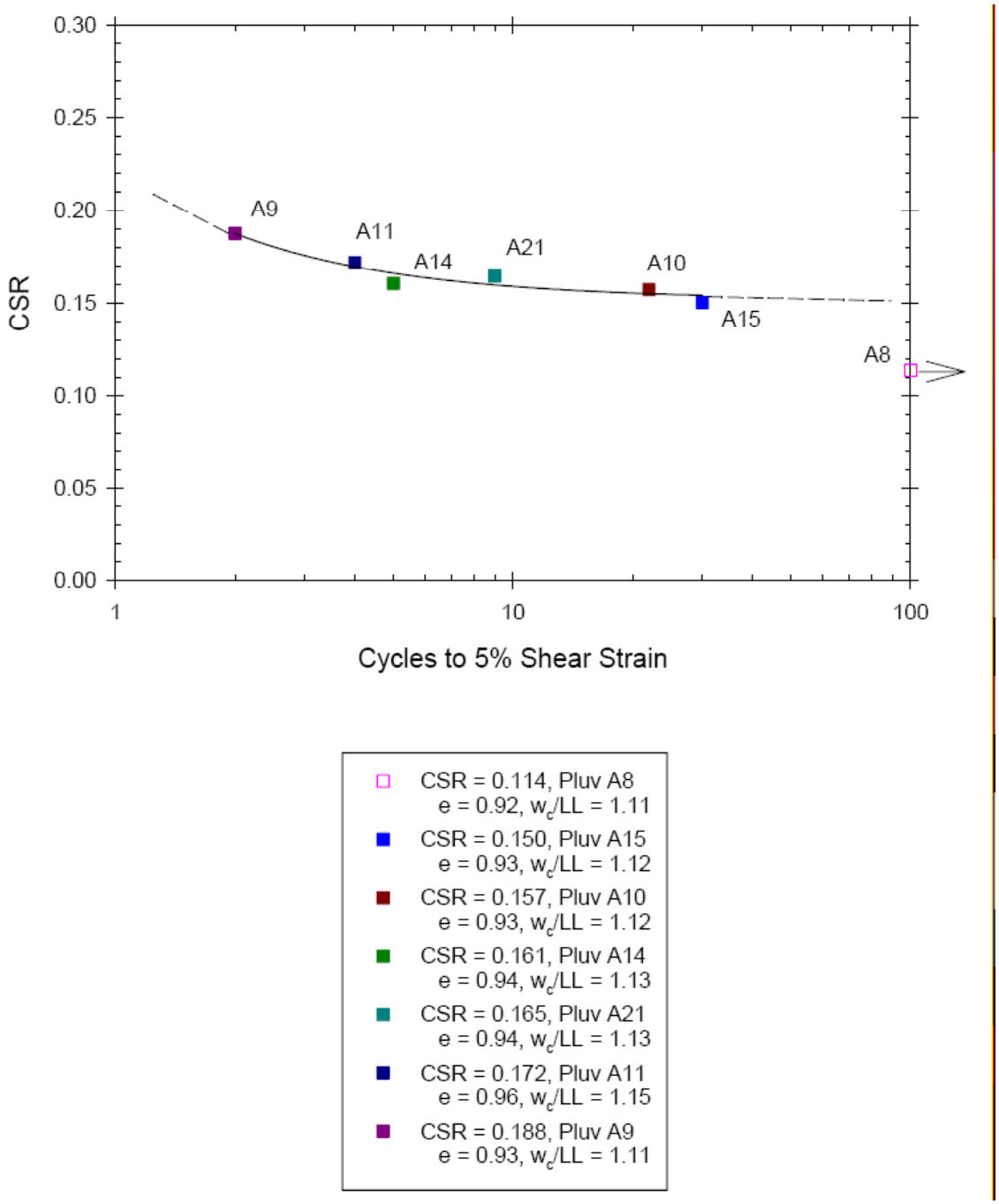

Figure 6.22 CSR Chart of Soil A prepared using In-Place Wet Pluviation tested by the cyclic simple shear, all tests at $\sigma'_v \approx 137$ kPa.

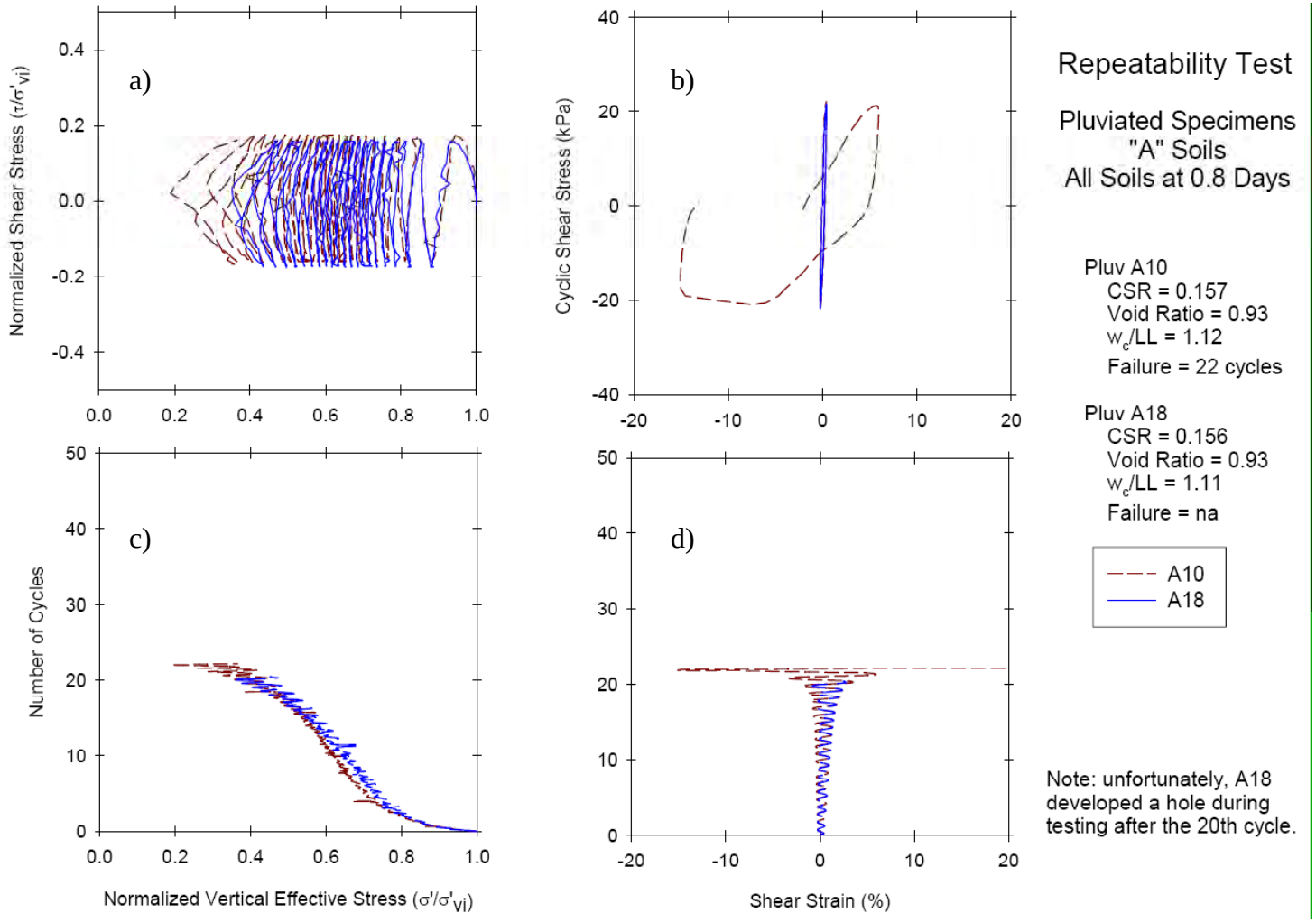

Figure 6.23 4-way plot comparison of Repeatability Test on Soil A prepared using In-Place Wet Pluviation tested by the cyclic simple shear, $\sigma'_v \approx 137$ kPa: a) effective stress path, b) stress-strain diagram, c) normalized vertical effective stress to number of cycles, and d) shear strain to number of cycles of loading.

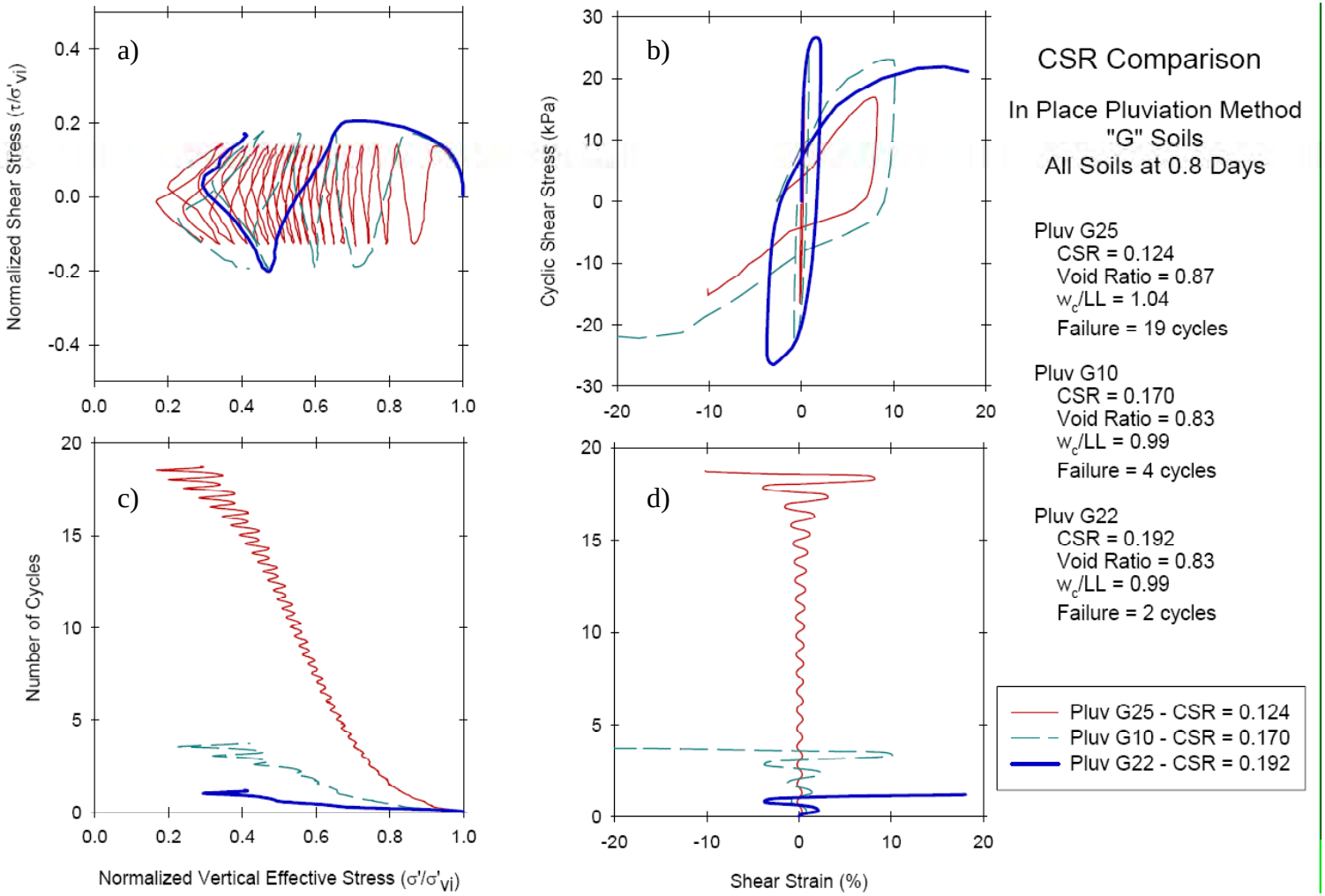

Figure 6.24 4-way plot comparison of CSR for Soil "G-Loose" prepared using In-Place Wet Pluviation tested by the cyclic simple shear, $\sigma'_v \approx 137$ kPa: a) effective stress path, b) stress-strain diagram, c) normalized vertical effective stress to number of cycles, and d) shear strain to number of cycles of loading.

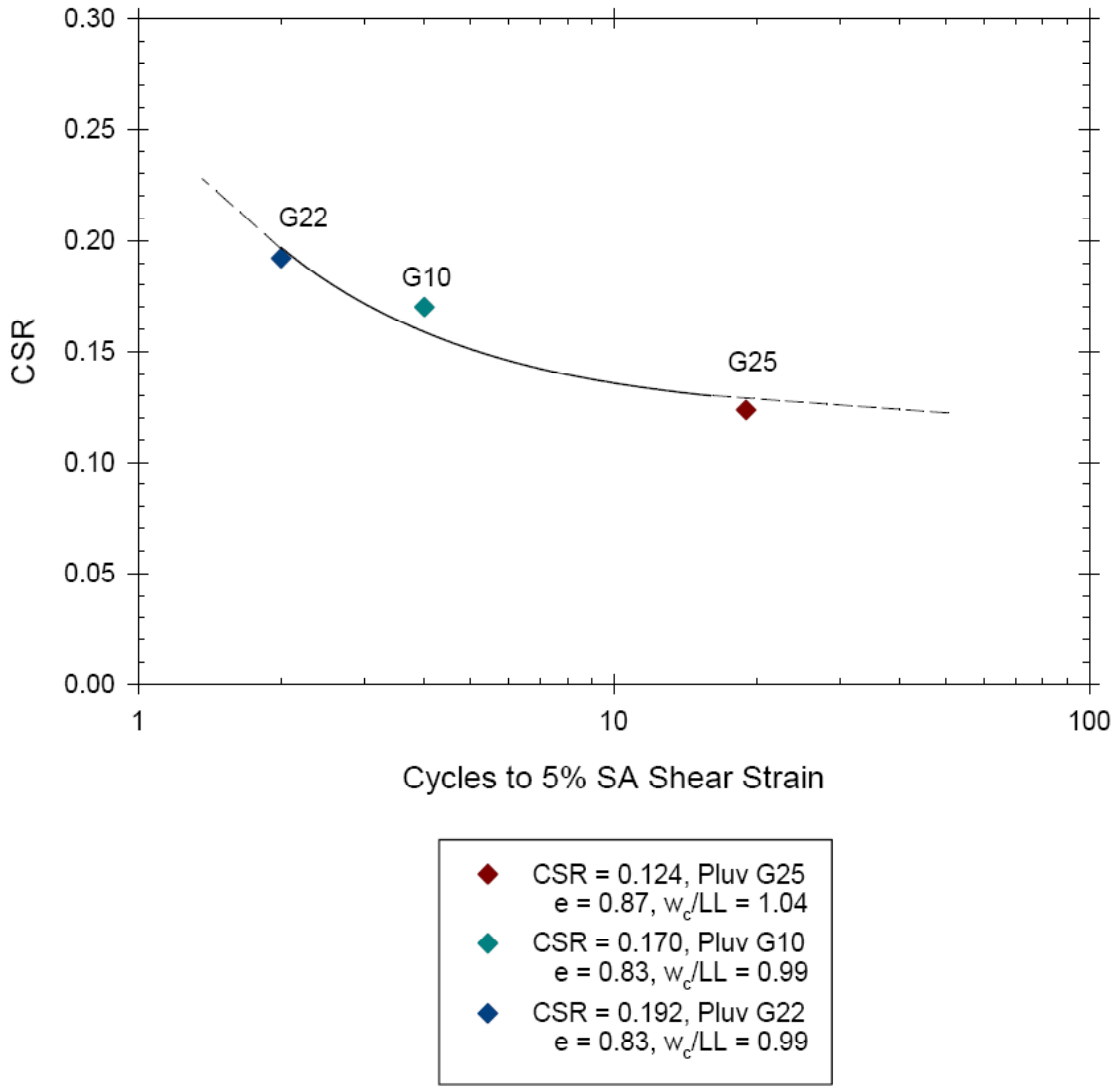

Figure 6.25 CSR Chart of Soil "G-Loose" prepared using In-Place Wet Pluviation tested by the cyclic simple shear, all tests at $\sigma'_v \approx 137$ kPa.

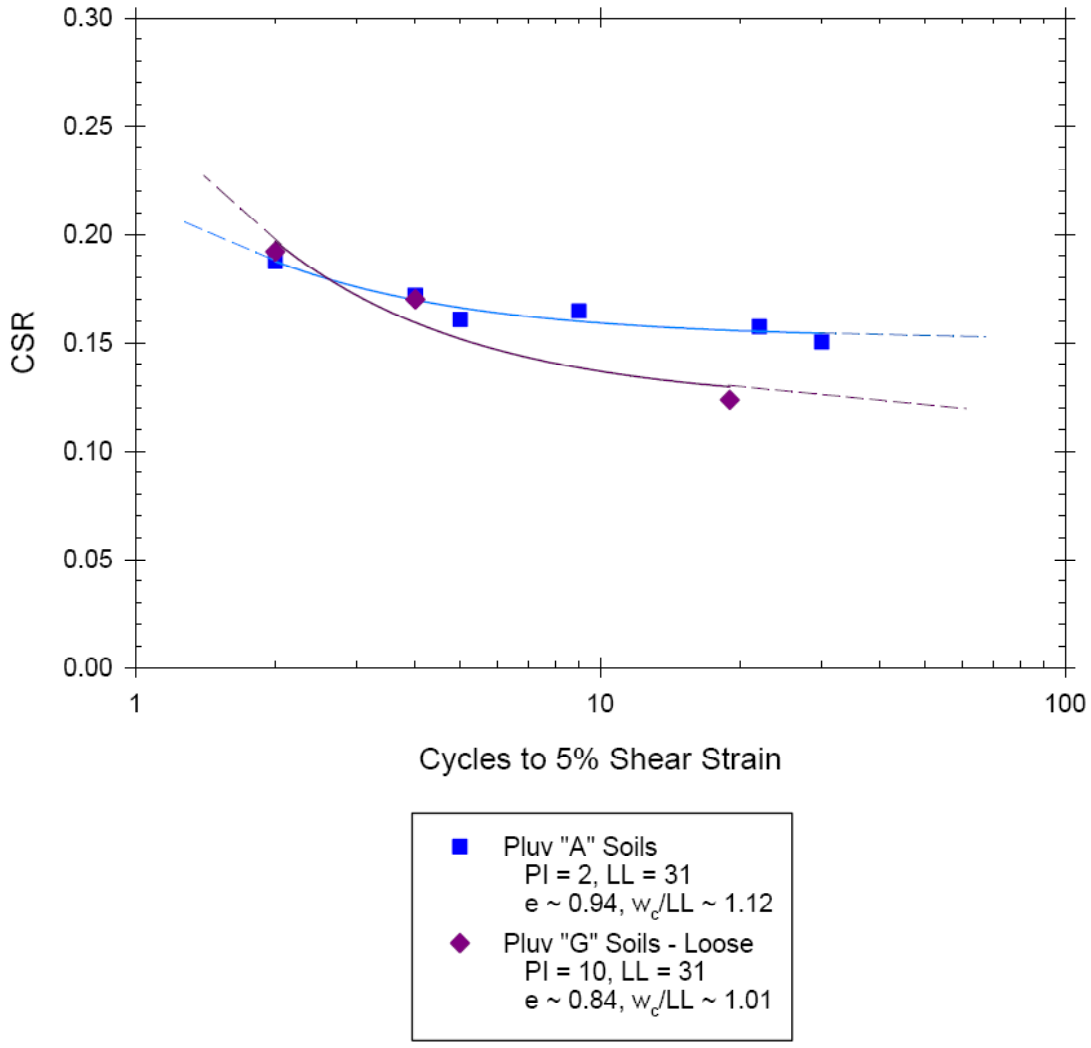

Figure 6.26 CSR Chart comparing Soil A and Soil G prepared using In-Place Wet Pluviation tested by the cyclic simple shear, all tests at $\sigma'_v \approx 137$ kPa.

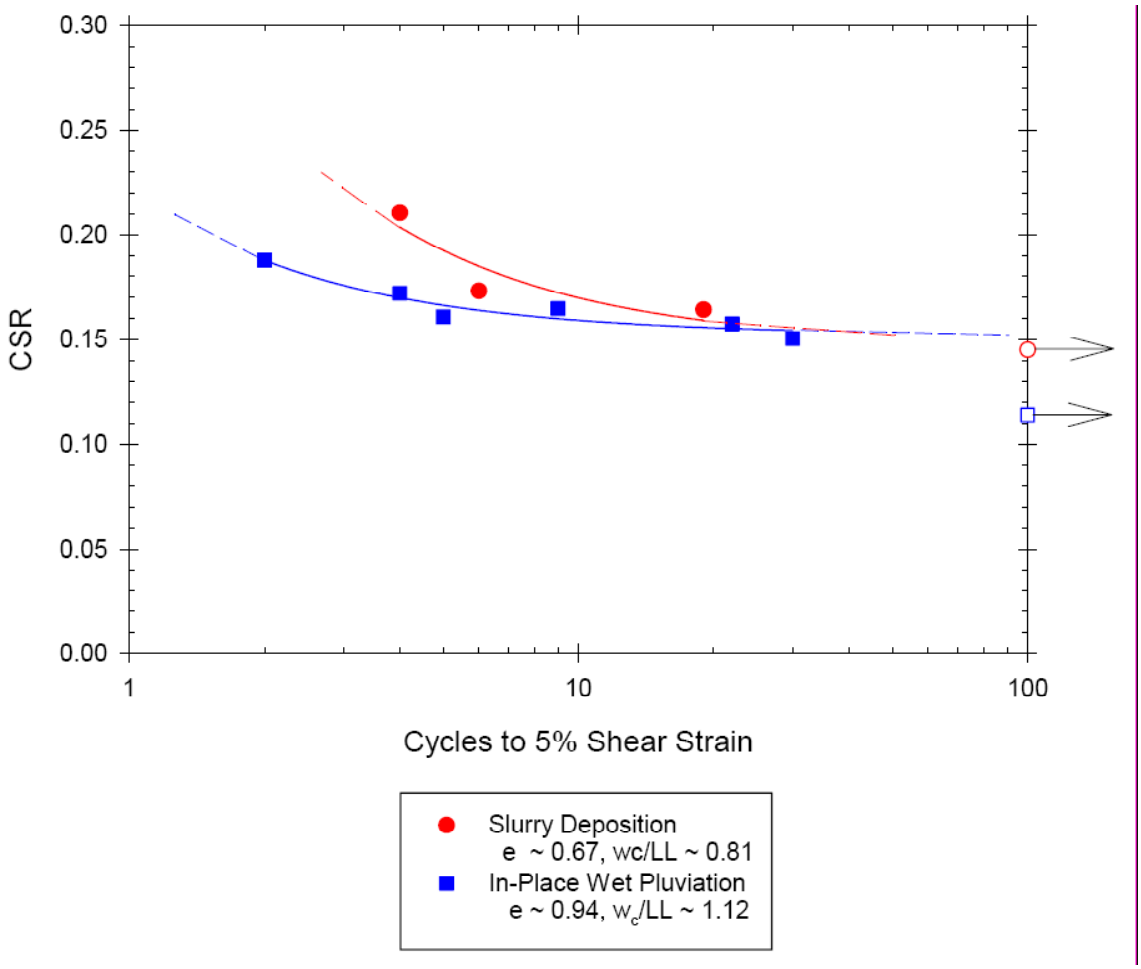

Figure 6.27 CSR Chart comparing Soil A prepared using the Slurry Deposition Method and In-Place Wet Pluviation tested by the cyclic simple shear, all tests at $\sigma'_v \approx 137$ kPa.

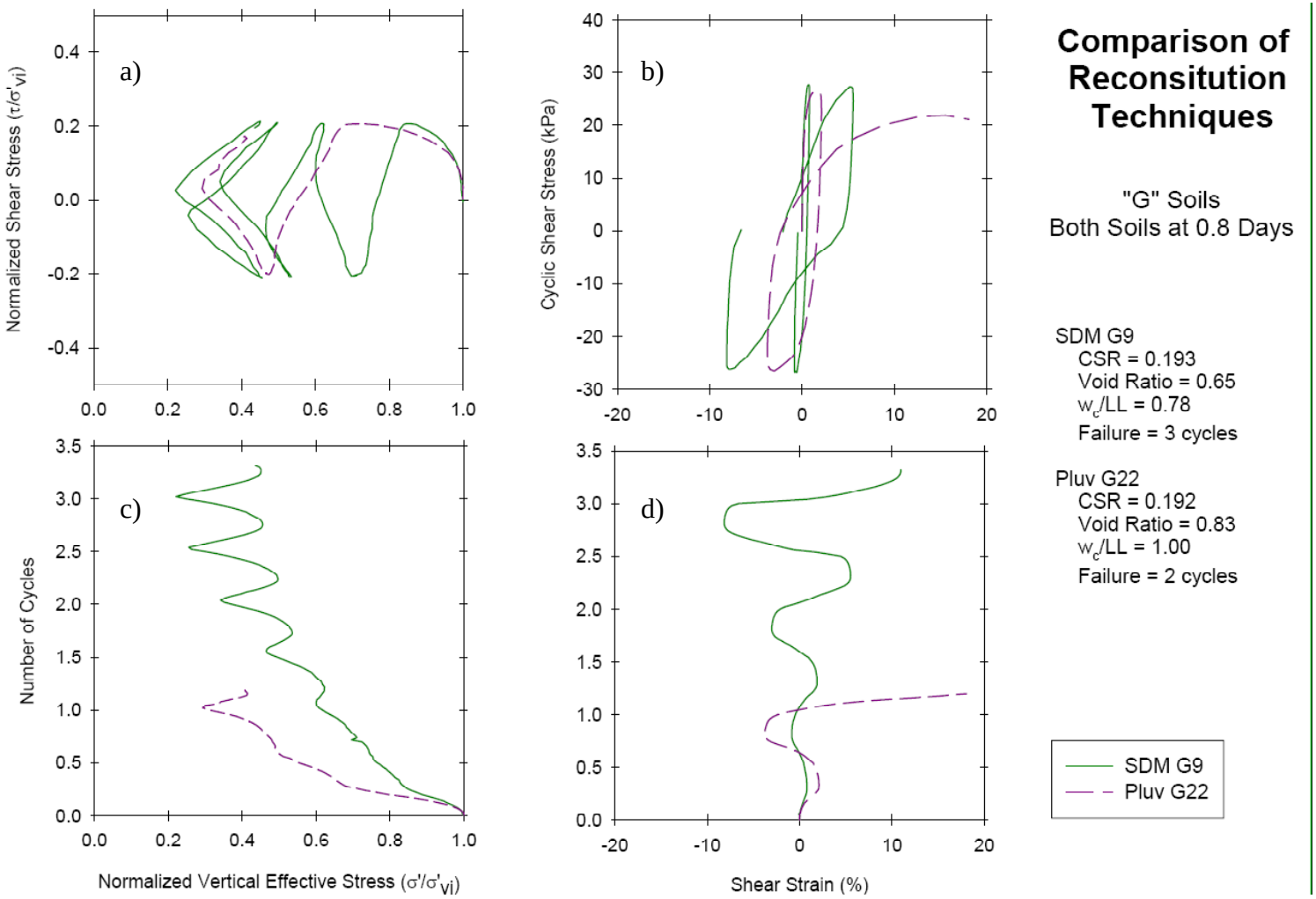

Figure 6.28 4-way plot comparison of Slurry Deposition Method specimen versus In-Place Wet Pluviation Specimens for Soil G tested by the cyclic simple shear, $\sigma'_v \approx 137$ kPa: a) effective stress path, b) stress-strain diagram, c) normalized vertical effective stress to number of cycles, and d) shear strain to number of cycles of loading.

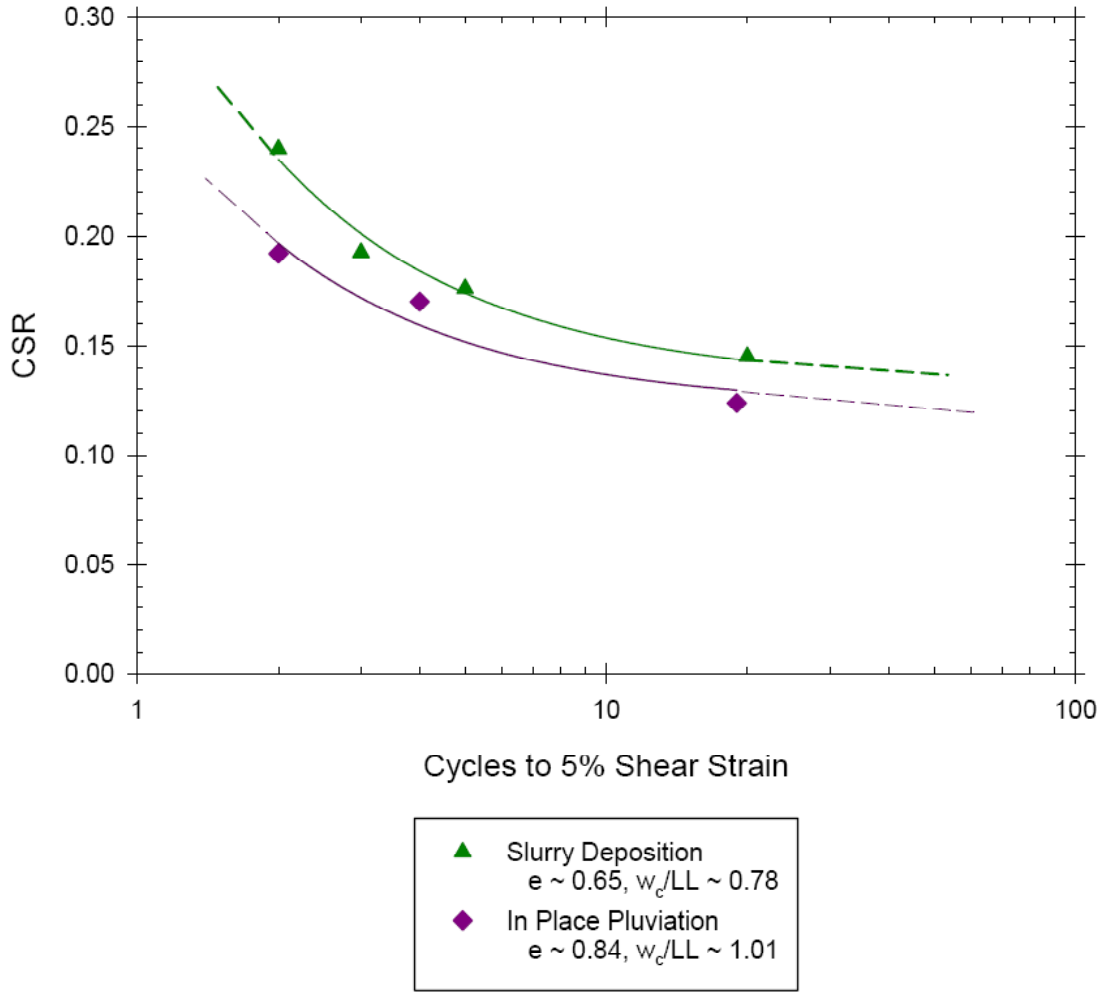

Figure 6.29 CSR Chart comparing Soil G prepared using the Slurry Deposition Method and In-Place Wet Pluviation tested by the cyclic simple shear, all tests at $\sigma'_v \approx 137$ kPa.

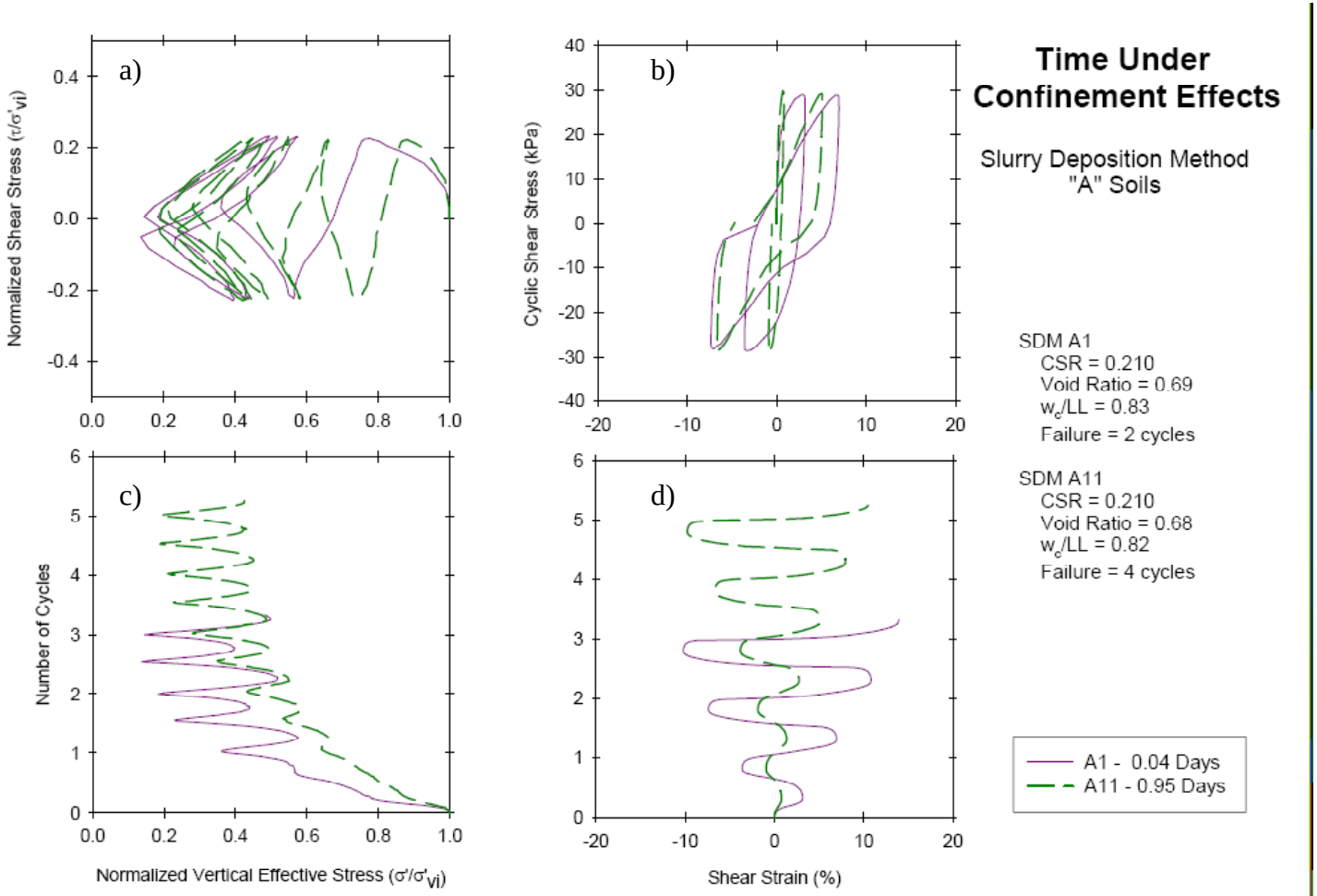

Figure 6.30 4-way plot comparison of time under confinement for Soil A prepared using the Slurry Deposition Method tested by the cyclic simple shear, $\sigma'_v \approx 137$ kPa: a) effective stress path, b) stress-strain diagram, c) normalized vertical effective stress to number of cycles, and d) shear strain to number of cycles of loading.

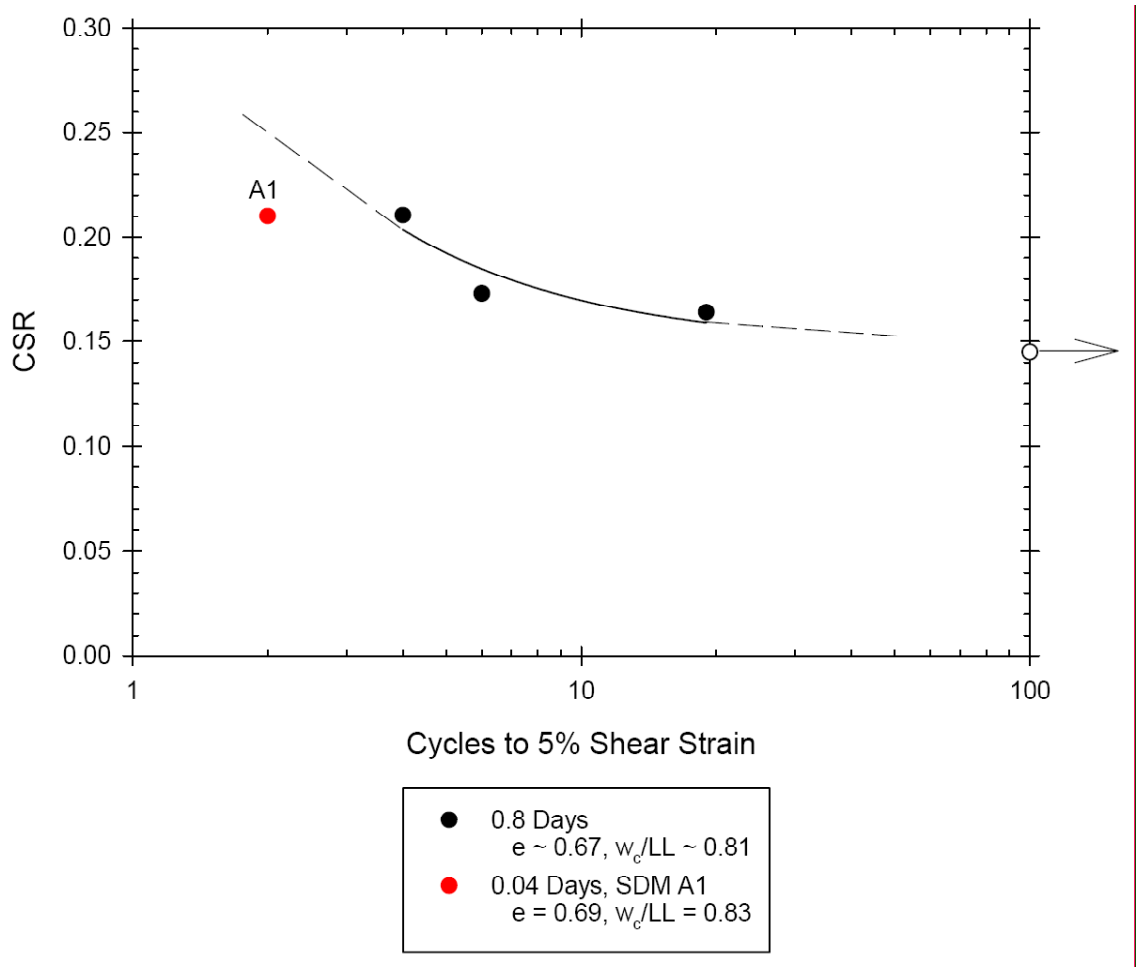

Figure 6.31 CSR Chart of Soil A prepared using the Slurry Deposition Method tested by the cyclic simple shear for different times under confinement, all tests at $\sigma'_v \approx 137$ kPa.

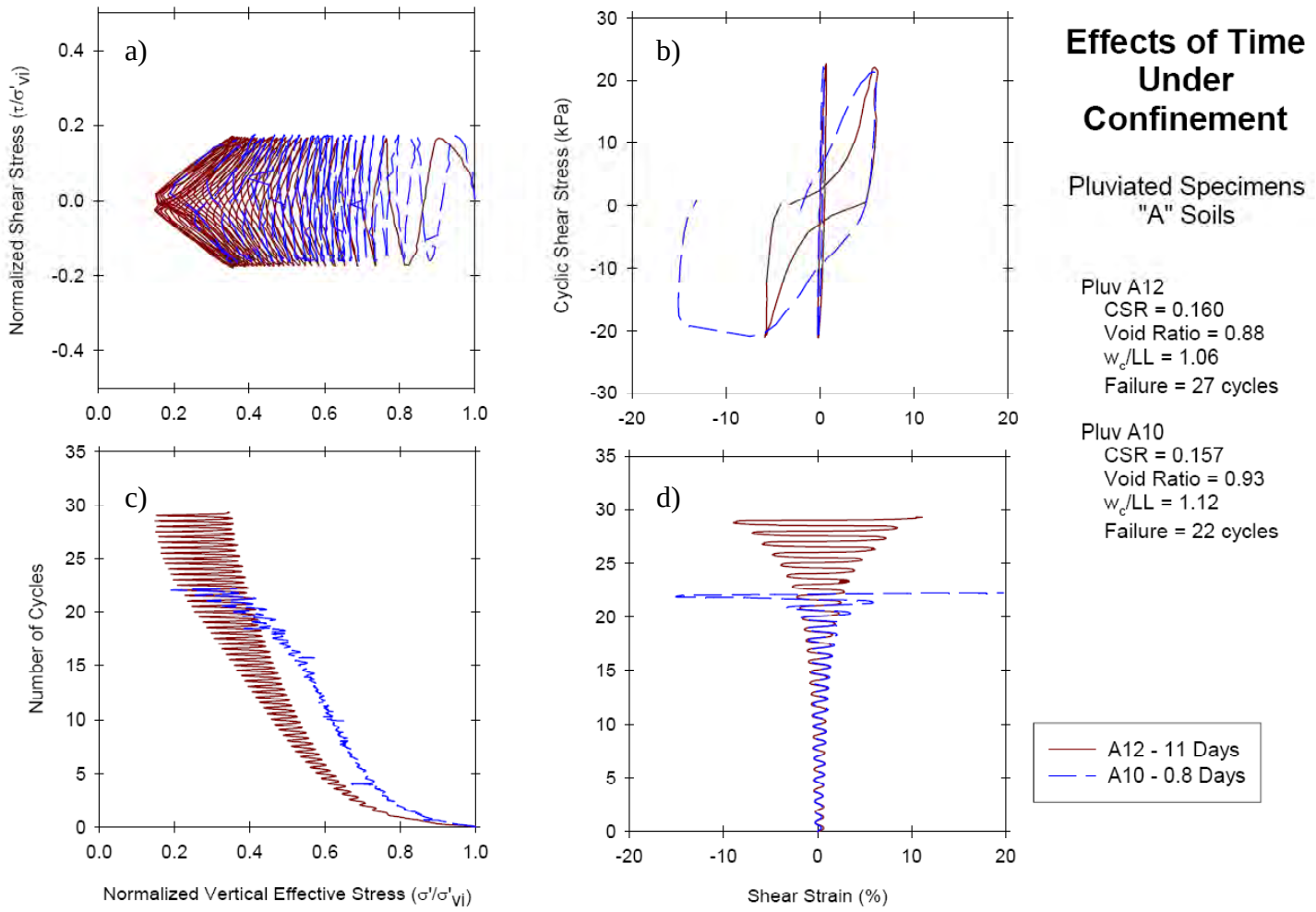

Figure 6.32 4-way plot comparison of time under confinement for Soil A prepared using In-Place Wet Pluviation tested by the cyclic simple shear for 0.8 and 11 Days, $\sigma'_v \approx 137$ kPa: a) effective stress path, b) stress-strain diagram, c) normalized vertical effective stress to number of cycles, and d) shear strain to number of cycles of loading.

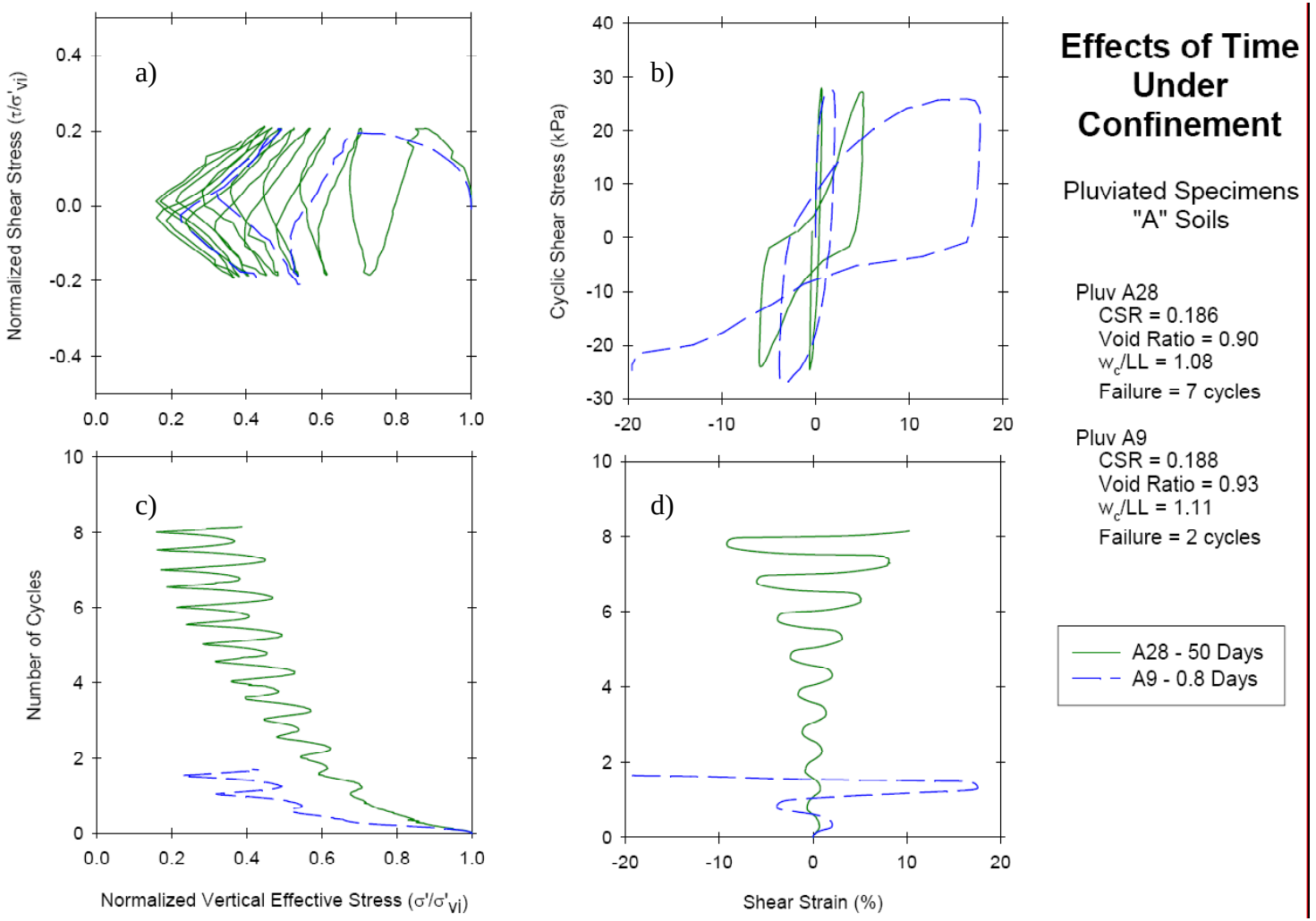

Figure 6.33 4-way plot comparison of time under confinement for Soil A prepared using In-Place Wet Pluviation tested by the cyclic simple shear for 0.8 and 50 Days, $\sigma'_v \approx 137$ kPa: a) effective stress path, b) stress-strain diagram, c) normalized vertical effective stress to number of cycles, and d) shear strain to number of cycles of loading.

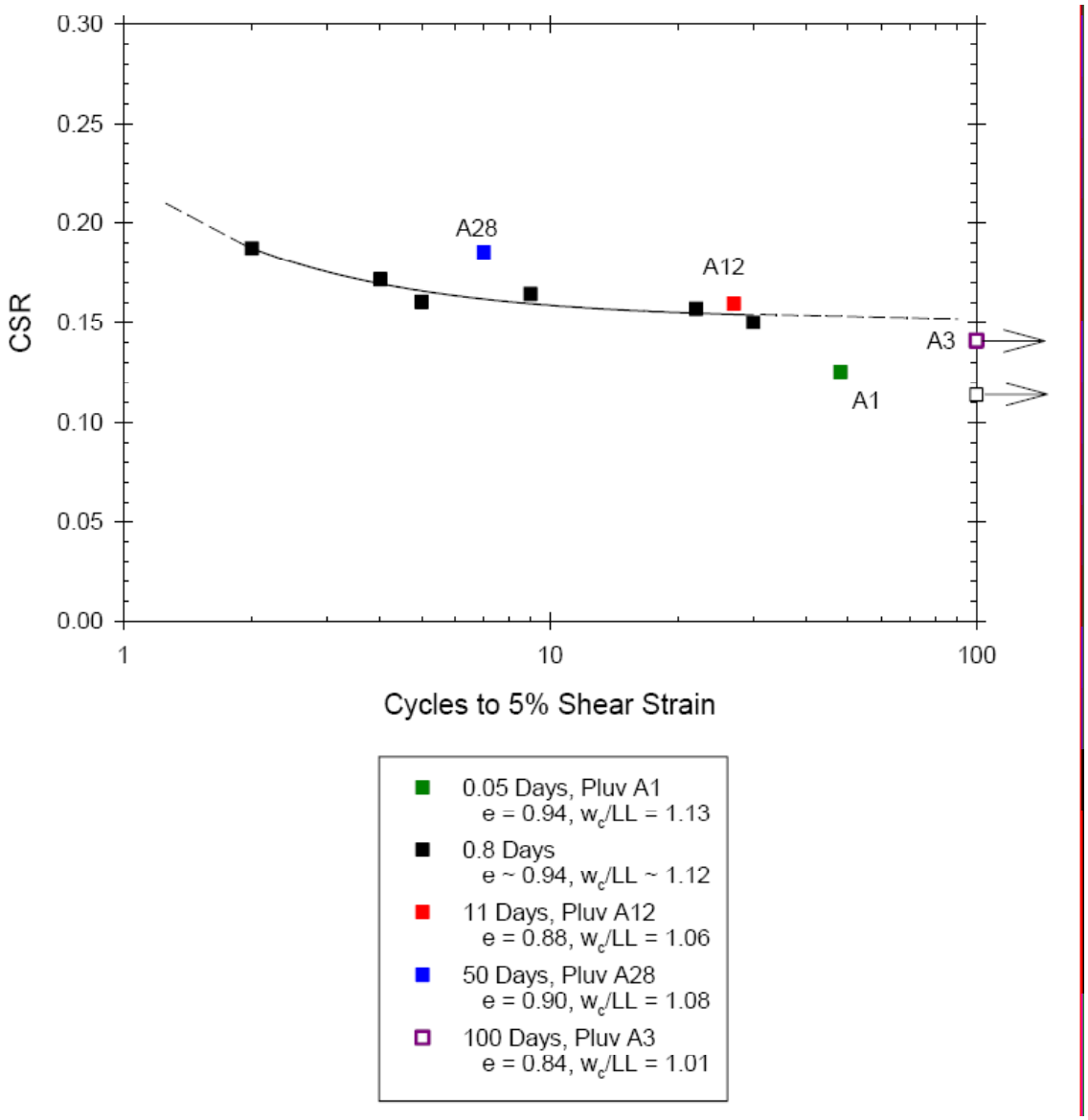

Figure 6.34 CSR Chart of Soil A prepared using In-Place Wet Pluviation tested by the cyclic simple shear for different times under confinement, all tests at $\sigma'_v \approx 137$ kPa.

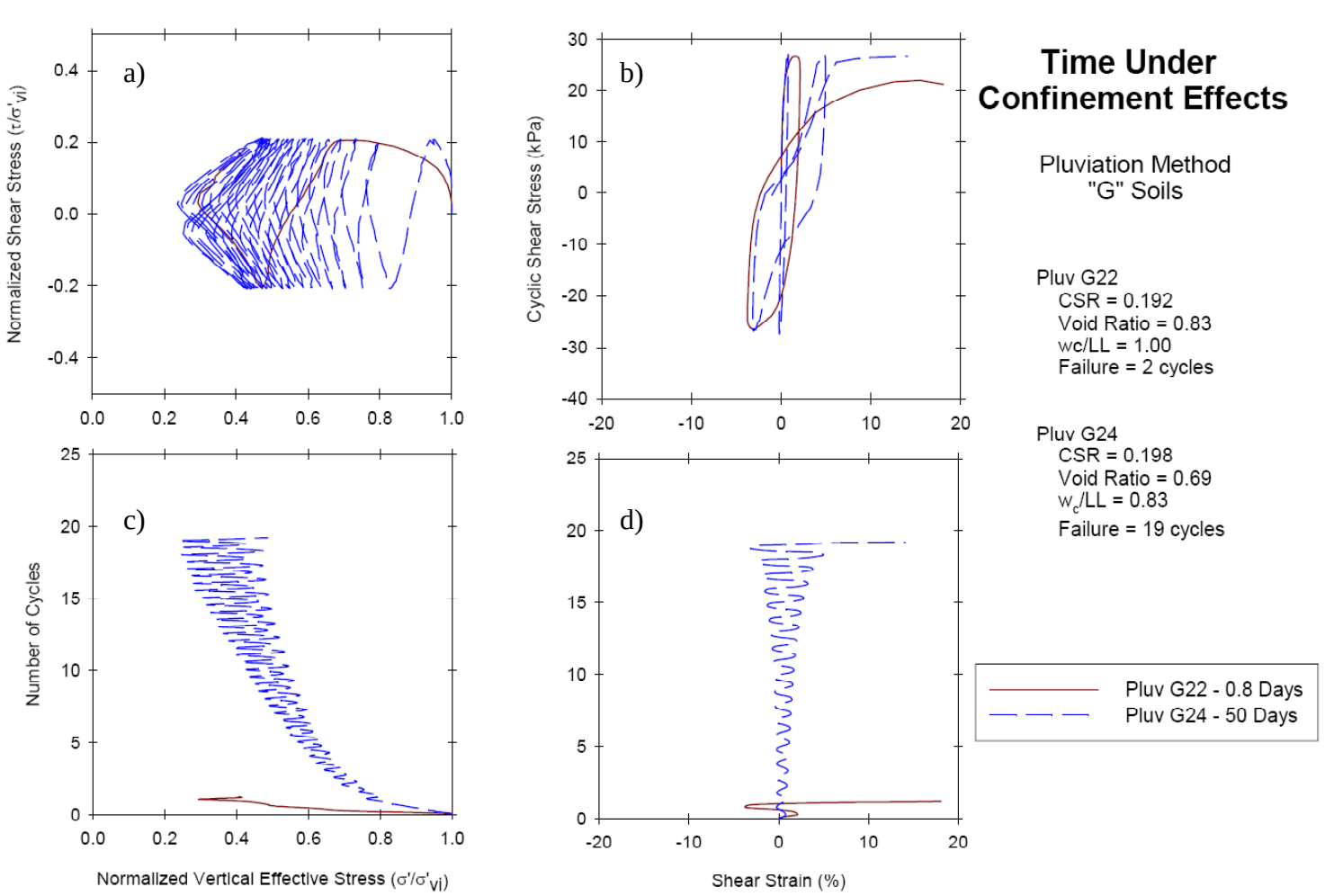

Figure 6.35 4-way plot comparison of time under confinement for Soil G prepared using In-Place Wet Pluviation tested by the cyclic simple shear for 0.8 and 50 Days, $\sigma'_v \approx 137$ kPa: a) effective stress path, b) stress-strain diagram, c) normalized vertical effective stress to number of cycles, and d) shear strain to number of cycles of loading.

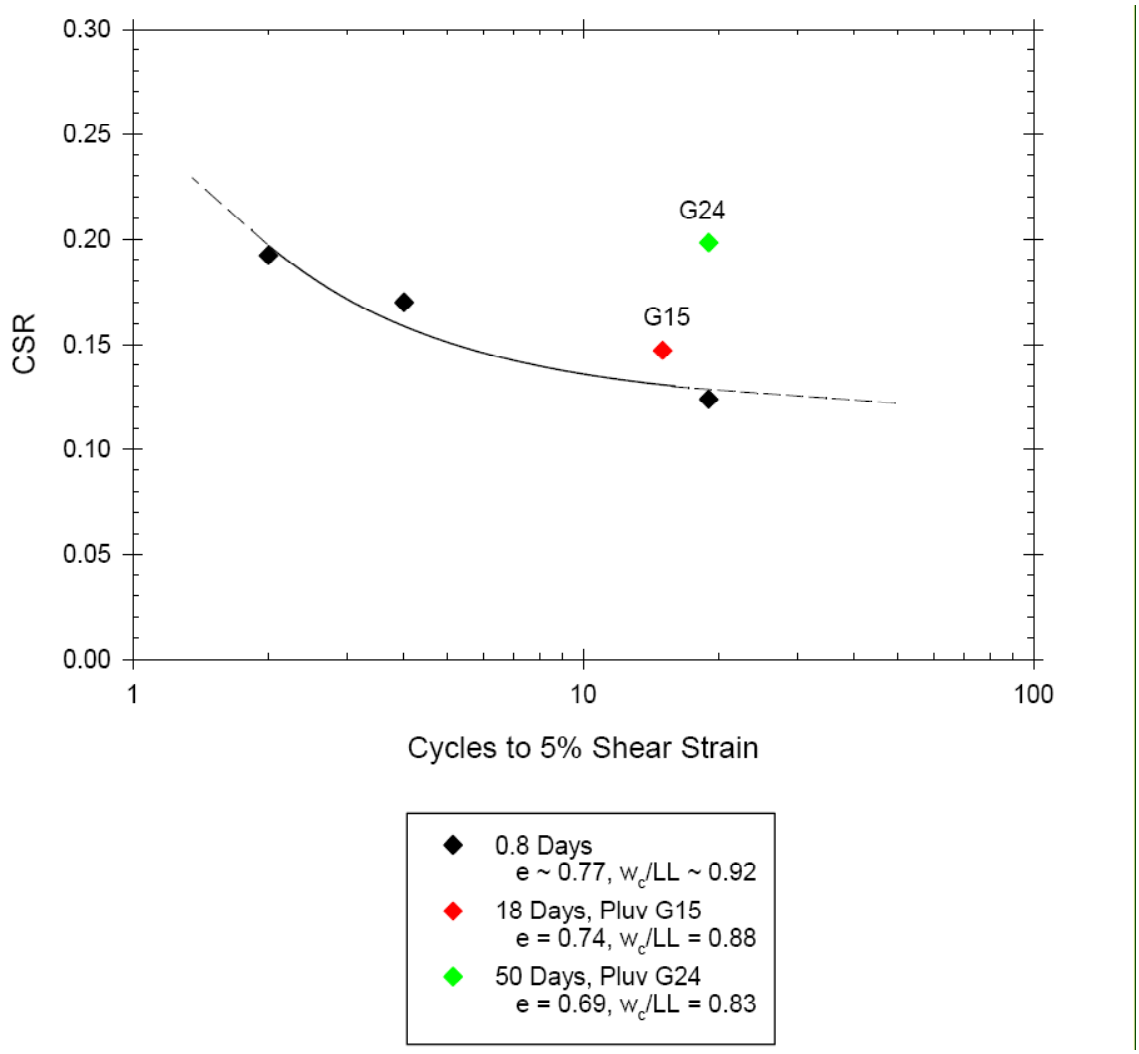

Figure 6.36 CSR Chart of Soil G prepared using In-Place Wet Pluviation tested by the cyclic simple shear for different times under confinement, all tests at $\sigma'_v \approx 137$ kPa.

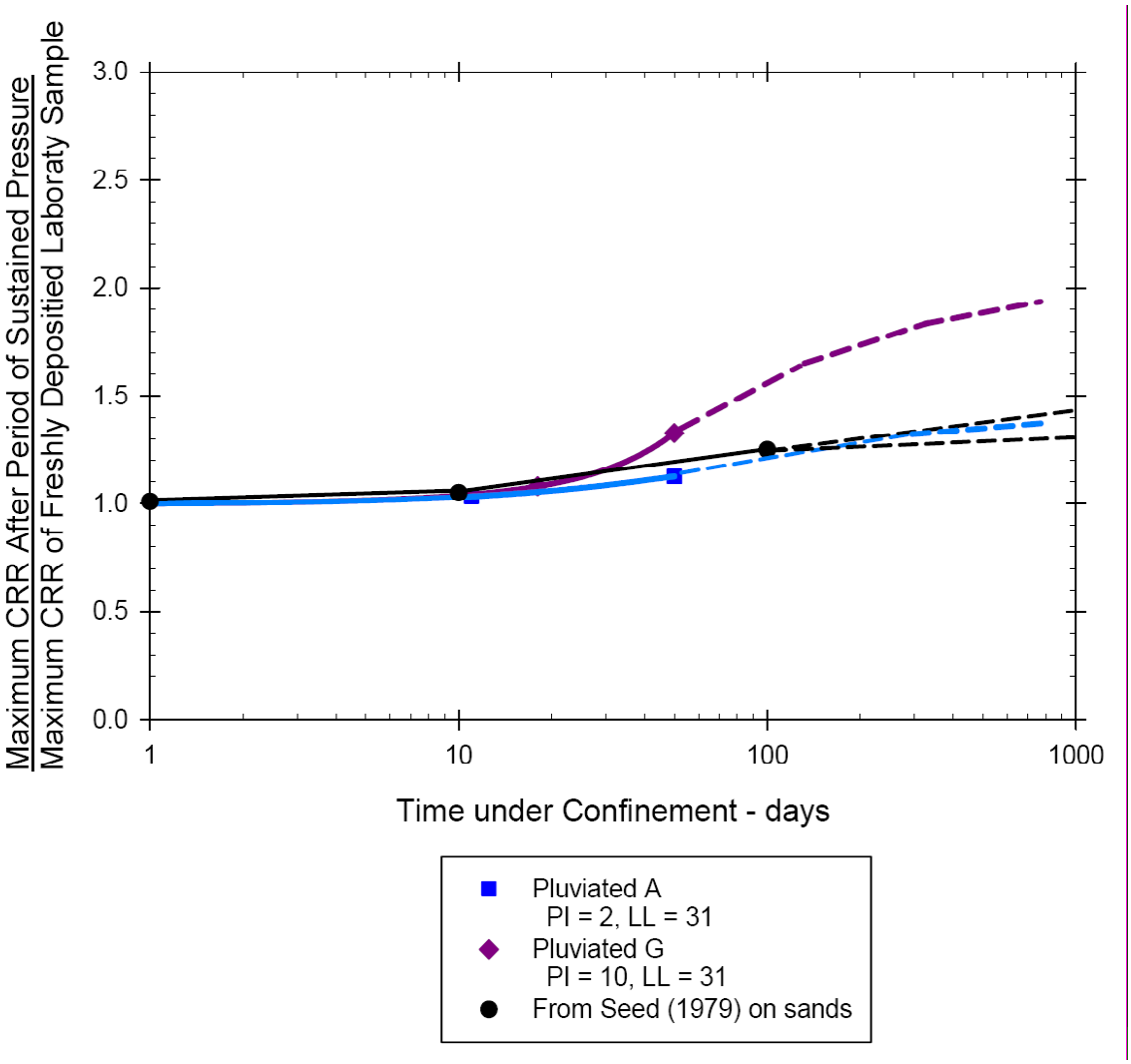

Figure 6.37 Influence of time under confinement on maximum undrained shear strength.

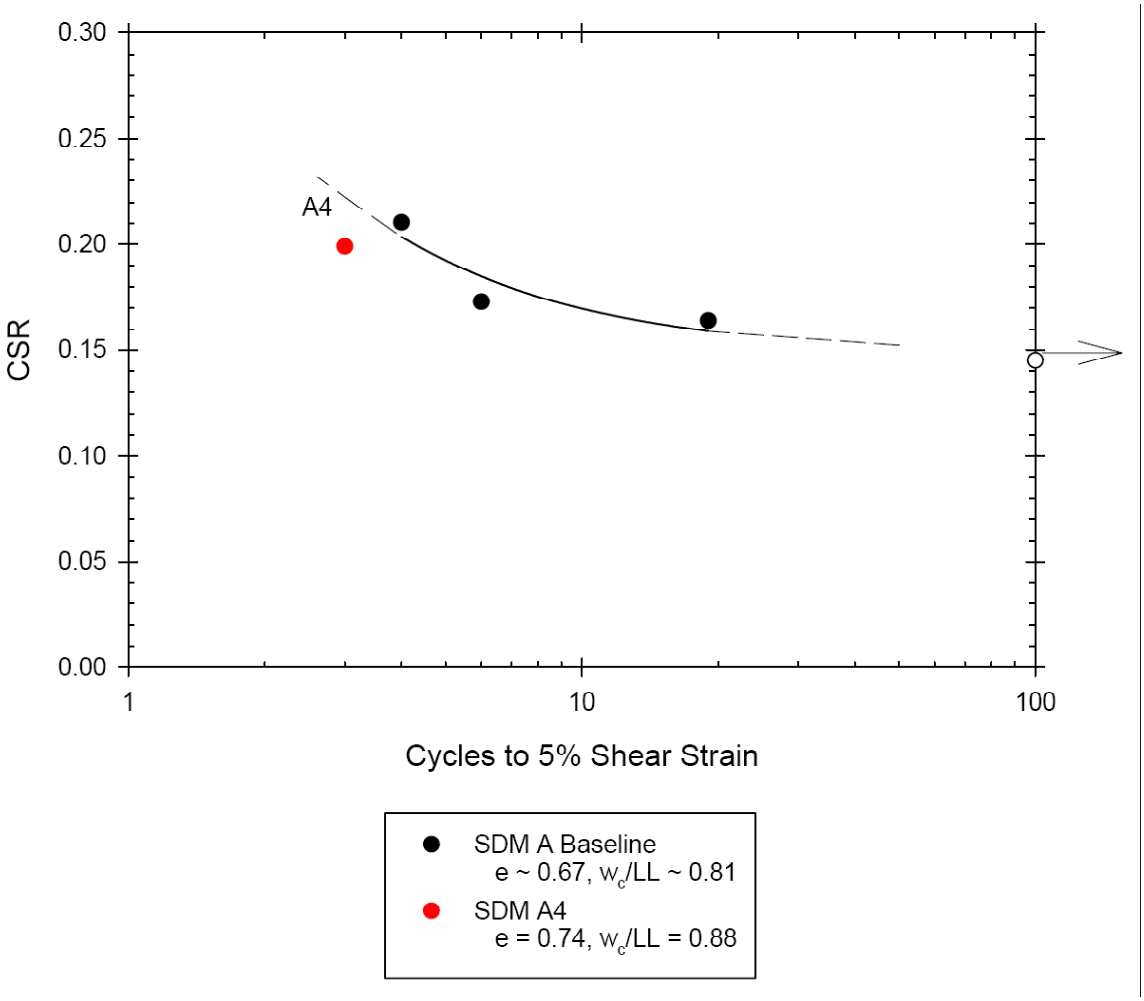

Figure 6.38 CSR Chart of Soil A prepared using the Slurry Deposition Method tested by the cyclic simple shear for different densities, all tests at $\sigma'_v \approx 137$ kPa.

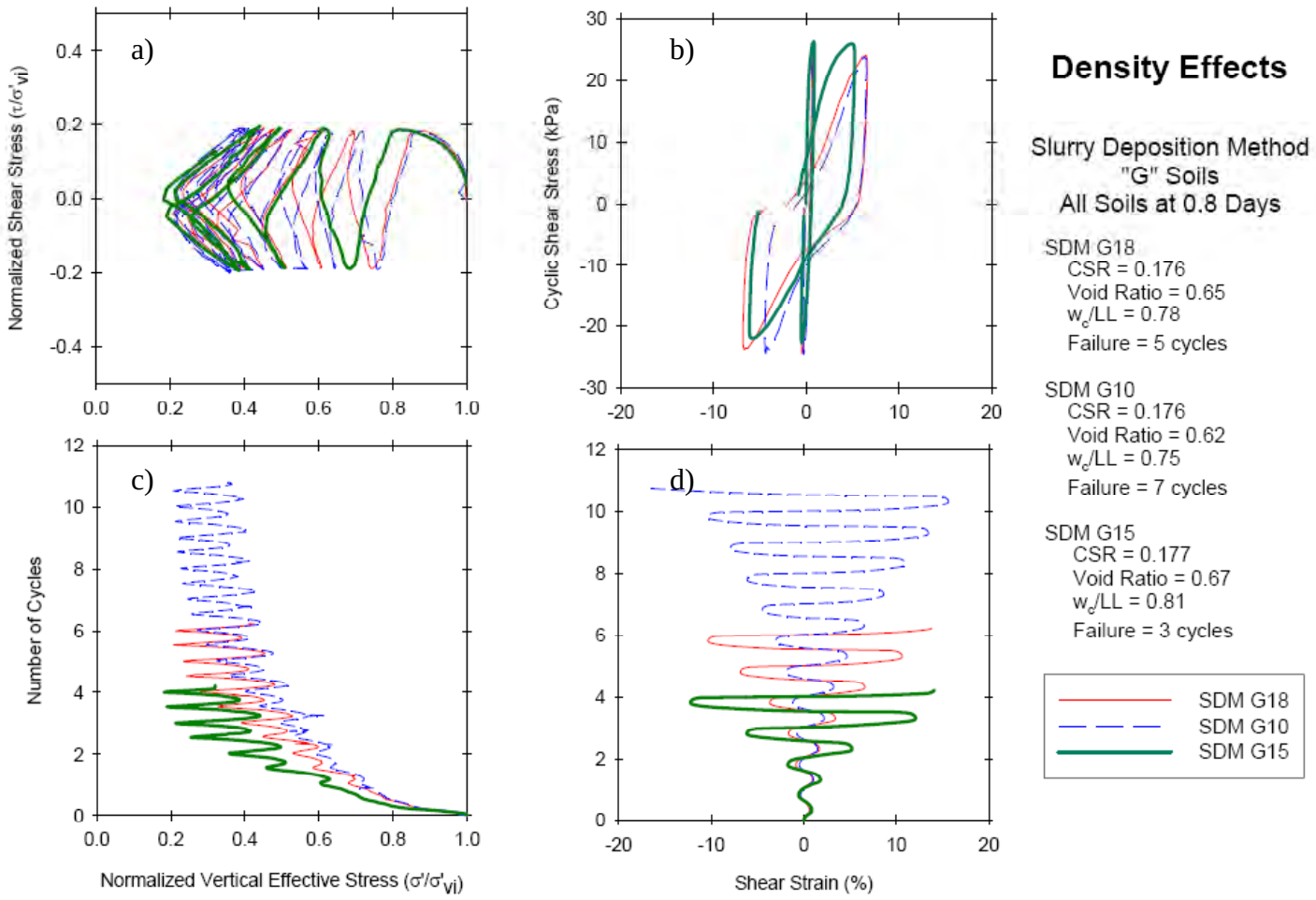

Figure 6.39 4-way plot comparison of density effects for Soil G prepared using the Slurry Deposition Method tested by the cyclic simple shear, $\sigma'_v \approx 137$ kPa: a) effective stress path, b) stress-strain diagram, c) normalized vertical effective stress to number of cycles, and d) shear strain to number of cycles of loading.

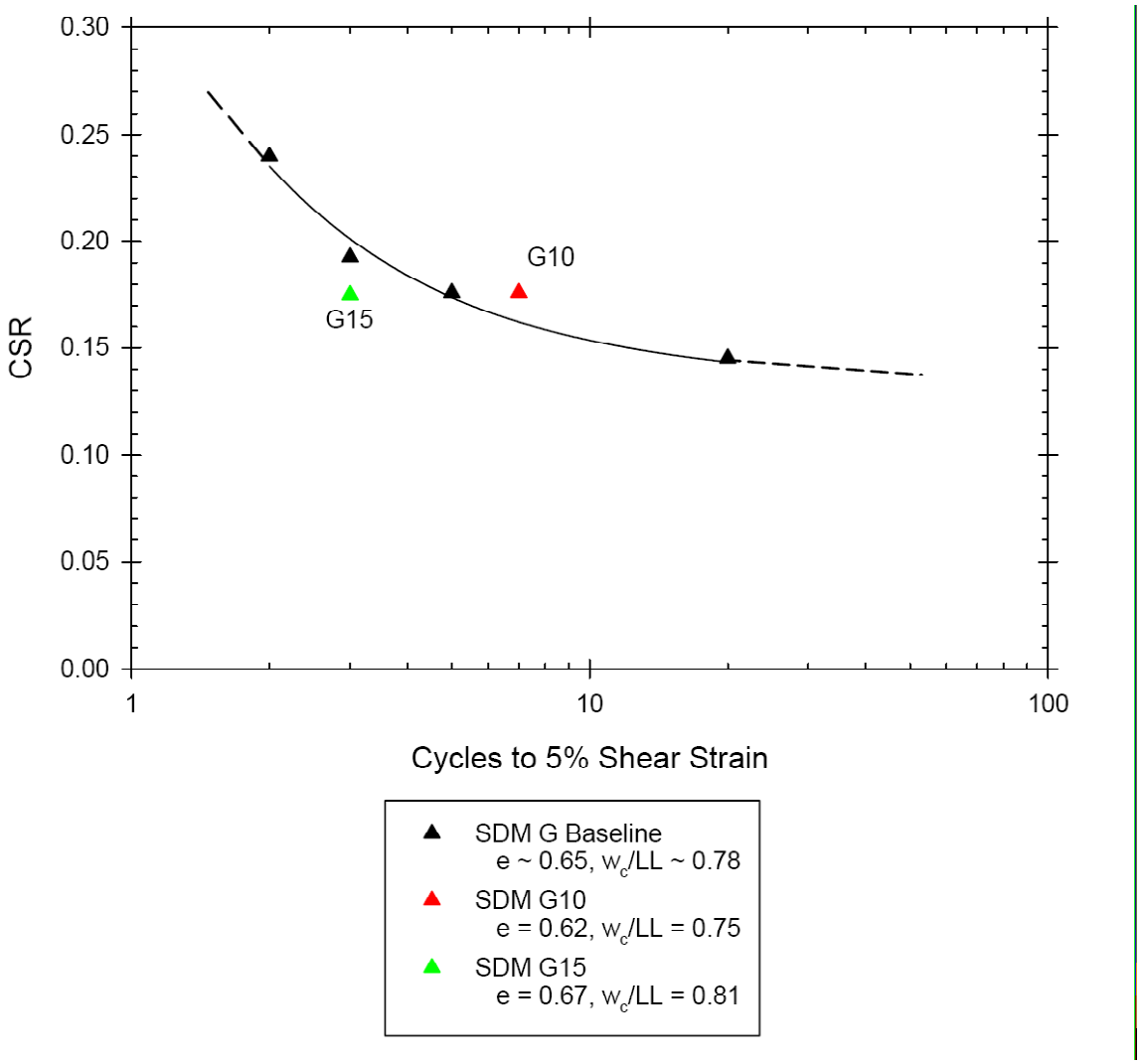

Figure 6.40 CSR Chart of Soil G prepared using the Slurry Deposition Method tested by the cyclic simple shear for different densities, all tests at $\sigma'_v \approx 137$ kPa.

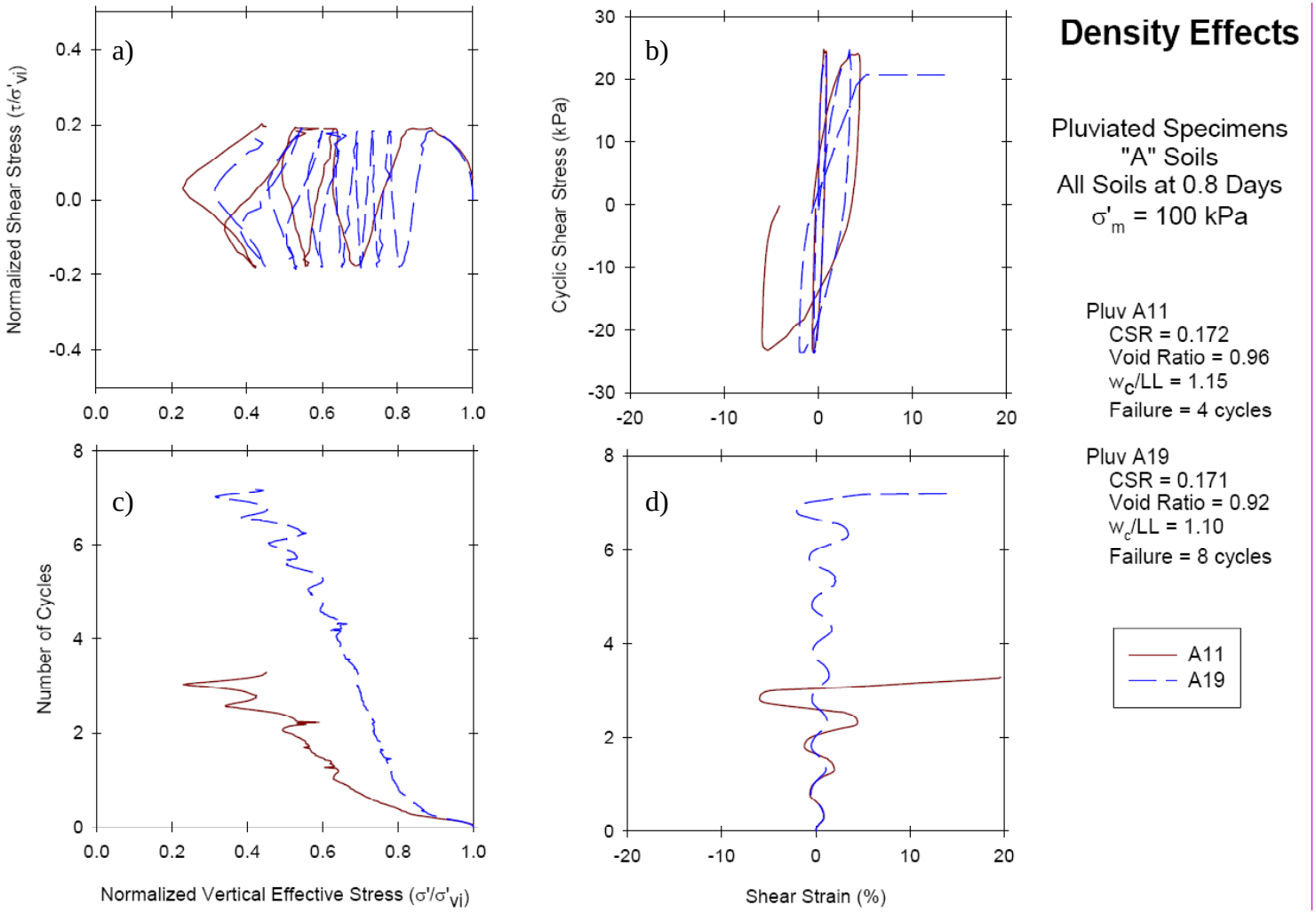

Figure 6.41 4-way plot comparison of density effects for Soil A prepared using In-Place Wet Pluviation tested by the cyclic simple shear at $\sigma'_v \approx 137$ kPa: a) effective stress path, b) stress-strain diagram, c) normalized vertical effective stress to number of cycles, and d) shear strain to number of cycles of loading.

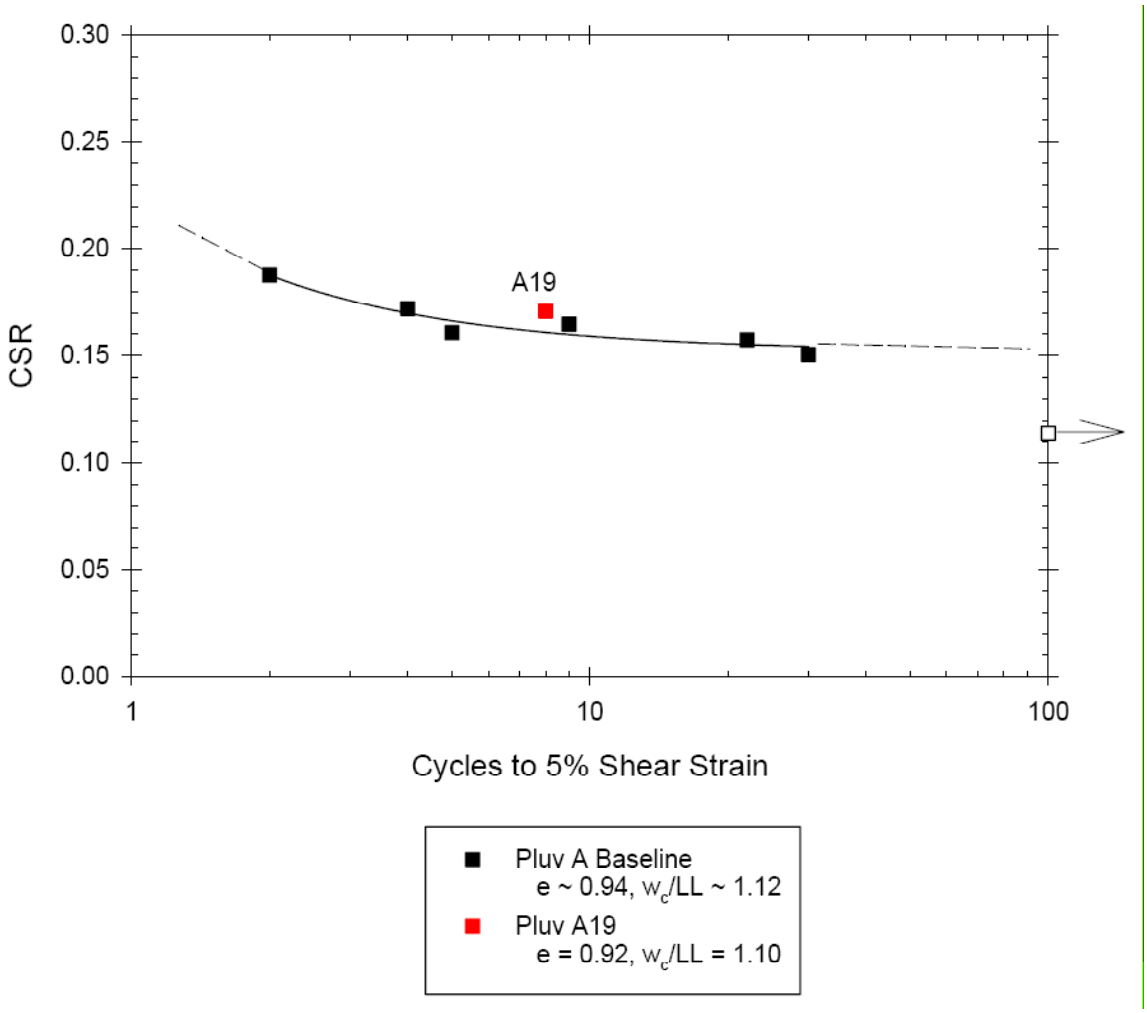

Figure 6.42 CSR Chart of Soil A prepared using In-Place Wet Pluviation tested by the cyclic simple shear for different densities, all tests at $\sigma'_v \approx 137$ kPa.

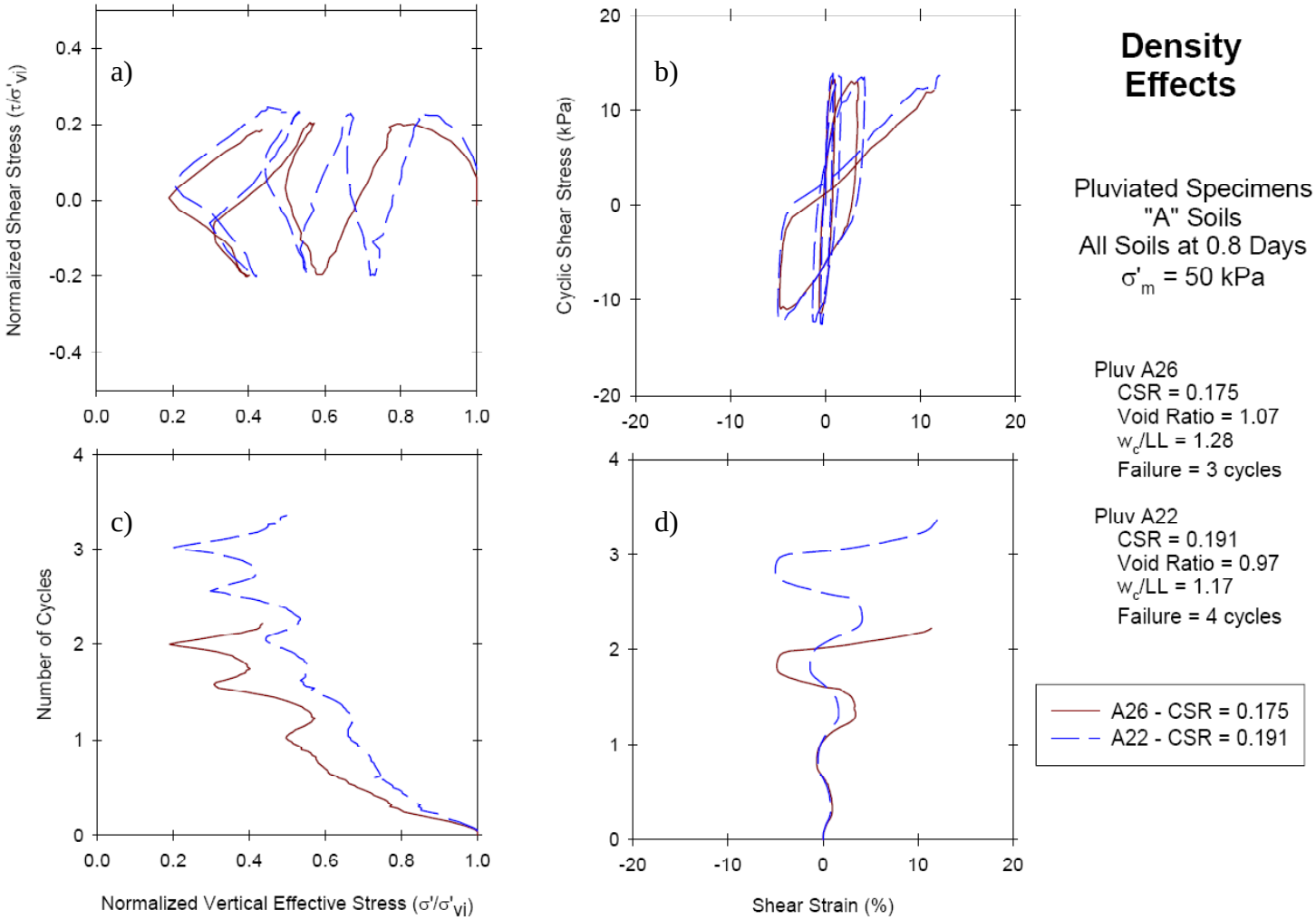

Figure 6.43 4-way plot comparison of density effects for Soil A prepared using In-Place Wet Pluviation tested by the cyclic simple shear at σ'_v = 68 kPa: a) effective stress path, b) stress-strain diagram, c) normalized vertical effective stress to number of cycles, and d) shear strain to number of cycles of loading.

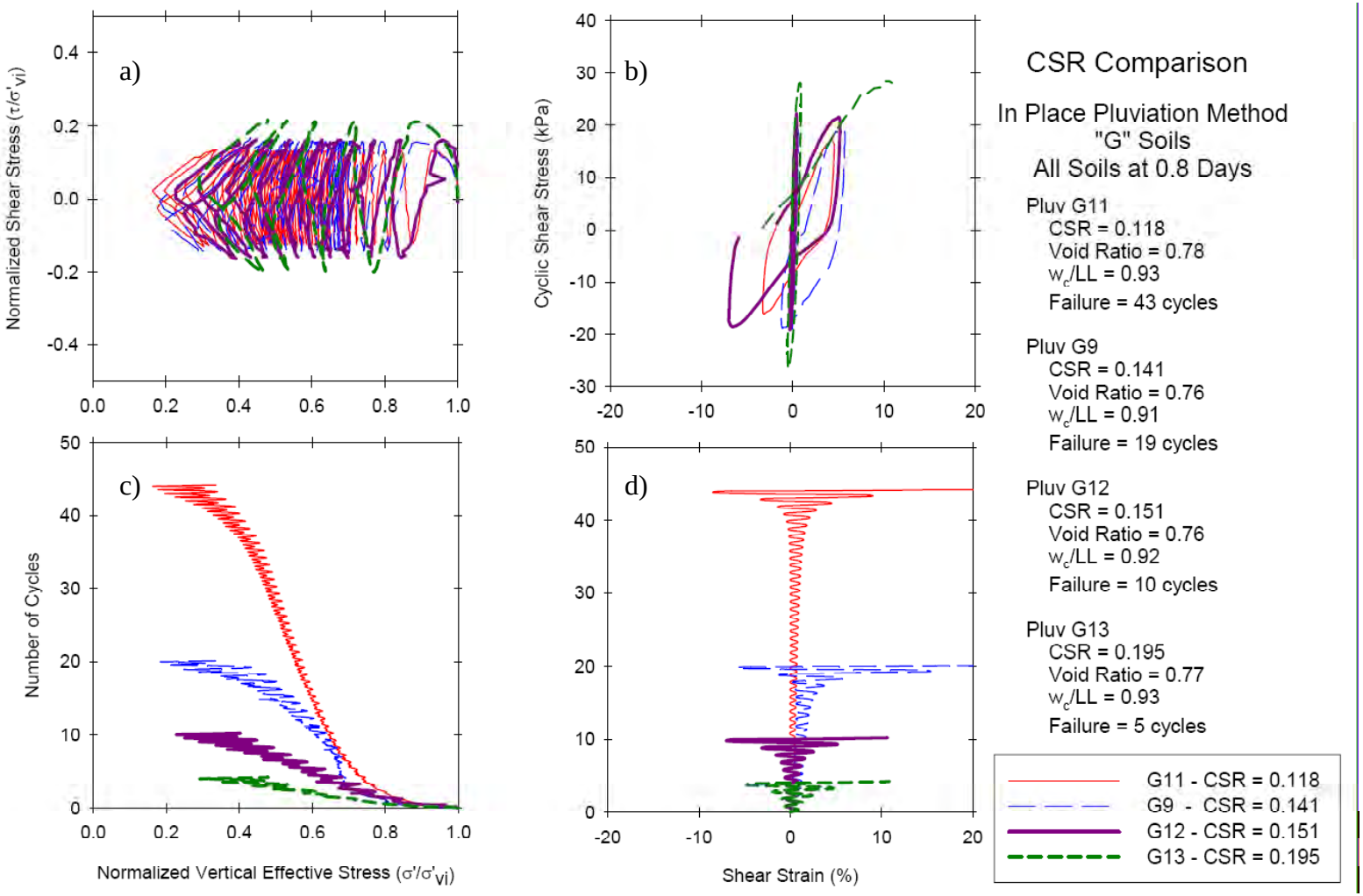

Figure 6.44 4-way plot comparison of CSR for Soil "G-Dense" prepared using In-Place Wet Pluviation tested by the cyclic simple shear, $\sigma'_v \approx 137$ kPa: a) effective stress path, b) stress-strain diagram, c) normalized vertical effective stress to number of cycles, and d) shear strain to number of cycles of loading.

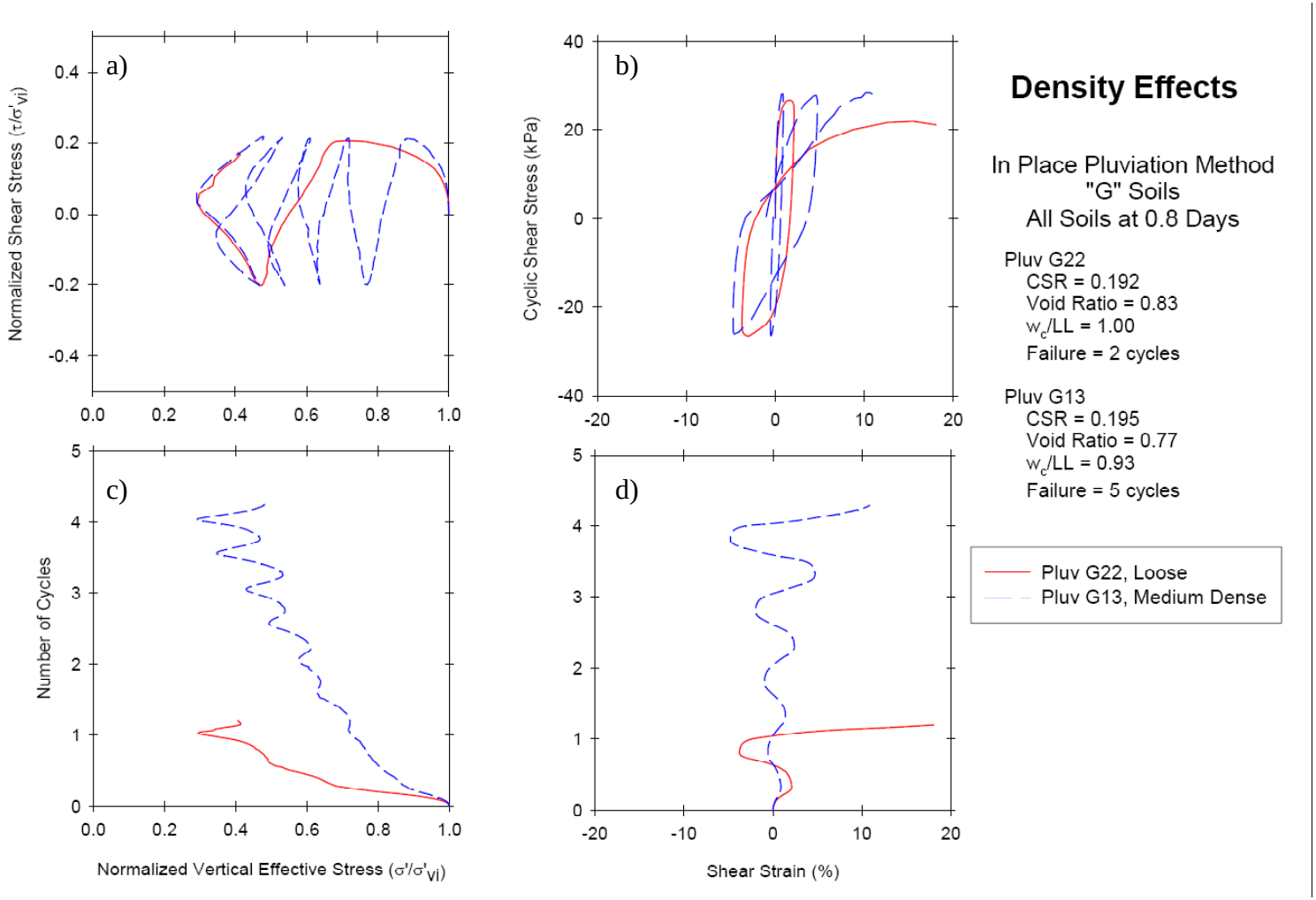

Figure 6.45 4-way plot comparison of densities, loose and medium dense, for Soil "G-Dense" prepared using In-Place Wet Pluviation tested by the cyclic simple shear, $\sigma'_v \approx 137$ kPa: a) effective stress path, b) stress-strain diagram, c) normalized vertical effective stress to number of cycles, and d) shear strain to number of cycles of loading.

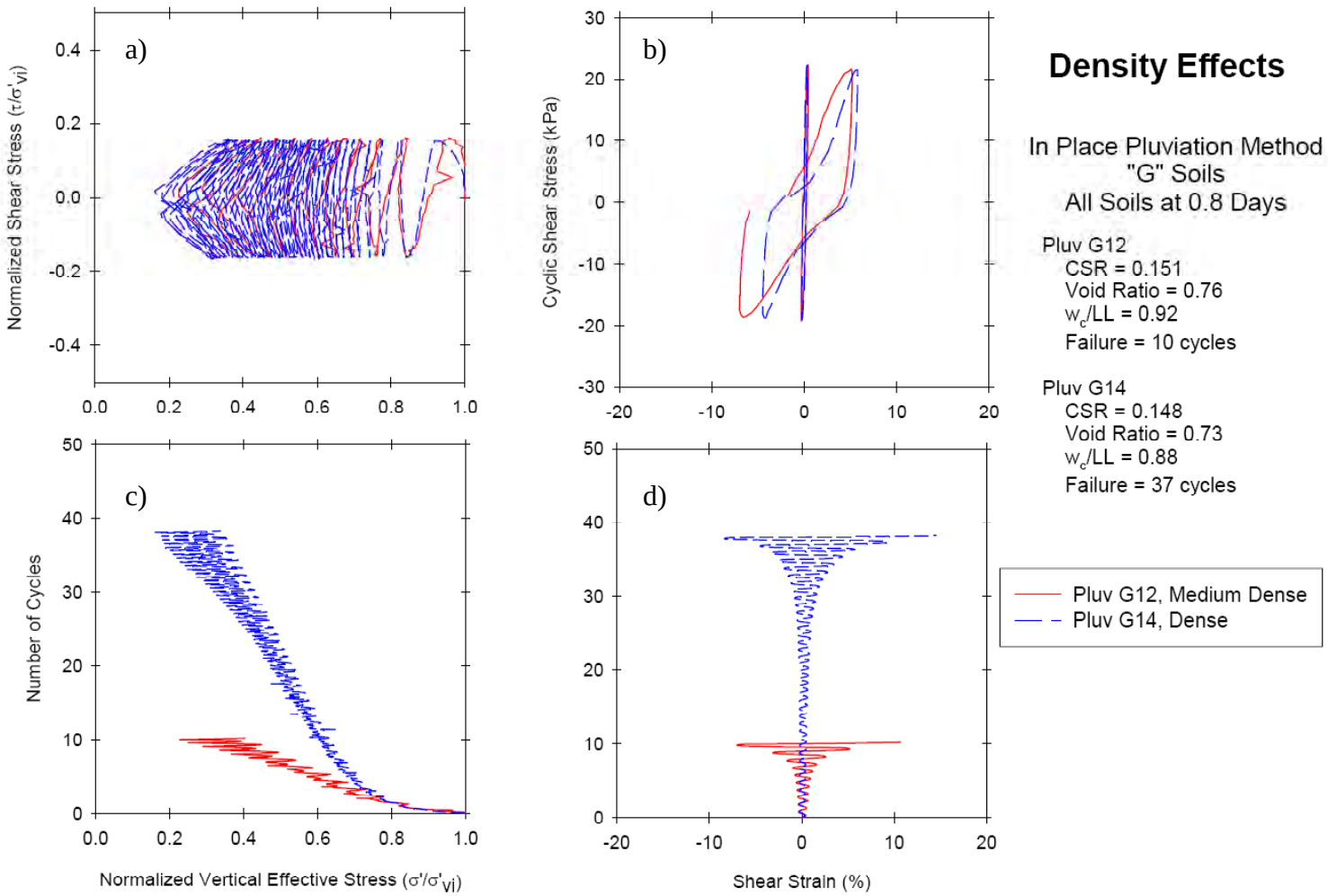

Figure 6.46 4-way plot comparison of density, medium dense and dense, for Soil "G-Dense" prepared using In-Place Wet Pluviation tested by the cyclic simple shear, $\sigma'_v \approx 137$ kPa: a) effective stress path, b) stress-strain diagram, c) normalized vertical effective stress to number of cycles, and d) shear strain to number of cycles of loading.

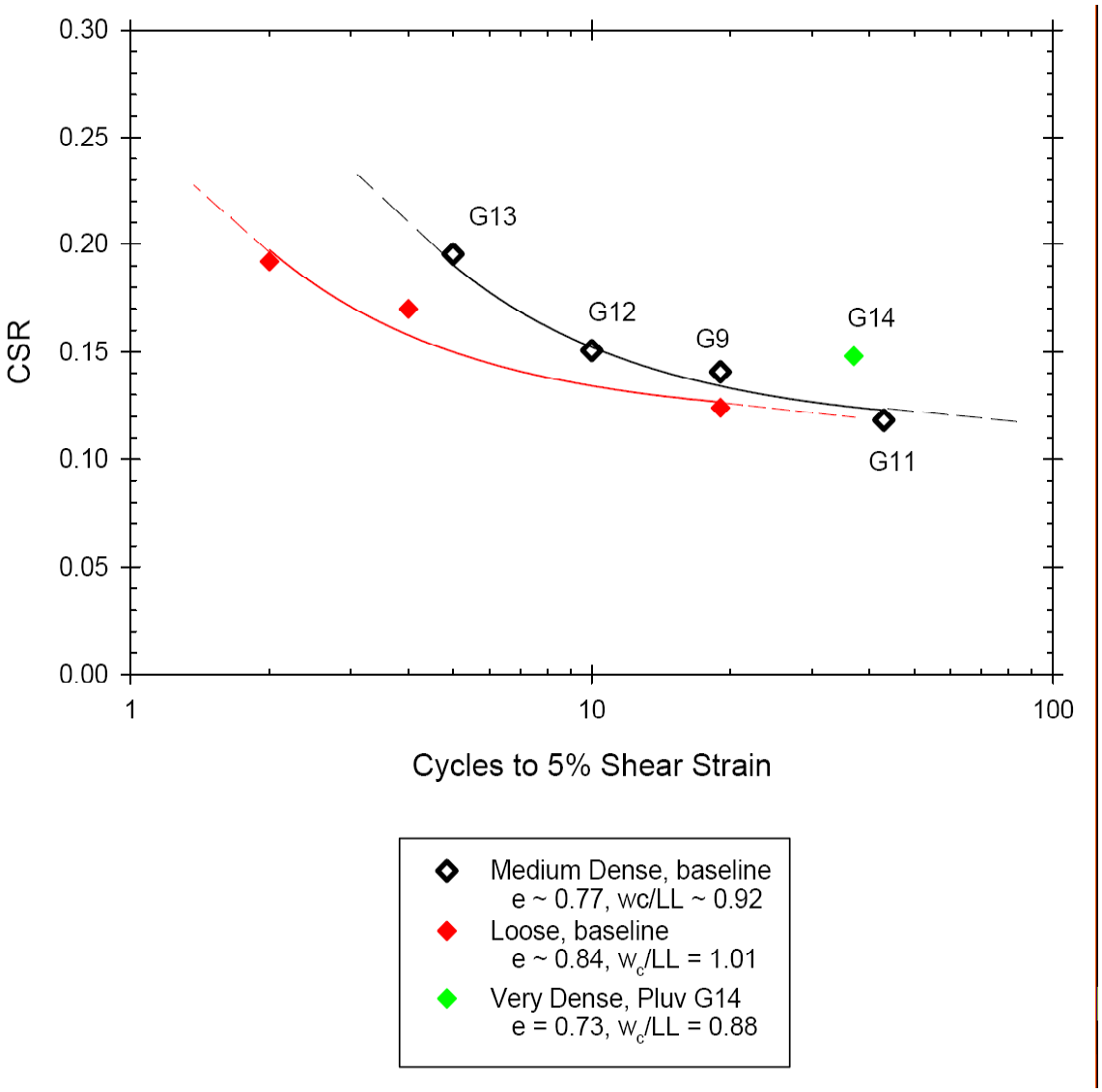

Figure 6.47 CSR Chart of Soil G prepared using In-Place Wet Pluviation tested by the cyclic simple shear for different densities, all tests at $\sigma'_v \approx 137$ kPa.

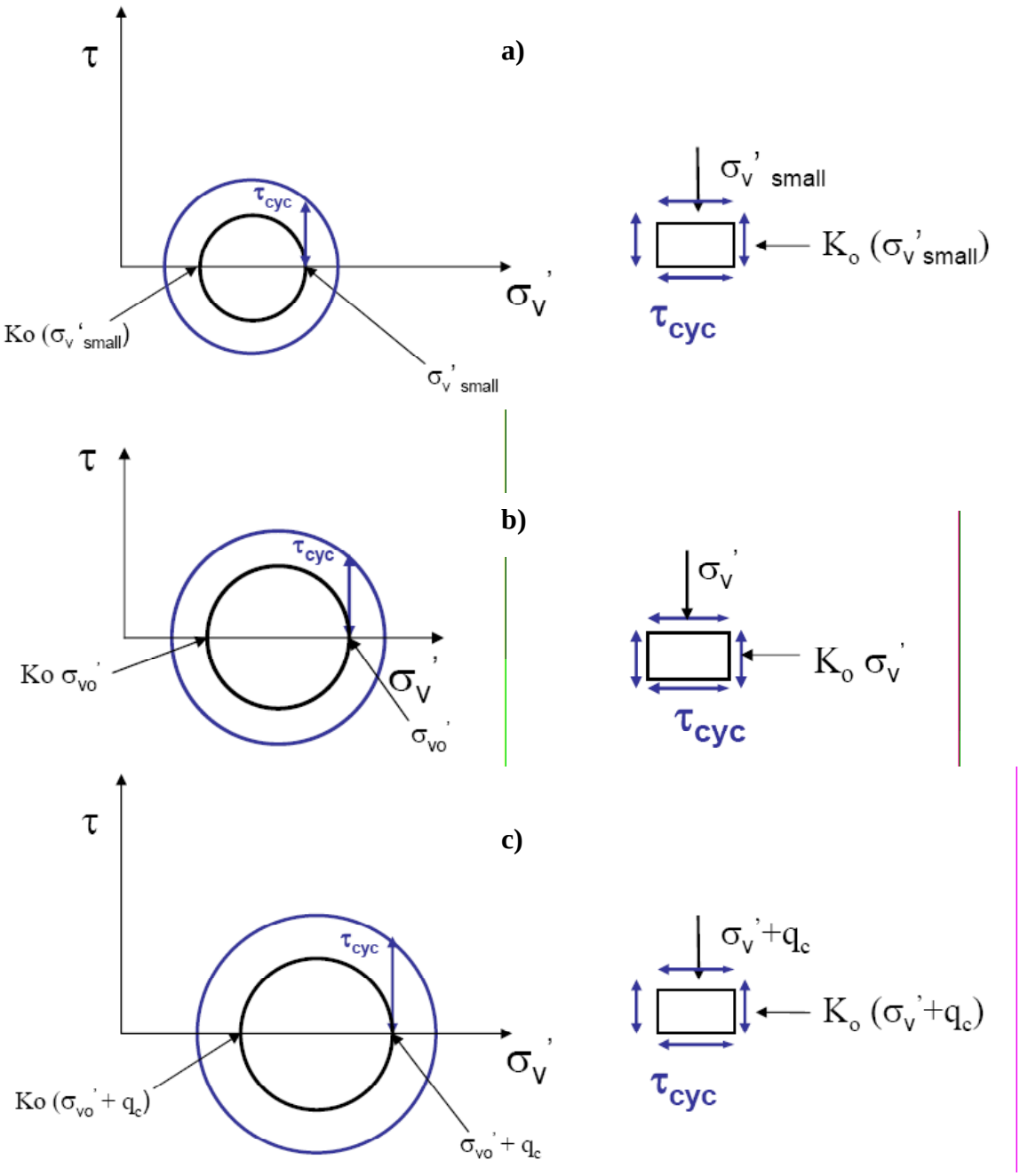

Figure 6.48 Stresses during anisotropically consolidated cyclic simple shear testing on specimens with: a) decreased effective confining pressure, b) baseline effective confining pressure, and c) increased effective confining pressure.

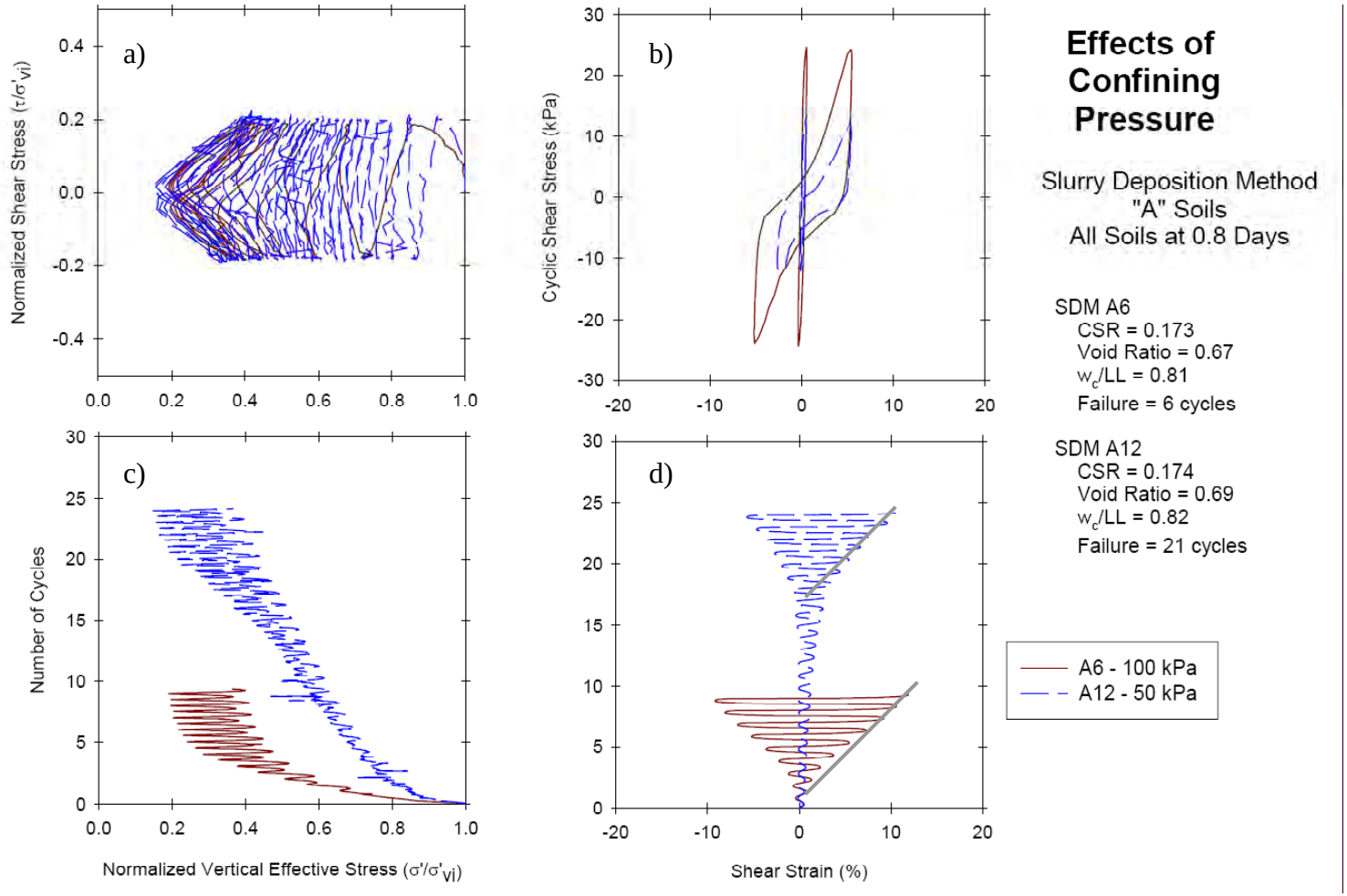

Figure 6.49 4-way plot comparison of a decrease in effective confining pressure effects for Soil A prepared using the Slurry Deposition Method tested by the Cyclic simple shear: a) effective stress path, b) stress-strain diagram, c) normalized vertical effective stress to number of cycles, and d) shear strain to number of cycles of loading.

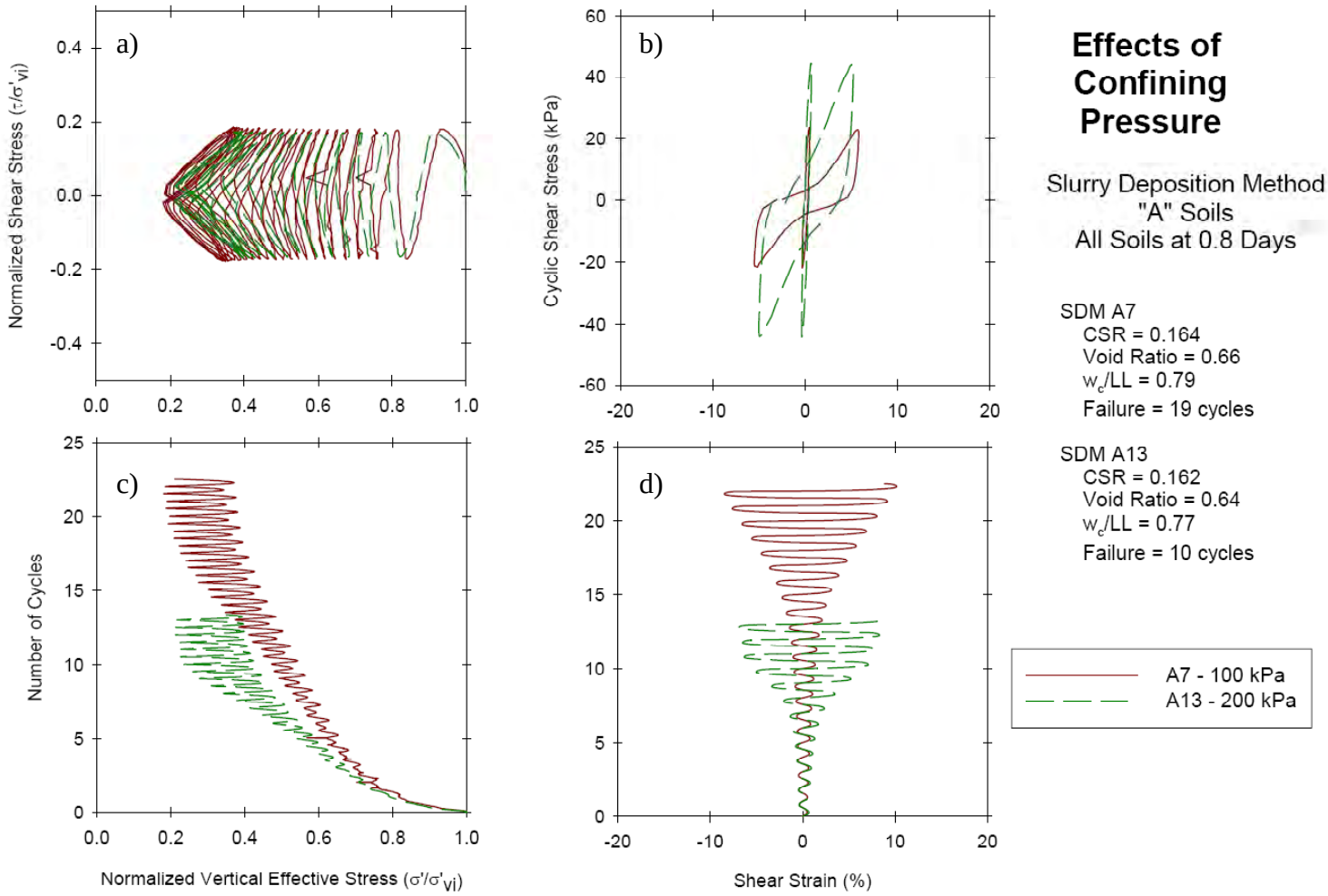

Figure 6.50 4-way plot comparison of an increase in effective confining pressure effects for Soil A prepared using the Slurry Deposition Method tested by the Cyclic simple shear: a) effective stress path, b) stress-strain diagram, c) normalized vertical effective stress to number of cycles, and d) shear strain to number of cycles of loading.

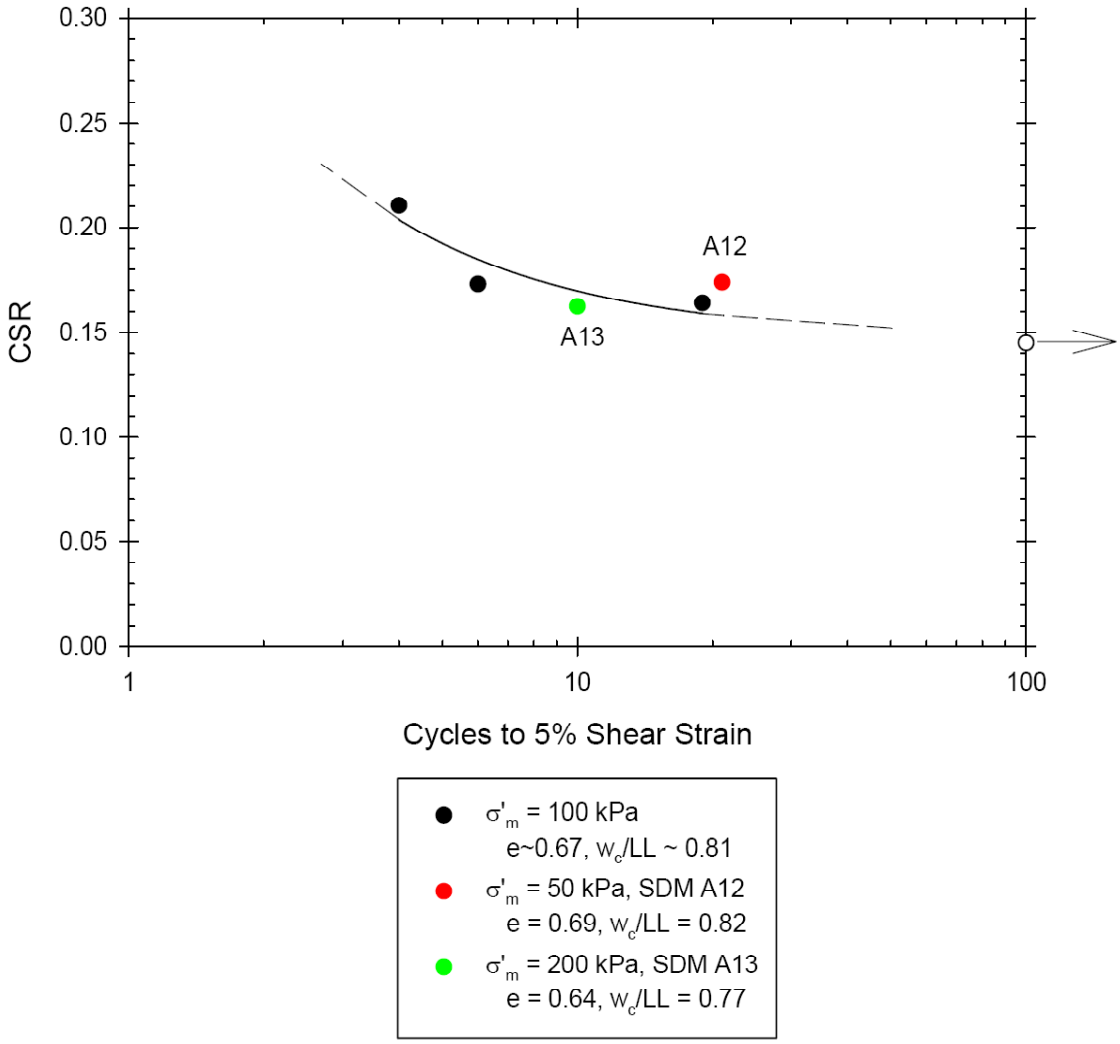

Figure 6.51 CSR Chart of Soil A prepared using the Slurry Deposition Method tested by the cyclic simple shear for different effective confining pressures.

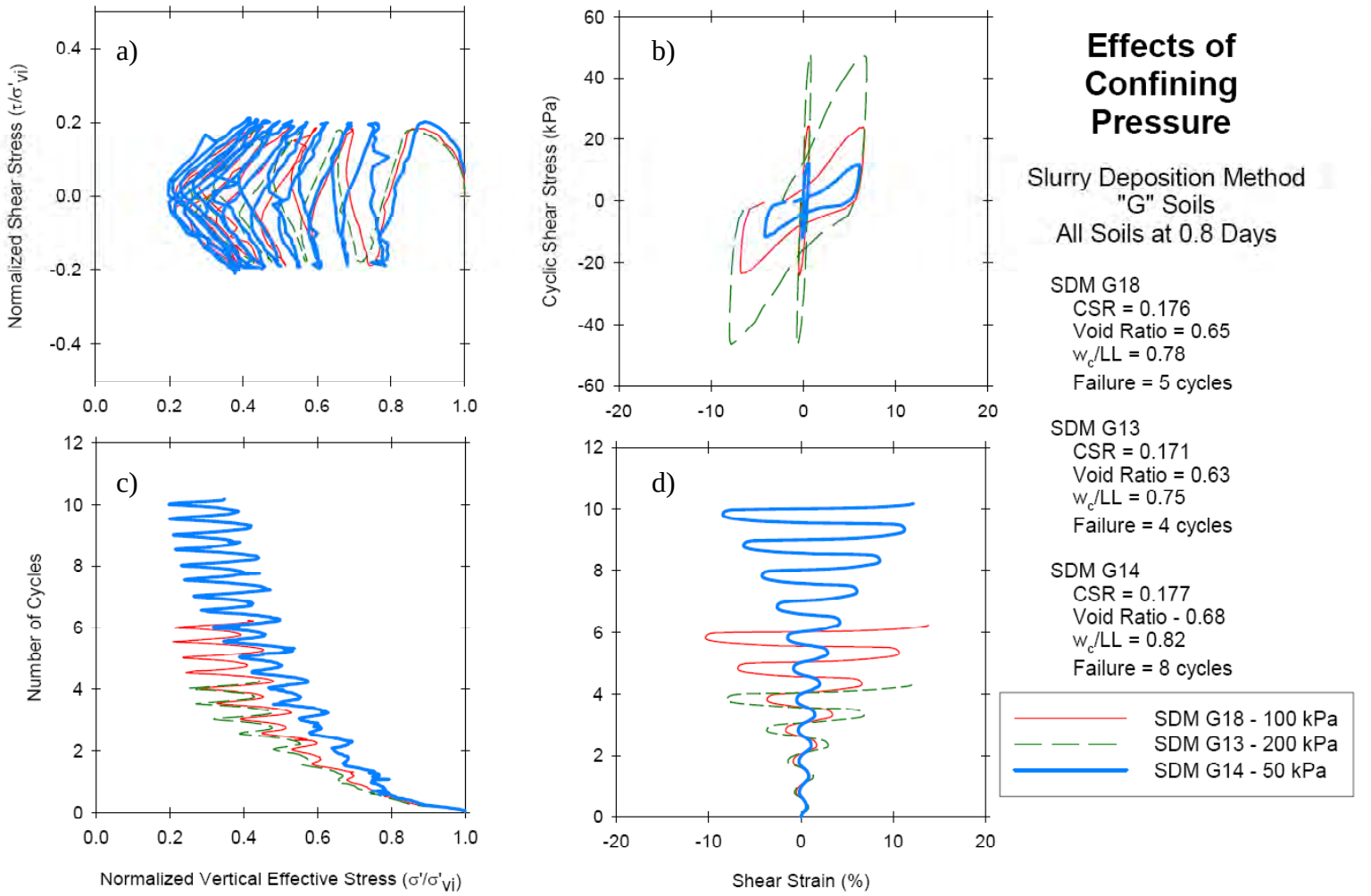

Figure 6.52 4-way plot comparison of effective confining pressure effects for Soil G prepared using the Slurry Deposition Method tested by the cyclic simple shear: a) effective stress path, b) stress-strain diagram, c) normalized vertical effective stress to number of cycles, and d) shear strain to number of cycles of loading.

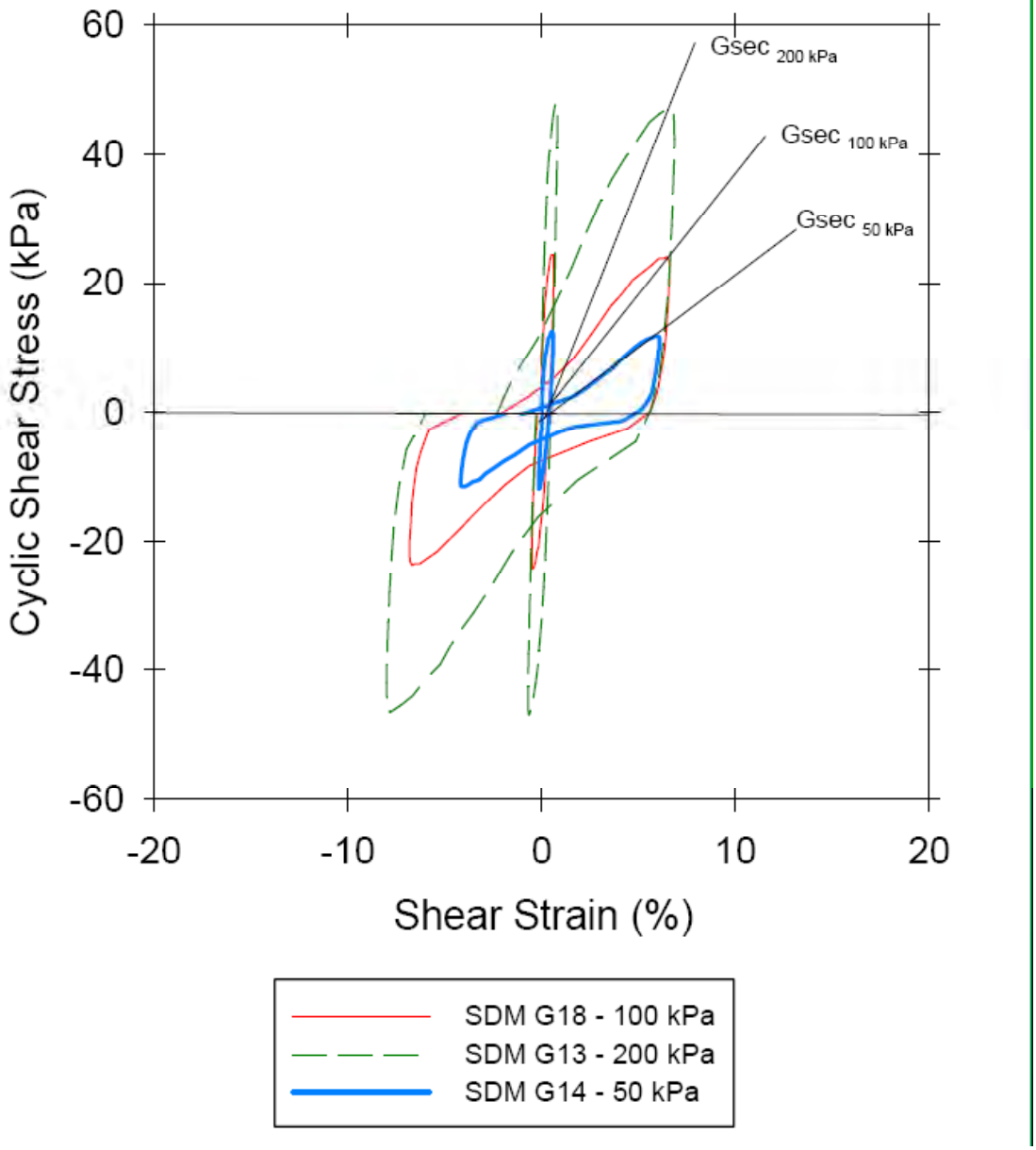

Figure 6.53 Gsec given different effective confining pressures for Soil G prepared using the Slurry Deposition Method.

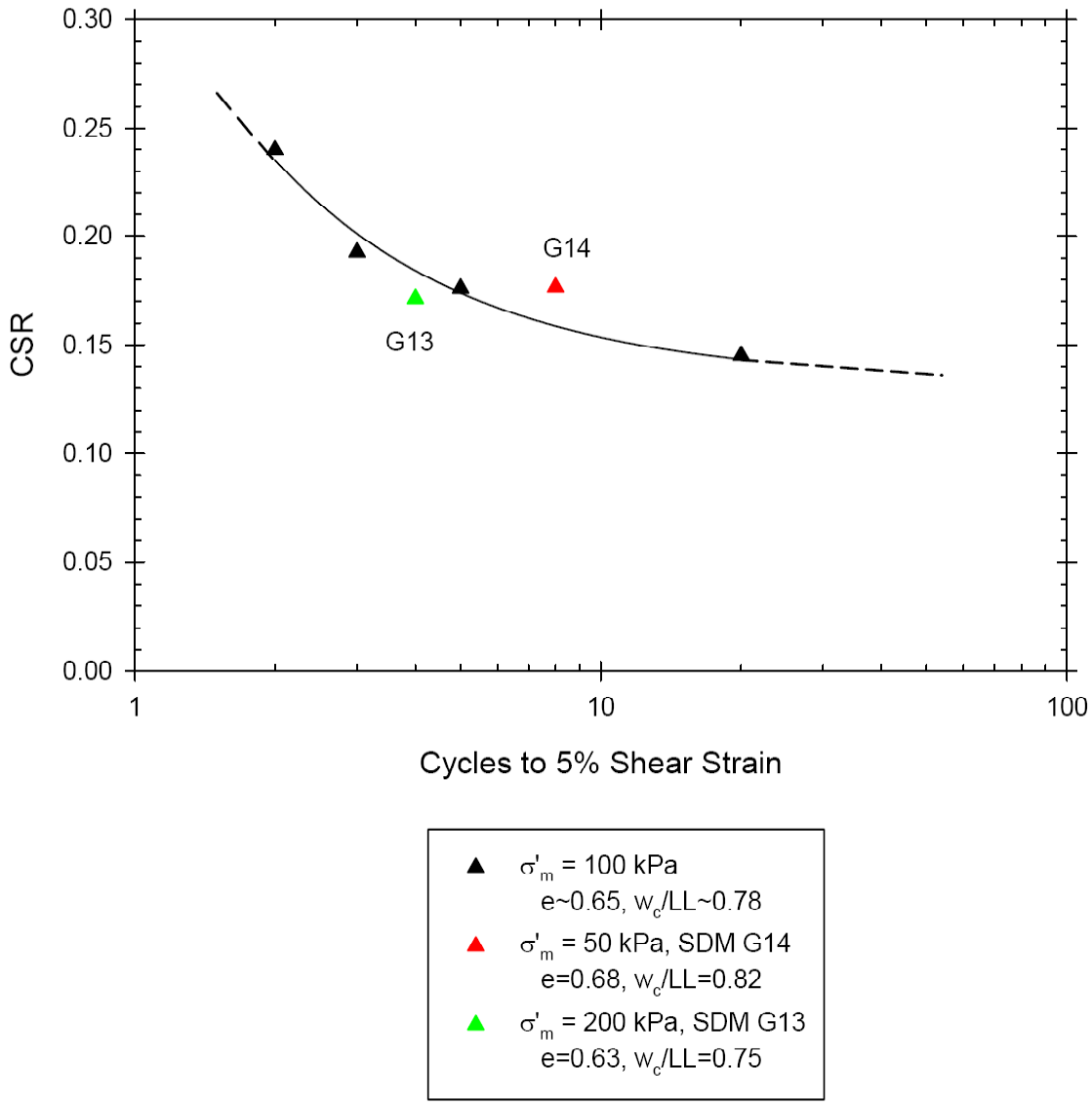

Figure 6.54 CSR Chart of Soil G prepared using the Slurry Deposition Method tested by the cyclic simple shear for different effective confining pressures.

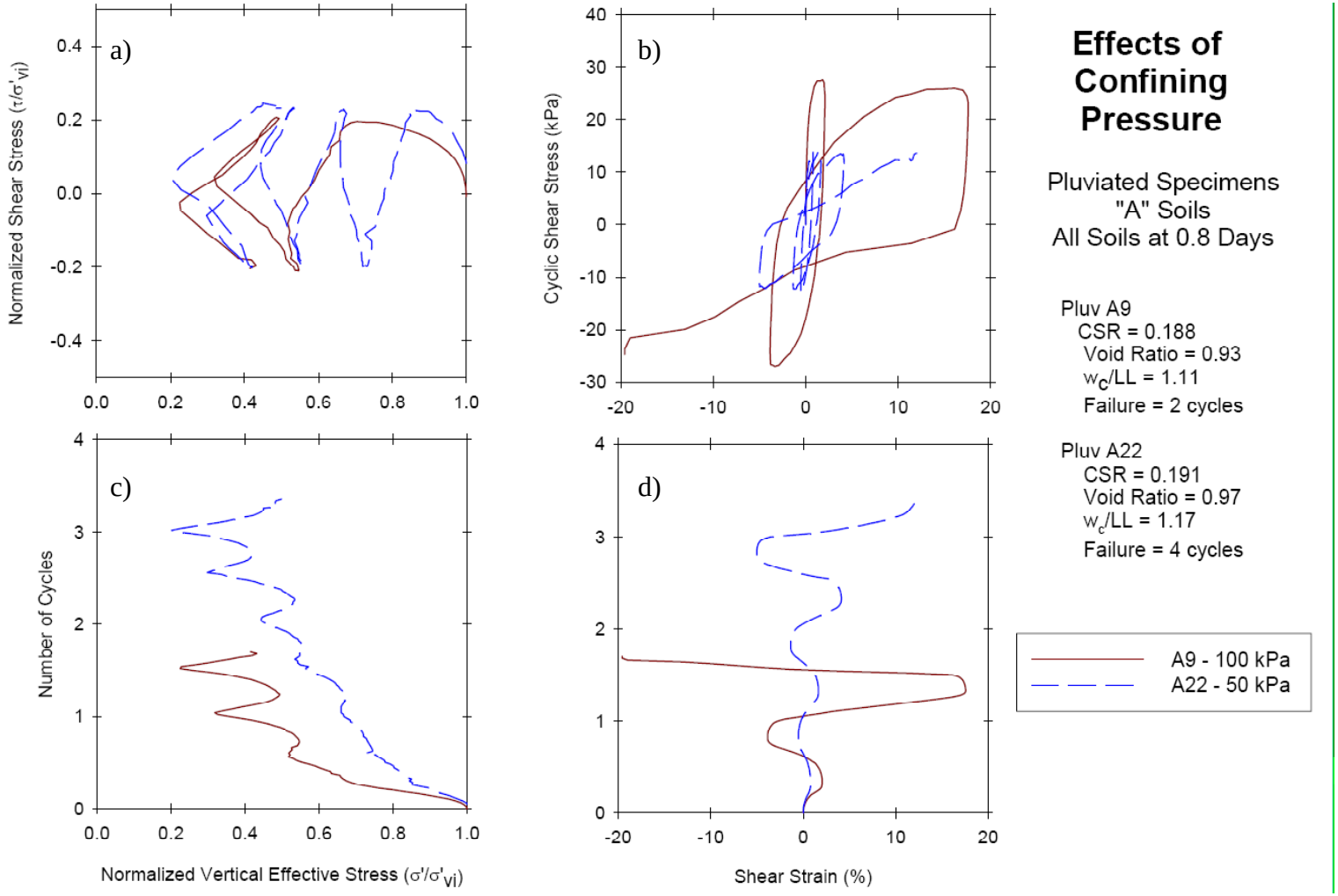

Figure 6.55 4-way plot comparison of a decrease in effective confining pressure effects for Soil A prepared using In-Place Wet Pluviation tested by the cyclic simple shear: a) effective stress path, b) stress-strain diagram, c) normalized vertical effective stress to number of cycles, and d) shear strain to number of cycles of loading.

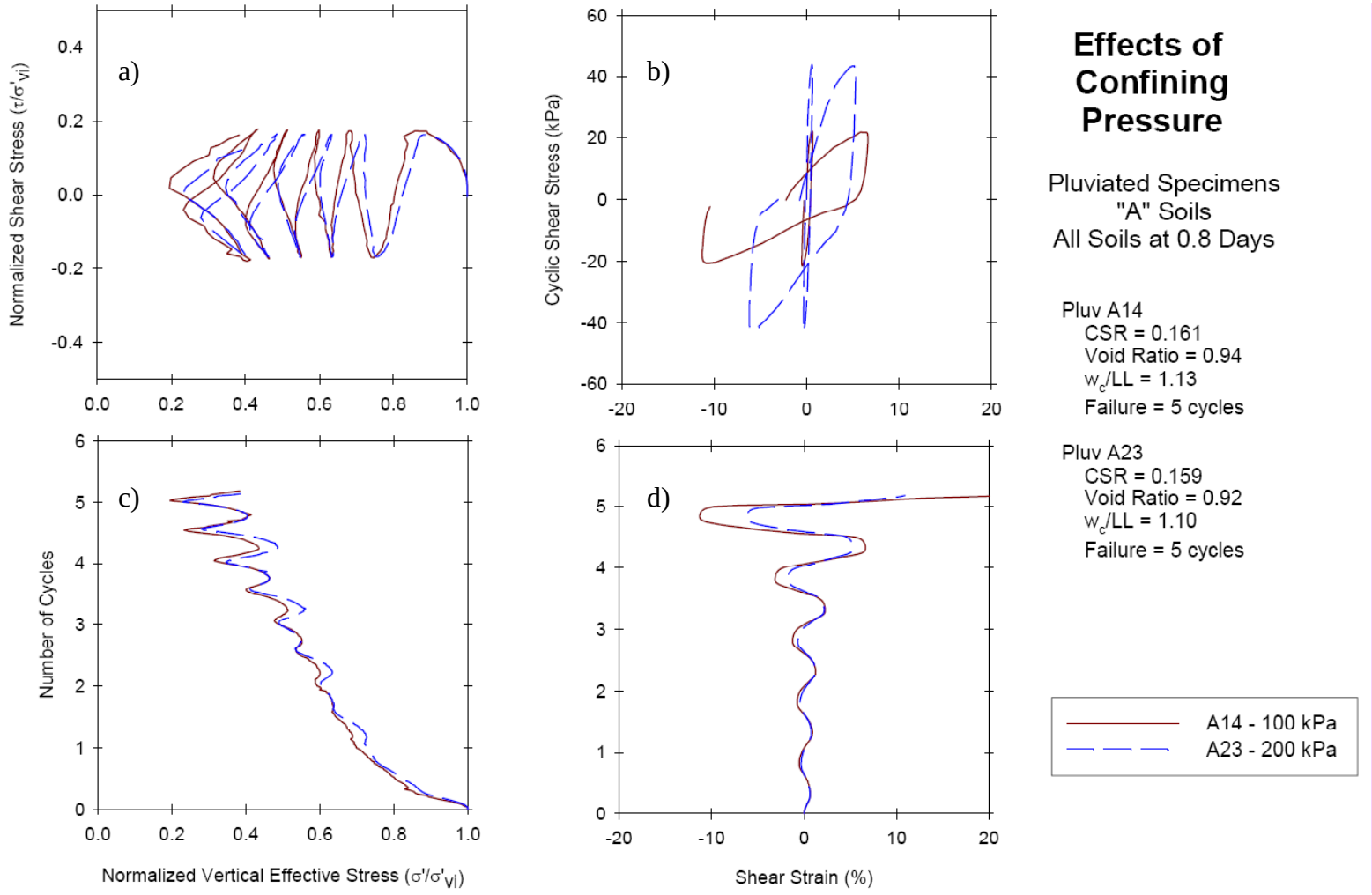

Figure 6.56 4-way plot comparison of an increase in effective confining pressure effects for Soil A prepared using In-Place Wet Pluviation tested by the cyclic simple shear: a) effective stress path, b) stress-strain diagram, c) normalized vertical effective stress to number of cycles, and d) shear strain to number of cycles of loading.

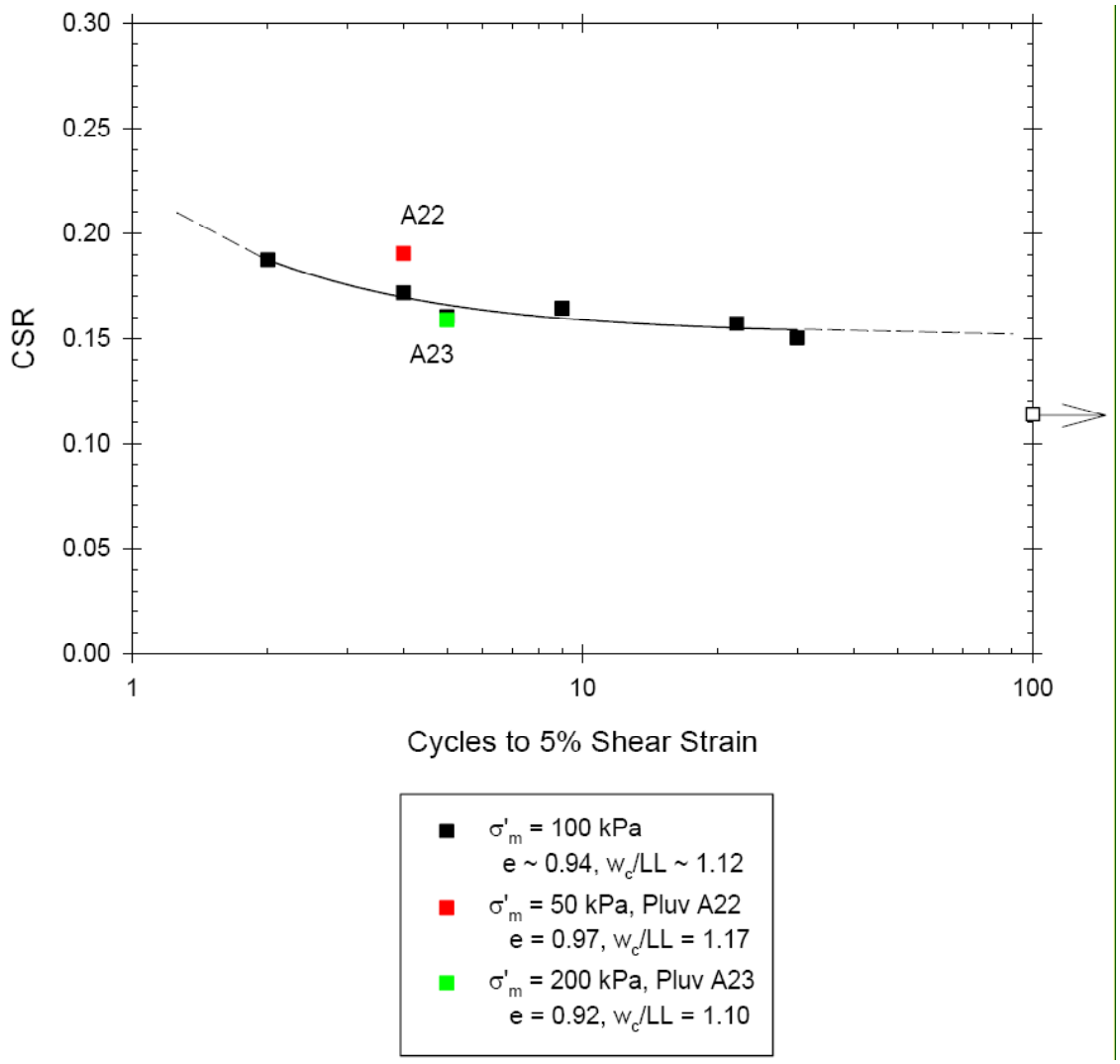

Figure 6.57 CSR Chart of Soil A prepared using In-Place Wet Pluviation tested by the cyclic simple shear for different effective confining pressures.

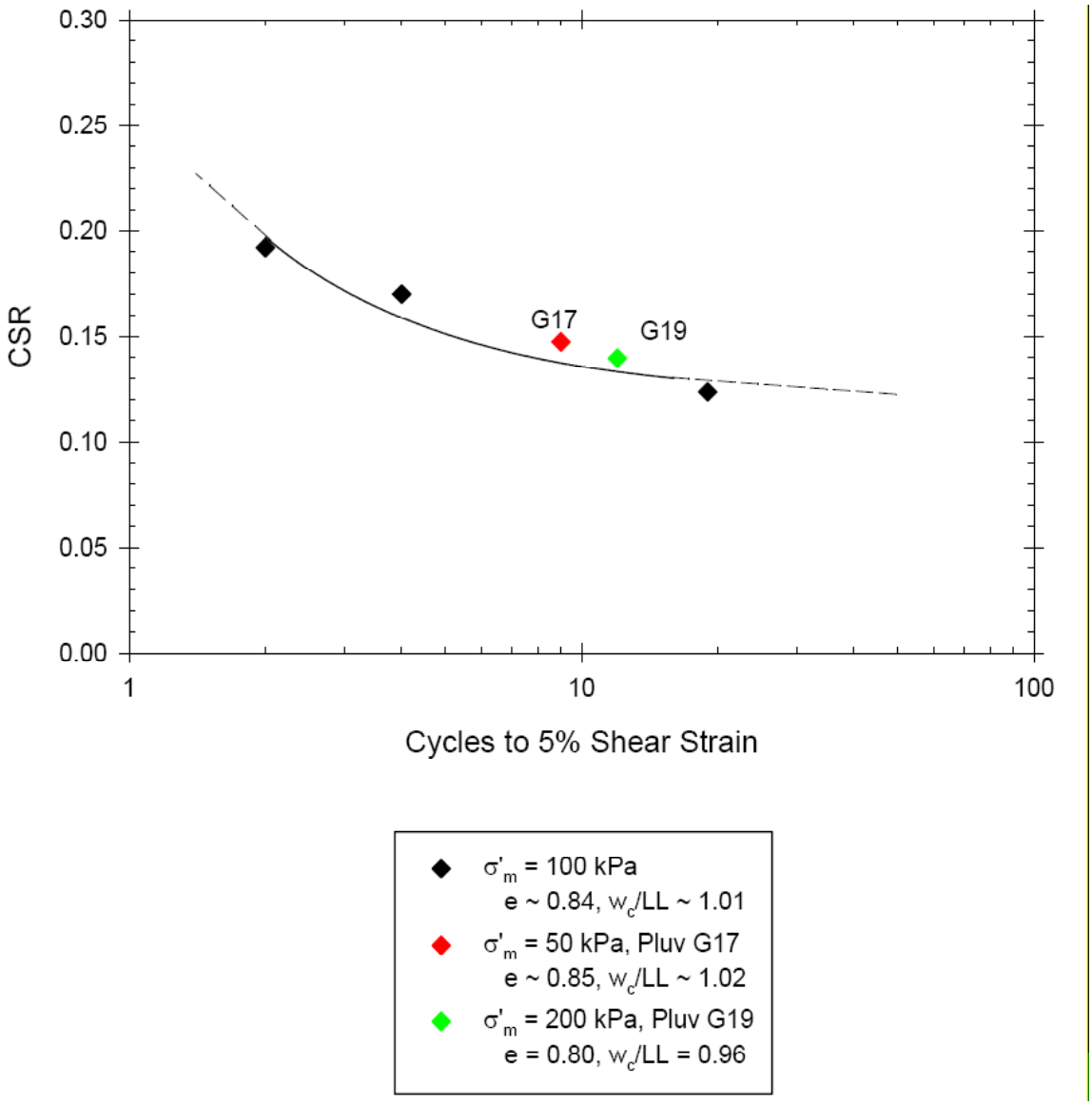

Figure 6.58 CSR Chart of Soil G prepared using In-Place Wet Pluviation tested by the cyclic simple shear for different effective confining pressures.

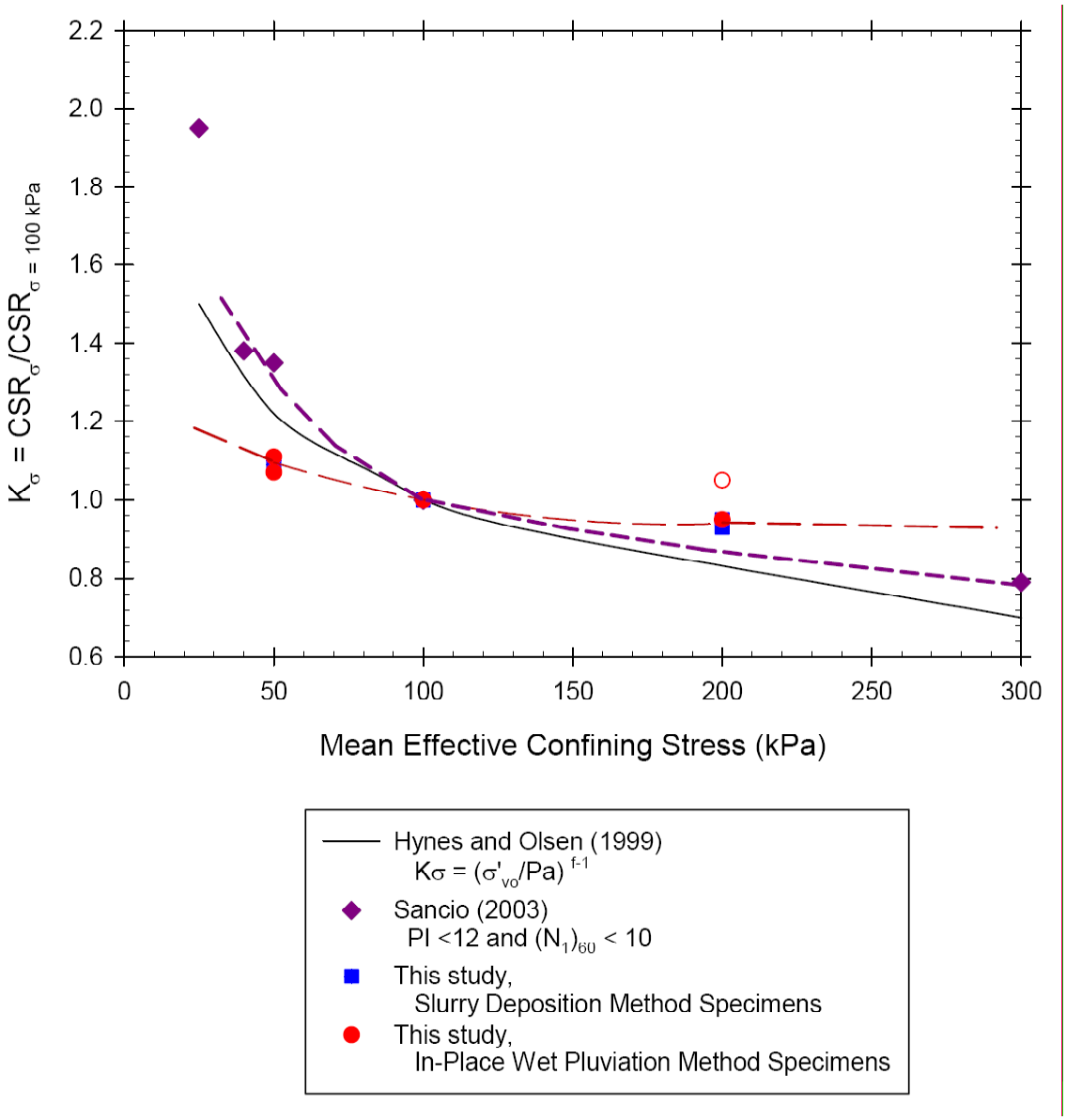

Figure 6.59 Normalized effect of the effective confining pressure on the liquefaction resistance of soils.

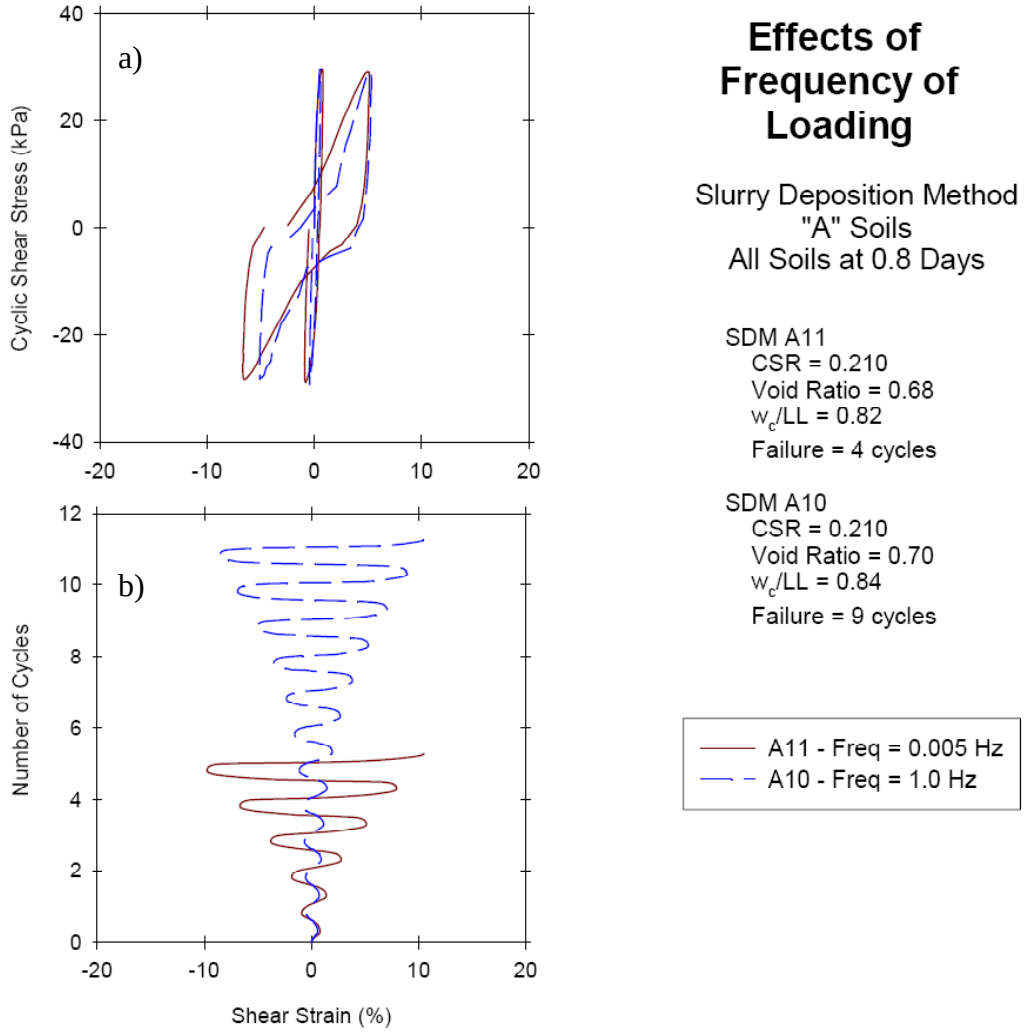

Figure 6.60 4-way plot comparison of frequency of loading effects for Soil A prepared using the Slurry Deposition Method tested by the cyclic simple shear, $\sigma'_v \approx 137$ kPa: a) stress-strain diagram and b) shear strain to number of cycles of loading.

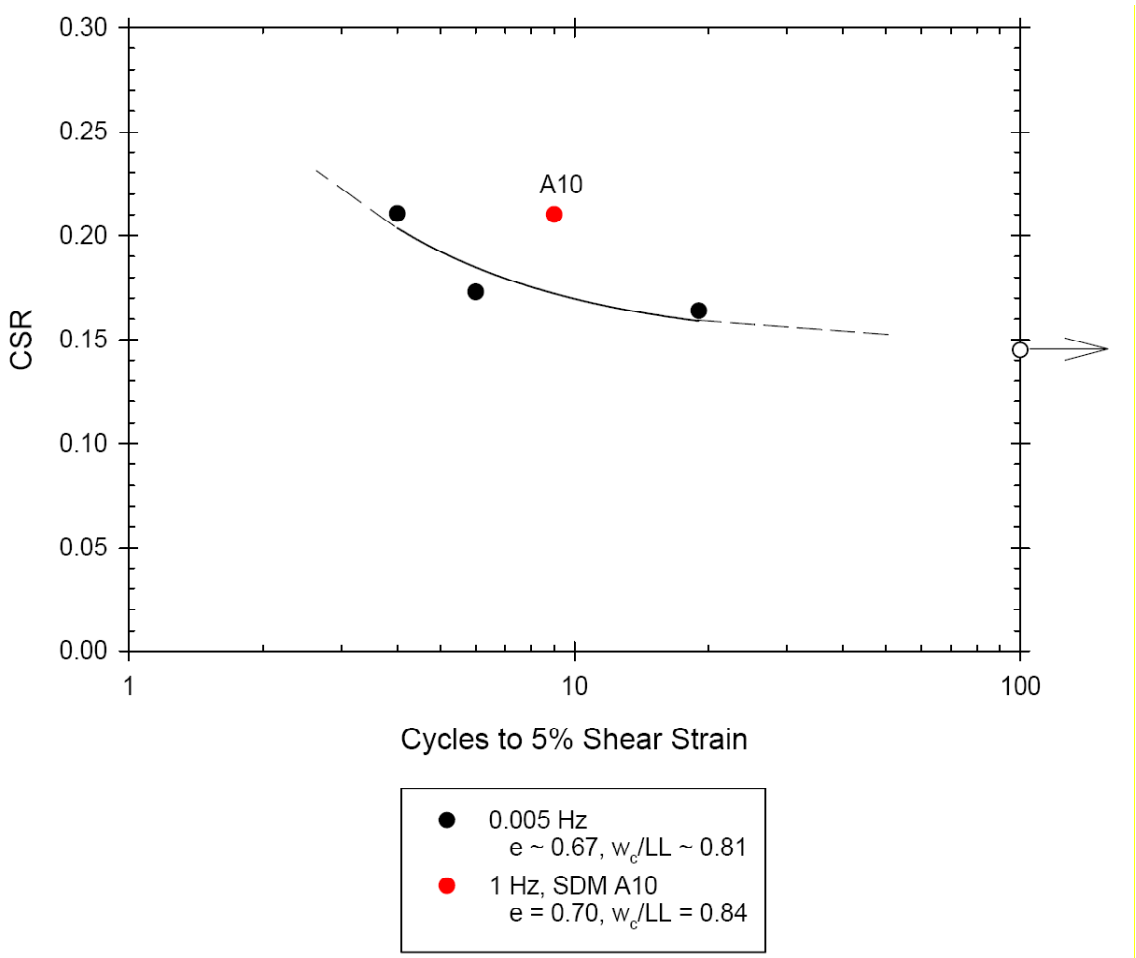

Figure 6.61 CSR Chart of Soil A prepared using the Slurry Deposition Method tested by the cyclic simple shear for different frequencies of loading, all tests at $\sigma'_v \approx 137$ kPa.

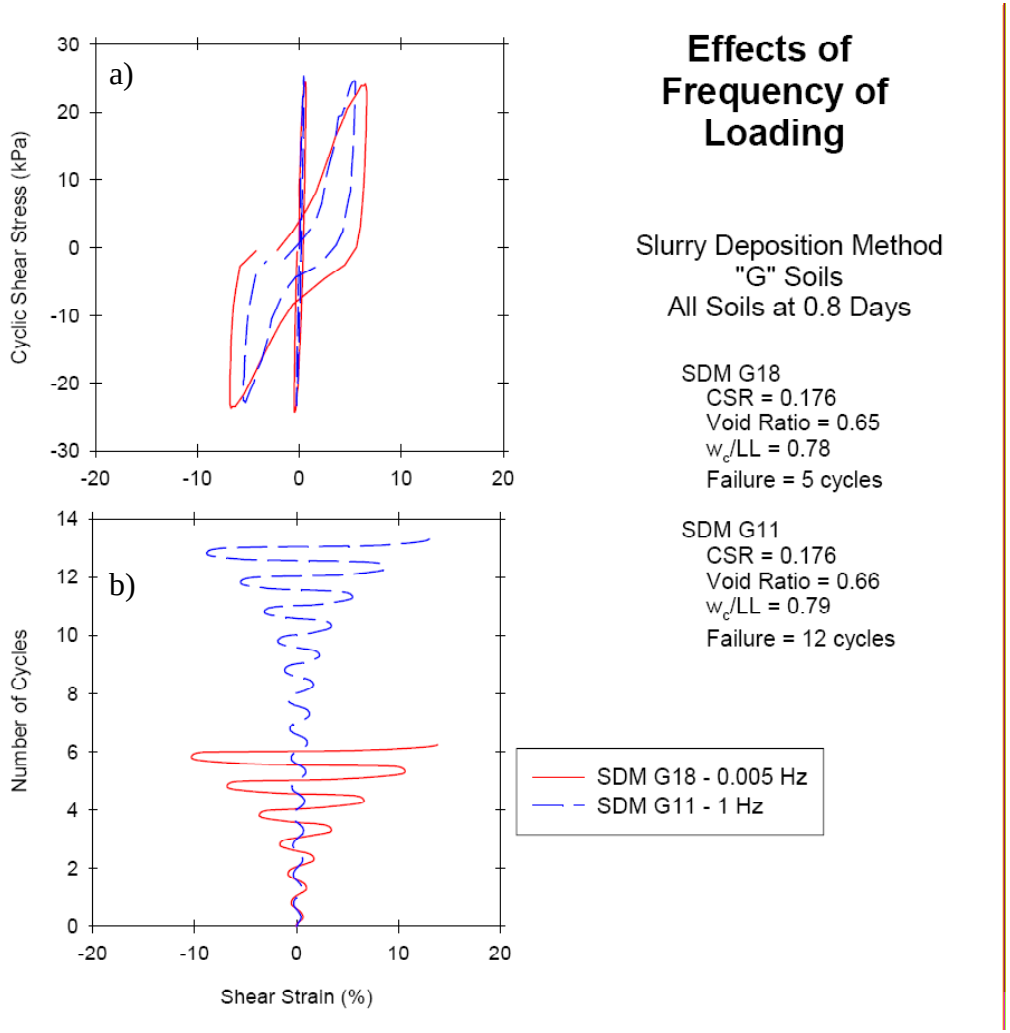

Figure 6.62 4-way plot comparison of frequency of loading effects for Soil G prepared using the Slurry Deposition Method tested by the cyclic simple shear, $\sigma'_v \approx 137$ kPa: a) stress-strain diagram and b) shear strain to number of cycles of loading.

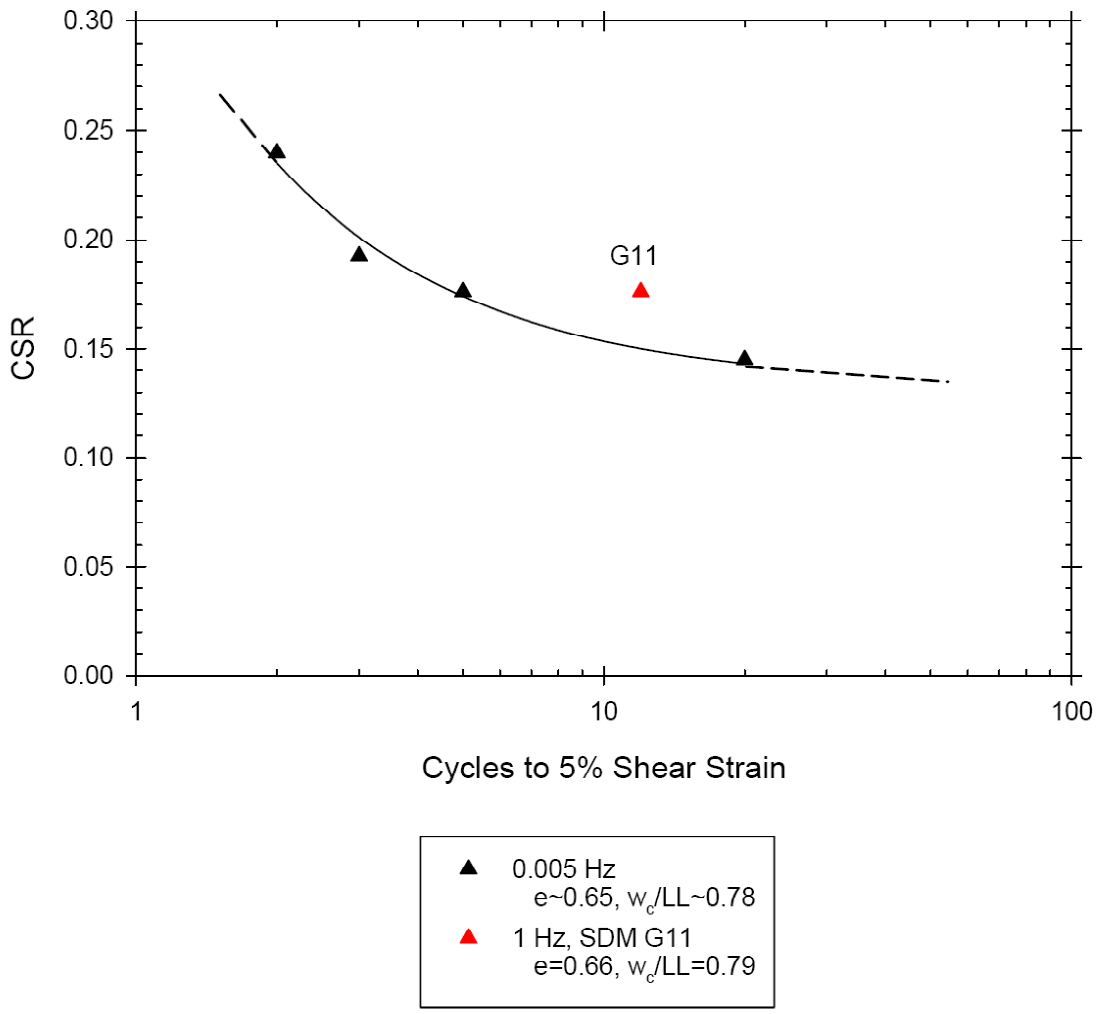

Figure 6.63 CSR Chart of Soil G prepared using the Slurry Deposition Method tested by the cyclic simple shear for different frequencies of loading, all tests at $\sigma'_v \approx 137$ kPa.

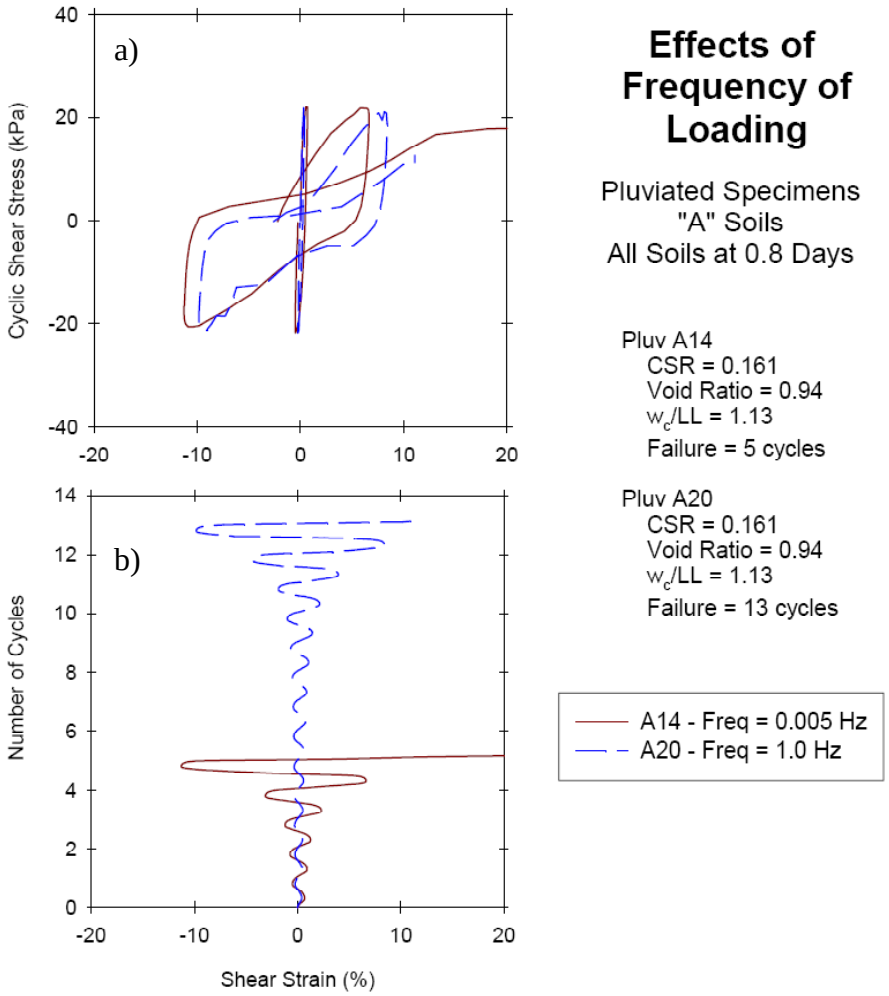

Figure 6.64 4-way plot comparison of frequency of loading effects for Soil A prepared using In-Place Wet Pluviation tested by the cyclic simple shear, $\sigma'_v \approx 137$ kPa: a) stress-strain diagram and b) shear strain to number of cycles of loading.

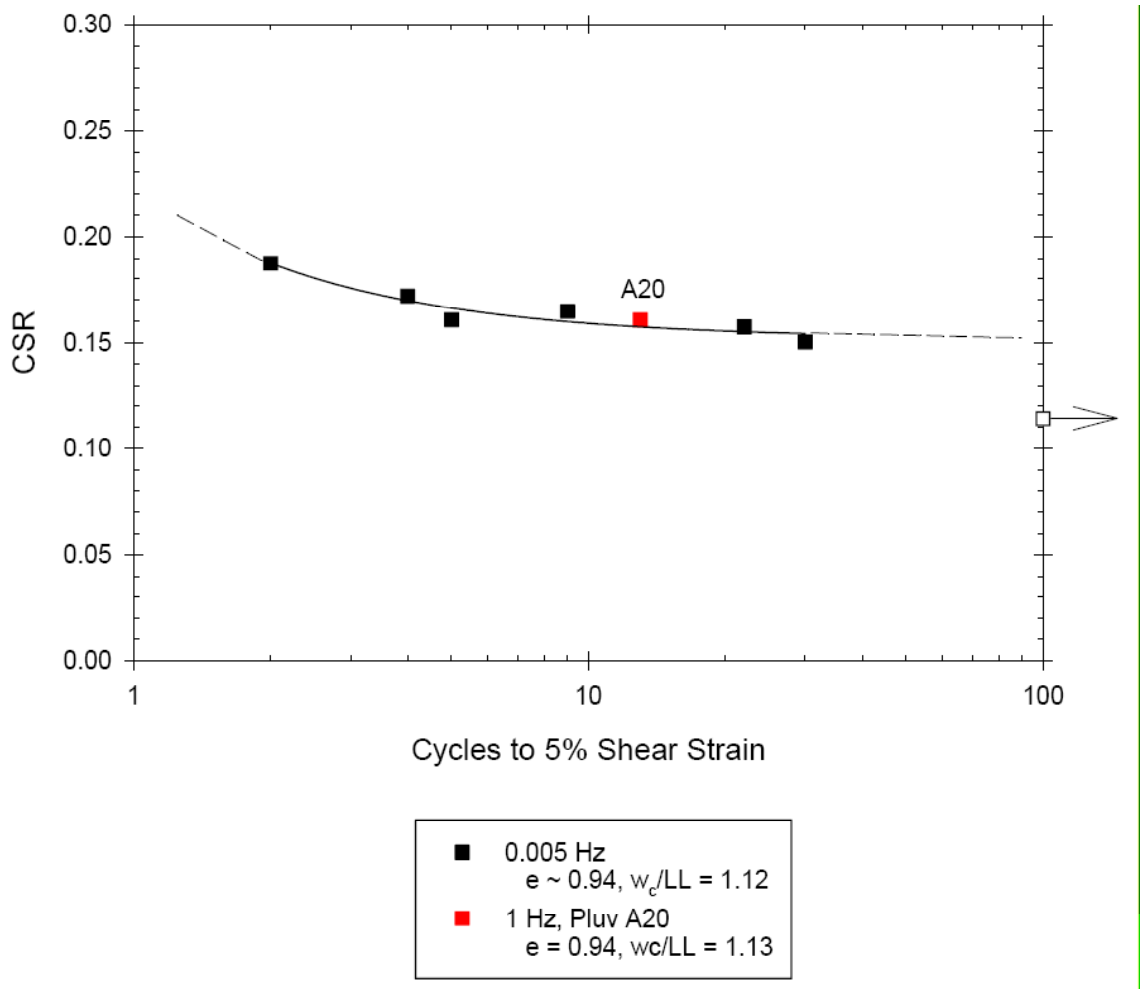

Figure 6.65 CSR Chart of Soil A prepared using In-Place Wet Pluviation tested by the cyclic simple shear for different frequencies of loading, all tests at $\sigma'_v \approx 137$ kPa.

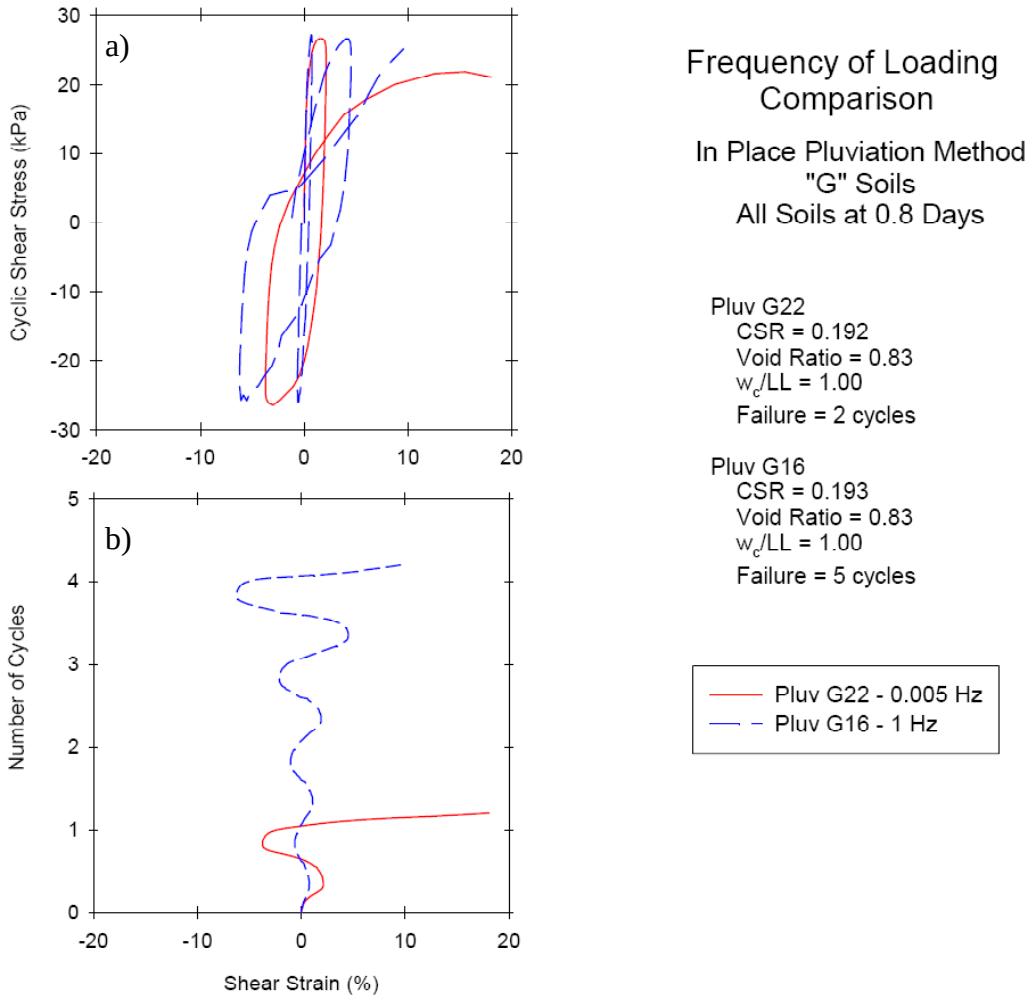

Figure 6.66 4-way plot comparison of frequency of loading effects for Soil G prepared using In-Place Wet Pluviation tested by the cyclic simple shear, $\sigma'_v \approx 137$ kPa: a) stress-strain diagram and b) shear strain to number of cycles of loading.

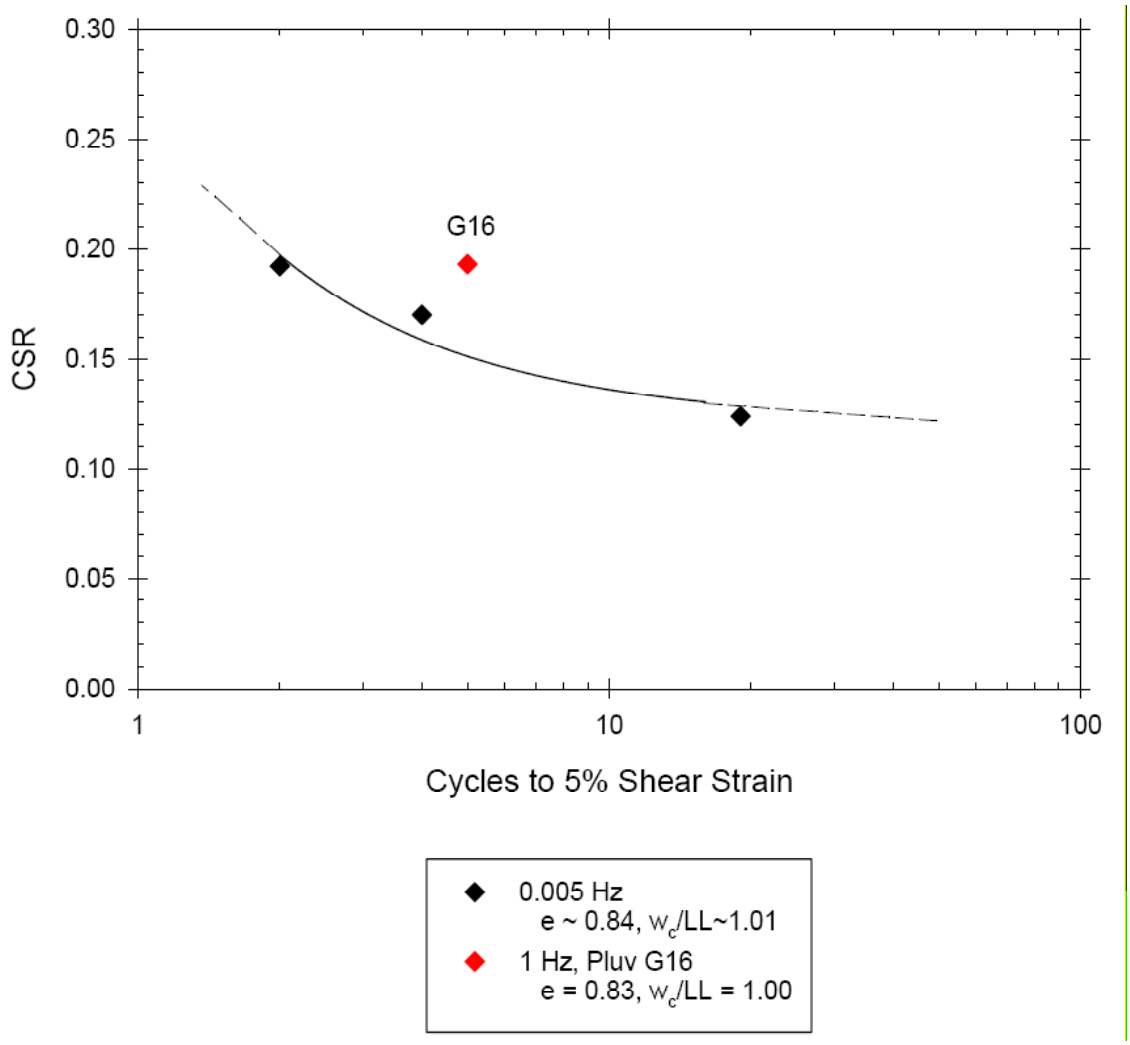

Figure 6.67 CSR Chart of Soil G prepared using In-Place Wet Pluviation tested by the cyclic simple shear for different frequencies of loading, all tests at $\sigma'_v \approx 137$ kPa.

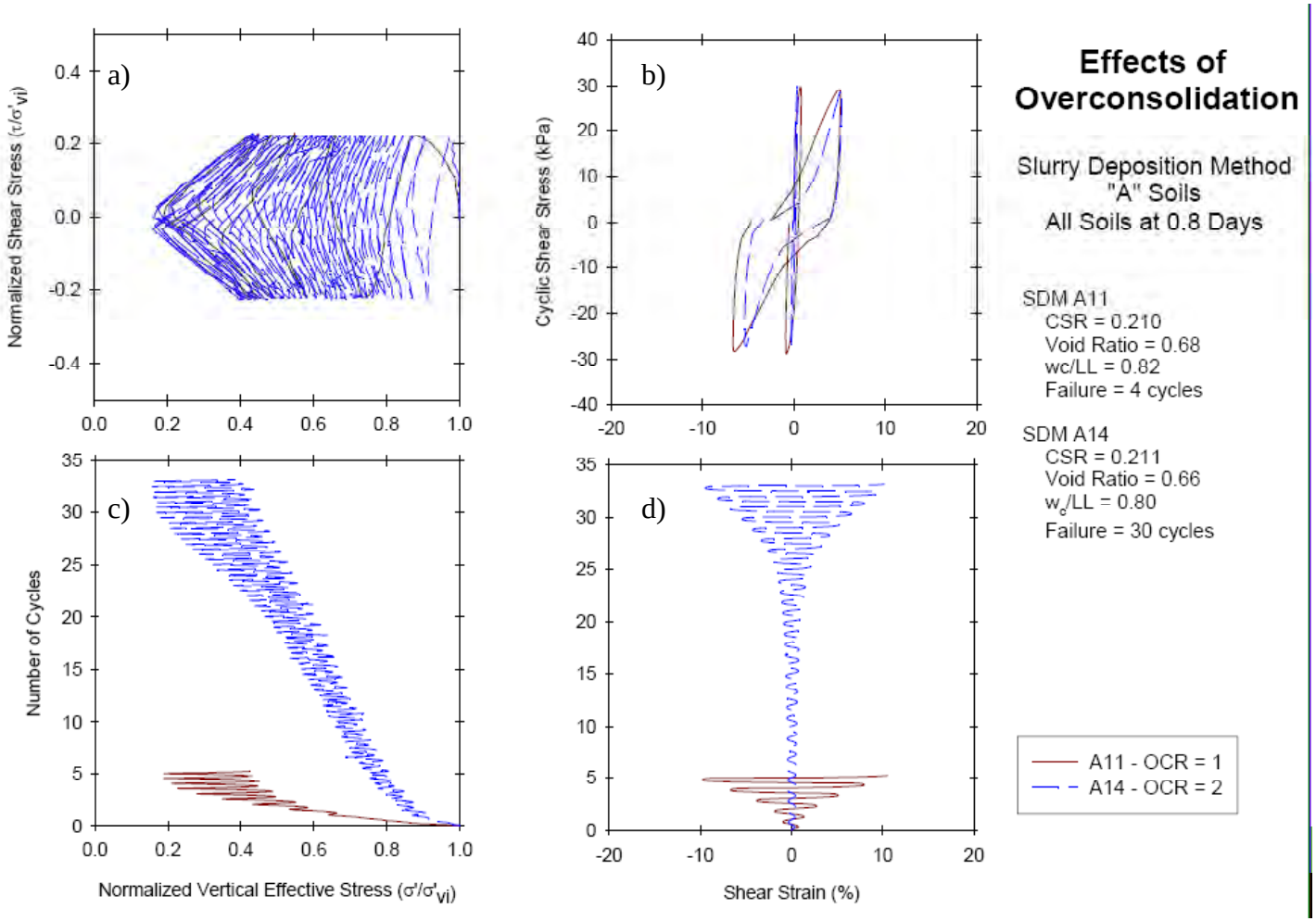

Figure 6.68 4-way plot comparison of OCR effects for Soil A prepared using the Slurry Deposition Method tested by the cyclic simple shear, $\sigma'_v \approx 137$ kPa: a) effective stress path, b) stress-strain diagram, c) normalized vertical effective stress to number of cycles, and d) shear strain to number of cycles of loading.

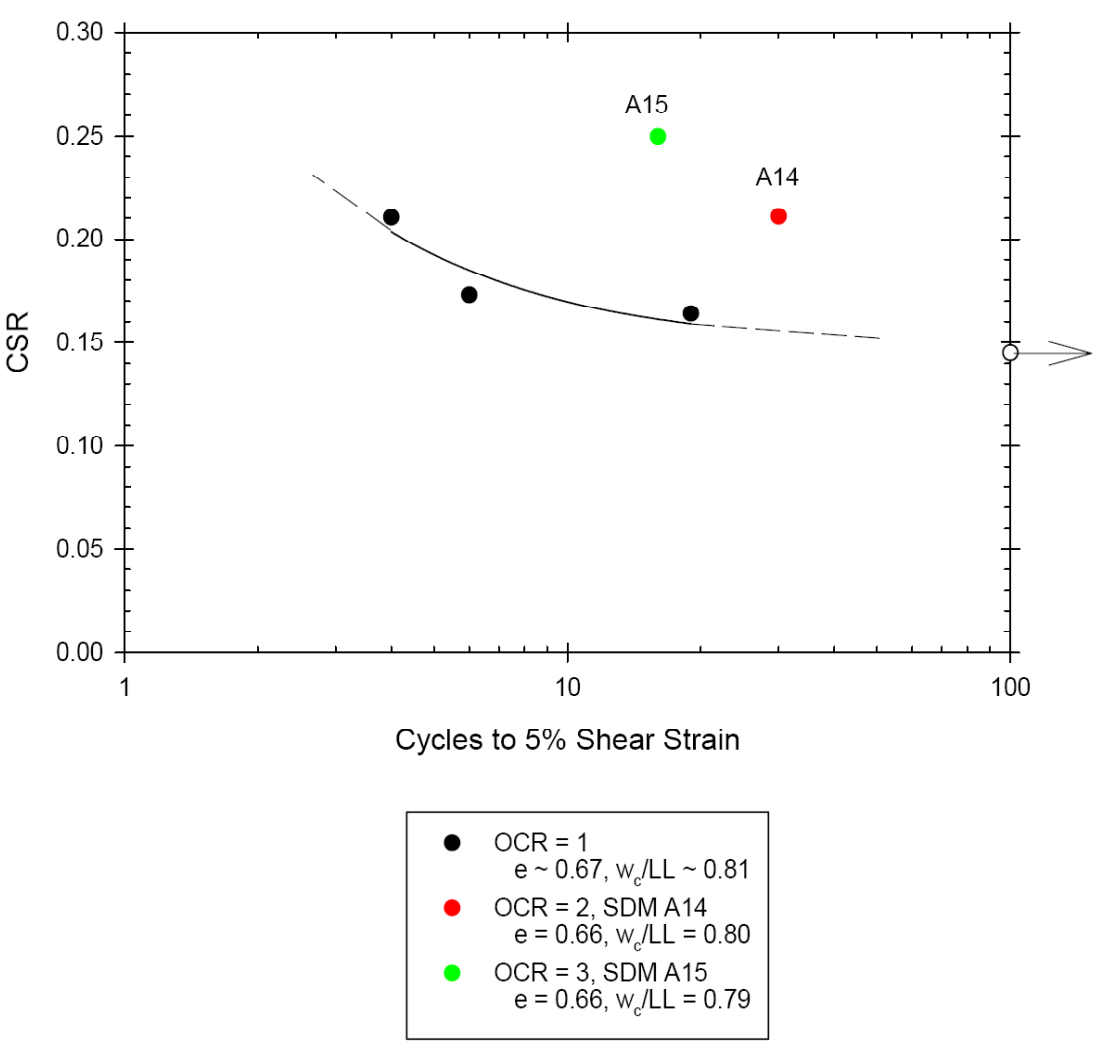

Figure 6.69 CSR Chart of Soil A prepared using the Slurry Deposition Method tested by the cyclic simple shear for different OCRs, all tests at $\sigma'_v \approx 137$ kPa.

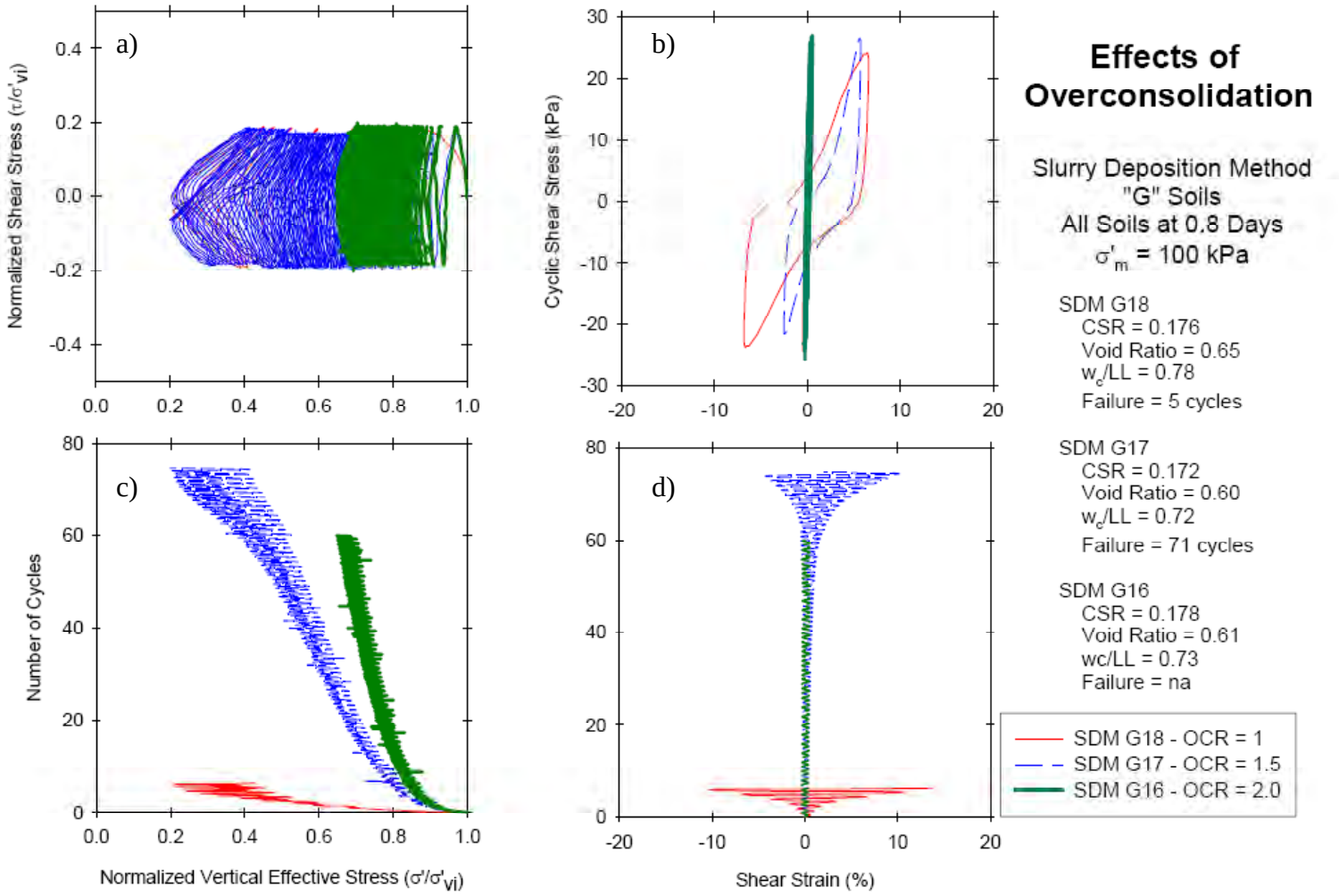

Figure 6.70 4-way plot comparison of OCR effects for Soil G prepared using the Slurry Deposition Method tested by the cyclic simple shear, $\sigma'_v \approx 137$ kPa: a) effective stress path, b) stress-strain diagram, c) normalized vertical effective stress to number of cycles, and d) shear strain to number of cycles of loading.

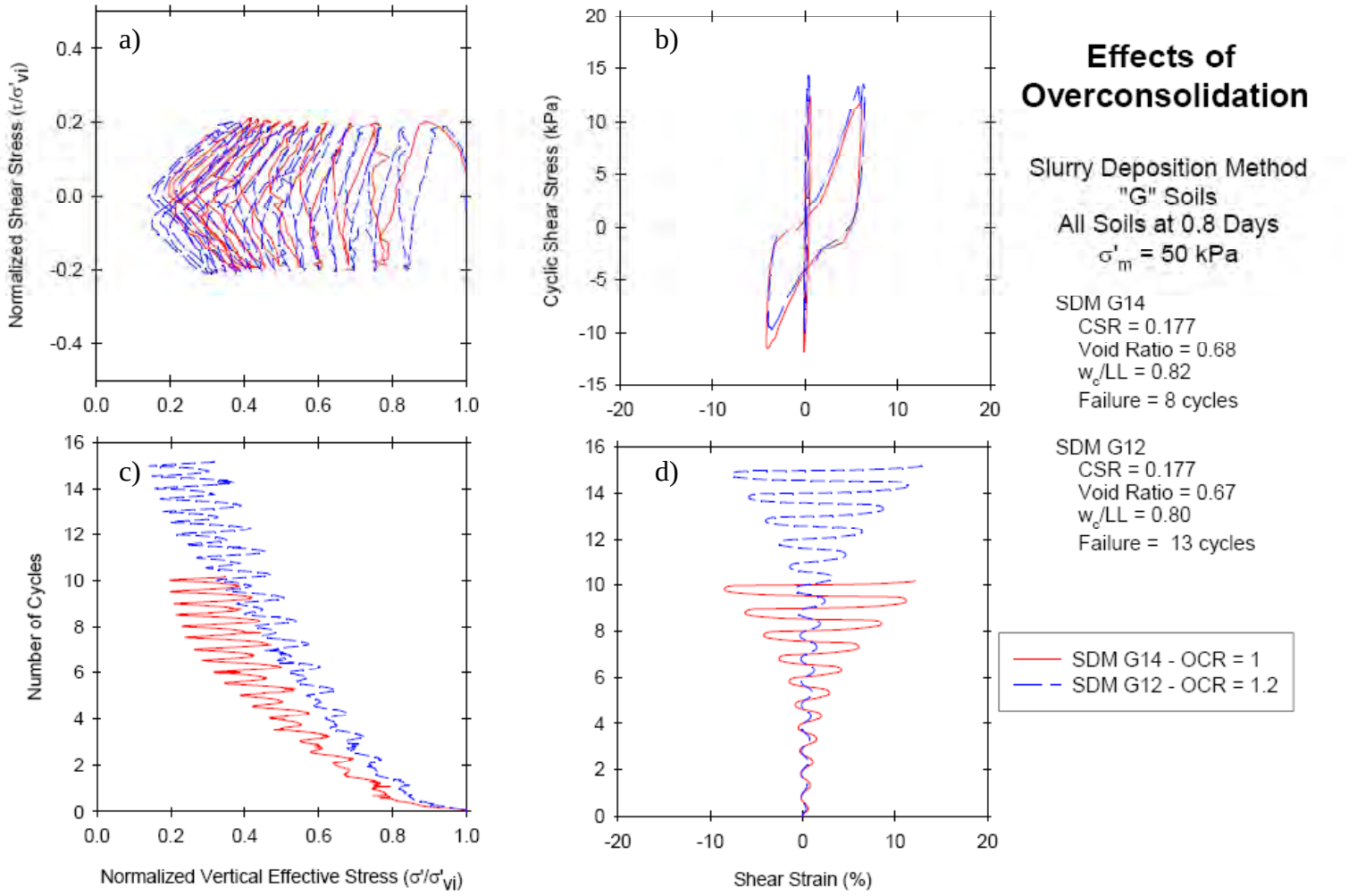

Figure 6.71 4-way plot comparison of OCR effects for Soil G prepared using the Slurry Deposition Method tested by the cyclic simple shear, $\sigma'_v \approx 68$ kPa: a) effective stress path, b) stress-strain diagram, c) normalized vertical effective stress to number of cycles, and d) shear strain to number of cycles of loading.

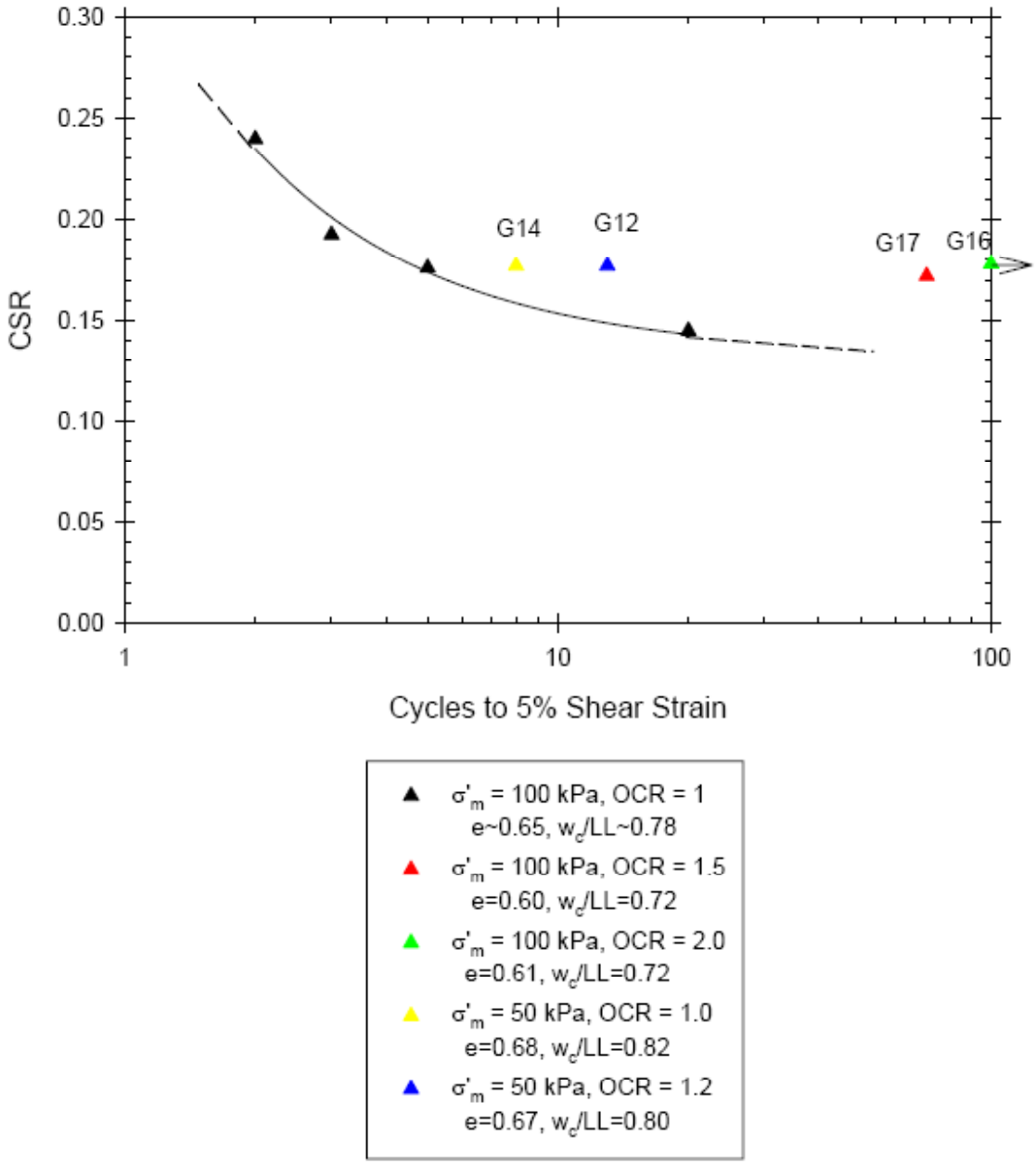

Figure 6.72 CSR Chart of Soil G prepared using the Slurry Deposition Method tested by the cyclic simple shear for different OCRs.

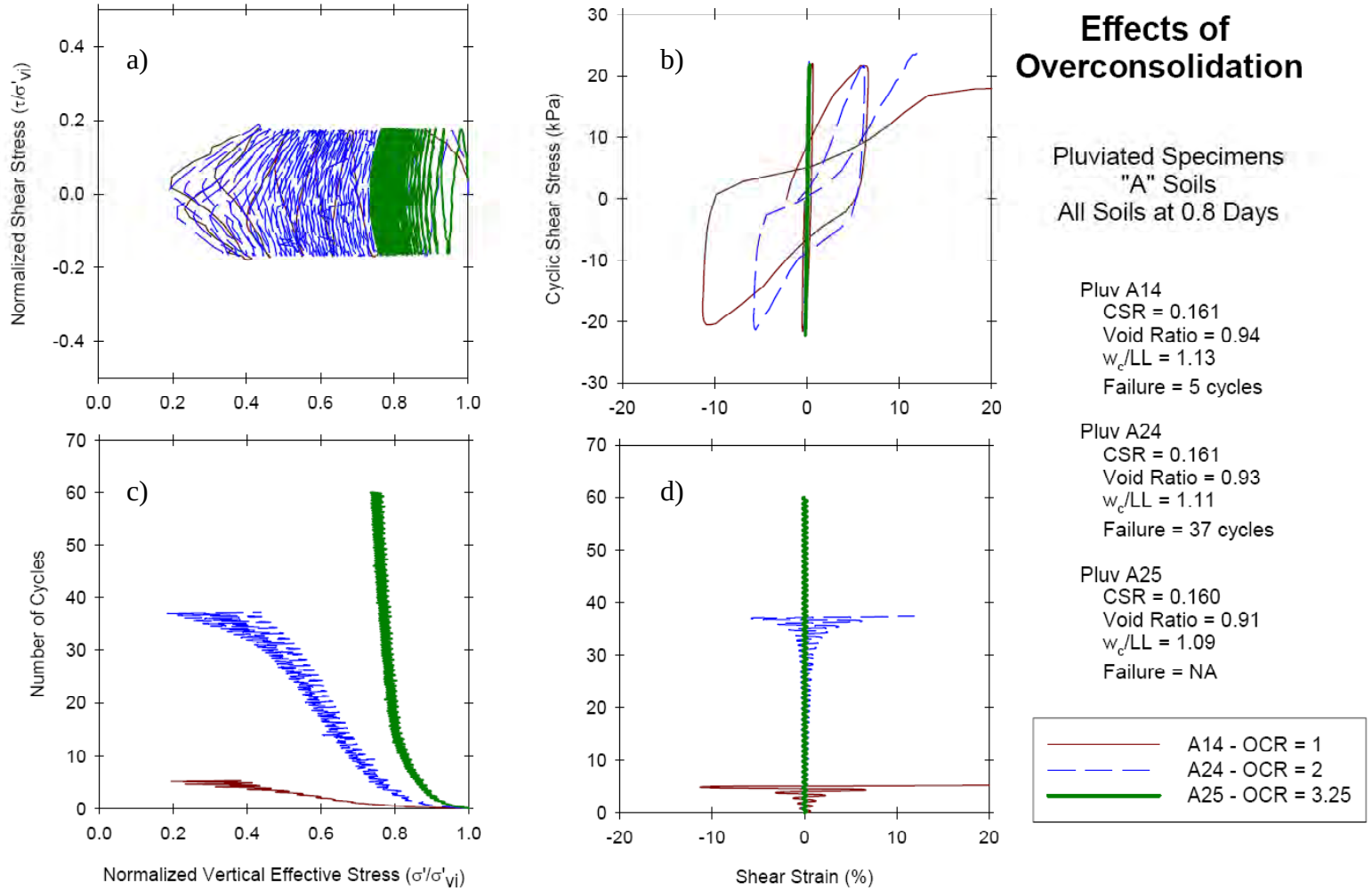

Figure 6.73 4-way plot comparison of OCR effects for Soil A prepared using In-Place Wet Pluviation tested by the cyclic simple shear, $\sigma'_v \approx 137$ kPa: a) effective stress path, b) stress-strain diagram, c) normalized vertical effective stress to number of cycles, and d) shear strain to number of cycles of loading.

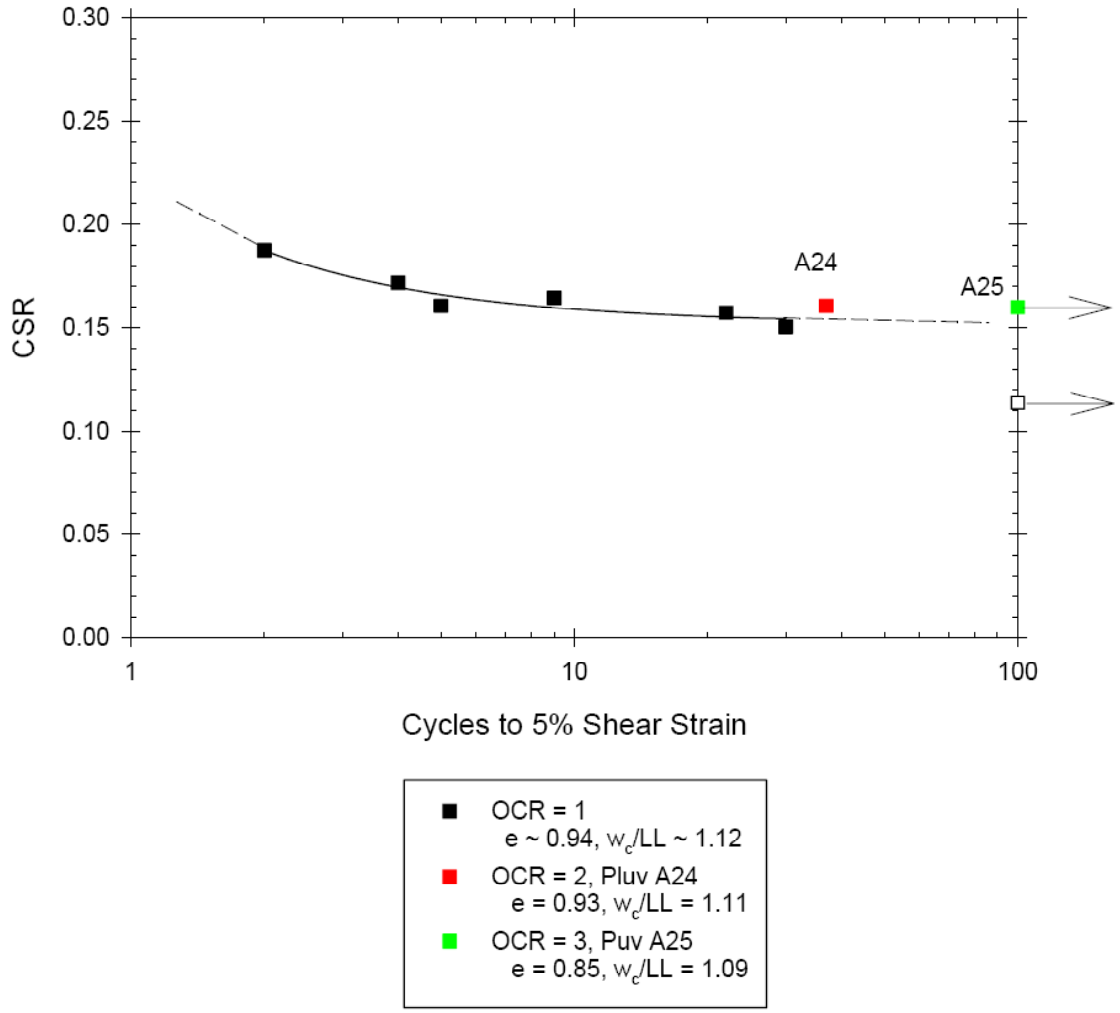

Figure 6.74 CSR Chart of Soil A prepared using In-Place Wet Pluviation tested by the cyclic simple shear for different OCRs, all tests at $\sigma'_v \approx 137$ kPa.

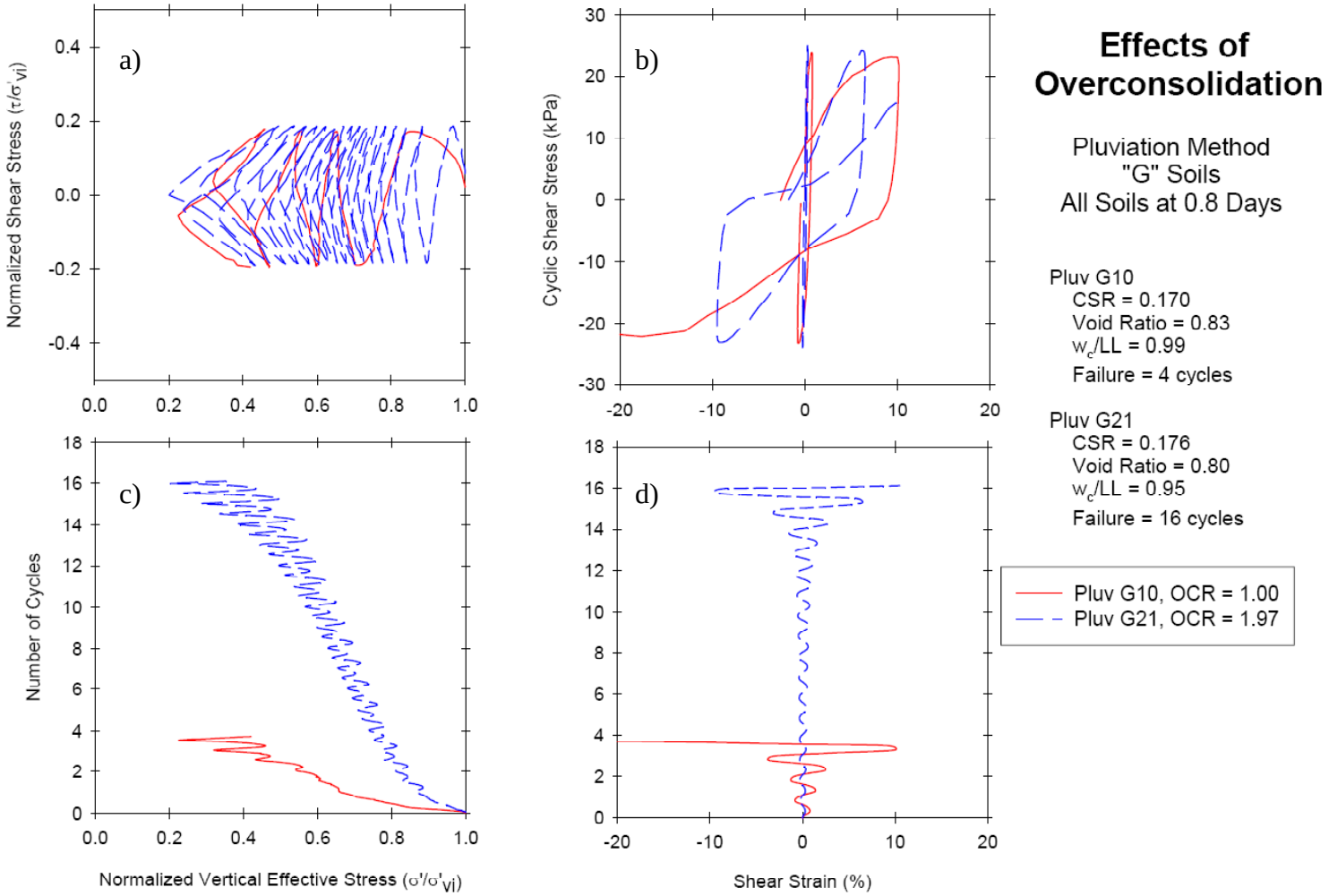

Figure 6.75 4-way plot comparison of OCR effects for Soil A prepared using In-Place Wet Pluviation tested by the cyclic simple shear, $\sigma'_v \approx 137$ kPa: a) effective stress path, b) stress-strain diagram, c) normalized vertical effective stress to number of cycles, and d) shear strain to number of cycles of loading.

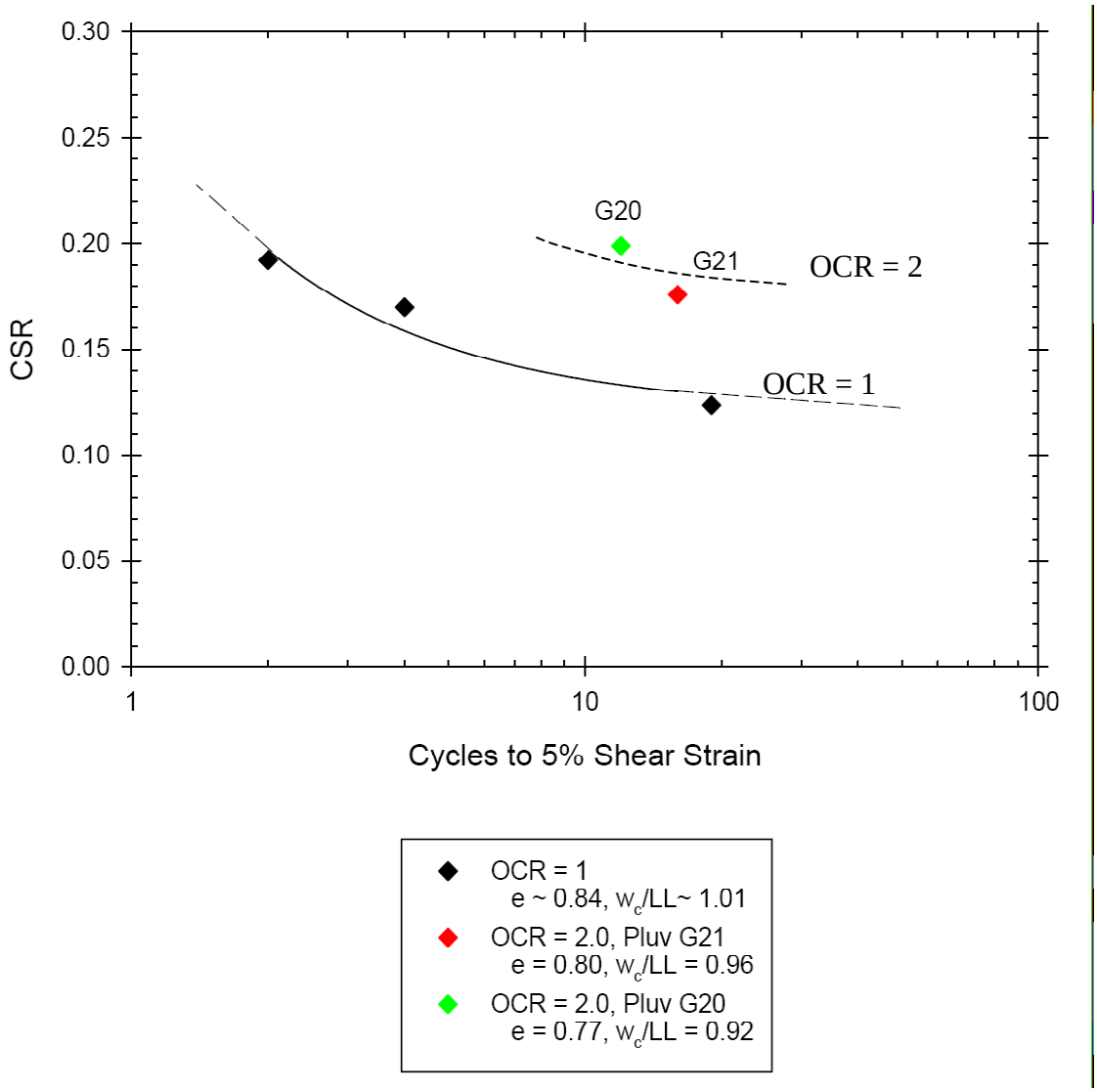

Figure 6.76 CSR Chart of Soil G prepared using In-Place Wet Pluviation tested by the cyclic simple shear for different OCRs, all tests at $\sigma'_v \approx 137$ kPa.

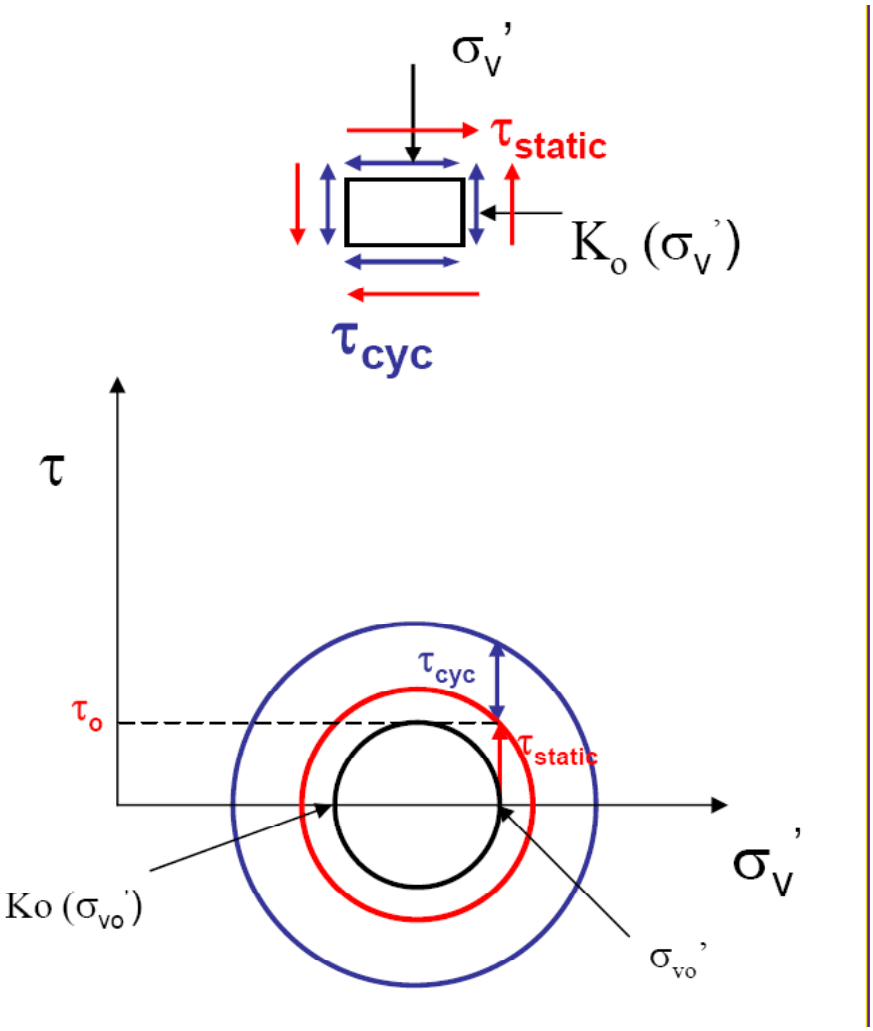

Figure 6.77 Stresses during anisotropically consolidated cyclic simple shear testing on specimens with initial static shear stress.

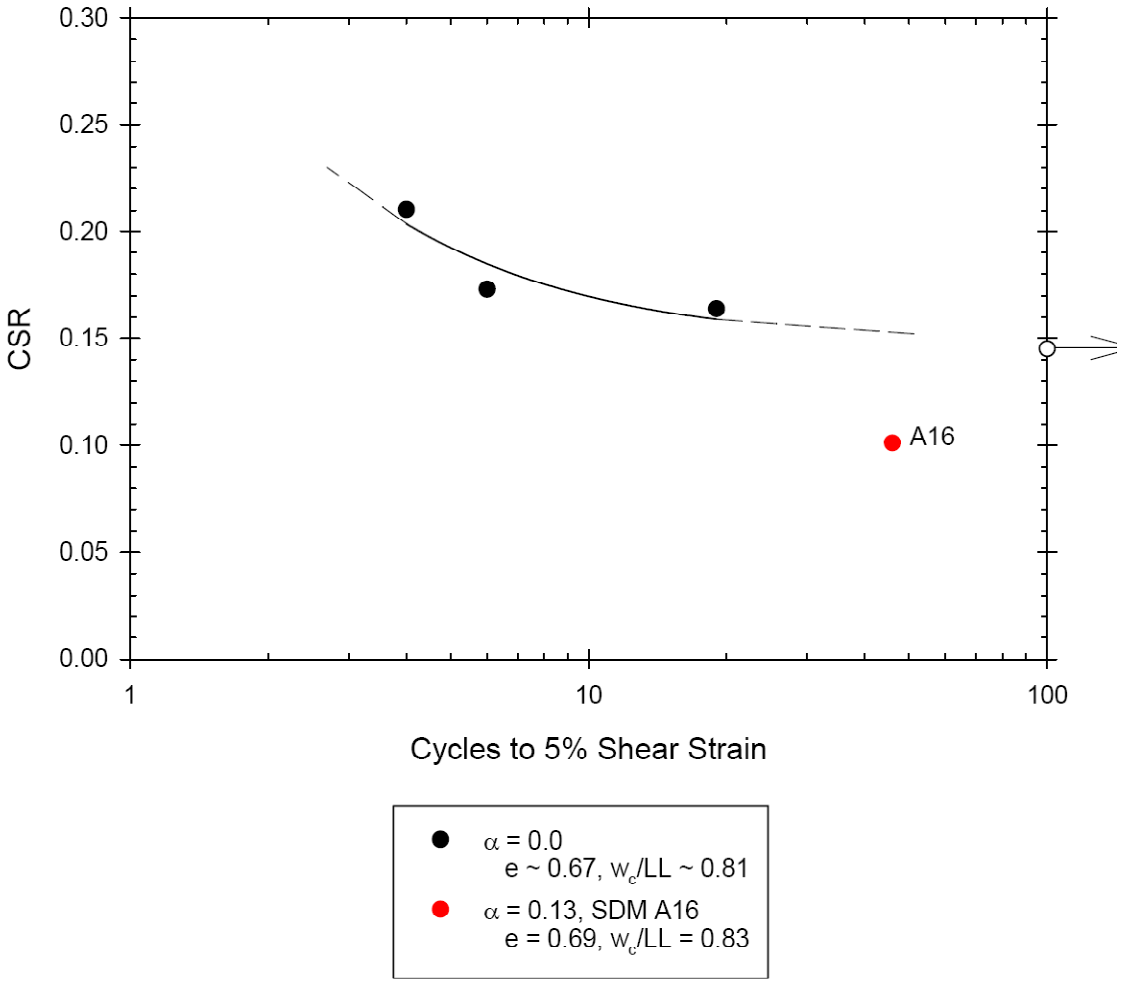

Figure 6.78 CSR Chart of Soil A prepared using the Slurry Deposition Method tested by the cyclic simple shear for initial static shear, all tests at $\sigma'_v \approx 137$ kPa.

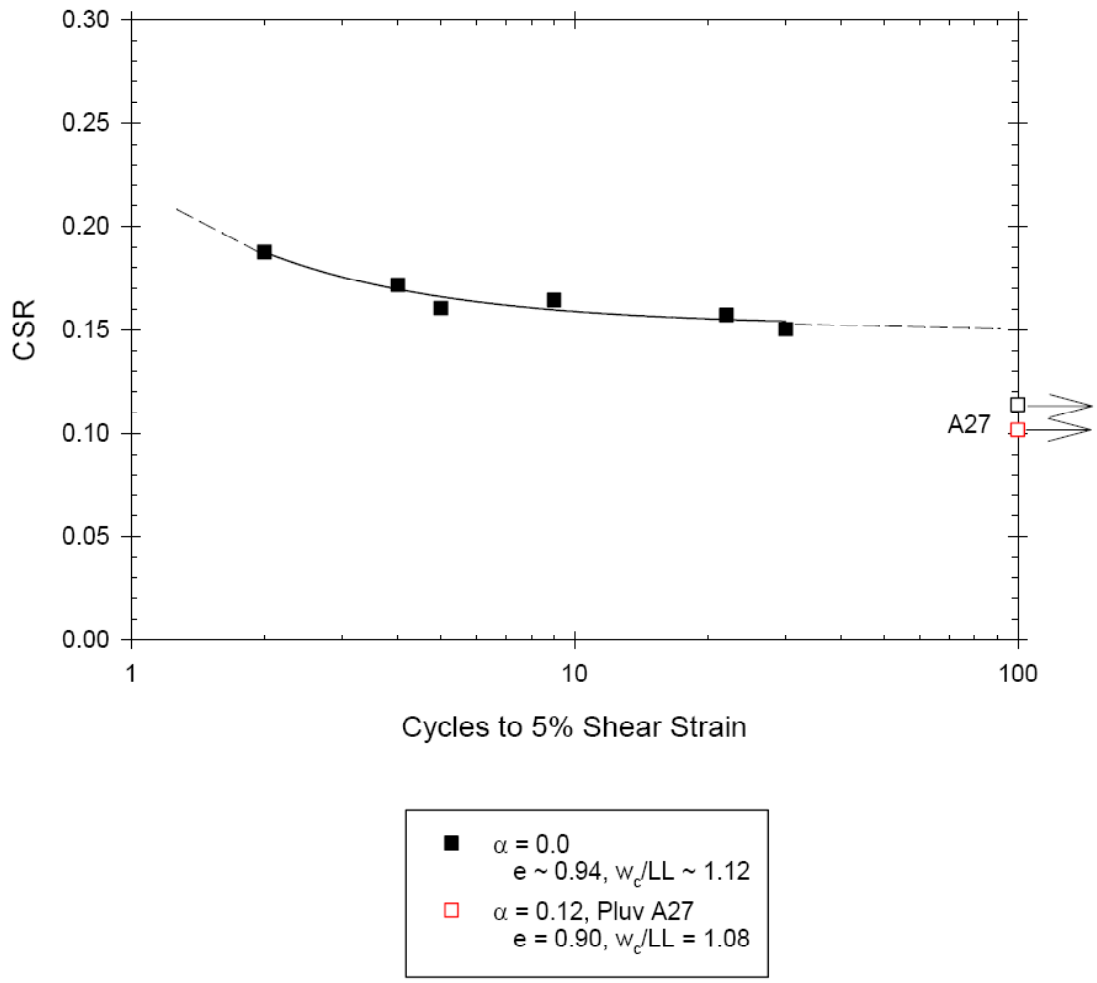

Figure 6.79 CSR Chart of Soil A prepared using In-Place Wet Pluviation tested by the cyclic simple shear for initial static shear, all tests at $\sigma'_v \approx 137$ kPa.

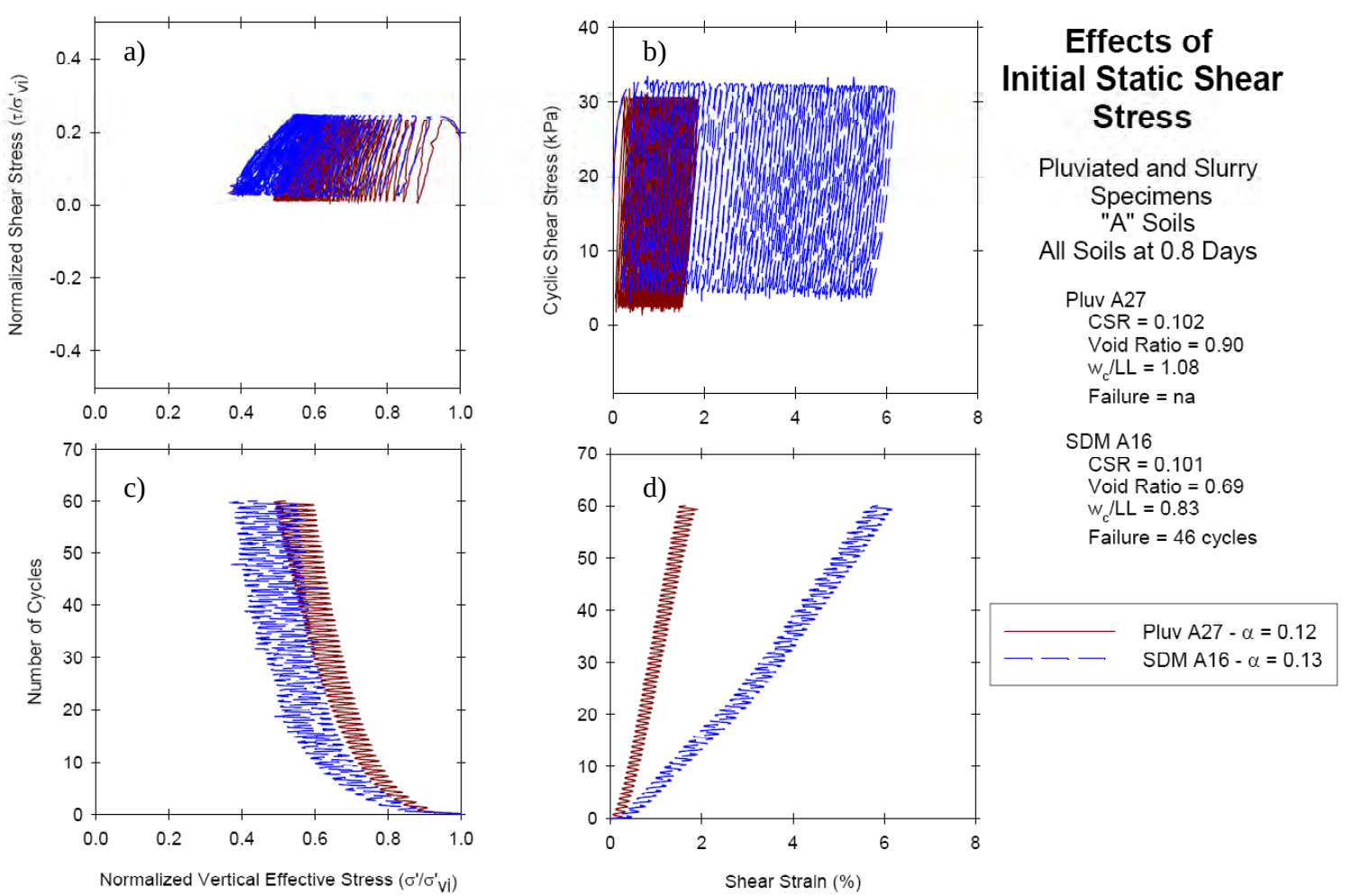

Figure 6.80 4-way plot comparison of initial static shear on Soil A using both reconstitution methods tested by the cyclic simple shear, $\sigma'_v \approx 137$ kPa: a) effective stress path, b) stress-strain diagram, c) normalized vertical effective stress to number of cycles, and d) shear strain to number of cycles of loading.

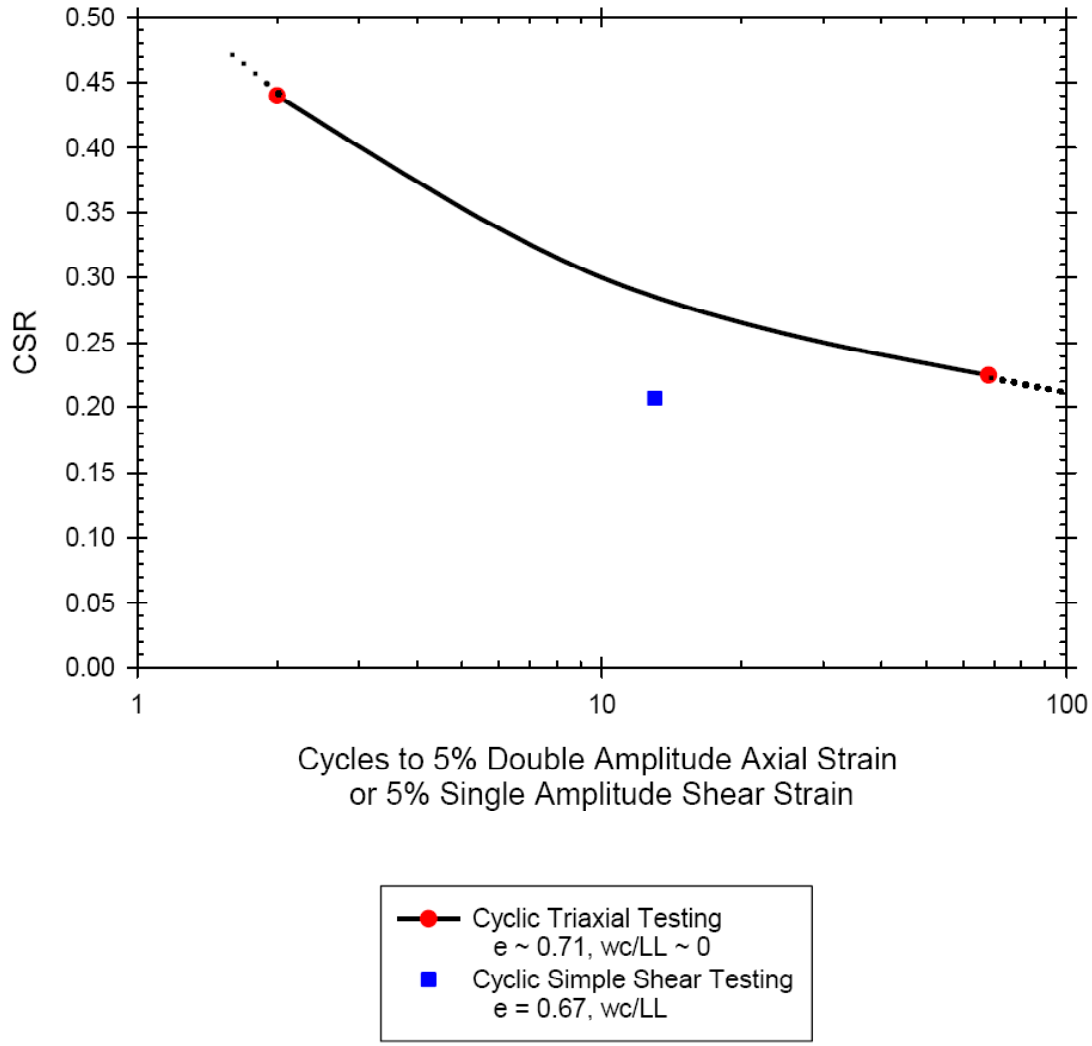

Figure 6.81 CSR Chart for comparison of Cyclic Triaxial Testing and Cyclic Simple Shear Testing, prepared using the Slurry Deposition Method, all tests at $\sigma'_m \approx 50$ kPa.

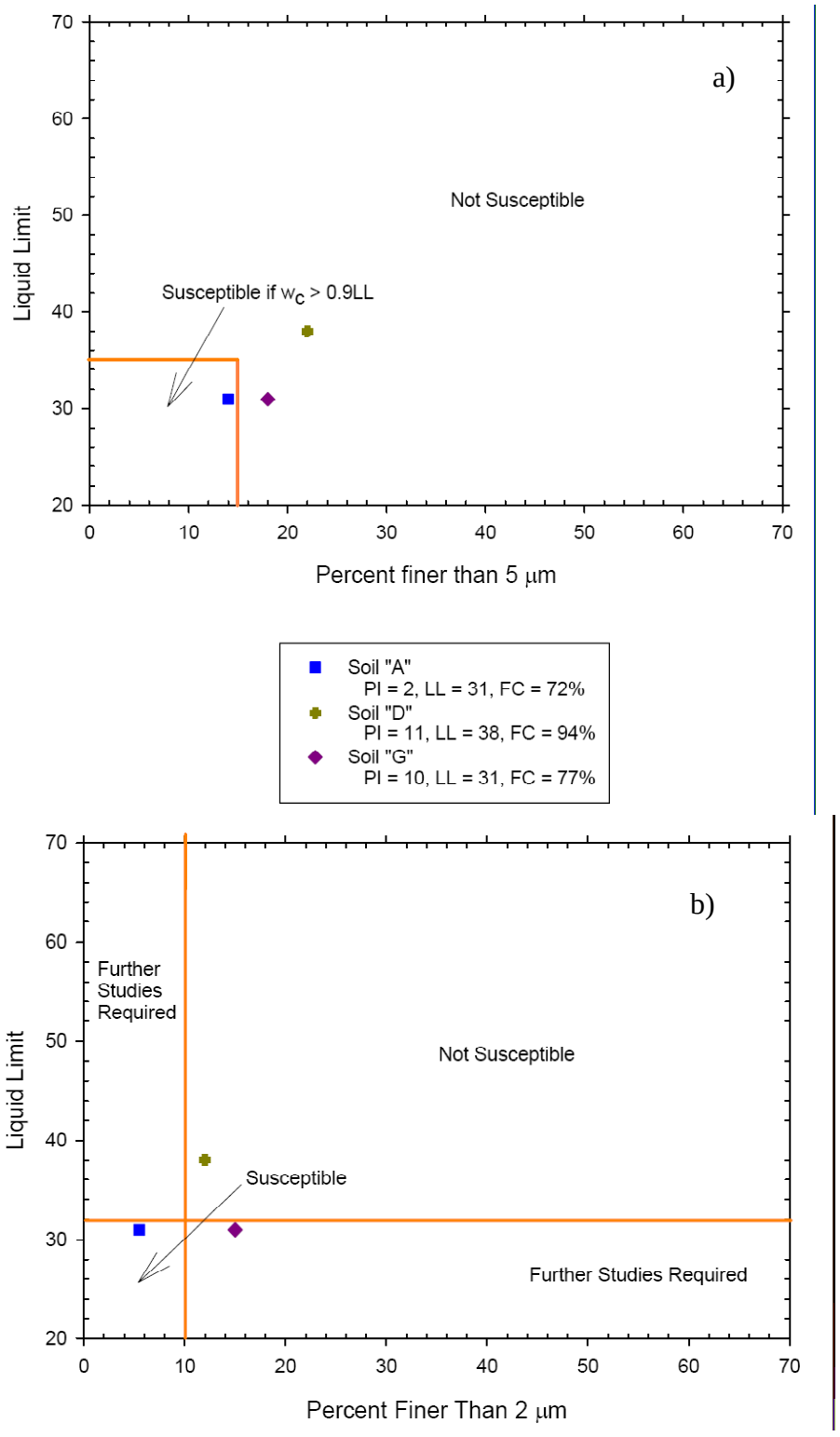

Figure 6.82 Graphical representation of liquefaction criteria: a) Chinese Criteria after Wang (1979), and b) Andrews and Martin (2000).

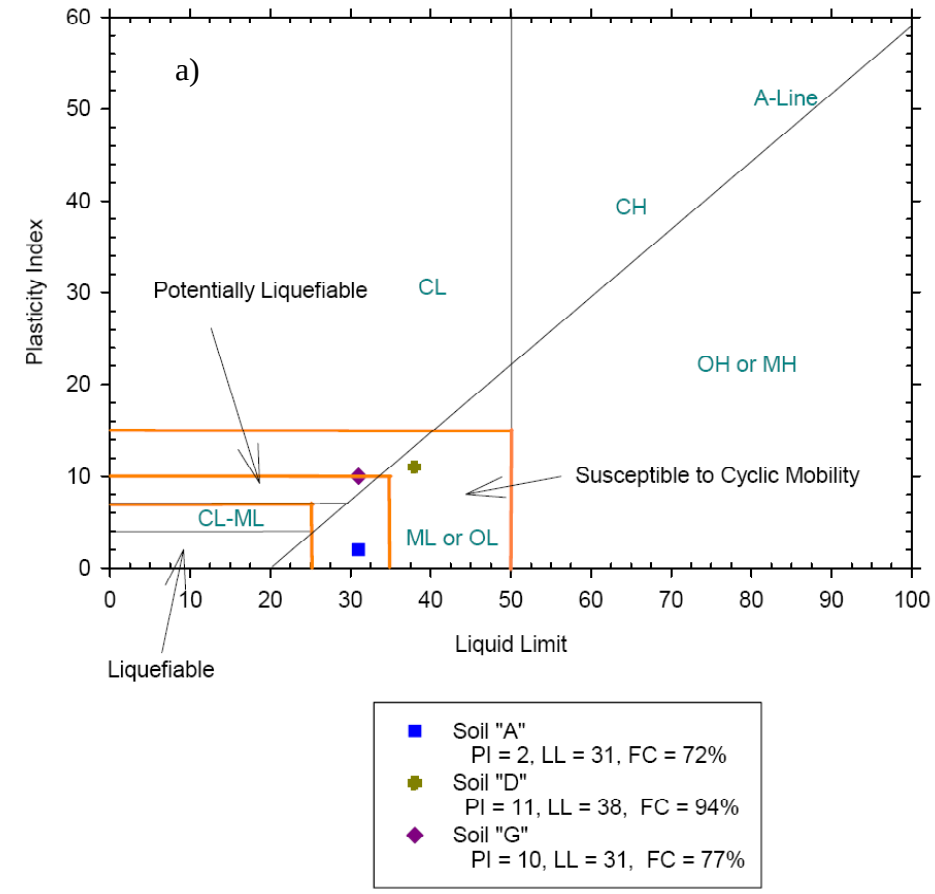

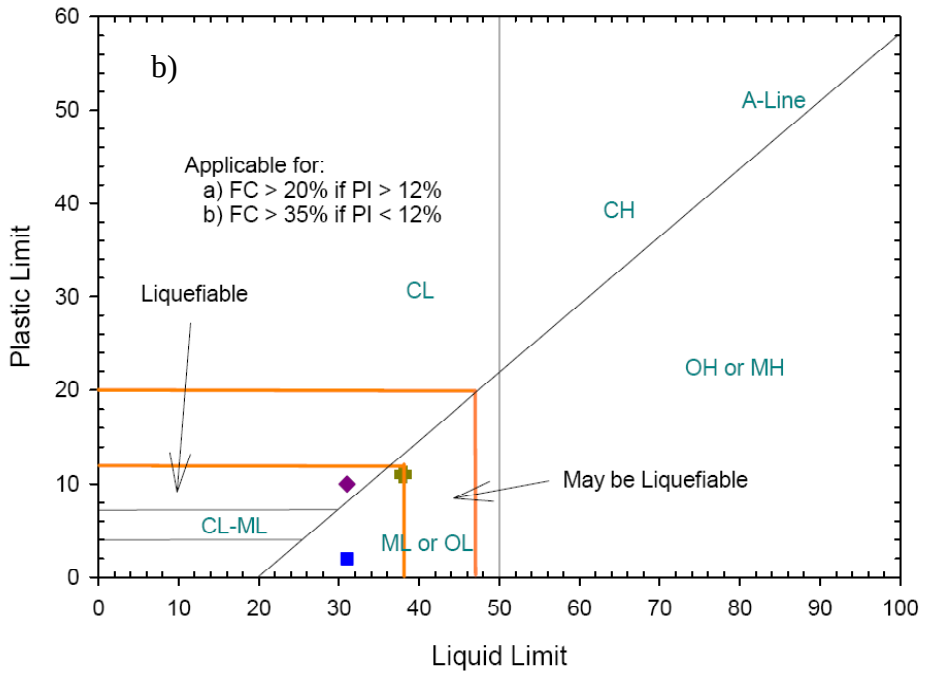

Figure 6.83 Graphical representation of liquefaction criteria: a) Polito and Martin (2001), and b) Seed et al (2003).

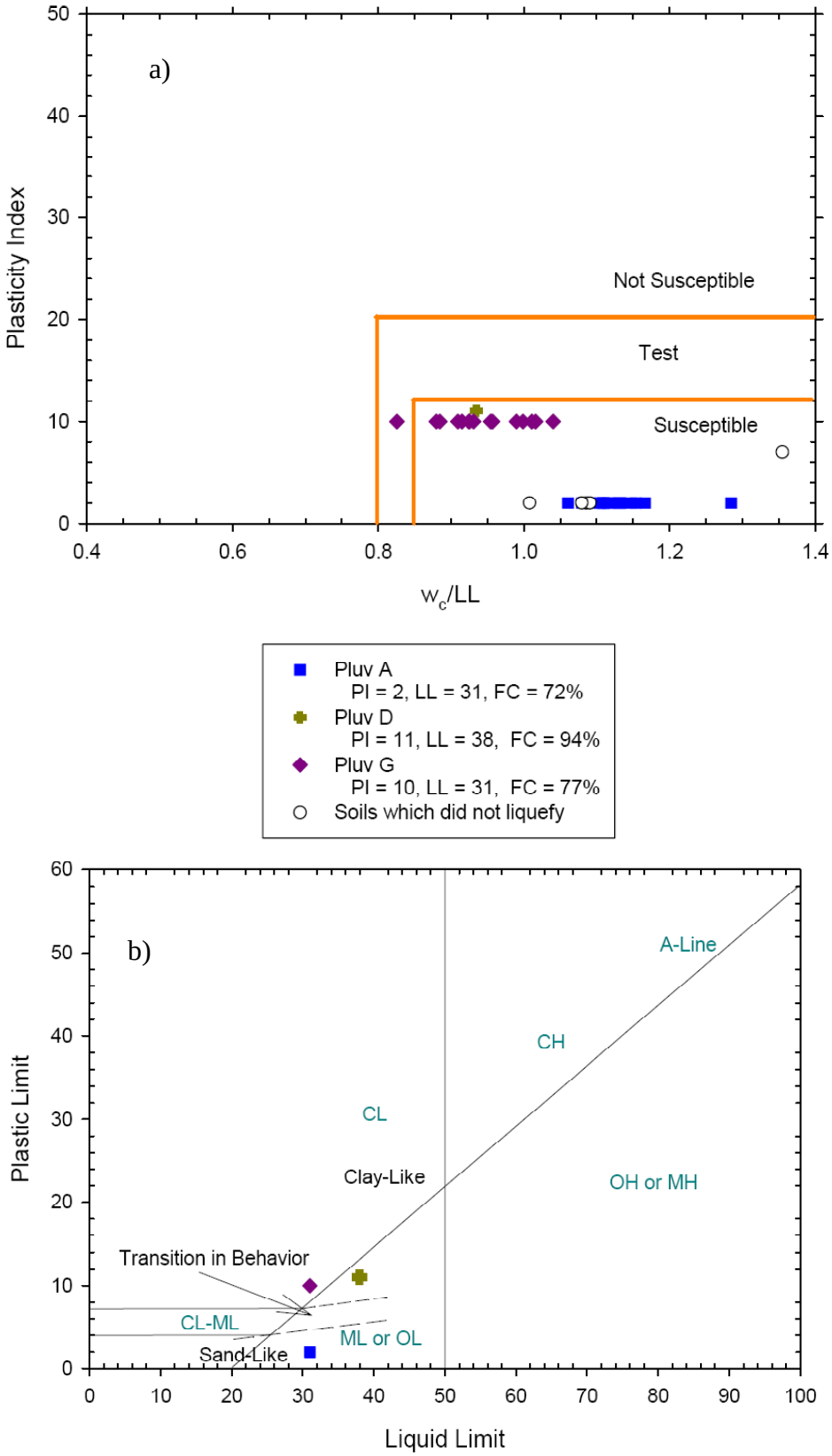

Figure 6.84 Graphical representation of liquefaction criteria: a) Sancio (2003) and Bray and Sancio (2006), and b) Boulanger and Idriss (2006).

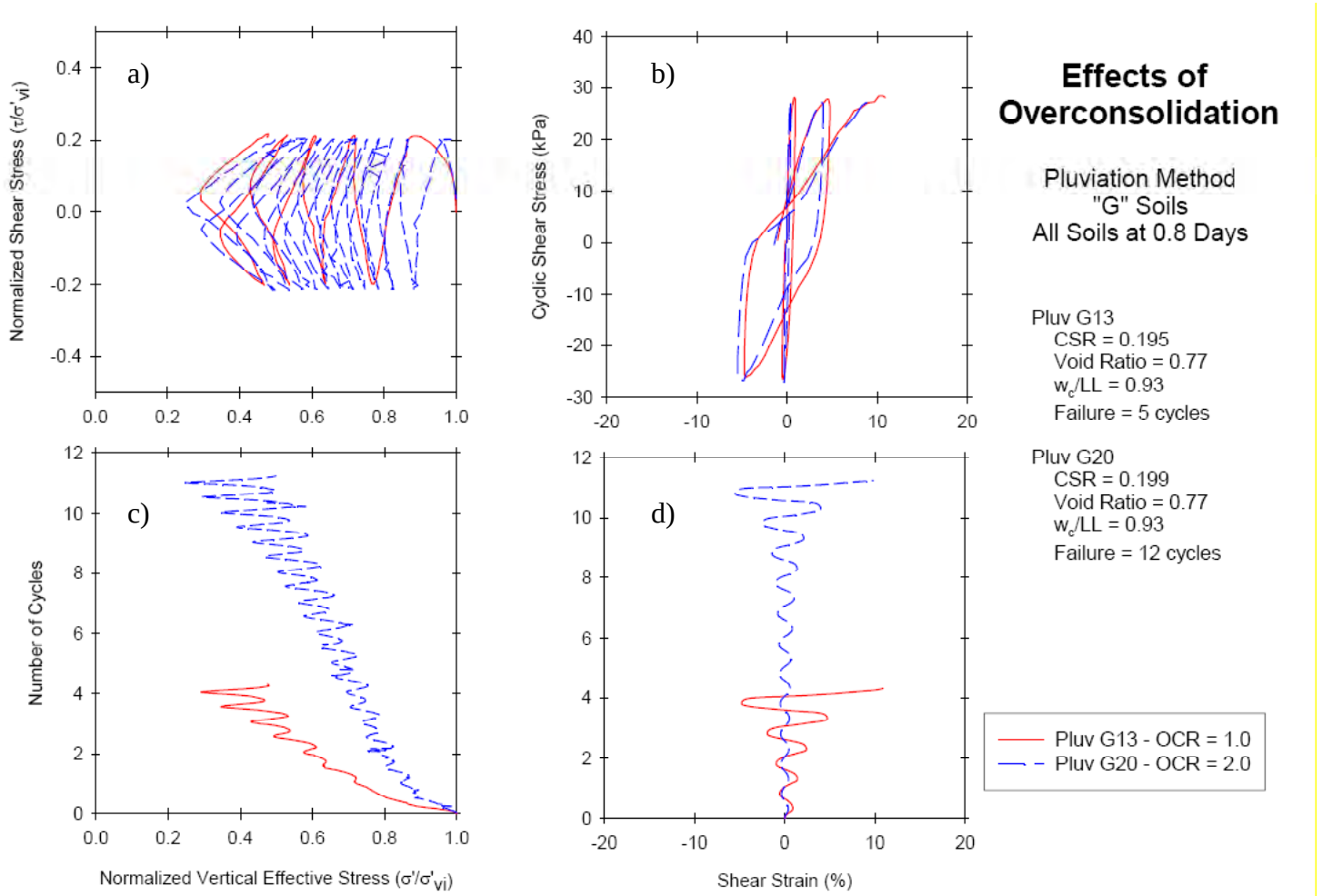

Figure 6.85 4-way plot comparison of two soils with the same void ratio and different OCRs for Soil G prepared using the In-Place Wet Pluviation Method tested by the cyclic simple shear: a) effective stress path, b) stress-strain diagram, c) normalized vertical effective stress to number of cycles, and d) shear strain to number of cycles of loading.

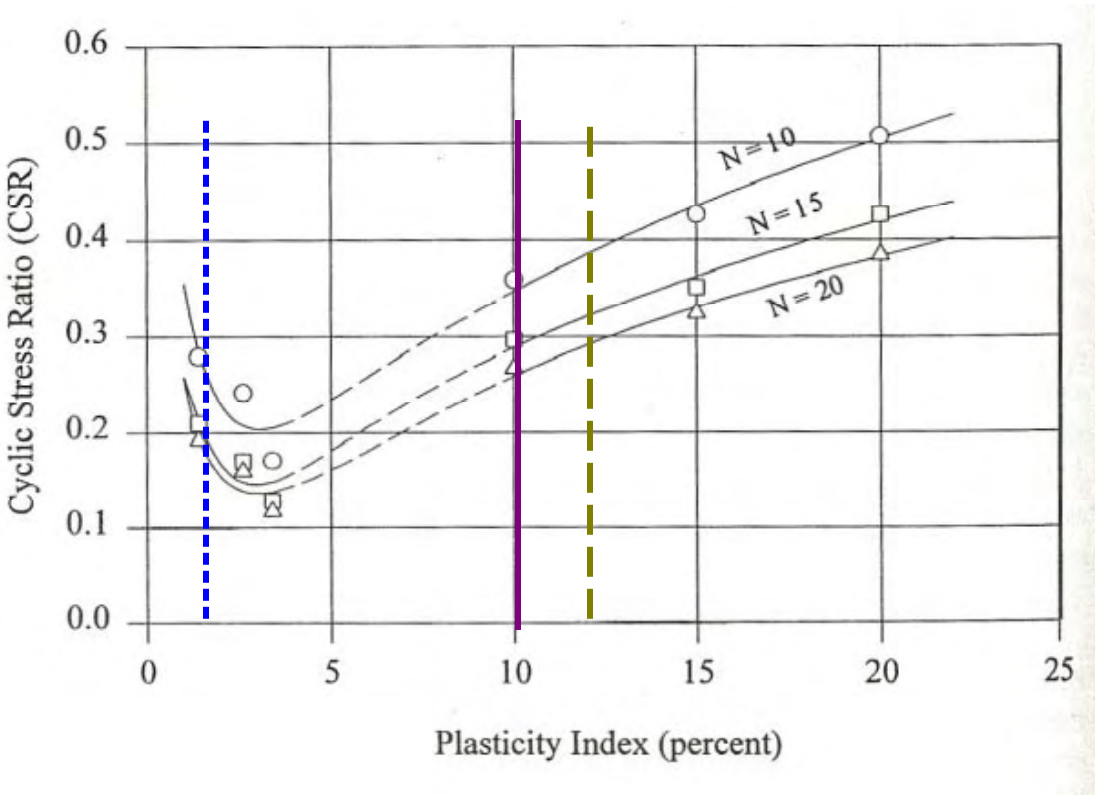

Figure 6.86 Graphical representation of Prakash and Guo (1998) liquefaction assessment for reconstituted specimens.

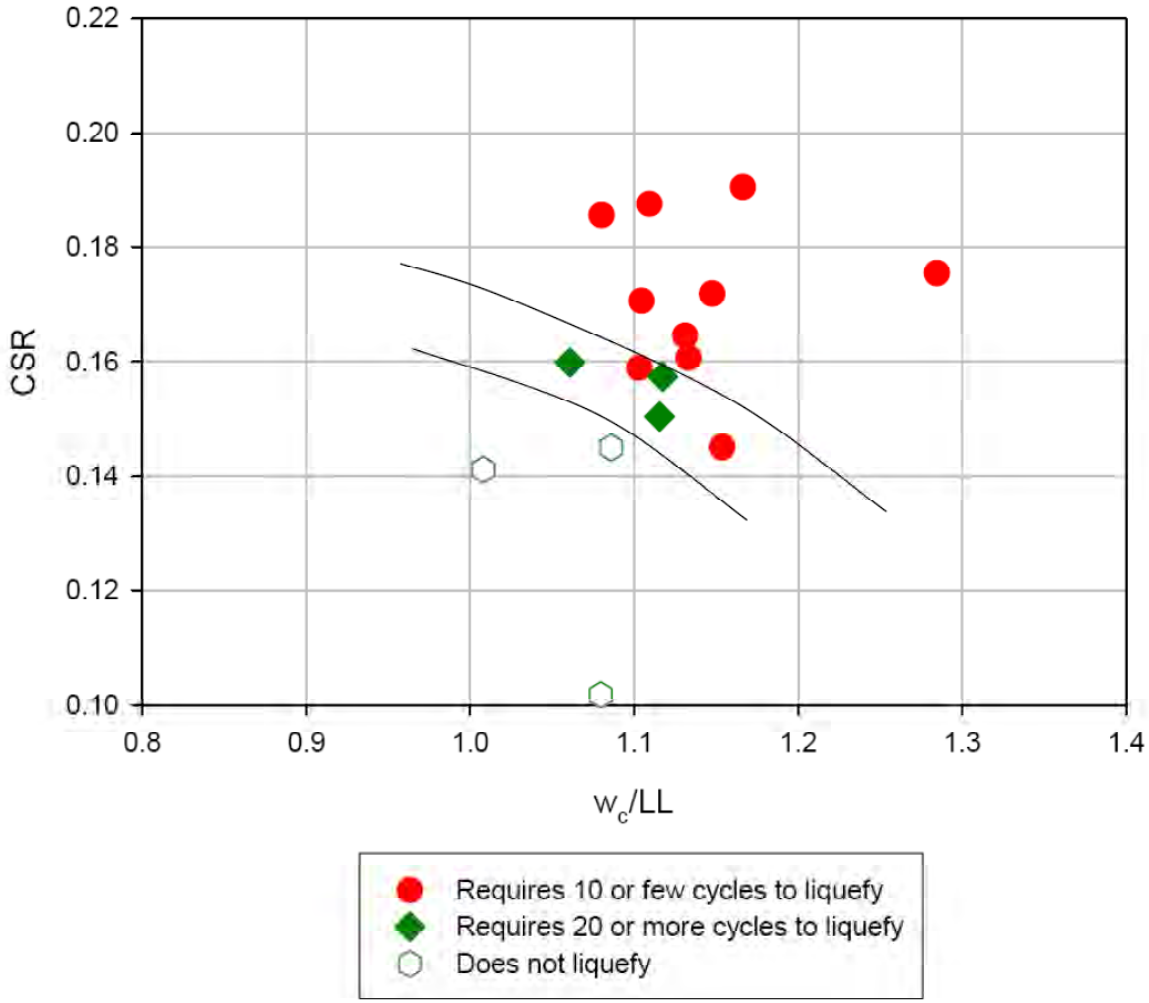

Note: no Soil "A" specimens required 10 – 20 cycles to liquefy

Figure 6.87 Insight for CSR vs. w_c/LL and number of cycles to liquefy for Soil A (PI = 2, LL = 31).

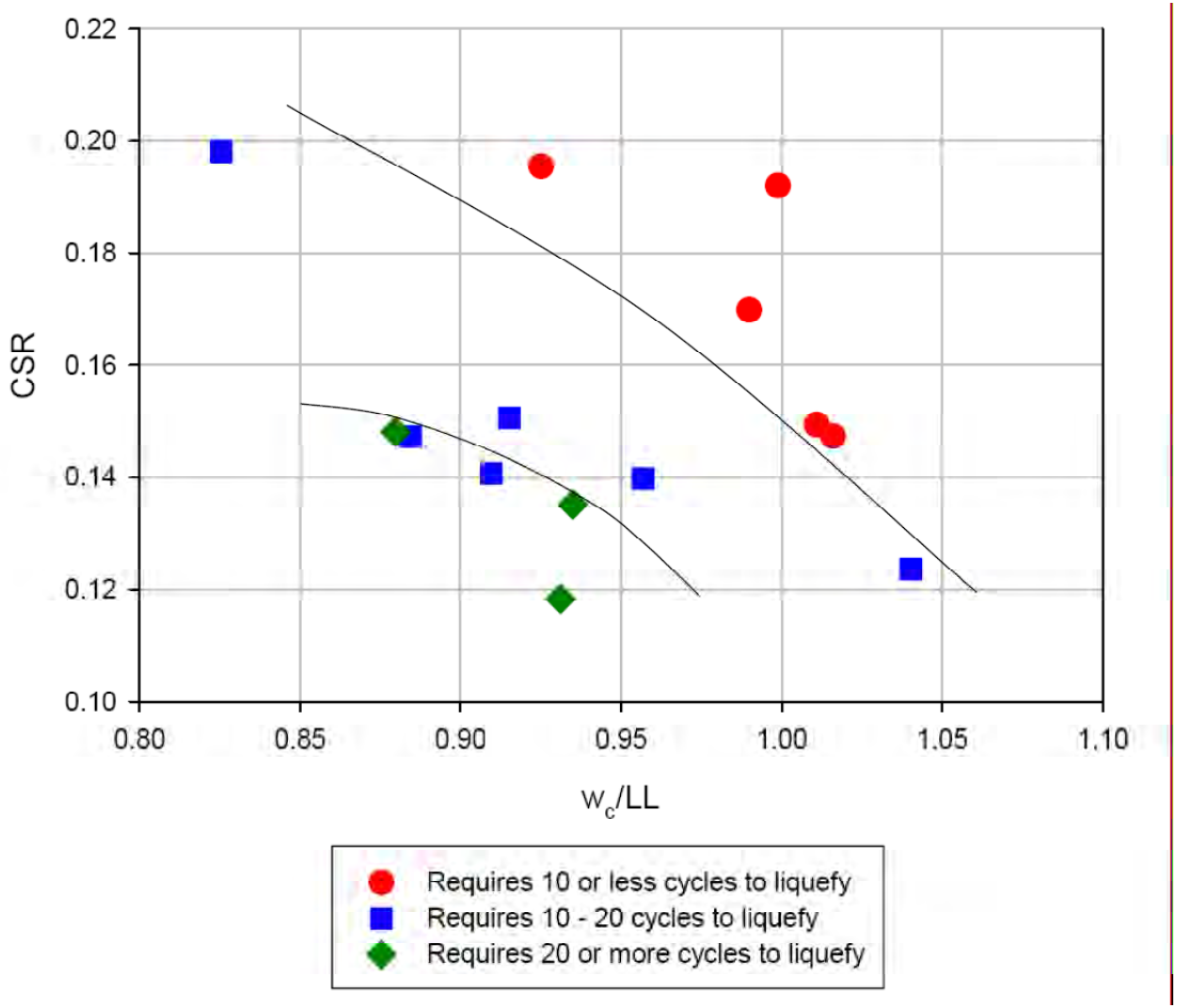

Figure 6.88 Insight for CSR vs. w_c/LL and number of cycles to liquefy for Soil D (PI = 11, LL = 38) and Soil G (PI = 10, LL = 31).

Chapter 7 SUMMARY AND CONCLUSIONS

7.1 Summary

An extensive laboratory testing program, which included static and dynamic tests, was carried out to evaluate the properties of fine-grained soils retrieved from Adapazari, Turkey. These retrieved soils were separated into seven distinct batches that represented the fine-grained soils that exhibited liquefaction in Adapazari during the 1999 Kocaeli earthquake. Soils from the seven batches were then reconstituted using two methods modified for use in this research, i.e., the Slurry Deposition Method and In-Place Wet Pluviation Method.

The monotonic stress-strain-strength relationship of the reconstituted soil specimens was first investigated by performing 47 soil characterization tests and 22 static strength tests. Grain size analysis, constant rate of strain consolidation tests, consolidation tests, undrained monotonic triaxial tests, and undrained simple shear tests were performed to develop an understanding and a framework for interpreting the cyclic experiments. The effects of changes to the reconstituted specimens were evaluated based on static strength using the undrained monotonic triaxial tests and undrained monotonic simple shear tests by varying the reconstitution method, effective confining stress, soil index properties, loading rate, and time under confinement.

After a framework for interpreting the static strength of the reconstituted fine-grained soils was established, the cyclic responses of these soils were investigated. This was achieved by performing 82 cyclic triaxial and cyclic simple shear tests on soil specimens that were reconstituted using the Slurry Deposition Method and the In-Place Wet Pluviation Method. The cyclic strength of the soil was assessed by initially performing tests at specified baseline conditions, and then performing tests with the following testing conditions varied systematically: time under confinement, void ratio, overconsolidation ratio (OCR), effective confining stress (σ'_m), frequency of loading, and initial static shear stress (α).

7.2 Principal Findings

The principal findings of this study are:

- Two useful methods for specimen reconstitution were developed and successfully utilized during this testing program. The modified Slurry Deposition Method was shown to consistently produce uniformly reconstituted specimens that minimize the significant inherent variability found in naturally deposited soils. The In-Place Wet Pluviation Method was shown to provide consistent, layered specimens that better replicate in situ fluvial deposits of fine-grained soils.

- The method of reconstitution, either by Slurry Deposition or by In-Place Wet Pluviation, significantly influenced the consolidation parameters. As an example the coefficient of consolidation, c_v, was greater for the In-Place Wet Pluviated specimens than for the Slurry

Deposition specimens. The parameter c_v was instrumental in determining the loading rate and consolidation characteristics of the soil.

- The method of specimen preparation influences the undrained static shear strength and undrained cyclic shear strength of the reconstituted soil specimens. During simple shear monotonic testing, the Slurry Deposition Method specimens consistently had greater static strength than the In-Place Wet Pluviated specimens. For cyclic testing, the Slurry Deposition Method specimens also consistently displayed greater cyclic shear strength than the In-Place Wet Pluviated specimens.

- Fine-grained soils that have lower PIs will not always have lower formation void ratios than fine-grained soils that have higher PIs. Whether the specimens were reconstituted using the Slurry Deposition Method or In-Place Wet Pluviation Method, Soil G (PI = 10) consistently had a lower void ratio and water content than Soil A (PI = 2). The difference in the formation void ratio of the In-Place Wet Pluviation Method specimens (i.e., Soil A: e = 0.94 vs. Soil G: e = 0.84) was much greater than that of the Slurry Deposition Method specimens (i.e., Soil A: e = 0.67 vs. Soil G: e = 0.65).

- The method of reconstitution also significantly influenced the density of the specimens. The void ratios and w_c/LL ratios were consistently lower for the Slurry Deposition Method specimens than the In-Place Wet Pluviated specimens.

- The static shear strength and cyclic shear strength of the soil specimens was influenced by their index properties. For example, Soil A (PI = 2) displayed greater static shear strength than Soil G (PI = 10) when tested under similar conditions. In cyclic testing under similar test conditions, the cyclic shear strength of Soil A was greater than that of Soil G, whether the specimens were reconstituted using the Slurry Deposition Method or the In-Place Wet Pluviation method.

- For Soil A and Soil G, using the cyclic simple shear test, the loading frequency of 0.005 Hz was chosen to reliably measure excess pore water pressures. The parameter c_v was used to find t_{50}; and $16t_{50}$ was used as the duration for one loading cycle. Specimen response depends on loading rate. Increases in the loading rate led to higher cyclic shear strengths.

- The specimen's effective confining stress controls its static shear strength and cyclic response. For static monotonic testing, when the measured effective stress is normalized by the initial vertical effective stress (σ'/σ'_{vi}) and the measured shear stress is normalized by the initial vertical effective stress (τ/σ'_{vi}), an increase in effective confining stress results in lower normalized static shear strength. For cyclic testing, when the measured effective stress is normalized by the initial vertical effective stress (σ'/σ'_{vi}), comparing the response for each loading cycle will show that an increase in effective confining stress results in lower normalized cyclic shear strength.

- An increase in the time under confinement led to a significant increase in the static and cyclic shear strength of the soil. For example, the maximum shear stress on the horizontal

plane for Soil D increased by approximately 10% per log cycle of time. In the cyclic testing, the Soil A and Soil G specimens typically showed an increase in cyclic strength of 13% and 33%, respectively, for time under confinement of 50 days when compared to the baseline case that had a time under confinement of 0.8 days. The results from this test series confirmed that soils with characteristics similar to Soil G (i.e., PI = 10, LL = 31, FC = 77%) have a greater increase in cyclic strength for time under confinement than soils with characteristics similar to Soils A (i.e., PI = 2, LL = 31, FC = 72%).

- The failure mechanism of the Pluviated specimens is not fully understood. The Slurry Deposition specimens are relatively homogeneous, and the response of a soil reconstituted by this method is that of a soil with a relatively uniform PI and water content throughout the test specimen. For the In-Place Wet Pluviated specimens, it remains unclear whether it was the entire specimen that failed, or whether it was the coarser-grained seams within the specimen that failed. If these seams are the cause of failure, the lower PI, higher void ratio, and lower fines content within these seams is one explanation for differences in the cyclic strength response between the two reconstitution methods.

- The CSRs applied to the reconstituted soil specimens prepared in this research are significantly smaller than those for field specimens from Adapazari. Sancio (2003) was able to test field specimens of similar soil up to CSR = 0.5. Previous research on reconstituted fine-grained specimens (e.g., Xenaki and Athanasopoulos, 2002; Wijewickreme and Sanin, 2004; Wijewickreme et al., 2005; Boulanger and Idriss, 2006) and the testing presented herein, rarely reached loading as high as CSR = 0.25. Specimen preparation method, time under confinement effects, ageing, as well as other factors, caused laboratory prepared specimens to be weaker than corresponding field fine-grained specimens.

- Previous researchers have recommended liquefaction screening criteria based on Liquid Limit, Fines Content, the percentage of particles finer than 5 μm or 2 μm, Plasticity Index, and w_c/LL. Laboratory tests confirmed that the "Chinese Criteria," after Wang (1979), and the Andrews and Martin (2000) criteria are not effective for the evaluation of liquefaction susceptibility of fine-grained soils due primarily to the ineffectiveness of the criterion on the amount of particles smaller than 5μm or 2 μm. The Polito and Martin (2001), Seed et al. (2003), and Bray and Sancio (2006) methods captured the liquefaction susceptibility of these soils well. The Boulanger and Idriss (2006) PI criterion (i.e., "sand-like" for PI < 7 and "clay-like" for PI ≥ 7) suggests that there is a significant difference in the cyclic response of fine-grained soils due to minor changes in PI for low plasticity soils. The results from this testing program do not support this view.

- The threshold of significant increases in shear strains per cycle is about r_u = 60% for Slurry Deposition Method specimens and 70% for In-Place Wet Pluviated specimens. Before this threshold, Soils A and G, have minimal shear strains per cycle. After this threshold, the shear strain increase with each additional cycle of loading until liquefaction. For a stress-based definition of liquefaction triggering, 5% shear strain typically coincides with r_u = 80%.

- All laboratory prepared specimens tested within this program of research, would liquefy if the applied cyclic loading was sufficiently intense. For this body of research, liquefaction could be described as either cyclic mobility with limited shear strains or cyclic mobility with unlimited shear strains. For these fine-grained soils, cyclic mobility with limited strain potential occurred after the r_u threshold (described above) was reached; then the specimens developed a nearly linear increase in shear strain for each additional cycle of loading. The following specimens exhibited cyclic mobility with limited shear strains:
    - Slurry Deposition Soil A specimens
    - Slurry Deposition Soil G specimens
    - Pluviated Soil A and G specimens with significant time under confinement
    - Pluviated Soil A and G specimens with OCR > 1
    - Pluviated Soil A and G specimens tested at a loading frequency of 1 Hz
    - Pluviated Soil G specimens constructed to be very dense (low void ratio)

  Cyclic mobility with unlimited shear strain also occurred after the r_u threshold (described above) was reached, but these specimens would typically fail in only 1 to 2 more cycles of loading after reaching this threshold. The following specimens exhibited cyclic mobility with unlimited shear strains:
    - Pluviated Soil A and G specimens prepared to baseline conditions (0.8 Days under confinement, OCR = 1, loading frequency of 0.005 Hz, σ'_m = 100 kPa, average void ratio)
    - Pluviated Soil A and G specimens tested at condition similar to the baseline conditions, except σ'_m = 50 kPa or 200 kPa

- Testing on reconstituted specimens should be used to provide insight regarding the trends that result due to changes in time under confinement, density, effective confining stress, and overconsolidation ratios. Although it is premature to recommend a new liquefaction criterion for in situ fine-grained soil deposits based on this research, important factors were identified. Factors such as w_c/LL and OCR were found to be important, as well as the time under confinement. PI remains a useful index of soil mineralogy, but it failed to discern differences in soil response over small changes in PI for these soils of low plasticity (i.e., PI < 12).

7.3 Recommendations for Future Work

Research concerning the liquefaction resistance and susceptibility of the reconstituted fine-grained soils has only recently attracted much attention. This study helps to advance understanding in this new area of research. There are topics in the liquefaction susceptibility and resistance of the reconstituted fine-grained soils that were not addressed during the course of this research. To improve our knowledge on the liquefaction susceptibility and resistance of the reconstituted fine-grained soils, future research should consider the following:

- An extensive laboratory testing program should be performed to investigate further the effects of time under confinement of reconstituted soil specimens. As learned from Chapters 5 and 6, the specimen's static and cyclic shear strength increases with increased time under confinement. Increasing the specimen's time under confinement to 100+ days will provide valuable insight on the increase in strength and make the specimens more comparable to specimens retrieved from the field.

- Additional testing on the effects of effective confining stress for the cyclic strength of the soil should be performed to constrain the uncertainty in the estimates of the K_σ curve. To properly plot points on the K_σ graph, the CSR at 10 cycles to 5% shear strain for a given effective confining stress is compared to the CSR at 10 cycles to 5% shear strain for an effective confining stress of 100 kPa. Due to the limited number of data points at low and high effective confining stresses, the K_σ curve presented in Section 6.3.4 is only an approximation.

- Additional In-Place Wet Pluviation tests should be performed to constrain the uncertainty in the estimates of the static and cyclic strength of the soil given the variations in testing conditions. For many tests, only one test was performed for a specific testing condition from which comparisons were drawn. This was often insufficient to develop firm conclusions concerning the response of the soil to the varied soil parameters or to develop a robust estimate of the 95% confidence intervals for each testing condition.

- Bi-directional cyclic simple shear testing should be performed because it betters captures actual earthquake motions. Previous research by Seed et al. (1975), Ishihara and Yamazaki (1980), and Kammerer (2002) found that materials loaded under bi-directional shear conditions exhibit larger shear strains than when loaded in one horizontal direction.

- More monotonic loading tests using either strain-control or stress-control should be performed to constrain the static strength response of the soil specimens given the method of preparation. The soils reconstituted using the Slurry Deposition Method had the same response for both strain-control and stress-control up to 5% shear strain; whereas the response of the soils reconstituted using the In-Place Wet Pluviated were dissimilar.

REFERENCES

Anantanavanich, T. (2002) “Modeling the rate dependent dynamic response of submarine soft clay deposits,” Ph.D. Thesis, University of California, Berkeley.

Andersen, K. H., Kleven, A., and Heien, D. (1988) “Cyclic soil data for design of gravity structures,” Journal of Geotechnical and Geoenviromental Engineering, ASCE, Vol. 114, No. 5, pp. 517-539.

Andrews, D. C. A. and Martin, G. R. (2000) "Criteria for liquefaction of silty soils," Proceedings of the 12th World Conference on Earthquake Engineering, New Zealand, Paper No. 0312

Assimaki, D., Kausel, E., and Whittle, A. (2000) “Model of dynamic shear modulus and damping for granular soils,” Journal of Geotechnical and Geoenvironmental Engineering, ASCE, Vol. 126, No. 10, pp. 859-869.

ASTM D 4186-06 (2006) “Standard test method for one-dimensional consolidation properties of soils using controlled-strain loading,” American Society for Testing and Materials, Annual Book of ASTM Standards, Vol. 04.08.

ASTM D D422-63 (2002)e1 “Standard test method for particle-size analysis of soils” American Society for Testing and Materials, Annual Book of ASTM Standards, Vol. 04.08.

Biscontin, G. (2001) “Modeling the dynamic behavior of lightly overconsolidated soil deposits on submerged slopes,” Ph.D. Thesis, University of California, Berkeley

Bishop, A. W. and Henkel, D. J. (1957) “The measurement of soil properties in the triaxial test,” Edward Arnold Publishers LTD, London, England. 190 pages.

Black, D. K. and Lee, K. L. (1973) “Saturating laboratory samples by back pressure,” Journal of the Soil Mechanics and Foundations Division, ASCE, Vol. 99, No 1, pp. 75-93.

Boulanger, R. W. (1990) “Liquefaction behavior of saturated cohesionless soils subjected to unidirectional and bi-directional static and cyclic loads,” Ph.D. Thesis, University of California, Berkeley.

Boulanger, R. W., Chan, C. K., Seed, H. B., Seed, R. B., and Sousa, J. (1993) “A low compliance bi-directional cyclic simple shear apparatus,” Geotechnical Testing Journal, Vol. 16, No. 1, pp. 36-45.

Boulanger, R. W. and Idriss, I. M. (2004) “Evaluating the potential for liquefaction or cyclic failure of silts and clays”, Report No. UCD/CGM-04/01, December.

Boulanger, R. W. and Idriss, I. M. (2006) “Liquefaction susceptibility criteria for silts and clays,” Journal of Geotechnical and Geoenviromental Engineering, ASCE, Vol. 132 No. 11, pp. 1413-1426.

Boulanger R. W., Mejia L. H. and Idriss L. M. (1997) "Liquefaction at Moss Landing during Loma Prieta Earthquake," Journal of Geotechnical and Geoenviromental Engineering, ASCE, Vol. 123, No. 5, pp. 453-467.

Boulanger R. W., Meyers M. W., Mejia L. H. & Idriss I. M. (1998) “Behavior of a fine-grained soil during the Loma Prieta earthquake,” Canadian Geotechnical Journal, Vol. 35, pp. 146-158.

Boulanger, R. W. and Seed, R. B. (1995) “Liquefaction of sand under bi-directional monotonic and cyclic loading,” Journal of Geotechnical and Geoenvironmental Engineering, ASCE, Vol. 121, No. 12, pp. 870-878.

Bray, J. D., Sancio, R. B., Riemer, M. F., and Durgunoglu, H. T. (2004a) “Liquefaction susceptibility of fine-grained soils,” Proceedings of 11th Inter. Conf. On Soil Dynamics and Earthquake Engineering and 3rd Inter. Conf. On Earthquake Geotechnical Engineering, Doolin et al., Eds., Berkeley, 1, 655-662.

Bray, J. D., Sancio, R. B., Durgunoglu, H. T., Onalp, A., Seed R. B., Stewart J. P., Youd T. L., Baturay, M. B., Cetin, K. O., Christensen, C., Karadayilar, T., and Emrem, C. (2001a) "Ground failure In Adapazari, Turkey," in Proc., Earthquake Geotechnical Engineering Satellite Conference of the XVth International Conference on Soil Mechanics & Geotechnical Engineering, Istanbul, Turkey, August 24-25.

Bray, J.D., Sancio, R. B., Youd, L. F., Christensen, C., Cetin, O., Onalp, A., Durgunoglu, T., Stewart, J. P., C., Seed, R. B., Baturay, M. B., Karadayilar, T., and Oge, C. (2001b) "Documenting incidents of ground failure resulting from the August 17, 1999 Kocaeli, Turkey Earthquake," Pacific Earthquake Engineering Research Center website: http://peer.berkeley.edu/turkey/adapazari/.

Bray, J. D., Sancio, R. B., Durgunoglu, H. T., Onalp, A., Youd, T. L., Stewart, J. B., Seed, R. B., Cetin, O. K., Bol, E., Baturay, M. B., Christensen, C., and Karadayila T. (2004b) “Subsurface characterization at ground failure sites in Adapazari, Turkey,” Journal of Geotechnical and Geoenvironmental Engineering, ASCE, Vol. 130, No. 7, pp. 1 – 13.

Bray, J. D. and Sancio, R. B. (2006) “Assessment of the liquefaction susceptibility of fine-grained soils,” Journal of Geotechnical and Geoenvironmental Engineering, ASCE, Vol. 132, No. 9, pp. 1165-1177.

Budhu, M. and Britto, A. M. (1987) “Numerical Analysis of Soils in Simple Shear Devices,” Soils and Foundations, Vol. 27, No. 2, pp. 31-41.

Campanella, R. G. and Lim, B. S. (1981) “Liquefaction characteristics of undisturbed soils,” Proceedings of the International Conference on Recent Advances in Geotechnical Earthquake Engineering and Soil Dynamics, Vol. 1, pp. 227-230.

Carraro, J. A. H., Bandini, P., and Salgado, R. (2003) “Liquefaction resistance of clean and nonplastic silty sands based on cone penetration resistance,” Journal of Geotechnical and Geoenviromental Engineering, ASCE, Vol. 129, No. 11, pp. 965-976.

Castro, G. and Poulos, S. J. (1977) “Factors affecting liquefaction and cyclic mobility,” Journal of the Geotechnical Engineering Division, ASCE, Vol. 101, No. 6, pp. 551-569.

Chan C. K. (1982) “An electropneumatic cyclic loading system,” Geotechnical Testing Journal, Vol. 4, No. 4, pp. 183-187.

Dobry, R., Yokel, F. Y., and Ladd, R. S. (1981) “Liquefaction potential of overconsolidated sands in areas with moderate seismicity,” Proceedings of Earthquakes and Earthquake Engineering: the Eastern United States, pp. 643-664.

Donahue, J. L., Bray, J. D., and Riemer, M. (2007) “Liquefaction testing on fine-grained soils prepared using slurry deposition,” Proceedings of the 4th International Earthquake Geotechnical Engineering, Thessaloniki, Greece, Paper 1226.

Duncan, J. M. and Chang, C. Y. (1970) “Nonlinear Analysis of Stress and Strain in Soils,” Journal of the Soil Mechanics and Foundations Division, ASCE, Vol. 96, No. 5, pp. 1629-1653.

El Hosri, M. S., Biarez, H., and Hicher, P. Y. (1984) “Liquefaction characteristics of silty clay, “ Proceedings of the 8th World Conference on Earthquake Engineering, Prentice-Hall, Englewood Cliffs, N.J., Vol. 3, pp. 277-284.

Franke, E., Kiekbusch, M., and Schuppener, B. (1979) “A new direct simple shear device,” Geotechnical Testing Journal, Vol. 2, No. 4, pp. 190-199.

Germaine, J. T. and Ladd, C. C. (1988) “Triaxial testing of saturated cohesive soils,” Advanced Triaxial Testing of Soil and Rock; American Society for Testing and
Materials, Philadelphia, 1988, pp. 421-459.

Guo, T. and Prakash, S. (1999) "Liquefaction of silts and silt-clay mixtures," Journal of the Geotechnical Engineering Division, ASCE, Vol. 125, No. 8, pp. 706-710.

Guo, T. and Prakash, S. (2000) "Liquefaction of silt-clay mixtures," Proceedings of the 12th World Conference on Earthquake Engineering, New Zealand, Paper No. 0561.

Gratchev I., Sassa, K., Fukuoka, H. (2006) “How reliable is the plasticity index for estimating the liquefaction potential of clayey sands?” Journal of the Geotechnical Engineering Division, ASCE, Vol. 132, No. 1, pp. 124-127.

Harder, L. F. (1988) “Use of penetration tests to determine the cyclic loading resistance of gravelly soils during earthquake shaking,” Ph.D. Thesis, Univ. of California, Berkeley.

Harder, L. F. and Boulanger, R. W. (1997) “Application of Kσ and Kα Correction Factors,” Rep. No. NCEER-97-0022, NCEER, Buffalo, NY.

Holtz, R. D. and Kovacs, W. D. (1981) “An introduction to geotechnical engineering.” Prentice Hall, New Jersey, USA. 733 pages.

Holzer, T. L., Bennett, M. J., Ponti, D. J., and Tinsley, J. C. (1999) "Liquefaction and soil failure during 1994 Northridge Earthquake," Journal of Geotechnical and Geoenvironmental Engineering, Vol. 125, No. 6, pp. 438-452.

Hynes, M. E. and Olsen, R. S. (1999) “Influence of confining stress on liquefaction resistance,” Physics and Mechanics of Soil Liquefaction, Lade and Yamamuro (editors), pp. 145-151.

Ishihara, K. (1996) “Soil behaviour in earthquake geotechnics,” The Oxford engineering science series, No. 46.

Ishihara, K., Iwamoto, T., Yasuda, S., and Takatsu, H. (1977) “Liquefaction of anisotropically consolidated sand” Proceedings of the 9th International Conference on Soil Mechanics and Foundation Engineering, Japanese Society of Soil Mechanics and Foundation Engineering, Tokyo, MAA Pub. Co., Vol. 2, pp. 261-264.

Ishihara, K. and Okada, S. (1978) “Yielding of overconsolidated sand and liquefaction model under cyclic stresses,” Soils and Foundations, Vol. 18, No. 1, pp. 57-72.

Ishihara, K., Sodekawa, M., and Tanaka, Y. (1978) “Effects of overconsolidation on liquefaction characteristics of sands containing fines,” Rep. No. 654, American Society for Testing of Materials.

Ishihara, K. and Takatsu, H. (1979) “Effects of overconsolidation and K_o conditions on the liquefaction characteristics of sands,” Soils and Foundations, Vol. 19, No. 4, pp. 59-68.

Ishihara, K. and Yamazaki, F. (1980) “Cyclic simple shear tests on saturated sand in multi-directional loading,” Soils and Foundations, Vol. 20, No. 1, pp. 45-59.

Kammerer, A. (2002) “Undrained response of Monterey 0/30 sand under multidirectional cyclic simple shear loading conditions,” Ph.D. Thesis, University of California at Berkeley.

Koester J.P., (1992) “The influence of test procedure on correlation of Atterberg limits with liquefaction in fine-grained soils,” Geotechnical Testing Journal, Vol. 15, No. 4, pp. 352-361.

Kuerbis R. and Vaid Y. P. (1998) “Sand sample preparation – the Slurry Deposition Method”, Soils and Foundations, 28, No. 4, pp. 107-118.

Ladd, C. C. and Edgers, L (1972) “Consolidated-undrained direct-simple shear tests on saturated clays,” MIT Research Report R72-82, Massachusetts Institute of Technology.

Lee, K. L. (1977) “End restraint effects on undrained static triaxial strength of sand,” Journal of the Geotechnical Engineering Division, ASCE, Vol. 104, No. 6, pp. 687-704.

Lee, K. L. and Focht, J. A. (1975) “Liquefaction potential of Ekofisk Tank in North Sea,” Journal of the Geotechnical Engineering Division, ASCE, Vol. 100, No. 1, pp. 1-18.

Lee, K. L. and Roth, W. (1977) “Seismic stability analysis of Hawkins hydraulic fill dam,” Journal of the Geotechnical Engineering Division, ASCE, Vol. 103, No. 6, pp. 627-644.

Lee, K. L. and Seed, H. B. (1967a) “Cyclic stress conditions causing liquefaction of sands,” Journal of Soil Mechanics and Foundations Division, ASCE, Vol. 93 No. 5, pp. 47-70.

Martin, G. R. and Lew, M., eds. (1999) "Recommended procedures for implementation of DMG Special Publication 117: Guidelines for analyzing and mitigating liquefaction hazards in California," Southern California Earthquake Center, Univ. of Southern Calif., March.

Mulilis, J. P., Seed, H. B., Chan, C. K., Mitchell, J. K., and Arulanandan, K. (1977) “Effects of Sample Preparation on San Liquefaction,” Journal of the Geotechnical Engineering Division, ASCE, Vol. 103, No. 2, pp. 91-105.

Naeini S. and Baziar M. (2003) “Effect of fines content on steady-state strength of mixed and layered samples of a sand,” Soil Dynamics and Earthquake Engineering, Vol. 24, p 181-187.

Nagase, H., Yasuda, S., Tsujino, S. Shinji, R., and Yanagihata, T. (1996) “Liquefaction Strength characteristics of overconsolidated sand samples,” Proceedings of the Eleventh World Conference on Earthquake Engineering, Oxford, England, Paper 1089.

Perlea, V. G. (2000) “Liquefaction of cohesive soils,” Soil Dynamics and Liquefaction 2000, The 2000 Specialty Conference, Denver CO. ASCE Geotechnical Special Publication No. 107, pp. 58-75.

Polito, C. P. and Martin, II, J. R. (2001) "Effects of nonplastic fines on the liquefaction resistance of Sands," Journal of Geotechnical and Geoenvironmental Engineering, ASCE, Vol. 127, No. 5, pp. 408-415.

Prakash, S., Guo, T., and Kumar, S. (1998) “Liquefaction of silts and silt-clay mixtures”, Geotechnical Earthquake Engineering and Soil Dynamics III, Special Publication No. 75, Vol. 1, ASCE, pp. 357 – 348

Puri, V. K. (1984) “Liquefaction behavior and dynamic properties of loessial (silty) soils,” Ph.D. Thesis, University of Missouri-Rolla, Missouri

Riemer, M. (1992) “The effects of testing conditions on the constitutive behavior of loose, saturated sands under monotonic loading” Ph.D. Thesis, University of California at Berkeley.

Rollins, K. M. and Seed, H. B. (1988) “Influence of buildings on potential liquefaction damage,” Journal of the Geotechnical Engineering Division, ASCE, Vol. 116, No. 2, pp. 165-185.

Romero, S. (1995) “The behavior of silt as clay content is increased,” MS Thesis, University of California, Davis.

Sancio, R. B. (2003) “Ground failure and building performance in Adapazari, Turkey,” Ph.D. Thesis, University of California, Berkeley.

Sancio, R. B., Bray, J. D., Riemer, M. F. and Durgunoglu, T. (2003) "An assessment of the liquefaction susceptibility of Adapazari silt," 2003 Pacific Conference on Earthquake Engineering, Christchurch, New Zealand.

Sancio R. B., Bray J. D., Stewart J. P., Youd T. L., Durgunoglu H. T., Onalp A., Seed R. B., Christensen C., Baturay M. B., and Karadayilar T. (2002) “Correlation between ground failure And soil conditions In Adapazari, Turkey,” Soil Dynamics and Earthquake Engineering Journal, Vol. 22 (9-12), pp. 1093 – 1102.

Sandoval, J. (1989) “Liquefaction and settlement characteristics of silt soils,” Ph.D. Thesis, University of Missouri-Rolla, Missouri

Seed, H. B. (1979) “Soil liquefaction and cyclic mobility evaluation for level ground during earthquakes,” Journal of Geotechnical Engineering, ASCE, Vol. 105, No. 2, pp. 201-255.

Seed, H. B. and Idriss, I. M. (1982) “Ground motions and soil liquefaction during earthquakes,” EERI Monograph, Berkeley, California, 134 pages.

Seed, H. B. and Lee, K. L. (1966) “Liquefaction of saturated sands during cyclic loading,” Journal of Soil Mechanics and Foundations Division, ASCE, Vol. 92, No. 6, pp. 105-134.

Seed, H. B. and Peacock, W. H. (1971) “Test procedures for measuring soil liquefaction characteristics,” Journal of Soil Mechanics and Foundations Division, ASCE, Vol. 97, No 8, pp. 1099-1119.

Seed, H. B., Pyke, R. M., and Martin, G. R. (1975b) “Effect of multi-directional shaking on liquefaction of sands,” Rep. No. EERC 75-41, University of California, Berkeley.

Seed, H. B., Tokimatsu, K., Harder, L. F., and Chung, R. M. (1985) "Influence of SPT procedures in soil liquefaction resistance evaluation," Journal of Geotechnical Engineering, Vol. 111, No. 12, pp. 1425-1445.

Seed, R. B. and Harder, L. F. (1990) "SPT-based analysis of cyclic pore pressure generation and undrained residual strength" H. B. Seed Memorial Symposium, BiTech Publishing, Ltd., Vol. 2, pp. 351-376.

Seed, R. B., Cetin, K. O. & Moss, R. E. S. (2001). Recent advances in soil liquefaction hazard assessment. 15th international conference on soil mechanics and geotechnical engineering, TC4 satellite conference on "Lessons learned from recent strong earthquakes," Istanbul, Turkey.

Seed, R. B., Cetin, K. O., Moss, R. E. S., Kammerer, A. M., Wu, J., Pestana, J. M., Riemer, M. F., Sancio, R. B., Bray, J. D., Kayen, R. E., Faris, A. (2003) "Recent Advances in Soil Liquefaction Engineering: A Unified and consistent framework," 26th Annual ASCE Keynote Presentation, 71 pages.

Silver M. L., Chan C. K., Ladd R. S., Lee K. L., Tiedemann D. A., Townsend F. C., Valera J. E. & Wilson J. H. (1976) "Cyclic triaxial strength of standard test sand," Journal of the Geotechnical Engineering Division, ASCE, Vol. 102, No. 5, pp. 511-523.

Stamatopoulos, C., Stamatopoulos, A., and Kotzias, P. (1995) "Effect of pressures on the liquefaction potential of silty sands," Soil Dynamics and Earthquake Engineering VII, Computational Mechanics Publications, pp. 181- 188.

Thevanayagam, S. (2000) "Liquefaction potential and undrained fragility of silty soils," Proceedings of the 12th World Conference on Earthquake Engineering, New Zealand, Paper No. 2383.

Thevanayagam, S. and Martin, G. (2002) "Liquefaction in silty soils-screening and remediation issues," Soil Dynamics and Earthquake Engineering Journal, Vol. 22 (9-12), pp 1035-1042.

Thevanayagam, S., Shenthan, T., Mohan, S., and Liang, J. (2002) "Undrained fragility of clean sands, silty sands, and sandy silts," Journal of Geotechnical and Geoenvironmental Engineering, Vol. 128, No. 10, pp. 849-859.

Vaid, Y. P. and Chen, J. C. (1983) "Effects of static shear on resistance to liquefaction," Soils and Foundations, Vol. 22, No 13, pp. 47-60.

Vaid, Y. P. and Finn, W. D. L. (1979) "Static shear and liquefaction potential," Journal of the Geotechnical Engineering Division, ASCE, Vol. 105, No 10, pp. 1233-1246.

Vaid, Y. P. and Sivathayalan, S. (2000) "Fundamental factors affecting liquefaction susceptibility of sand, "Canadian Geotechnical Journal, Vol. 37, pp. 592-606.

Vaid, Y. P., Sivathayalan, S., and Steadman, D. (1999) "Influence of specimen-reconstituting method on the undrained response of sand" Geotechnical Testing Journal, GTJODJ, Vol. 22, No. 3, pp. 187-195.

Vasquez-Herrera, A., Dobry, R., and Ng, T. T. (1988) “Pore pressure buildup and liquefaction failure of anisotropically consolidated sand due to cyclic straining,” Hydraulic Fill Structures, D. Van Zyl, ed., pp. 346-366.

Vasquez-Herrera, A. and Dobry, R. (1989) “Re-evaluation of the lower San Fernando Dam,” Rep. No. GL-89-2, Report 3, Department of the Army, US Army Corps of Engineers, Vicksburg, Miss, U.S. Army Engineer Waterways Experiment Station.

Wang, W. (1979) “Some findings in soil liquefaction,” Water Conser. And Hydroelect. Power Scien. Res. Inst., Beijing, China.

Wijewickreme, D. and Sanin, M. (2004) “Cyclic shear loading response of Fraser River Delta Silt,” 13th World Conference on Earthquake Engineering, Vancouver, B.C., Canada, No. 499.

Wijewickreme, D., Sanin, M., and Greenaway, G. (2005) “Cyclic shear response of fine-grained mine tailings,” Canadian Geotechnical Journal, Vol. 42, pp. 1408-1421.

Willamette Geological Service Report on X-Ray Diffraction, 2005.

Wroth, C. P. (1984) “The interpretation of in situ soil tests,” 24th Rankine Lecture, Geotechnique, Vol. 34, No. 4, pp. 449-489.

Wroth, C. P. (1987) “The behaviour of normally consolidated clay as observed in undrained direct shear tests,” Geotechnique, Vol. 37, No. 1, pp. 37-43.

Wu, J. (2002) “Liquefaction triggering and post-liquefaction deformation of Monterey 0/30 sand under uni-directional cyclic simple shear loading,” Ph.D. Thesis, University of California at Berkeley.

Xenaki V. C. and Athanasopoulos, G. A. (2003) “Liquefaction resistance of sand – silt mixtures: an experimental investigation of the effects of fines,” Soil Dynamics and Earthquake Engineering, Vol. 23, pp. 183-194.

Yamamuro, J. A. and Covert, K. M. (2001) “Monotonic and cyclic liquefaction of very loose sands with high silt content,” Journal of Geotechnical and Geoenviromental Engineering, ASCE, Vol. 127, No. 4, pp. 314 – 324.

Yamamuro, J. A., and Lade, P. V. (1998) "Steady-State Concepts and Static Liquefaction of Silty Sands," Journal of Geotechnical and Geoenvironmental Engineering, ASCE, Vol. 124, No. 9, pp. 868-877.

Yasuhara, K., Murahami, S., Song, B., and Hyde, A. (2003) “Post-cyclic degradation of strength and stiffness for low plasticity silt,” Journal of Geotechnical and Geoenviromental Engineering, ASCE, Vol. 129, No. 8, pp. 756-769.

Yilmaz, M. T., Pekcan, O., and Bakir, B. S. (2004) “Undrained cyclic shear and deformation behavior of silt-clay mixtures of Adapazari, Turkey,” Soil Dynamics and Earthquake Engineering, Vol. 24, pp. 497-507.

Yoshimi, Y. and Oh-oka, H. (1975) “Influence of degree of shear stress reversal on the liquefaction potential of saturated sand,” Soils and Foundations, Vol. 15, No. 3, pp. 27-40.

Yoshimi, Y. and Tokimatsu, K. (1978) “Two-dimensional pores pressure changes in sand deposits during earthquakes,” 2nd International Conference on Microzonation for Safer Construction, Vol. 2, pp. 853-863.

Youd, T. L. (1998) “Screening guide for rapid assessment of liquefaction hazard at highway bridge sites,” Multidisciplinary Center for Earthquake Engineering, Technical Report MCEER-98-0005, June.

Youd, T. L., Idriss, I. M., Andrus, R. D., Arango, I., Castro, G., Christian, J. T., Dobry, R., Finn, W. D., Harder, Jr., L. F., Hynes, M. E., Ishihara, K., Koester, J. P., Liao, S. S. C., Marcuson, III, W. F., Martin, G. R., Mitchell, J. K., Moriwaki, Y., Power, M. S., Robertson, P. K., Seed, R. B., and Stokoe, II, K. H. (2001) “Liquefaction Resistance of Soils: Summary Report” from the 1996 NCEER and 1998 NCEER/NSF Workshops on Evaluation of Liquefaction Resistance of Soils, Journal of Geotechnical and Geoenvironmental Engineering, ASCE, Vol. 127, No. 4, pp. 297-313.

Zdravkovic, L. (1998) “The stress-strain-strength anisotropy of a granular medium under general stress conditions”, Ph.D. Thesis, University of London, Imperial College of Science, Technology and Medicine.

Zergoun, M. and Vaid, Y. P. (1994) “Effective stress response of clay to undrained cyclic loading,” Canadian Geotechnical Journal, Vol. 31, pp. 7 14-727.

Zhang, J., Andrus, R., and Juang, C. H. (2005) “Normalized shear modulus and material damping ratio relationships,” Journal of Geotechnical and Geoenvironmental Engineering, Vol. 131, No. 4, pp. 453-464.

BIBLIOGRAPHY

[Publications produced by this research at the time of this report]

Donahue, J. L., Bray, J. D., and Riemer, M. (2007) "Liquefaction testing on fine-grained soils prepared using slurry deposition," Proceedings of the 4th International Earthquake Geotechnical Engineering, Thessaloniki, Greece, Paper 1226.

Donahue, J.L. (2007) "The liquefaction susceptibility, resistance, and response of silty and clayey soils," Ph.D. Dissertation, in partial fulfillment of the requirements for a Ph.D. within the Department of Civil and Environmental Engineering, University of California, Berkeley, Fall.